AD NUMBER
AD240849
LIMITATION CHANGES
TO: **Approved for public release; distribution is unlimited.**
FROM: **Distribution authorized to U.S. Gov't. agencies and their contractors; Administrative/Operational Use; 10 AUG 1960. Other requests shall be referred to Army Transportation Research Command, Fort Eustis, VA.**
AUTHORITY
TRECOM ltr 21 Dec 1972

UNCLASSIFIED

AD 240849

UNCLASSIFIED

REPUBLIC AVIATION

REPUBLIC AVIATION CORPORATION

Farmingdale, L. I., N. Y.

749 600

U. S. Army Transportation Research Command
Fort Eustis, Virginia

Contract No. DA 44-177-TC-606
Project No. 9R38-01-017-24

THEORETICAL INVESTIGATION OF DUCTED PROPELLER AERODYNAMICS

by

Dr. Th. Theodorsen
Director of Scientific Research

Volume II

Th. Theodorsen
Th. Theodorsen

Republic Aviation Corporation
Farmingdale, Long Island, New York
August 10, 1960

"The findings and recommendations contained in this report are those of the contractor and do not necessarily reflect the views of the Chief of Transportation."

crd 3860

DISCLAIMER NOTICE

When Government drawings, specifications, or other data are used for any purpose other than in connection with a definitely related Government procurement operation, the United States Government thereby incurs no responsibility nor any obligation whatsoever; and the fact that the Government may have formulated, furnished, or in any way supplied the said drawings, specifications, or other data is not to be regarded by implication or otherwise as in any manner licensing the holder or any other person or corporation, or conveying any rights or permission to manufacture, use, or sell any patented invention that may in any way be related thereto.

* * *

ASTIA AVAILABILITY NOTICE

Qualified requestors may obtain copies of this report from

Armed Services Technical Information Agency
Arlington Hall Station
Arlington 12, Virginia

* * *

This report has been released to the Office of Technical Services, U. S. Department of Commerce, Washington 25, D. C., for sale to the general public.

* * *

The information contained herein will not be used for advertising purposes.

* * *

The publication of this report does not constitute approval by USATRECOM of the findings and conclusions contained herein. It is published only for the exchange and stimulation of ideas.

SECTION II

REVIEW AND ANALYSIS OF EXPERIMENTAL INVESTIGATIONS ON DUCTED FANS

TABLE OF CONTENTS

SECTION II

TABLE OF CONTENTS (Cont'd.)

I. INTRODUCTION

Theoretical methods used in treating the ducted fan problem are dealt with in the previous part of this report where also specific extensions to the theory are given. Theoretical methods are indispensible for a rational treatment of the subject. To verify theoretical solutions, to determine deviations due to the real properties of the medium, and to treat configurations too complicated for analysis, experiments are needed.

A comprehensive survey of published experimental work on ducted fan configurations is made in the following. This survey gives an outline of some analytic relations used to document and analyze experimental result. It then selects a number of experimental papers which make significant and consistent contributions and analyzes their results in detail. Major subsections are dealing with the performance in the static or hovering case of the configuration, with performance fields for the case where the fan is moving in axial direction and with the analysis of the performance in non-axial flow which is the flow encountered by a configuration making a transition from hovering to forward flight. Specific observations derived from the analysis and concerning, e.g. the distribution of rolling and pitching moments for a

shrouded and unshrouded propeller, evidence and recognition of flow separation on the shroud, etc. follow. Special arrangements of fans in wing, multiple fan arrangements, and ground proximity effects are reviewed in the following section. The concluding part of this report briefly reviews the general considerations that go into the design of ducted fan systems.

II. ANALYTIC RELATIONS

II A. Dimensionless Representation of Experimental Data

In the theory of models, rules are derived to present the performance of a system from observations made on a different scale system (model). In application to fluid flow it is common practice to express the performance of a turbo machine by characteristic dimensionless quantities (coefficients) which are obtained through combinations of observed physical quantities and which in turn can be used to predict the performance of geometrically similar machines of arbitrary size.

Without going further into detail reference is made to the list of symbols where all the coefficients used are listed and defined. Attention is called to the fact that two systems of coefficients are used, distinguished by the symbol K and C respectively. The K-coefficients are based on the r.p.m. and the diameter of the propeller, and the C-coefficients are based on the flight velocity and the propeller disc area. These systems are used generally in the literature, however variations occur with respect to constants (radius instead of diameter, factor π, etc.). The K-coefficient representation is used for the majority of the experimental results shown in this report.

Inspection of the coefficients listed and of the data given in Section III will demonstrate their usefulness in describing the performance of existing machines by dimensionless quantities independent of scale and measuring system.

II B. Classification According to Specific Speed and Specific Diameter

A different situation exists when the problem is to either classify a given machine with respect to other machines of the same kind (but not geometrically similar) or to design a new machine for a given task. Such classification or orientation for a new design can be obtained by forming a dimensionless or specific speed n_S and a dimensionless or specific diameter d_S using the essential physical dimensions of the machine as mass flow density and energy imparted to unit mass.

For application to ducted fans we define

$$n_S = n(\rho, v_e, v_o, d) = \frac{\sqrt{K_T}}{J^2}\sqrt{8\pi}$$

and

$$d_S = d(\rho, v_e, v_o, d) = \frac{J}{\sqrt{K_T}}\sqrt{\frac{\pi}{8}}$$

(The constants are carried here to conform with other sources and facilitate comparison).

If these specific values are evaluated with the values obtained at or near best performance (highest efficiency) for various machines

and entered in a logarithmic plot n_S vs. d_S they are found to group closely to one universal curve. A plot of this kind is discussed in the subsequent paragraph III B 1 where it serves to give a summary representation of the axial performance of a large number of different ducted fan systems.

II C. Effect of Viscosity and Compressibility

The simple similarity law which is the basis of the derivation of performance coefficients (II A), assumes a perfect fluid medium. In reality the medium, be it air or water, is viscous as well as compressible. The similarity parameters governing viscosity and compressibility are the Reynolds number and the Mach-number. Since it is usually not possible to carry out model tests satisfying the correct similarity conditions it is correct practice to describe deviations observed under the simplified similarity assumptions as functions of Reynolds number or Mach-number. Those deviations are commonly called scale effects and compressibility effects. A recent survey on ducted fans (ref. 62) observes that little is known on such effects with respect to ducted fans. This is literally true and due to a general lack of systematic tests on the subject. Nevertheless these effects have been thoroughly explored by developers of propellers as well as axial compressors. Since the ducted fan is very closely related to propellers

and axial flow compressors, it is desirable to compare scale and compressibility effects with recourse to such data. An example of experimental determination of scale and compressibility effects on axial compressors is given in Section III B 10.

II D. Relations Derived From Momentum Theorem

For the analysis of the experimental data the following relations are derived for the forces and the power of a propeller system.

II D 1. Forces

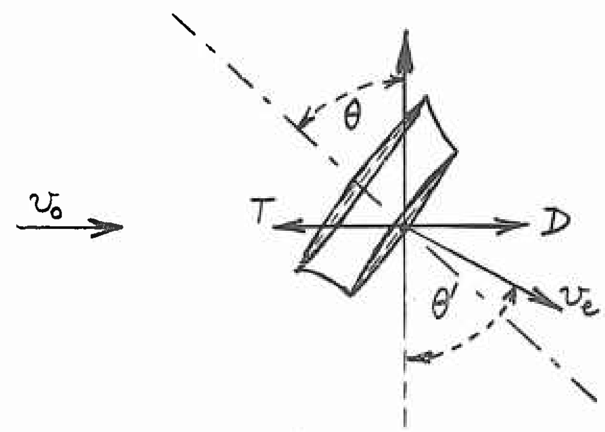

$$T_N = T - D$$

A coordinate system is considered which is fixed on the propeller.

The mass flow is

$$\dot{M}_s = \rho A_e v_e \cos(\theta' - \theta) \tag{1}$$

The lift is

$$L = \dot{M}_s v_e \cos\theta' = \rho A_e v_e^2 \cos(\theta' - \theta) \cos\theta' \tag{2}$$

The net horizontal force is

$$T_N = \dot{M}_s\left(v_e \sin\theta' - v_0\right) - C_D \frac{1}{2}\rho v_0^2 S \qquad (3)$$

where the last term represents the aerodynamic drag of the system and $S = kA_e$ is the reference area.

For steady flight with velocity v_0 the net horizontal force is

$$T_N = 0$$

i.e.,

$$\dot{M}_s v_e \sin\theta' = \dot{M}_s v_0 + C_D \frac{k}{2}\rho v_0^2 A_e \qquad (4)$$

and the lift should be

$$L = W - C_L \frac{k}{2}\rho v_0^2 A_e \qquad (5)$$

where W is the weight and the last term is the aerodynamic lift of the system.

Making use of Eqs. (2) & (5) and (1) & (4) we find respectively

$$\left.\begin{aligned} v_e^2 \cos\theta' \cos(\theta'-\theta) &= \frac{W}{\rho A_e} - C_L \frac{k}{2} v_0^2 \\ v_e^2 \sin\theta' \cos(\theta'-\theta) &= v_e v_0 \cos(\theta'-\theta) + C_D \frac{k}{2} v_0^2 \end{aligned}\right\} \qquad (6)$$

This is a system of two equations with two unknowns v_e & θ . Thus, for any given value of the velocity v_o we can find v_e & θ provided that we know the aerodynamic coefficients C_D & C_L and a relationship between the angles θ' & θ .

Assuming $\theta' = \theta$ the system of Eqs. (6) becomes:

$$v_e^2 \cos\theta = \frac{W}{\rho A_e} - C_L \frac{k}{2} v_o^2$$

$$v_e^2 \sin\theta = v_e v_o + C_D \frac{k}{2} v_o^2 \tag{7}$$

A graphical solution of this system is readily obtained after squaring and adding the two equations so that the angle θ will be eliminated. Then we solve for θ from any of the two equations.

II D 2. Power

The ideal power of the propeller is given by the change in the kinetic energy of the mass flow

$$P = \dot{M}_s \left(\frac{v_e^2}{2} - \frac{v_o^2}{2} \right) = \rho A_e \frac{v_e^3}{2} \cos(\theta' - \theta) \left[1 - \left(\frac{v_o}{v_e} \right)^2 \right] \tag{8}$$

Thus, for a given steady state and aerodynamic characteristics of the system, we can find:

the exit velocity v_e.

the angle of inclination θ and

the ideal power of the propeller P.

From Eq. (8), it is obvious that the power of the propeller is a function of both the exit velocity v_e and the ratio v_o/v_e.

Since for steady state the net horizontal force should be zero, the thrust component of the propeller counterbalances the total drag, and the inclination of the propeller axis θ is found from Eq. (4).

If two separate propellers are used, one in the horizontal and the other in the vertical direction, then the power required is given by

$$P = P_1 + P_2$$

where:

$$\text{(vertical)} \qquad P_1 = \dot{M}_{s1}\left(\frac{v_{e1}^2}{2} - \frac{v_o^2}{2}\right)$$

$$\text{(horizontal)} \qquad P_2 = \dot{M}_{s2}\left(\frac{v_{e2}^2}{2} - \frac{v_o^2}{2}\right) \tag{9}$$

For

$$\dot{M}_{s1} = \dot{M}_s \qquad\qquad v_{e1} = v_e \cos\theta'$$

$$\dot{M}_{s2} = \dot{M}_s \frac{v_{e2}}{v_{e2} - v_o} \qquad\qquad v_{e2} = v_e \sin\theta' \tag{10}$$

we have that the net thrust and lift are the same, i.e.,

$$L = L_1 + L_2 = \dot{M}_{s1} v_{e1} + 0 = \dot{M}_s v_e \cos\theta' \tag{2a}$$

$$T_N = T_1 + T_2 = -\dot{M}_{s1} v_o + \dot{M}_{s2}(v_{e2} - v_o) - C_D \frac{k}{2} \rho v_o^2 A_e$$

$$= \dot{M}_s (v_{e2} - v_o) - C_D \frac{k}{2} \rho v_o^2 A_e \tag{3a}$$

Solving for A_{e1} and A_{e2} from Eqs. (1) and (10), we find ($\theta_1' = 0$, $\theta_2' = \theta_2 = 90^\circ$)

$$\dot{M}_s = \rho A_{e1} v_{e1} \cos\theta_1 \qquad A_{e1} = A_e \frac{\cos(\theta' - \theta)}{\cos\theta' \cos\theta_1} \tag{11}$$

$$\dot{M}_s = \rho A_{e2} v_{e2} \frac{v_{e2} - v_o}{v_{e2}} \qquad A_{e2} = A_e \frac{\cos(\theta' - \theta)}{\sin\theta' - \frac{v_o}{v_e}} \tag{12}$$

Making use of Eqs. (9), (10), (11) and (12), the required power becomes

$$P = P_1 + P_2 = \dot{M}_{s1} \frac{v_{e1}^2 - v_o^2}{2} + \dot{M}_{s2} \frac{v_{e2}^2 - v_o^2}{2}$$

$$= \frac{\dot{M}_s}{2} \left[v_{e1}^2 - v_o^2 + \frac{v_{e2}}{v_{e2} - v_o} (v_{e2}^2 - v_o^2) \right]$$

or

$$\mathcal{P} = \frac{\dot{M}_s}{2}\left[v_{e_1}^2 + v_{e_2}^2 - v_o^2 + v_{e_2}v_o\right]$$

$$= \frac{\dot{M}_s}{2}\left(v_e^2 - v_o^2\right) + \frac{\dot{M}_s}{2} v_{e_2}v_o \tag{13}$$

Thus from Eqs. (8) and (13), it is obvious that if we use two separate propulsion units to produce the same velocity and momentum in the vertical and horizontal direction, then more ideal power is required than that of a single properly inclined propeller unit.

II D 3. Axial Flow

For the experimental case of axial flow through a ducted propeller supported at the test section of a wind tunnel we have the following:

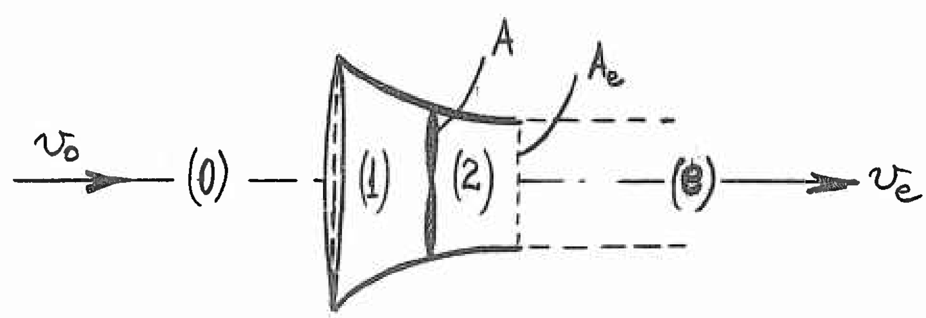

From Bernoulli's equation at the regions (0) & (1) and (2) & (e), we have

$$p_0 + \frac{1}{2}\rho v_0^2 = p_1 + \frac{1}{2}\rho v_1^2$$

$$p_e + \frac{1}{2}\rho v_e^2 = p_2 + \frac{1}{2}\rho v_2^2 \tag{14}$$

For the same static pressure at (0) and (e), we have $p_0 = p_e$, and from continuity $v_1 = v_2$.

Thus, subtracting Eqs. (14) and multiplying by A we get:

$$T_p = A(p_2 - p_1) = \frac{1}{2}\rho A_e v_e^2 \frac{A}{A_e}\left[1 - \left(\frac{v_0}{v_e}\right)^2\right] \tag{15}$$

which is the propeller thrust T_p.

The net thrust is equal to:

$$T_N = \rho A_e v_e (v_e - v_0) - C_D \frac{k}{2} \rho v_0^2 A_e$$

or

$$T_N = \rho A_e v_e^2 \left[1 - \frac{v_0}{v_e} - \frac{k}{2} C_D \left(\frac{v_0}{v_e}\right)^2\right] \tag{16}$$

and is equal to the force measured on the balance of the wind tunnel where:

$$T_N = T_p + T_S \tag{17}$$

T_S is the shroud thrust.

Making use of Eqs. (15), (16) and (17) we find

$$T_s = \rho A_e v_e^2 \left\{ 1 - \frac{v_o}{v_e} - \frac{k}{2} C_D \left(\frac{v_o}{v_e}\right)^2 - \frac{1}{2}\frac{A}{A_e}\left[1 - \left(\frac{v_o}{v_e}\right)^2\right]\right\} \tag{18}$$

Dividing Eqs. (15) and (18) by Eq. (16). we find respectively,

$$\frac{T_p}{T_N} = \frac{\frac{1}{2}\frac{A}{A_e}\left[1 - \left(\frac{v_o}{v_e}\right)^2\right]}{1 - \frac{v_o}{v_e} - \frac{k}{2} C_D \left(\frac{v_o}{v_e}\right)^2} \tag{19}$$

and

$$\frac{T_s}{T_N} = 1 - \frac{\frac{1}{2}\frac{A}{A_e}\left[1 - \left(\frac{v_o}{v_e}\right)^2\right]}{1 - \frac{v_o}{v_e} - \frac{k}{2} C_D \left(\frac{v_o}{v_e}\right)^2} \tag{20}$$

II D 4. Efficiency

The efficiency of a propeller system is defined as the ratio of the ideal power to the actual power used:

$$\eta = \frac{P_{\text{ideal}}}{P_{\text{actual}}} \tag{21}$$

Making use of Eq. (8), the above equation becomes

$$\eta = \frac{\rho A_e v_e^3 \cos(\theta' - \theta)\left[1 - \left(\frac{v_o}{v_e}\right)^2\right]}{2 P_{\text{actual}}} \tag{22}$$

For $v_o = 0$ then $\theta' = \theta$ and the efficiency η becomes

$$\eta_{ST} = \frac{\rho A_e v_e^{*3}}{2P^*_{\text{actual}}} \tag{23}$$

where v_e^* is the exit velocity and P^*_{actual} is the actual power for the case of $v_o = 0$. This efficiency η_{ST} is sometimes called figure of merit.

III. EXPERIMENTAL DATA

III A. List of Experiments Reviewed in Detail, Order of Presentation

Experiments reduced and analyzed in detail, are listed below. The exact quote is given in the list of references.

	Fig. No.	Reference
Hoehne, V. O. and Wattson, R. K. University of Wichita (7) Reports	8-49	17-23
Gill, W. J. Hiller Aircraft Corporation	50-108	7
Grose, R. M. United Aircraft Corporation	109-114	12
Platt, R. J. NACA	115-121	60
Krüger, W. AVA Goettingen, Germany	122-130	31
Van Manen, J. D. Wageningen, Holland	131-138	80, 81
Allen, H. J. and Rogallo, F. M. Stanford University	139-141	1
Moser, H. H., Livingston, C. L., MIT	142-151	52
Taylor, R. T. NACA	152-154	74
McLemore, H. C., and Cannon, M. D. NACA	155-167	47

The above list shows those experimental reports which were

found to contribute significantly either by dealing with a configuration correlated to theoretically determined shapes or by investigating a fairly wide range of performance of a specific configuration, or by illustrating certain characteristics of specific interest. Inclusion in this list does not indicate that the results obtained were particularly outstanding.

The experimental results were reduced uniformly using the quantities and coefficients listed in the list of symbols. The following order is used: The data curves from one investigation are arranged in a group and within the various groups the sequence is: configuration (sketch and designation), static performance data, axial performance data, non-axial performance data and additional related data, e.g., velocity distributions, etc.

The static performance representation requires only two plots per configuration namely, static efficiency η_{ST} vs. thrust coefficient K_T and the thrust division T_S/T vs. K_T. Various blade angles are noted along the curves.

The axial performance is represented in the performance field K_T vs. advance ratio J with the blade angle β as parameter and curves of constant propulsive efficiency η_P shown in the same graph. The

thrust division is shown as T_S/T vs. J. Thus, again two plots describe the axial performance.

All non-axial performance data are shown vs. the angle of tilt θ. The performance is described in a set of graphs showing in coefficient form the resultant force R and its components lift L and drag D. This is followed by a graph of dimensionless fan power K_P and graphs showing the shroud lift K_{LS} and drag K_{DS} and the division of lift L_S/L. Pitching and rolling moments of the configuration are shown as the moment arms e_m and e_ℓ respectively, made dimensionless with the fan diameter and defined as the arm on which the resultant R acts to produce the observed moment. Thus, a total of eight graphs is used to describe non-axial performance.

In the following sections it is attempted to point out characteristic features of ducted fan systems. To keep the text within reasonable proportions the discussions are based on and limited to a few selected examples.

III B. Experimental Results, Discussion and Specific Deductions

III B 1. Summary Plots

Figures 6 and 7 show summaries of static performance of ducted fans. Static efficiency η_{ST} is plotted versus exit area loading

in figure 6 and versus thrust coefficient K_T in figure 7. Most of the data fall within the 80% $\pm$ 8% band.

A static summary plot can also be obtained by entering corresponding values of thrust and power into a plot of T/P versus T/A_e as discussed in II D 3a. This has been done in figures 2 and 3.

A summary of axial performance of ducted fans is shown in figure 5. Corresponding values of specific speed n_S and specific diameter d_S taken for optimum performance are entered in a logarithmic plot. These specific values were derived and defined in II B. It is seen that all values group closely to one universal curve. It may be mentioned that this curve is universal for all kind of turbomachinery and may be extended downward through propellers, axial compressors, Kaplan turbines, radial compressors, to Pelton turbines (ref. 5).

Figure 5 can also serve for selecting the basic dimensions and speed of a new design. Determining from prescribed design data d_S and selecting a n_S from the universal curve, or vice-versa, assures a configuration with which high propulsive efficiency can be obtained.

III B 2. Static Performance Data

Static performance data are contained in figures 9 to 12, 52 to 58, 110, 111, 116 to 121, 123 to 125, 132 to 135, 143 and 144, and for a free propeller in figure 155.

As an example figures 9 and 11 shall be discussed. The curves shown were produced by varying the inlet stator blade angles. (Similar curves can be produced by varying rotor blade angles, figures 10 and 12. Highest efficiency is associated with a certain thrust, i.e., the fan operates with best efficiency at a mass flow corresponding to this thrust. The bellmouth inlet shows higher efficiency than the high speed inlet because it is able to carry more thrust (fig. 11, 43% against 30% of total). The loss of thrust on the sharp lipped high speed inlet is due to flow separation and the attendant loss of suction areas on this inlet. Flow separation on sharp lipped inlets can be demonstrated experimentally. In references (7) and (12), it is demonstrated through pictures of tufts and oilflow patterns. Figures 52 to 57 and 110 & 111 show the static data for these references.

It is possible however, for a relatively sharp lipped shroud to carry a sizeable portion of the total thrust. In figures 115 to 121, data from reference 60 have been plotted. Note that in figure 116, efficiency is high for all configurations. The accompanying shroud thrust data of

figure 119 show that about 60% of the total thrust is carried by the shroud. Shroud thrust data presented in the figures were obtained from pressure measurements. This thrust, therefore, represents an upper limit which probably could not be attained in practice, for it does not include skin-friction drag and support-strut drag and interference. Check points taken with strain gages indicated a shroud thrust about 10% lower than the pressure measurements. Total thrust therefore, is probably about 6% too high. Corresponding efficiencies should be about 9% lower than indicated since efficiency is related to the 3/2 power of thrust for the same power. A typical shroud pressure distribution is shown in figure 117. Note the high negative peak at the inlet, and the slight discontinuities caused by the propellers. It is seen also that the static pressure for this short shroud is restored to ambient pressure at the exit, indicating no contraction or expansion in the wake. Velocity distributions presented in figure 118 show that the propeller renders more uniform the initial non-uniform distribution induced by the shroud.

Fan blade stall can, severely hamper static performance of a system. This is demonstrated, e.g., in figure 123. Static efficiency falls off rapidly at a certain blade angle ($\beta = 50^\circ$ for the uppermost curve) and for increasing blade angles the curves fold under due to the concurrent

loss of thrust. Shroud thrust under those conditions may considerably exceed 50% (figure 128, $J \approx 0$) which of course is due to diffusion behind the propeller.

That shroud thrust can increase above 50% of total thrust with a diffusing shroud is also seen in figure 154 where experimental results are compared with the theoretical momentum relation $T_S/T = 1 - (1/2)\, A/A_e$.

Figure 123 also demonstrates the effect of an exit stator which for this case of a fairly highly loaded fan is seen to improve static efficiency by more than 10%.

That a correctly designed shroud induces additional velocities at the propeller is also evident in the same figure 123. The unshrouded propeller begins to stall at a blade angle of $\beta = 25^\circ$ while this same propeller with a shroud does not reach best efficiency before $\beta = 35^\circ$ to 40°.

The water tests of van Manen (refs. 80 and 81) figures 132 to 135, appear to exhibit little evidence of shroud separation with the exception of a model consisting of a propeller in an axial circular cylinder. The relatively good performance of the other configurations is due to the use of a design procedure similar to that outlined by Küchemann and

Weber in reference 33 and the choice of slopes which induces fairly high velocities on the inside. It is obvious that the axial circular cylinder is the correct design for only the trivial case of infinitesimally small propeller loading in axial flow, and therefore, is to be expected not to demonstrate good efficiency at static conditions.

In general, it can be observed that high efficiencies can be obtained with free propellers as well as with ducted propellers provided the ducted propeller is correctly designed as a unit.

III B 3. Axial Performance

Axial performance data are contained in figures 13 to 20, 59, 60, 112, to 114, 126 to 130, 136 to 138, 140 to 141.

The performance field is used throughout to describe axial performance. This is a plot of corresponding values of thrust coefficient and advance ratio. Fan blade angle β (occasionally stator blade angle β_V) is parameter to the K_T vs. J curves. Points of constant propulsive efficiency η_P are connected and form (generally closed) curves which are labelled with the respective propulsive efficiency value. Supplementing the performance plots are plots of thrust division T_S/T vs. advance ratio J with β again as parameter.

Figure 19 and its corresponding plot of shroud thrust, Fig. 20,

shall serve as an example to illustrate the kind of information that can be extracted from such plots. Thrust is seen to vary directly with blade angle and inversely with advance ratio. Maximum efficiency occurs at a particular blade angle and advance ratio. An area of good efficiency is found in the middle of the field allowing for some variation in β and J without severe loss of efficiency. From figure 20 it appears that the point where shroud thrust becomes zero corresponds closely to operation near best efficiency for a given value of blade angle β. This situation was found consistently in all the data examined figures 13, 14; 15, 16; 17, 18; 112, 113, with the exception of the data of reference 31 figures 127 and 128.

Comparing the performance field of a high speed shroud, fig. 19 and 22 with the performance field of a bellmouth shroud, figure 17 and 18 shows typical differences. The most pronounced difference is an increase of the slope of the K_T vs. J curves caused by the better performance of the bellmouth shroud at low J and its higher drag at high advance ratios. This high drag is also the reason why the bellmouth shroud shows lower peak efficiency. In contrast, the high speed shroud may exhibit loss in thrust at low advance ratios (unstable characteristic, fig. 19) due to shroud separation or blade stall or a combination of both. Blade stall may be quite severe particularly if the fan is an aerodynamically highly loaded efficient limit design, fig. 127, $\beta=65^\circ$.

Pressure distributions on a shroud for various advance ratios are shown in figure 129. At near static conditions (low J), high suction pressures are observed which quickly decrease with increasing advance ratio, while the pressure distribution approaches the distribution on the shroud without a propeller. Accompanying velocity surveys in the inlet, figure 130 show the same trend. It is interesting to note that changes in the normalized velocity distribution with advance ratio are small. The low values near the hub at high advance ratio are not typical but are due to a thick boundary layer developing over the long forebody, see fig. 122.

Performance fields of a free propeller and this same propeller in a duct from reference 7 are shown in figures 59 and 60. The performance fields shown are fragmentary because the tests were not extended far enough to include optimum performance. The effect of the duct to shift the area of best performance toward higher advance ratios can, nevertheless, be seen from a comparison of the figures. Also apparent are the higher thrust and the lower efficiency obtained with the shrouded configuration at low advance ratios.

Early tests by Allen and Rogallo, ref. 1, figures 139 to 141, show that little advantage is to be gained with the addition of a shroud to a lightly loaded propeller ($T/A \approx 3$ lb/ft^2). Figure 140 shows that

shroud thrust is a very low fraction of the total thrust, and a comparison of figures 140 and 141 will show that the unshrouded propeller operated at higher efficiency than the shrouded propeller. The tip clearance for these tests was very large (.0185 of propeller radius) and the blade tips were well rounded. It is evident that the deleterious effects of tip clearance as shown in figure 170, are responsible for the low shroud thrust.

When the propeller is designed to operate within a shroud as is the case with reference 31, operation of this propeller unshrouded should result in a lower efficiency. A comparison of figures 126 and 127 shows that the shrouded propeller operated more efficiently than the same propeller without a shroud.

The water tests of van Manen (references 80 and 81) showed that at sizeable forward speed, higher efficiency was obtained with a straight circular cylinder of one diameter length than with shrouds having airfoil profile cross sections. (Figure 136 compared to figures 137 and 138. The reason is probably that the straight cylinder has only a small separated region near its leading edge when operating under light propeller loading ($K_T = 0.13$) and that the flow is able to reattach before entering the propeller plane due to the considerable length of the shroud. Thus, this shroud acts essentially as an end plating device

insuring full loading over the blade span. In contrast the bellmouth shrouds probably incur separation on the outside and possibly cavitation and as a consequence, large drag. The distinct kink in the K_T vs. J curves of these shrouds (figs. 137 and 138) appears to confirm this deduction.

III B 4. Non-axial Performance

Non-axial performance data are contained in figures 21 to 49, 61 to 108, 145 to 148 and for the free propeller in figures 156 to 167.

The lift and drag forces on the shroud and the ratio of shroud lift to total lift are shown in figures 25 to 27, 33 and 34, 40 and 41, 47 and 48, 74 to 76, 86 to 88, 95 to 99, 104 to 106.

As an example, the lift division for a bellmouth and a high speed shroud figures 27 and 33 may be discussed. Shroud lift is seen to increase with advance ratio and the increase is relatively larger for the high speed inlet. The sudden fall-off of the shroud lift (figure 33, $J = 0.7$) is probably due to separation on the high speed shroud and is seen also in the total lift graph (figure 30).

It is interesting to note that in forward flight the shroud lift increases relative to that for static conditions. This is to be expected

in the case of the high speed inlets (see fig. 33) for unseparated flow, however, this characteristic is even demonstrated by the bellmouth shroud which when operated as ring wing without a propeller, has very poor lift/drag ratio (ref. 7).

Test results for a rigid unshrouded propeller are presented in figures 155 to 167. The propeller was operated as a thrust generator throughout the range of forward speed and angle of tilt. The values of advance ratio employed varied from 0.2 to 6.2 which correspond to ratios of forward speed to tip speed from ~ 0.06 to ~ 2.0. The lowest tilt angle tested was 7.5°.

Increasing J has an unloading effect at high tilt angles and the opposite effect at low tilt angles, the blade loading becoming more asymmetric with increasing J and decreasing tilt. The above points may be illustrated by reference to figures 156, 157, 158, 159 and 160 where the forces and power input are shown versus tilt angle for $\beta_{.75R} \cong 30^{\circ}$. Additional data for $\beta_{.75R} \cong 40^{\circ}$ may be seen in figures 162, 163 and 164. The effects of asymmetric blade loading may be seen in the moment data. (Fig. 161 and 165) Note that:

a. Rolling moment is about three times pitching moment.

b. Increasing J displaces the resultant vector outward.

c. Variations with tilt angle become more erratic with increasing blade angle as J increases.

The causes of these effects may be seen in figure 168 where the blade angle at .75 radius for zero net loading is expressed as a function of J and tilt angle. For a constant blade angle and $J < 2.36$, decreasing J or tilt angle has the tendency to increase the net section angle of attack at different rates, thus unevenly loading the blades. At values of J approaching 2.36, the retreating blade undergoes large changes in section angle of attack which is responsible for the erratic variations in the moment data in this range.

III B 5. Effect of Flow Separation on Performance

Flow separation on ducted fan configurations occurs quite frequently and has usually a marked effect on performance. Separation on the duct ahead of the fan can also have a compounding or triggering effect because it may cause blade stall with violent changes in performance. Some examples of experimental evidence of flow separation are therefore discussed in this paragraph.

Inspection of fig. 81 shows that as tilt angle is decreased the flow on the inside of the forward part of the bellmouth shroud separates. The separation increases as the tilt is decreased until finally at $\theta = 20^{\circ}$,

very little flow passes through the forward part of the shroud. This observed exit distribution is the result of inflow disturbances and whatever changes have been added by the propeller. It is reasonable to assume therefore that the inflow distribution is similar. A propeller operating in such a flow would experience higher section angles of attack during the forward traverse of the blade than the rear traverse, resulting in positive (nose up) propeller moments. This, in fact, is seen in fig. 79. At low values of tilt angle, the propeller moments are positive and the total moment is also positive (fig. 78). As the flow asymmetry is decreased, i.e., the tilt is increased, the propeller moment becomes negative while total moment remains positive. Reference to moment data for this propeller without the bellmouth shroud (fig. 65) shows that at low tilt angles, the propeller moment is also positive and of the same order of magnitude. This and the fact presented earlier that the mean wake direction at low tilt angles deviates rearward from the propeller axis strongly suggests that the flow through the Hiller bellmouth shroud resembles that through a free propeller as a result of flow separation from the shroud. It can be seen from the velocity distributions in fig. 81 that the separation becomes progressively worse as the tilt decreases.

Reference to data for a more highly loaded shrouded propeller

(ref. 17-23) reveals a different characteristic. As an example, figs. 36 to 40 may be consulted. It is seen that together with the variations described for reference 7 (fig. 72, 73 and 77), there are now sharp decreases in resultant lift and drag followed by increase in power at a tilt of less than 30^{o} and $J = 1.4$. It can be inferred that the sharp decreases in lift, drag and resultant at low tilts are the result of the compounded effects of a separation at the forward shroud lip and blade stall.

It must be realized that shroud separation and fan stall, or more precisely, cyclical fan blade stall in the forward section of the duct, are closely linked. It is therefore not always possible to distinguish clearly the two effects if only summary measurements of forces or exit velocity distributions are available. Qualitatively, however, the situation can be described. Incipient shroud separation first increases the aerodynamic loading on those parts of the fan blade which traverse the separated regions due to the reduced velocity in those regions. Depending on how closely the blade was originally operating near its maximum lift coefficient and on the size of the separated region this may lead to blade stall. As soon as blade stall occurs and spreads spanwise over a sizeable portion of the blade the shroud separation region will increase and take up even larger parts

of the cross section. Thus it is evident that mutually compounding effects are an essential feature of the whole process.

Static separation phenomena have been described by Platt, ref. 60, and Hubbard, in ref. 26, as function of propeller rotational speed. Platt has noted that at low rotational speeds the flow separates from the shroud at the leading edge. Operation in this condition is rough and accompanied by much noise; as the propeller speed is increased, the flow suddenly attaches at the inlet resulting in smooth, quiet operation with much higher shroud thrust. This is probably due to transition occurring in the shroud boundary layer as a consequence of increasing Reynolds number and the turbulent boundary layer being able to remain attached in the adverse pressure gradient. Comparison of shroud pressure distributions for the unseparated and separated flow conditions shows that they differ only in that the low-pressure region at the nose is lost in the separated condition. The shroud thrust in the separated flow condition is then only about .25 total thrust.

The report of Hubbard, (ref. 26) on sound pressures is consistent with the foregoing result of Platt, (ref. 60) in that higher sound levels were observed when the flow over the shroud inlet was separated. For these static tests which were conducted outdoors, wind direction

was critical in establishing the flow in the shroud. Cross winds and tail winds generally caused a separation of the flow on parts of the shroud surface, and head winds generally assisted in establishing unseparated flow. Flow conditions in this case were observed by means of tufts located around the periphery of the shroud on the inside surface near the leading edge.

The effect of shroud inlet radius is illustrated in fig. 153. Increasing lip radius is seen to improve the thrust performance. It must be pointed out that a simple radius is not the correct shape for an inlet and will not result in a highly effective minimum-length inlet. Such an inlet should be designed to avoid or minimize adverse pressure gradients. A large amount of literature exists on this subject and ref. 84 is mentioned as an example.

Shroud separation caused by small inlet radii is often the predominant factor in static performance tests, figs. 52 through 57. Although obvious, fig. 151 (b), it is occasionally not recognized. The picture is complicated when shroud separation affects the operation of the propeller and then may lead to contradictory results regarding required propeller pitch distribution ("washout" instead of "wash-in" at the blade tips) figs. 143 and 144.

In the axial case, increasing forward speed will of course always tend to reduce separation and at a certain forward speed even the most sharp lipped shrouds will have completely attached flow, resulting in good efficiency. See for example fig. 136 which shows good performance even for a thin-walled circular cylinder shroud provided the advance ratio is sufficiently high.

III B 6. Moment characteristics

Moment representation: Pitching moments are represented by the arm e_m on which the resultant force R must act to produce the observed moment. Corresponding rolling moments are expressed by the arm e_ℓ. The arms are made dimensionless by division with propeller diameter d.

A characteristic difference between the moments on a ducted fan and on a free propeller can be seen comparing figs. 28, 42 and 49 with figs. 161 and 165. The pitching moments (e_m/d) of the three shrouded configurations (figs. 28, 42, 49)are seen to vary with tilt angle approximately as a cosine function and to increase nearly linearly with forward speed; rolling moments are quite small. The opposite is true for a free propeller (figs. 161 and 165). Rolling moments are large and distinctly variable with advance ratio, while pitching moments are small and only slightly dependent upon forward speed.

The reasons are the following: on a free propeller rolling moments are caused by differences in section angle of attack of the advancing and retreating blades. Pitching moments on a free propeller are positive (nose-up). The addition of a shroud reduces the rolling moments of the configuration because the flow through the propeller is made more axial and differences felt by the advancing and retreating blades are reduced. The addition of a shroud increases the positive (nose-up) pitching moment of the configuration because due to high flow velocity over the leading part of the shroud, strong suction pressures are developed there. The propeller pitching moment is simultaneously reduced due to the shroud induced additional velocities (for the case of no separation) in the forward part of the propeller plane, but is overpowered by the duct moment.

The addition of stators to the shrouded configuration further affects the rolling moments. This latter effect is predominant in the experimental results shown in figs. 28, 42, 49. Further results on pitching moments substantiating the above remarks are contained in the material extracted from reference 7, figures 65, 70, 78, 79, 89, 90, 98, 107 and 108.

The effects of shroud separation on pitching moments have been discussed in detail in section III B 5. Flow separation can modify the

moments considerably. If the flow over the leading edge of a ducted propeller separates from the shroud, the low pressure on that part of the shroud is lost and consequently the positive duct pitching moment will be reduced. It has previously been shown that the flow over sharp lipped ducts is more prone to separation than the flow over gradually curving large bellmouth inlets. It is to be expected therefore that pitching moments for airfoil ducts will be lower than for bellmouth shrouds. This is illustrated in figs. 89 and 107. The moments shown in fig. 107 which are for an airfoil shape shroud are appreciably lower than those for the bellmouth shroud in fig. 89. Shroud lift for the airfoil duct is also appreciably lower, figs. 87 and 105.

III B 7. Lift Characteristics of Shroud and Propeller at Low Angle of Attack.

Figure 169 shows lift curve slope C_L versus power loading for two high speed shroud configurations. The first set of points taken from Hiller experiments (ref. 7) is for a small power loading of $K_P = 0.019$. The points shown refer to the propeller alone, the shroud alone, and the combination of shroud and propeller. It is evident that the lift curve slope of the combination is the sum of the component slopes. Values for $\alpha = 0$ are shown, however, $\overline{C}_{L_\alpha}$ -values remained constant up to $\alpha = 30^\circ$ in these experiments.

The other high speed shroud configuration is that of ref. 12. Data are presented for the isolated shroud, the propeller operating in the shroud, and the combination. Since isolated propeller lift was not available, additional data for a free propeller of similar geometry are presented. It is seen that the free propeller data and the data for the similar propeller operating in the shroud differ little. The sum of the latter data and the curve for the isolated shroud shows good agreement with the measured shrouded propeller lift at low power coefficients, again confirming the addition of lift curve slopes. Increasing deviation, however, occurs for increasing power loading, indicating increasing influence of the propeller flow upon the shroud flow. The tests showed constant lift curve slope up to the highest angle of attack investigated which was $\alpha = 6.3^\circ$.

Bellmouth shroud configurations exhibit for increasing angle of attack first a regime where $\overline{C}_{L_\alpha} = 0$ followed by a regime of constant C_{L_α}. (see ref. 7).

III B 8. The Effect of Tip Clearance

The experiments of Hubbard, ref. 26, show a highly deleterious effect of tip clearance on shroud thrust, the thrust dropping to 13% of its extrapolated zero clearance value at a ratio of tip clearance to propeller radius of only .0435. fig. 170. (The tip clearance ratio

in this report is not clearly defined and it has been assumed to be the ratio of clearance to propeller radius). The power consumed in these tests was about 20% lower at a tip clearance ratio of .0435. Tests by Hutton, ref. 27, show essentially the same trends. Measurements of axial velocity near the duct wall showed a decrease with an increase in tip clearance with an accompanying decrease in fan pressure rise of about 30% at a tip clearance of approximately 4% radius.

III B 9. Contra-rotating Propeller

Data for contra-rotating propellers at equal blade angle settings for both stages may be found in refs. 7 and 60. The former tests encompass a wide range of operating conditions while the latter were restricted to only static conditions. In the latter tests, however, individual measurements of propeller thrust and power and shroud thrust were made and these data are shown in figs. 119, 120 and 121. Sizeable differences in thrust and power exist between the two propeller components. No direct conclusions can be drawn from the latter tests as the number of blades differed in each component, and from the fromer tests because stage forces were not measured individually, nevertheless, certain general remarks may be made concerning contra-rotating propeller operation. When equal blade angle settings are used for each component, the second

stage operates at higher section blade angles of attack and is likely to stall first. If lower but still equal settings are used, the first stage is not fully loaded and both stages can of necessity never work at peak efficiency simultaneously.

III B 10. Viscosity and Compressibility Effects

Scale and compressibility effects are important whenever it is attempted to use small scale model tests to predict the performance of a larger configuration. Although direct investigation of these effects on ducted fans is almost completely missing, it is nevertheless possible to use systematic studies in neighboring fields to predict those effects.

Figure 4 taken from reference 6, may serve as an example. Figure 4a shows results of systematic Reynolds number variations on an axial flow compressor stage (rotor plus stator). Reynolds number is defined here with tip velocity and blade chord and these two quantities together with number of blades z were varied. Multiplication of Re with λ_p refers the Reynolds number to the axial velocity through the compressor. The stage efficiency is seen to increase with Reynolds number. The kink in the η_{stage}-envelope is probably due to the attainment of full turbulent attachment of the flow on the blade suction side.

The combined effect of Reynolds number and Mach number is shown in fig. 4b for another axial flow compressor stage. Mach number is defined as the ratio of tip velocity to local sound velocity. The same Reynolds number dependence is seen and in addition the sharp drop of efficiency when $M = 1$ is approached.

Some effects of changes in velocity are also shown in figures 112 and 114 and, following the practice of the source, the data are labelled with Mach numbers. Because the effects are produced in the tests by velocity changes, they are however the combined effects of Mach and Reynolds number changes. It is believed that the Reynolds number effect is predominant in the results shown.

III C. Special Configurations

III C 1. Fan in Wing

A comparison of fan-in-wing data with any data of open or shrouded propellers is afforded by figures 145-148 where data from ref. 52 are represented in identically the same fashion as the non-axial data of the other investigations. Distinct differences can be seen. The lift no longer shows a gradual increase at moderate forward speeds and $\theta \approx 0$, but shows instead a rather steep increase effected undoubtedly by and characteristic of the wing.

Drag, on the other hand, varies almost linearly with velocity in the range of tilt angles shown demonstrating that the momentum drag of the fan is predominant (fig. 146). Pitching moments increase with forward speed and decrease with tilt angle. Power for the data presented (fig. 147) increased with forward speed, and decreased with tilt.

In addition, experiments with fan-in-wing arrangements (refs. 16 and 83) show moment behavior which is analogous to that of ducted fan configurations described in section III B 6, i.e., propeller moments are negative while total moments are highly positive with the effects of shroud separation being similar to those described earlier.

The results of hovering tests with a cascade-wing vertically rising airplane model are reported in ref. 45. Included also, are force tests to determine the effectiveness of simple cascades in redirecting the propeller thrust. These latter results may be seen in fig. 171.

III C 2. Ground Proximity Effects

Ground proximity effects have been observed to be either positive or negative, i.e., the lift produced by a system has been observed to increase or decrease in the proximity of the ground. This irregular and

apparently contradicting behavior can be understood, however, if the flow pattern and surfaces over which the flow moves are considered in detail.

Take first the free propeller, (helicopter). Upon approaching the ground, a stagnation point is formed on the ground and the flow spreads outward from that point, i. e., the streamlines become divergent at the propeller plane and consequently the pressure becomes higher there than without ground interference. Therefore, a higher propeller thrust or a positive ground effect is to be expected. This picture is slightly over-simplified but will serve for the present purpose of comparison. A more detailed analysis is given, e. g., in reference 30, where also the question of power and torque dependency are treated. Essentially the same flow pattern exists with the shrouded propeller except that now the increased pressure at the propeller plane produces reduced flow velocities over the duct inlet so propeller thrust increases while duct thrust decreases. Figure 151 illustrates this effect for a ducted fan and a fan-in-wing arrangement. Figs. 149 and 150 show the resulting ground effect to be negative, i. e., show loss of lift in ground proximity.

Some experimental data will serve to illustrate the various points. Figure 172 shows typical data from six different sources. The

ratio of lift to lift at large distance from the ground is plotted versus height measured in fan diameters. The dashed curve (ref. 71) is taken from helicopter experiments and shows only positive ground effect. Almost the same behavior is obtained with a thin shroud with a relatively sharp nosed airfoil profile duct carrying only 20% of lift (ref. 9). In contrast, a shroud with a well rounded inlet, (ref. 52), shows negative ground effect. The remaining three curves, (refs. 15, 16, 74), are for fan in wing arrangements and the ground effect is seen to be most adverse with the fan operating in a large plane.

IV. CONCLUSION

The ducted fan experiments reviewed cover machines which are quite different in characteristics; for example, area loadings of these machines extend from 4 psf. to 150 psf. Operational conditions for the machines also vary from nearly static operation to operation with considerable forward speed. Usually the task is to design for a range of varying operational conditions, thus all the features of technical compromise enter the picture. Conclusions that hold for a wide range of applications can therefore hardly be expected.

Some general priciples are apparent nevertheless. Gains in efficiency over the free propeller cannot be obtained by a shrouded propeller or fan. This is true for configurations designed for static operation as well as for forward flight operation and holds even if mutual interference between shroud and propeller is carefully accounted for in the design. In oblique flow (non-axial) operation the shroud may cause considerable complications.

The shrouded propeller can however produce higher static thrust than a free propeller of the same diameter and can do this efficiently if correctly designed for operation in the shroud.

The ducted configuration also offers the opportunity to add stators easily. These are important for very highly loaded systems and it appears that in this area of extremely high loadings a case for the ducted fan can be made. The ducted fan configuration may also be the natural solution if the necessity exists to adapt a design to special constructive requirements, e.g., to stow away the fan for high speed flight.

It is evident therefore that the ducted fan system derives existence and justification more from constructive requirements and limitations than from aerodynamic considerations, i.e., from extraneous circumstance rather than from conditions inherent in the fluid mechanic problem.

V. LIST OF SYMBOLS

A	propeller area $\frac{\pi d^2}{4}$	
A_e	area at shroud exit $\frac{\pi d_e^2}{4}$	
A_p	shroud area at propeller plane	
a	velocity of sound	
C_R	resultant force coefficient $\frac{R}{q_o A}$	
C_T	thrust coefficient $\frac{T}{q_o A}$	
C_N	normal force coefficient $\frac{N}{q_o A}$	
C_L	lift coefficient $\frac{L}{q_o A}$	based on flight speed
$\overline{C}_L$	lift coefficient $\frac{L}{q_o c_s d}$	
C_D	drag coefficient $\frac{D}{q_o A}$	
C_ℓ	rolling moment coefficient $\frac{\ell}{q_o A d}$	
C_m	pitching moment coefficient $\frac{m}{q_o A d}$	
C_P	power coefficient $\frac{P}{q_o A v_o}$	
C_p	static pressure coefficient $\frac{p - p_o}{(\rho/2) v_o^2}$	
c_s	shroud length along axis of symmetry	

D	drag
d	propeller diameter
d_e	shroud exit diameter
d_h	hub diameter
d_S	propeller specific diameter $\frac{J}{\sqrt{K_T}}\sqrt{\frac{\pi}{8}}$
e_ℓ	lateral displacement of resultant force in a plane normal to the resultant vector (positive in negative y direction)
e_m	forward displacement of resultant force in a plane normal to the resultant vector
f	shroud profile camber
h	height above ground of duct exit plane
J	advance ratio, v_o/nd
J_p	propeller advance ratio, v_p/nd
K_R	resultant force coefficient, $\frac{R}{\rho n^2 d^4}$
K_T	thrust coefficient $\frac{T}{\rho n^2 d^4}$
K_N	normal force coefficient $\frac{N}{\rho n^2 d^4}$
K_L	lift coefficient $\frac{L}{\rho n^2 d^4}$
K_{L_s}	shroud lift coefficient $\frac{L_s}{\rho n^2 d^4}$
K_D	drag coefficient $\frac{D}{\rho n^2 d^4}$
k	ratio of reference area to fan exit area

based on propeller rotational speed

K_{D_s}	shroud drag coefficient $\frac{D_s}{\rho n^2 d^4}$	
K_ℓ	rolling moment coefficient $\frac{\ell}{\rho n^2 d^5}$	
K_m	pitching moment coefficient $\frac{m}{\rho n^2 d^5}$	based on propeller rotational speed
K_P	power coefficient $\frac{P}{\rho n^3 d^5}$	
K_p	pressure coefficient $\frac{p - p_o}{\rho n^2 d^2}$	
L	lift	
L_s	shroud lift	
ℓ	rolling moment about body axis	
M_o	free stream Mach number v_o/a	
M_{tip}	tip Mach number	
m	pitching moment about body axis	
N	normal force	
n	propeller rotational speed	
n_S	propeller specific speed $\frac{\sqrt{K_T}}{J^2}\sqrt{8\pi}$	
P	propeller power	
p	static pressure	
q	dynamic pressure $\frac{\rho v^2}{2}$	
R	resultant force	

R_e	Reynolds number $\frac{\rho v X}{\mu}$
r	radial distance along propeller blade
r'	shroud inlet radius
T	thrust
T_s	shroud thrust
t	shroud profile thickness
v	velocity
W	weight
X	body axis in direction of the axis of rotation, positive forward
Y	body axis in lateral direction; positive to the right when viewed from downstream
Z	body axis normal to X and Y in a right hand system
z	number of blades
α	angle of attack, angle between propeller axis and free stream velocity
$\beta_{.iR}$	propeller blade pitch angle at i percent radius
β_v	inlet guide vane angle, measured from axial plane (plus sign denotes flow deflection in direction of propeller rotation.)
η	efficiency $\frac{P_{ideal}}{P_{actual}}$
η_F	Froude efficiency $\frac{2}{\frac{v_e}{v_0}+1}$
η_P	propulsive efficiency $\frac{-K_D}{K_P} J$

η_{ST}	static efficiency $\frac{1}{\sqrt{\pi}\sqrt{A_e}}$	$\frac{1}{\sqrt{\pi}} \sqrt{\frac{A}{A_e}} \frac{K_L^{3/2}}{K_P}$
θ	tilt angle (angle between propeller axis and lift vector)	
θ'	angle between mean wake velocity and lift vector	
λ	ratio of forward to tip speed $\frac{v_o}{\pi n d}$	
λ_p	ratio of velocity at propeller to tip speed $\frac{v_p}{\pi n d}$	
μ	dynamic viscosity	
ν	hub ratio $\frac{d_h}{d}$	
ξ	shroud diffusion angle - angle between propeller axis and internal shroud surface of diffuser section	
ρ	fluid density	
σ	blade solidity $\frac{\text{blade area}}{\pi d^2/4}$	
σ'	ratio of fluid density to fluid density at sea level	
τ	ratio of tip clearance to propeller radius	
φ	angle between the resultant vector and the plane formed by the y axis and the lift vector	
φ'_a	angle formed by local velocity vector at .75 radius of advancing blade and plane of rotation	
φ'_r	angle formed by local velocity vector at .75 radius of retreating blade and plane of rotation	
Ψ	pressure coefficient $\frac{\Delta p}{\rho n^2 d^2}$	

SUBSCRIPTS

o	refers to free stream condition
p	generally refers to propeller
s	generally refers to shroud
tip	generally refers to conditions at the blade tip
∞	generally refers to conditions at an infinite height above ground
F	front component of contra-rotating propeller
R	rear component of contra-rotating propeller
ST	generally refers to static conditions
e	generally refers to conditions at shroud exit

Two systems of forces are used; one is referred to body axes, (T, N) and the other to wind axes (L, D). Only two of the three moments are considered, pitching moment (m) and rolling moment (ℓ) and these are referred to body axes.

Two systems of coefficients are used and distinguished by K and C respectively. All K coefficients are referred to nd, i.e., to propeller tip velocity / π and propeller diameter. All C coefficients are referred to forward or flight velocity and propeller disk area. These systems are used generally in the literature, however, variations occur with respect to constants (radius instead of diameter, factor π, etc) and of course with respect to the symbols used.

Some of the quantities not used in the present presentation but found more frequently are listed blow to facilitate orientation.

ζ	Bendemann coefficient $(\eta_{ST})^{2/3}$ (η_{ST} defined with $A/A_e = 2$)	
M	figure of merit equal to η_{ST}	
Ω	propeller rotational speed, rad/sec	
Q	propeller torque	e.g. NACA TN 3228
C_Q	torque coefficient $\frac{Q}{\rho n^2 d^5}$ equal to $2\pi \cdot$ power coefficient (K_P)	e.g. NACA TN 3228
Ψ	pressure coefficient (compressors) $\frac{\Delta p}{\frac{\rho}{2}(\pi n d)^2}$	
φ	flow coefficient (compressors) λ_p	

VI. LIST OF REFERENCES

1. Allen, J. J., and Rogallo, F. M.
   Ring Cowled Propellers
   Stanford University, Thesis, 1935

2. Chaplin, Harvey R.
   Theory of the Annular Nozzle in Proximity to the Ground
   David Taylor Model Basin, 1957

3. Claybourn, H. M., Sr.
   Study of a Shrouded Propeller with Distributed Suction on the Inlet Profile.
   Aerophysics Dept., Mississippi State University, Research Report No. 20, 1959

4. Colton, R. F.
   Preliminary Engineering Report on the .4 Scale Aerodyne Model Static Tests.
   Collins Aeronautical Research Laboratory, Report No. CER-924, February, 1959

5. Dickmann, H. E., Weissinger, J.
   Beitrag zur Theorie Optimaler Dusenschrauben (Kortdusen).
   Jahrbuch der Schiffbautechnischen Gesellschaft, Band 49, 1955.

6. Eckert, B.
   Axialkompressoren und Radial Kompressoren
   Springer-Verlag Berlin/Gottingen/Heidelberg, 1953

7. Gill, W. J.
   Wind Tunnel Tests of Several Ducted Propellers in Non-Axial Flow.
   Advanced Research Division of Hiller Aircraft Corp., Report No. ARD-224, April, 1959

8. Glauert, H.
   Airplane Propellers
   Div. L. of Aerodynamic Theory. W.F. Durand, Editor, Vol. IV
   Springer Verlag, Berlin, 1935

9. Gorton, J.V., Hamel, L. A.
   Aerial Jeep Vehicle Project - Phase I Final Report
   Chrysler Corporation, Defense Engineering, 1958

10. Grahame, W. E.
A Review of Ducted Fan Research at Grumman Aircraft Engineering Corporation
Ducted Fan Symposium at MIT, 1958

11. Greenman, R. N., Gaffney, M. G.
Dynamic Stability Analysis of Ducted Fan Type Flying Platforms
Advanced Research Division of Hiller Aircraft Corporation
Report No. ARD-233, 1959

12. Grose, R. M.
Wind Tunnel Tests of Shrouded Propellers at Mach Numbers from 0 to 0.60
United Aircraft Corporation, Research Department, WADC Technical Report 58-604, 1958

13. Ham, N. D., Moser, H. H.
Preliminary Investigation of a Ducted Fan in Lifting Forward Flight.
Massachusetts Institute of Technology, Institute of the Aeronautical Sciences 26th Annual Meeting, New York, 1958. Preprint No. 827.

14. Helmbold, H. B.
Range of Application of Shrouded Propellers.
Fairchild Aircraft Division of Fairchild Engine and Airplane Corp.
Engineering Report No. R221-011, 1955

15. Hickey, D. H.
Preliminary Investigation of the Characteristics of a Two-Dimensional Wing and Propeller with the Propeller Plane of Rotation in the Wing Chord Plane.
NACA RM A57F03, 1957

16. Hickey, David H. and Ellis, David R.
Wind-Tunnel Tests of a Semispan Wing with a Fan Rotating in the Plane of the Wing.
National Aeronautics and Space Administration
NASA TN No. D-88, 1959

17. Hoehne, V. O., Wattson, R. K.
Shrouded Propeller Investigations: Wind-Tunnel Tests of a Shrouded Propeller with a 17-Bladed Rotor, Inlet and Exit Stators, and Long Shroud with High-Speed Inlet and No Exit Diffusion.
Report No. 213-1, 1958

18. Hoehne, V. O., Wattson, R. K.
Shrouded Propeller Investigations: Wind-Tunnel Tests of a Shrouded Propeller with a 17-Bladed Rotor, Inlet and Exit Stators, and Long Chord Shroud with Static Inlet and No Diffusion.
Report No. 213-2, 1958

19. Hoehne, V. O.
Shrouded Propeller Investigations: Wind-Tunnel Tests of a Shrouded Propeller with a 17-Bladed Rotor, Inlet and Exit Stators, and Long Chord Shroud with Modified Static Inlet and No Diffusion.
Report No. 213-3, 1958

20. Hoehne, V. O., Wattson, R. K.
Shrouded Propeller Investigations: Static Performance of Two Highly-Loaded Shrouded Propellers as Measured in the Walter H. Beech Memorial Wind Tunnel.
Report No. 213-4, 1958

21. Hoehne, V. O.
Shrouded Propeller Investigations: Wind-Tunnel Tests of a Shrouded Propeller with a 10-Bladed Propeller, Exit Stators, and Long-Chord Shroud with High-Speed Inlet and No Exit Diffusion.
Report No. 213-5, 1959

22. Hoehne, V. O.
Shrouded Propeller Investigations: Wind-Tunnel Tests of a Shrouded Propeller with a 10-Bladed Propeller, Exit Stators, and Long Chord Shroud with Static Inlet and No Diffusion
Report No. 213-6, 1959

23. Hoehne, V. O.
Shrouded Propeller Investigations: Wind-Tunnel Tests of a Shrouded Propeller with a 10-Bladed Propeller, Exit Stators, and Long Chord Shroud with a Modified Static Inlet and No Diffusion.
Report No. 213-7, 1959

24. Horn, F.
Modell - und Grossversuche mit Kort-Dusenschiffen
Schiffbau, Bd. 36, Nr. 10, pp. 178-180, 1935

25. Horn, F.
Beitrag zur Theorie ummantelter Schiffsschrauben
Jahrbuch 1940 der Schiffbautechnischen Gesellschaft

26. Hubbard, H. H.
Sound Measurements for Five Shrouded Propellers at Static Conditions.
NACA TN 2024, 1950

27. Hutton, S. P.
Tip-Clearance and Other Three Dimensional Effects in Axial Flow Fans.
Zeitschrift fur angewandte Mathematik und Physik, Vol. IX b, pp. 357-371, Germany, 1958

28. Johnson, A. E.
Preliminary Investigation of the Effect of a Leading-Edge Slat on Static Thrust of a Shrouded Propeller.
David Taylor Model Basin, Aerodynamics Laboratory
Aero Memorandum 65, 1958

29. Kirby, R. H.
Dynamic Stability and Control Characteristics of a Ducted-Fan Model in Hovering Flight.
NACA RM L54C18, 1954

30. Knight, Montgomery, Hefner, Ralph A.
Analysis of Ground Effect on the Lifting Airscrew
NACA TN 835, 1941

31. Kruger, W.
On Wind Tunnel Tests and Computations Concerning the Problem of Shrouded Propellers.
Translation of ZWB Forschungsbericht Nr. 1949, January 21, 1944 by Mary L. Mahler, NACA
NACA TM 1202, 1949

32. Kuchemann, D., Weber, J.
Uber die Stroemung an ringformigen Verkleidungen
(Concerning the Flow over the Covering of Annular Shapes)
1942. Translated by H. R. Grumman Translation Report
No. F-TS-620-RE, Headquarters Air Material Command,
Wright Field, Dayton, Ohio, 1946

33. Kuchemann, D., Weber, J.
Aerodynamics of Propulsion
Chapter 6 - The Ducted Propeller
First Edition, McGraw-Hill Book Company, New York, 1956

34. Hayes, William C., Kuhn, Richard E., Sherman, Irving R.
Effects of Propeller Position and Overlap on the Slipstream
Deflection Characteristics of a Wing-Propeller Configuration
Equipped with a Sliding and Fowler Flap.
National Advisory Committee for Aeronautics, NACA TN 4404

35. Kuhn, Richard P, Draper, John W.
Investigation of the Aerodynamic Characteristics of a Model
Wing-Propeller Combination and of the Propeller Separately
at Angles of Attack up to 90°
NACA Report No. 1263, 1956

36. Lamb, H.
Hydrodynamics.
6th Edition, Dover Publications, New York, 1945

37. Lippisch, A. M., Navaratil, B. M.
Wing Tunnel Investigation of the Forward Flight Characteristics
of an Aircraft Model Composed of Two Shrouded Propellers.
Collins Aeronautical Research Laboratory, Report No. CER-355,
1954

38. Lippisch, A. M.
Some Basic Derivations About the Action of a Shrouded Propeller.
Collins Aeronautical Research Laboratory, 1956

39. Lippisch, A. M.
Final Engineering Report on Wind Tunnel Test Study-Part I.
Collins Aeronautical Research Laboratory,
Report No. CER-826, 1958

40. Lippisch, A. M.
Engineering Report on the Results of the Wind Tunnel Testing for the 1/10 Scale Aerodyne Model.
Collins Aeronautical Research Laboratory, Report No. CER-897, 1959

41. Malavard, L. C.
The Use of Rheoelectrical Analogies in Aerodynamics.
North Atlantic Treaty Organization
AGARDograph 18

42. Malavard, L., Hacques, G.
Problemes de L'Aile Annulaire Resolus par Analogie Rheo-electrique.
Laboratoire de Calcul Analogique du C.N.R.S., (Centre National de la Recherche Scientifique), Paris, France

43, Marcinowski, H.
Optimalprobleme bei Axialventilatoren
Heizung and Luftung, Vol. 8 (1957) 11, p. 273-285, and p. 295-296

44. Mathur, M. Ch.
A New Simplified Form of Navier-Stokes Equations for Curvilinear Flow
Aerophys. Dept. Mississippi State University, Report No. 24 1959

45. McKinney, Marion O., Tosti, Louis P., Davenport, Edwin E.
Dynamic Stability and Control Characteristics of a Cascade-Wing Vertically Rising Airplane Model in Take-Offs, Landings, and Hovering Flight.
National Advisory Committee for Aeronautics, NACA TN 3198 1954

46. McKinney, M. O., Parlett, L. P.
Flight Tests of a 0.4 Scale Model of a Stand-on Type of Vertically Rising Aircraft.
NACA RM L54B16b, 1954

47. McLemore, H. Clyde, Cannon, Michael D.
Aerodynamic Investigation of a Four-Blade Propeller Operating Through an Angle-of-Attack Range from 0^{o} to 180^{o}.
National Advisory Committee for Aeronautics, NACA TN 3228 1954

48. Minassian, B.
Analytical Study of Shrouded Propellers.
Longren Aircraft Company, Report No. PR-2, 1955

49. Minassian, B.
Analytical Study of Shrouded Propellers
Longren Aircraft Company, Report No. PR-3, 1955

50. Minassian, B.
Analytical Study of Shrouded Propellers
Longren Aircraft Company, Report No. PR-4, 1955

51. Minassian, B.
Analytical Study of Shrouded Propellers
Longren Aircraft Company, Report No. PR-5, 1956

52. Moser H. H., Livingston, C. L.
Experimental and Analytic Study of the Ducted Fan and Fan-in-Wing in Hovering and Forward Flight.
Aeroelastic and Structures Research Laboratory, Massachusetts Institute of Technology, Technical Report 79-1, 1959

53. Moser, H. H.
Analytic and Experimental Investigation of the Aerodynamics of the Ducted Fan.
Massachusetts Institute of Technology, Thesis, 1958

54. Nelson, N. E.
The Advantages of the Ducted Propeller in VTOL Aircraft Design.
Doak Aircraft Company, Presented at the American Helicopter Society 3rd Annual Western Forum, Dallas, Texas, 1956

55. Parlett, L. P.
Aerodynamic Characteristics of a Small-Scale Shrouded Propeller at Angles of Attack from 0 - 90°.
NACA TN 3547, 1955

56. Patterson, G. N.
Ducted Fans: Approximate Method of Design for Small Slipstream Rotation.
Australian Council for Aeronautics, Report ACA-8, August, 1944

57. Patterson, G. N.
Ducted Fans: Effect of the Straightener on Overall Efficiency.
Australian Council for Aeronautics, Report ACA-9, 1944

58. Patterson, G. N.
Ducted Fans: High Efficiency with Contra-Rotation.
Australian Council for Aeronautics, Report ACA-10, 1944

59. Payne, P. R.
Induced Aerodynamics of Helicopters - Part IV.
Aircraft Engineering, pp. 150-153, 1956

60. Platt, R. J.
Static Tests of a Shrouded and an Unshrouded Propeller.
NACA RM L7H25, 1948

61. Rethorst, Scott, Royce, W. W.
Lifting Systems for VTOL Vehicles
IAS Preprint No. 59-123, 1959

62. Sacks, A. H., Burnell, J. A.
Ducted Propellers - A Critical Review of the State of the Art.
Contract No. NONR 2677(00)
Advanced Research Division, Hiller Aircraft Corp. ARD-232
1959

63. Sacks, Alvin H.
The Flying Platform as a Research Vehicle for Ducted
Propellers.
IAS Preprint No. 832, 1958

64. Sacks, A. H.
The Flying Platform as a Research Vehicle for Ducted
Propellers.
Advanced Research Division, Hiller Aircraft Corporation
Preprint No. 832, 1958

65. Scholes, J. R. M., Patterson, G. N.
Wind Tunnel Tests on Ducted Contra-Rotating Fans.
Australian Council for Aeronautics, Report ACA-14, 1945
Stanford University Library

66. Sheets, H. E.
The Slotted-Blade Axial-Flow Blower.
Electric Boat Division, General Dynamics Corporation
Presented at the American Society of Mechanical Engineers,
Diamond Jubilee Annual Meeting, Chicago, Illinois, 1955
Paper No. 55-A-156

67. Siebold, W.
Naherungweise Berechnung des ummantelten Propellers
Zeitschrift fur, Flugwissenschaften (ZFW), Bd 3, Nr 5, 1955

68. Soloviev, U I , Churmack, D. A.
Marine Propulsion Devices
Publ. by Military Publishing House, Ministry of the Armed
Forces, Moscow, USSR, 1948. Translated by Rose Jermain,
Science Translations Service, University of Alabama, STS-101,
1951

69. Spreemann, K. P., Kuhn, R. E.
Investigation of the Effectiveness of Boundary Layer Control by
Blowing Over a Combinationof Sliding and Plane Flaps in
Deflecting a Propeller Slipstream Downward for Vertical take-off.
NACA TN 3904, 1956

70. Spreeman, Kenneth P.
Investigation of the Effects of Propeller Diameter on the Ability
of a Flapped Wing, with and Without Boundary Layer Control,
To Deflect a Propeller Slipstream Downward for Vertical Take-off.
NACA TN 4181, 1957

71. Stepniewski, W. Z.
Introduction to Helicopter Aerodynamics.
Rotary Aircraft Series No. 3
Rotorcraft Publishing Committee, Morton, Pa.

72. Stipa, L.
Experiments with Intubed Propellers.
L'Aerotechnica, Vol. XI, No. 4, 1931. Translated by A. A. Fanelli
for Aerophysics Department of Mississippi State College, 1956

73. Stone, A.
Ducted Propeller Development Status.
Department of the Navy, Bureau of Aeronautics, Research Division
Report No. DR-1910, 1957

74. Taylor, Robert T.
Experimental Investigation of the Effects of Some Shroud Design Variables on the Static Thrust Characteristics of a Small-Scale Shrouded Propeller Submerged in a Wing.
NACA TN 4126, 1958

75. Templin, R. J.
Note on the Minimum Power Required for Flight at Low Airspeeds.
National Research Council of Canada, Aeronautical Report LR-245, 1959

76. Tosti, Louis P.
Transition-Flight Investigation of a Four-Engine-Transport Vertical-Take-Off Airplane Model Utilizing a Large Flap and Extensible Vanes for Redirecting the Propeller Slipstream.
NACA TN 4131, 1957

77. Uberti, B. J., Reichert, J. B.
Design Philosophy and Test Experience of a VTOL Aircraft
IAS Preprint 59-122 1959

78. U.S. Army Transportation Research Command, Ft. Eusts, Va.
Proceedings of A National Aeronautics and Space Administration (NASA) Briefing on Aircraft Research.
1959

79. Van Manen, J. D.
The Design of Screw Propellers in Nozzles.
International Shipbuilding Progress, No. 55, 1959

80. Van Manen, J. D.
Recent Research on Propellers in Nozzles.
Research Department, Netherlands Ship Model Basin, Wageningen
Journal of Ship Research, pp.13-46, 1957

81. Van Manen, J. D.
Open-Water Test Series with Propellers in Nozzles.
Netherlands Ship Model Basin Publication No. 115a
Reprinted from International Shipbuilding Progress, Vol. 1, No. 2, 1954

82. Vidal, R. J.
A Theory of Wing-Propulsion Combinations in Slow Flight -
Cornell Aeronautical Lab.
Report No. AL-1190-A-1, AD 216 177, 1959

83. Wardlaw, R. L., McEachern, N. V.
A Wing-Submerged Lifting Fan: Wind Tunnel Investigations
and Analysis of Transition Performance.
National Research Council of Canada, Aeronautical Report
LR-243, 1959

84. Whitehead, L. G., Wu, L.Y., Waters, M. H. L.
Contracting Ducts of Finite Length
Aeronautical Quarterly Vol. II, (1951), 4, p. 254-271

FIG 1

NOTATION AND AXES SYSTEM

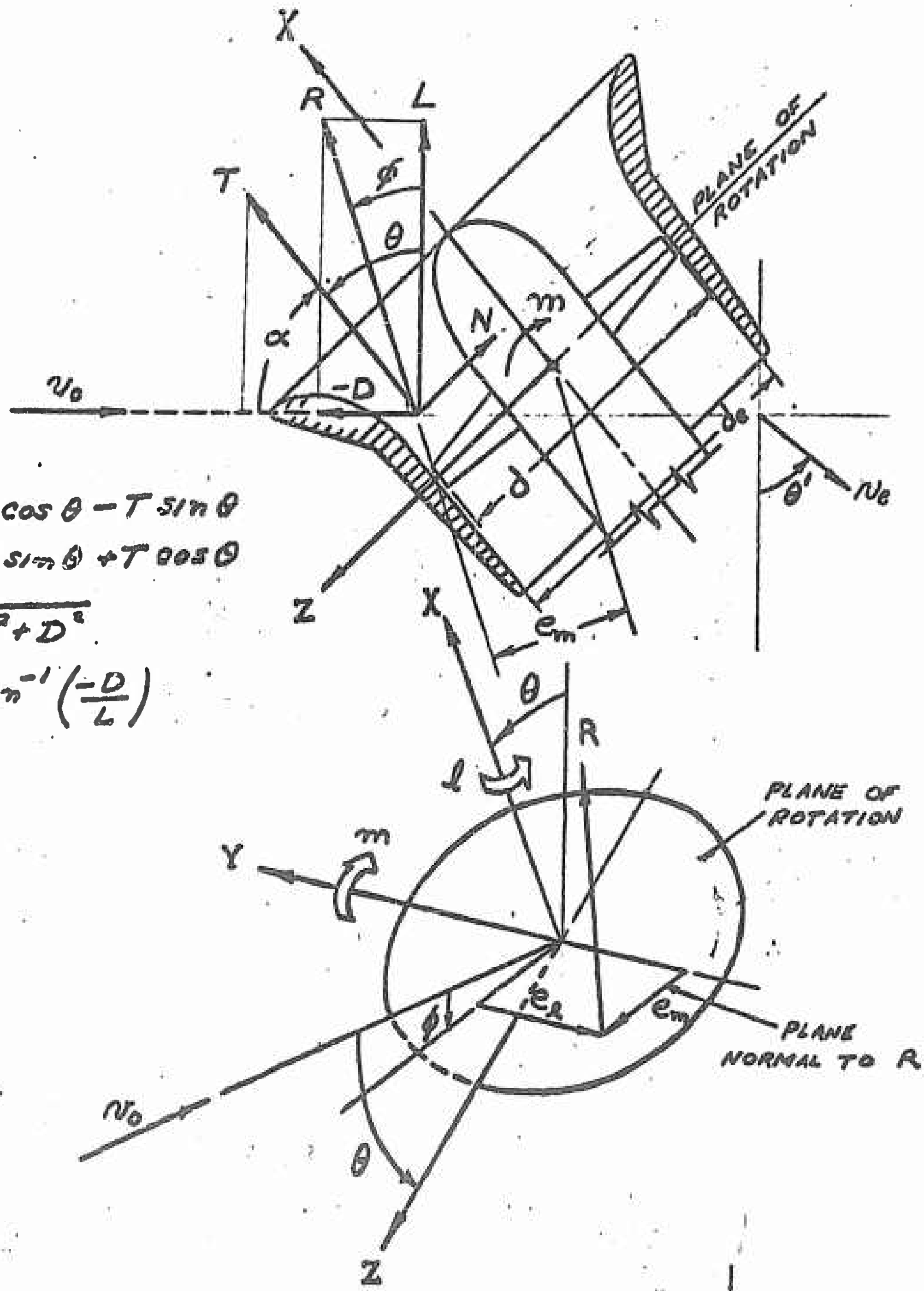

$$D = N\cos\theta - T\sin\theta$$

$$L = N\sin\theta + T\cos\theta$$

$$R = \sqrt{L^2 + D^2}$$

$$\phi = \tan^{-1}\left(\frac{-D}{L}\right)$$

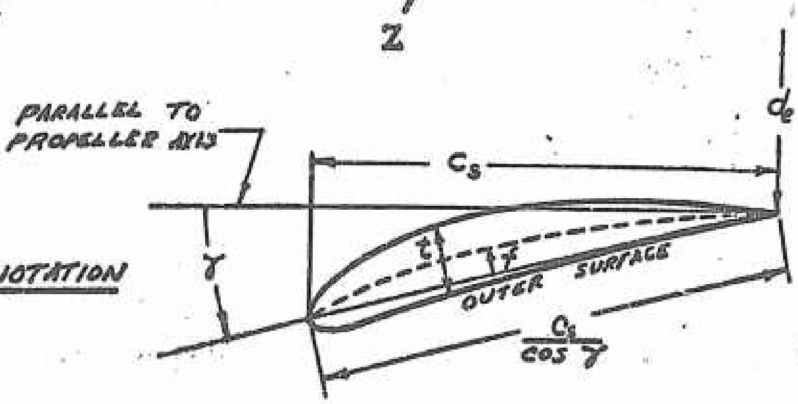

AIRFOIL SHROUD NOTATION

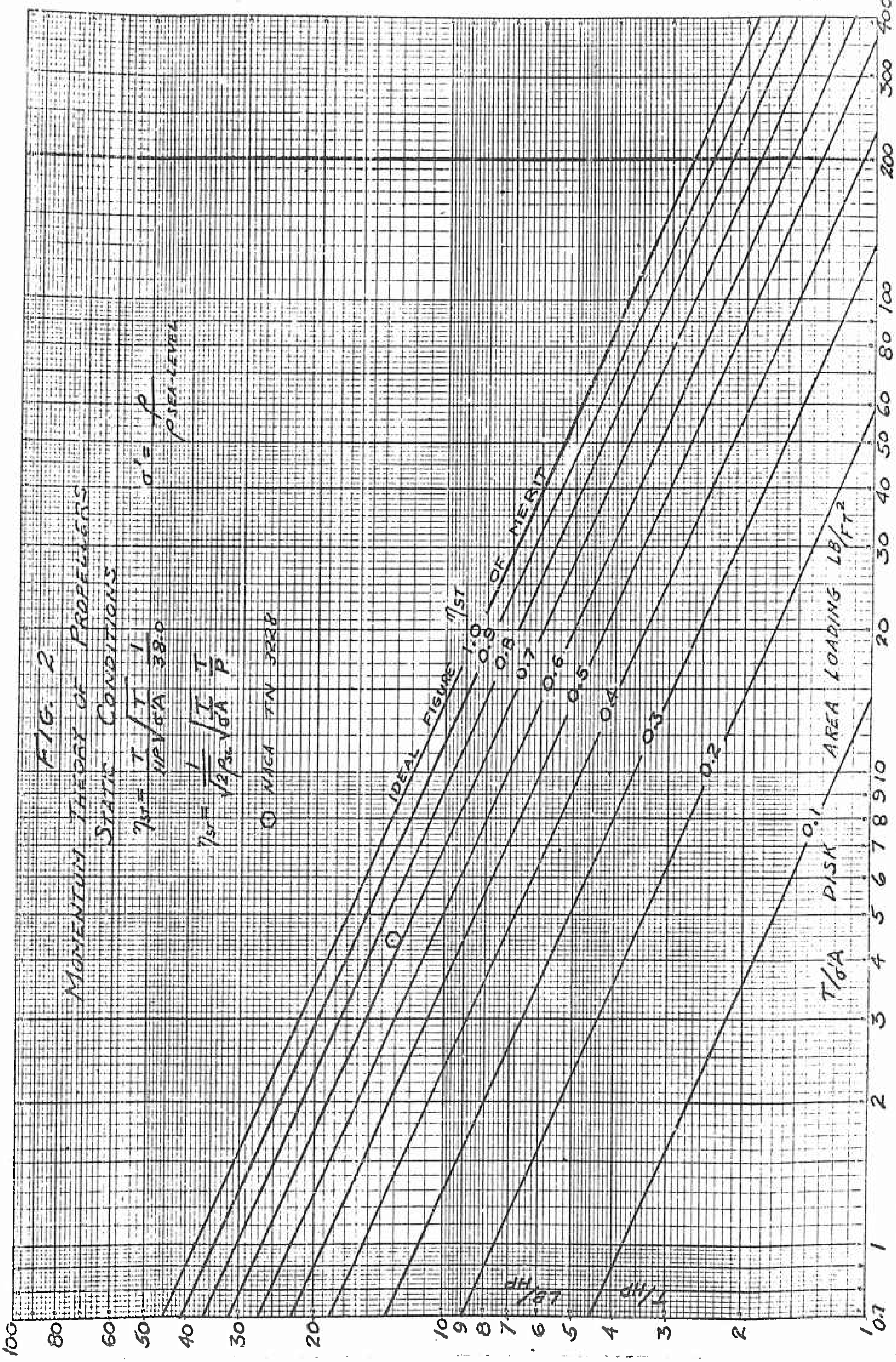
FIG. 2
MOMENTUM THEORY OF PROPELLERS
STATIC CONDITIONS
$\eta_{ST} = \frac{T}{HP}\sqrt{\frac{T}{\sigma' A}}\,\frac{1}{38.0}$
$\sigma' = \frac{\rho}{\rho_{SEA\text{-}LEVEL}}$
$\eta_{ST} = \frac{1}{\sqrt{2\rho_{SL}}}\sqrt{\frac{T}{\sigma' A}}\,\frac{T}{P}$
⊙ NACA TN 3228
IDEAL FIGURE OF MERIT η_{ST}
1.0
0.9
0.8
0.7
0.6
0.5
0.4
0.3
0.2
0.1
$T/\sigma' A$ DISK AREA LOADING LB/FT²
T/HP
T/P
0.1
1
2
3
4
5
6
7
8
9
10
20
30
40
50
60
80
100
200
300
400
100
80
60
50
40
30
20
10
9
8
7
6
5
4
3
2
1

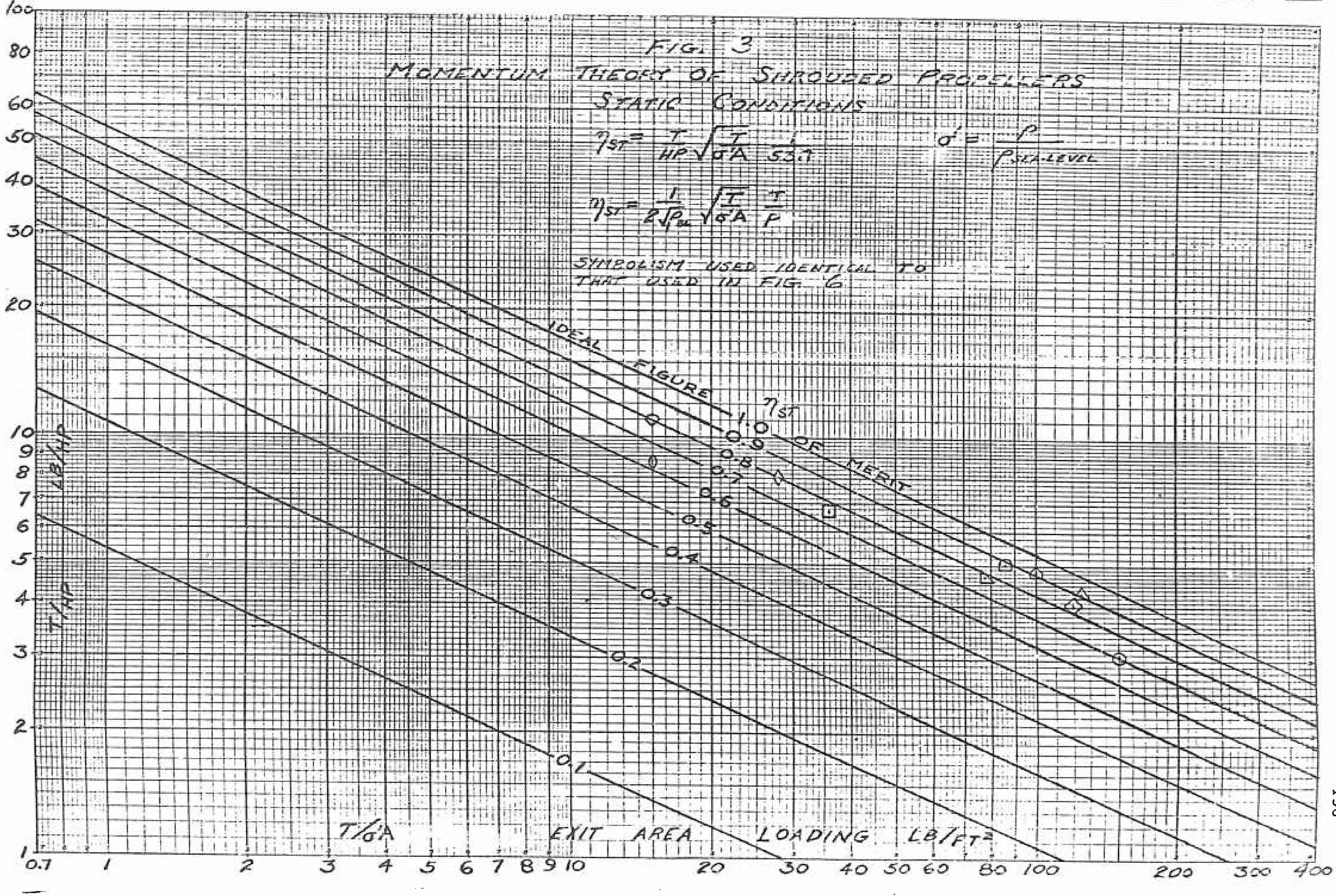
FIG. 3
MOMENTUM THEORY OF SHROUDED PROPELLERS
STATIC CONDITIONS
$\eta_{ST} = \frac{T}{HP}\sqrt{\frac{T}{\sigma A}}\,\frac{1}{53.1}$
$\sigma' = \frac{\rho}{\rho_{SEA\text{-}LEVEL}}$
$\eta_{ST} = \frac{1}{2\sqrt{\rho_{SL}}}\sqrt{\frac{T}{\sigma A}}\,\frac{T}{P}$
SYMBOLISM USED IDENTICAL TO THAT USED IN FIG. 6
IDEAL FIGURE OF MERIT
η_{ST}
1.0
0.9
0.8
0.7
0.6
0.5
0.4
0.3
0.2
0.1
T/HP LB/HP
$T/\sigma A$ EXIT AREA LOADING LB/FT^2
100
80
60
50
40
30
20
10
9
8
7
6
5
4
3
2
1
0.7
1
2
3
4
5
6
7
8
9
10
20
30
40
50
60
80
100
200
300
400

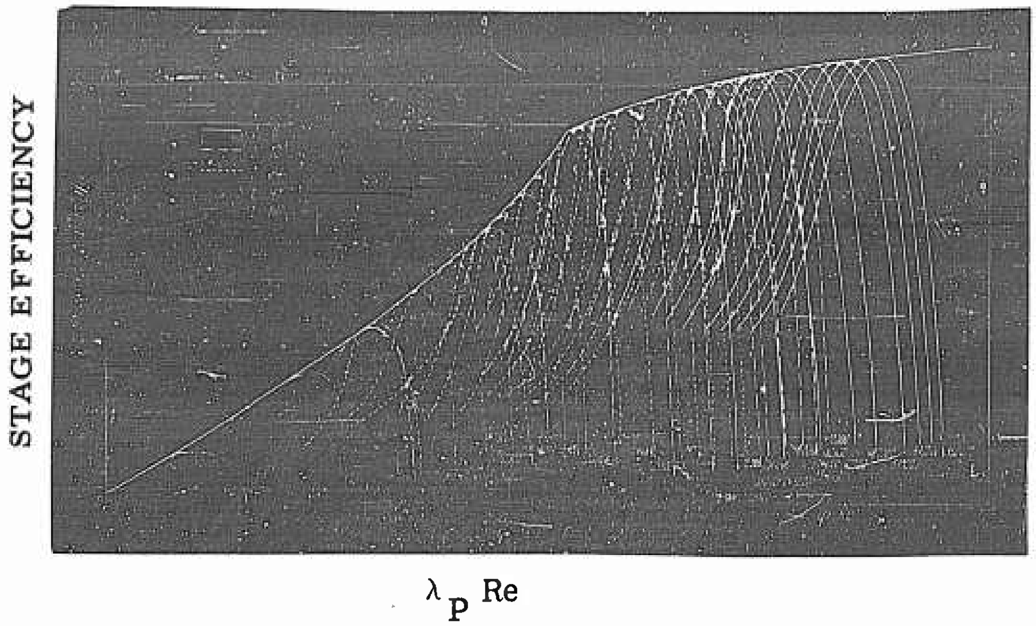

(a)

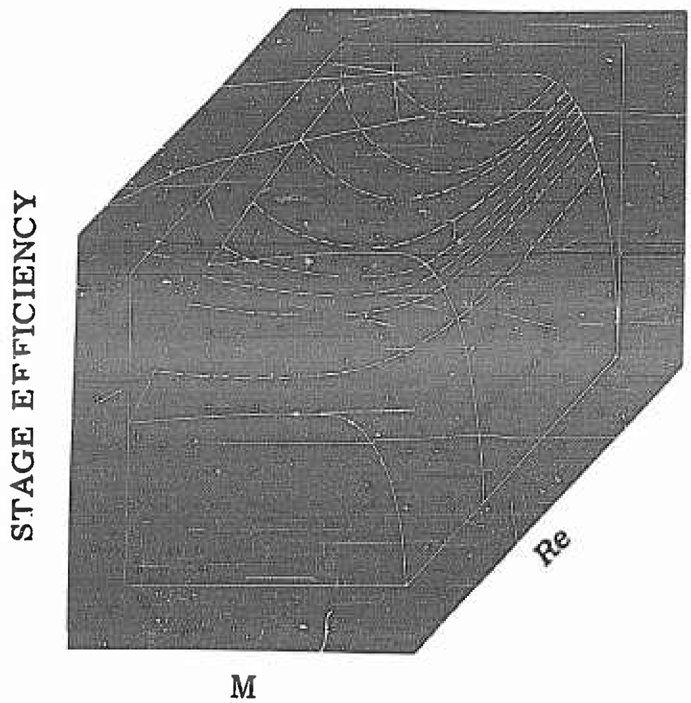

(b)

Fig. 4 COMPRESSOR PERFORMANCE AS FUNCTION OF REYNOLDS AND MACH NUMBER (Reference 6)

FIG. 5

AXIAL PERFORMANCE SUMMARY

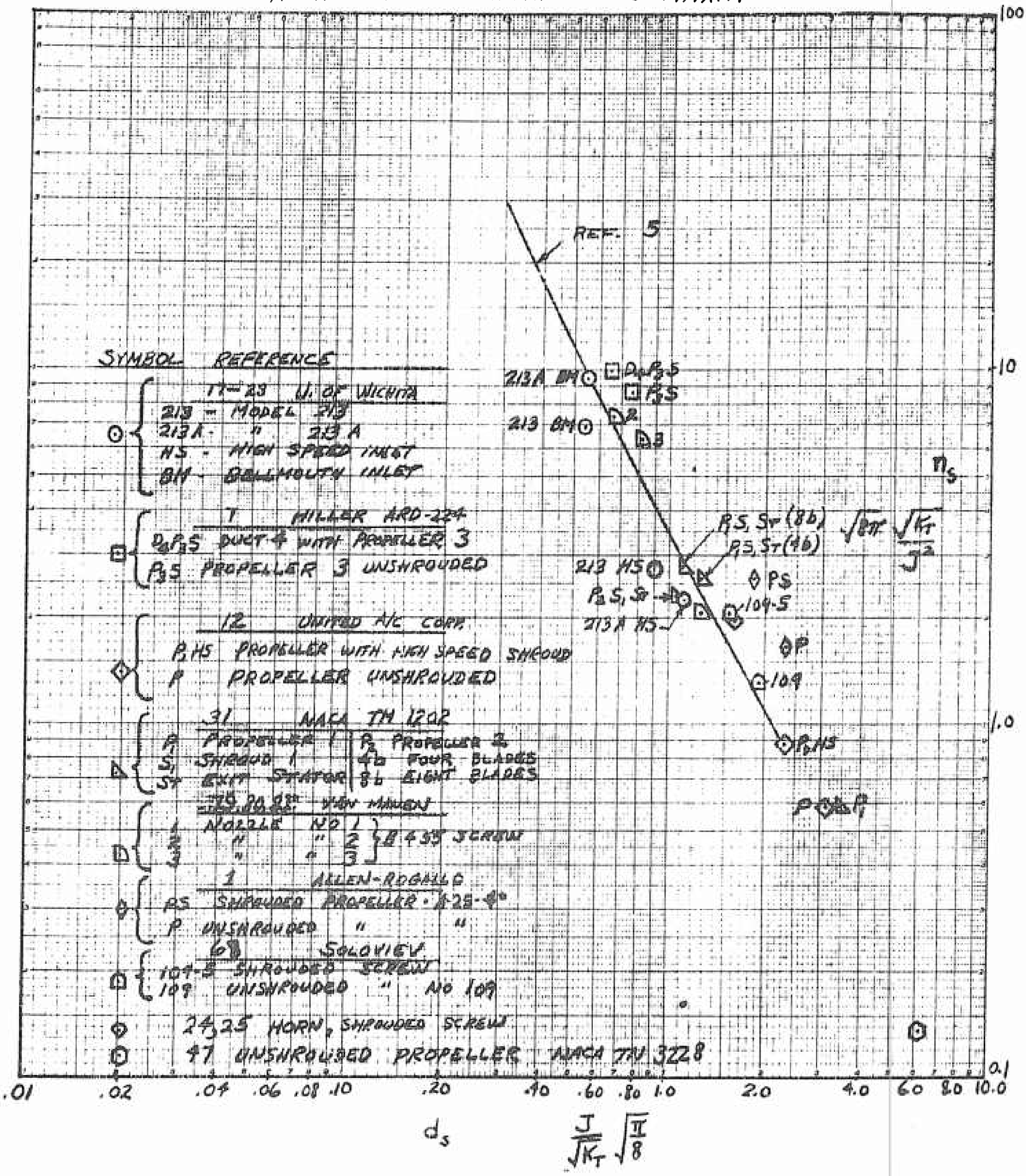

PREPARED
CHECKED
REVISED

REPUBLIC AVIATION

PAGE
REPORT NO
MODEL

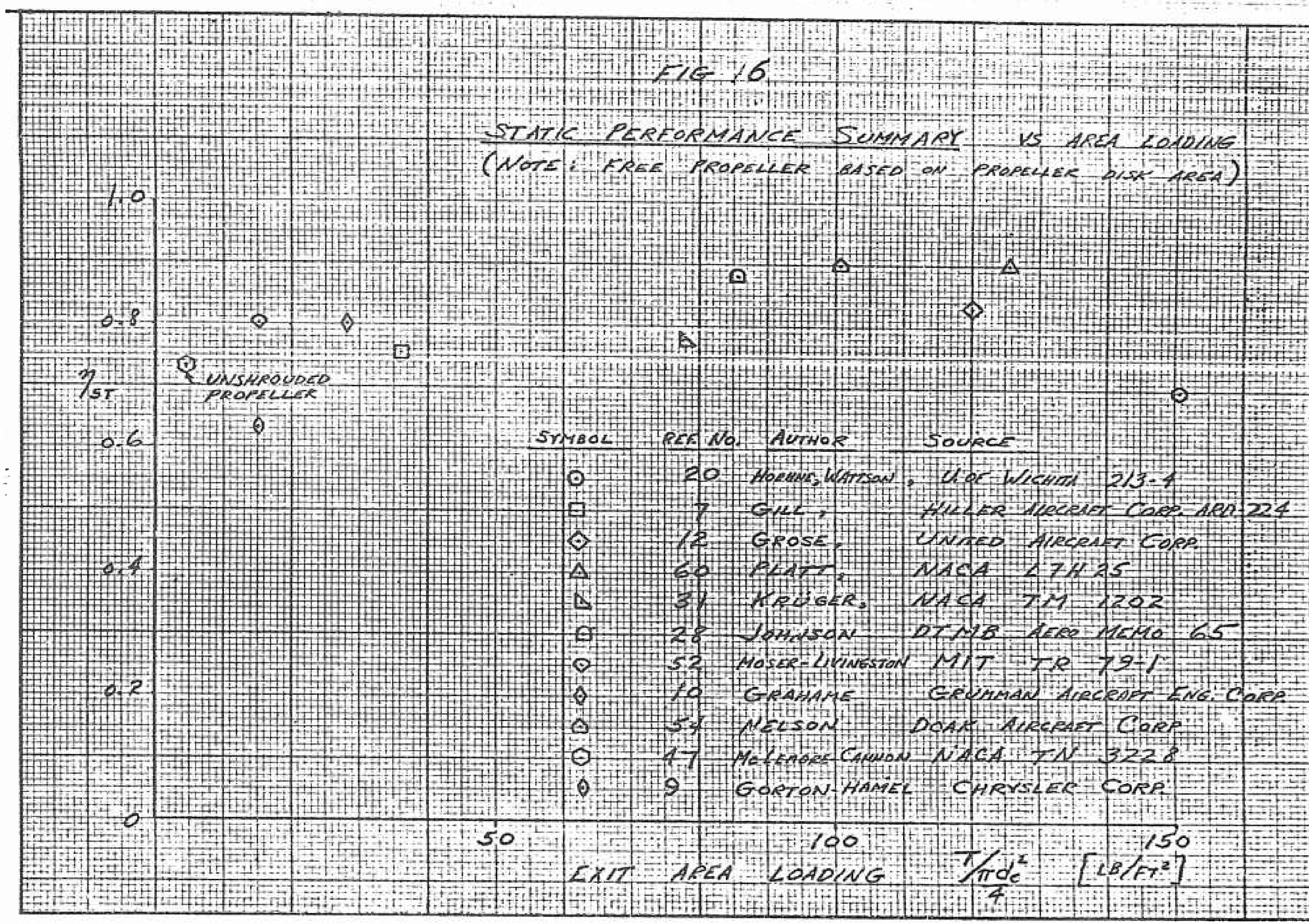

FIG 7:

STATIC PERFORMANCE SUMMARY VS THRUST COEFFICIENT

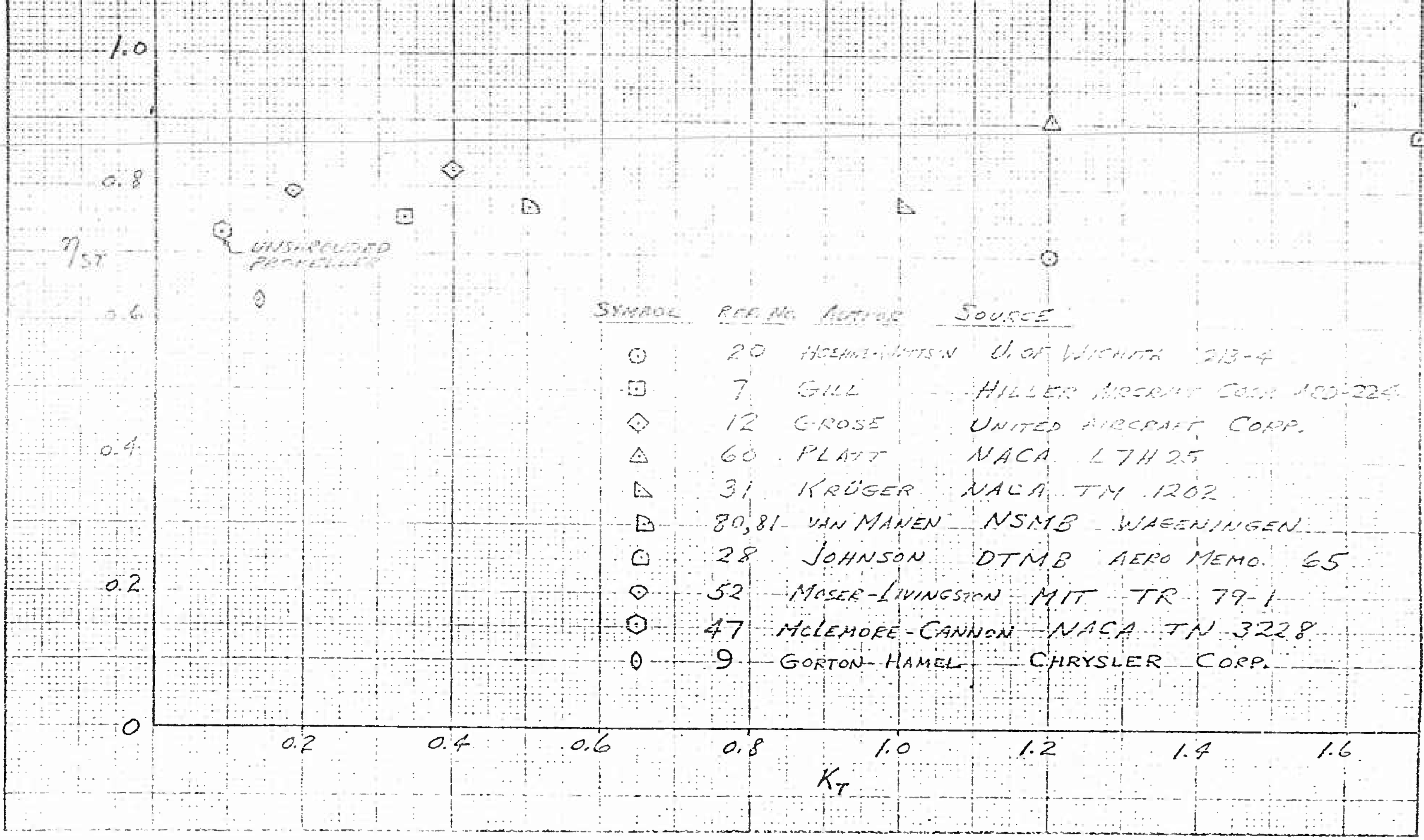

F-1-10A REV. 8/48

Reference	17-23
Authors	Hoehne, V. O. and Wattson, R. K.
Source	University of Wichita, (7) Reports
Figs.	8-49

FIG. 18

CONFIGURATION

REFS. 17-23; WATTSON, R.K., HOEHNE, V.O.
U. OF WICHITA REPORTS 213-1, 213-7, 1958

MODEL 213, 17 BLADED ROTOR, $d_h = 0.4d$
MODEL 213A, 10 BLADED ROTOR, $d_h = 0.3d$, (INLET VANES REMOVED)

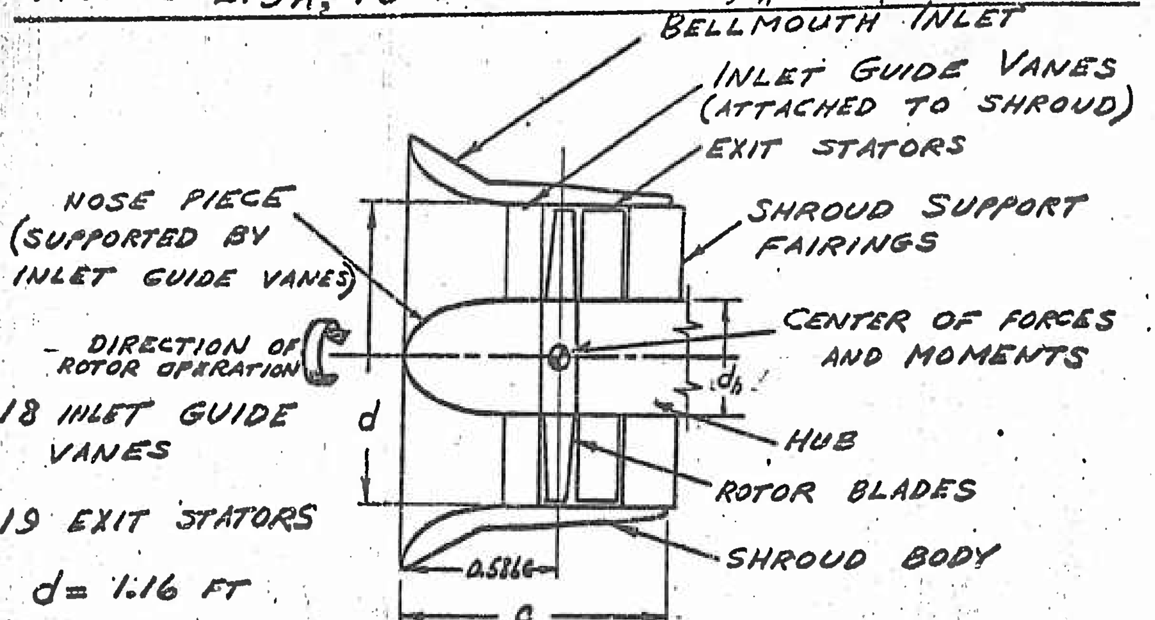

18 INLET GUIDE VANES

19 EXIT STATORS

$d = 1.16$ FT

$C_s = 0.896$ FT

TIP CLEARANCE = .00144d

BELLMOUTH SHROUD

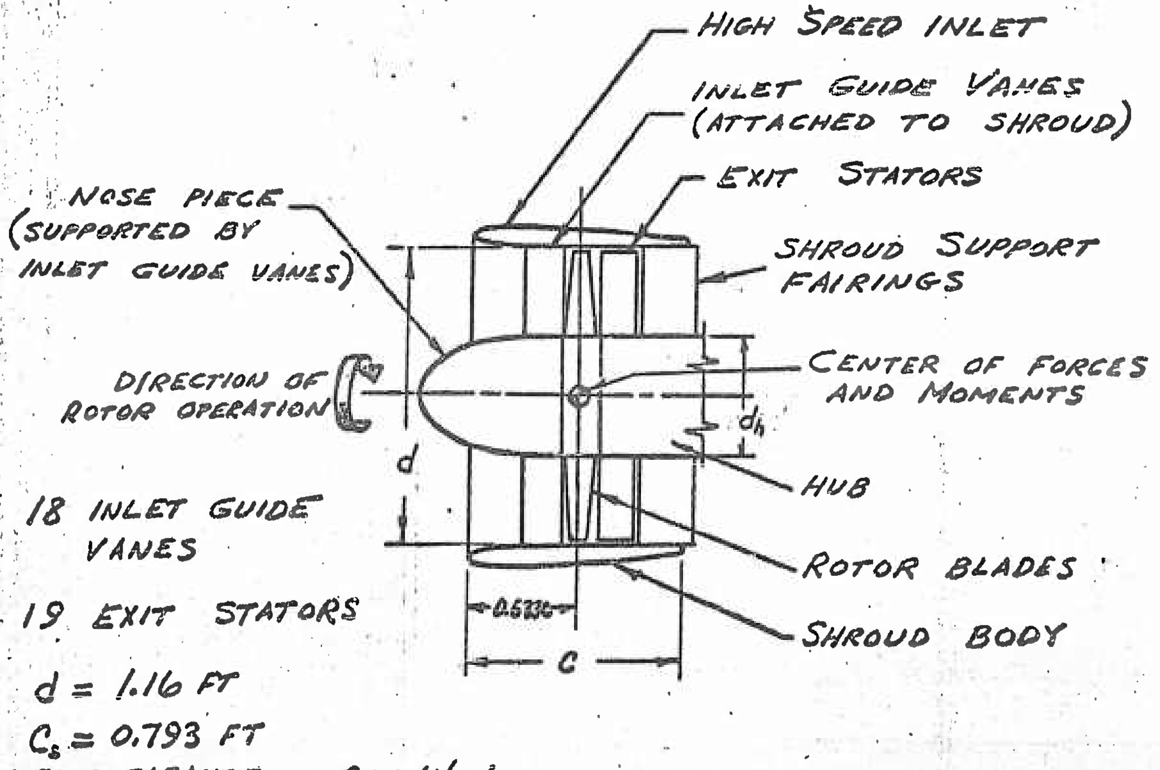

18 INLET GUIDE VANES

19 EXIT STATORS

$d = 1.16$ FT

$C_s = 0.793$ FT

TIP CLEARANCE = .00144 d

HIGH SPEED SHROUD

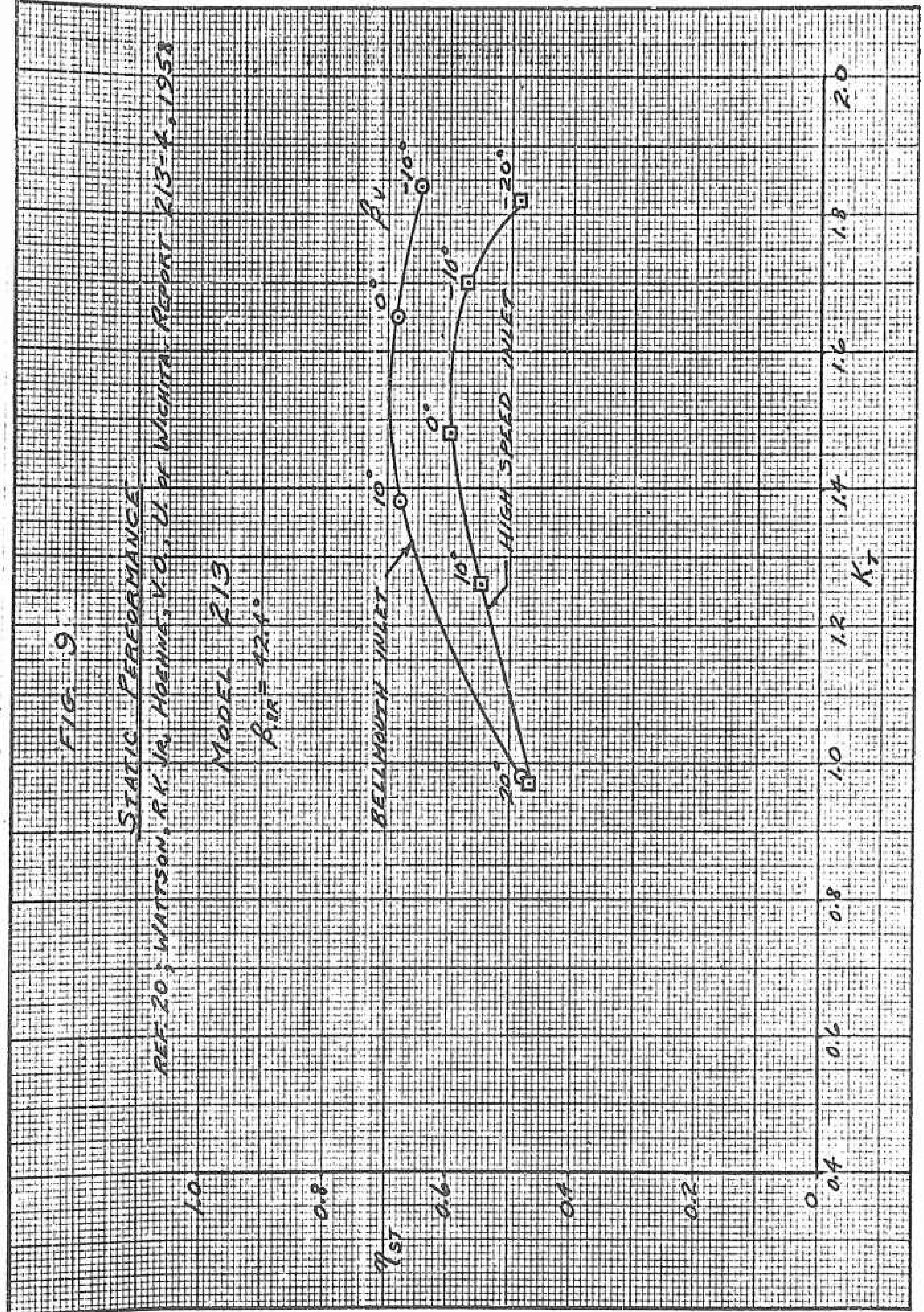
FIG. 9
STATIC PERFORMANCE
REF. 20; WATTSON, R.K. JR.; HOEHNE, V.O., U. of WICHITA, REPORT 213-2, 1958
MODEL 213
β0R = 42.1°
BELLMOUTH INLET
HIGH SPEED INLET
βV
-10°
0°
10°
20°
-20°
ηST
1.0
0.8
0.6
0.4
0.2
0
KT
0.4
0.6
0.8
1.0
1.2
1.4
1.6
1.8
2.0

PREPARED JBS 2-3-60

CHECKED

REVISED

REPUBLIC AVIATION

REPORT NO.

MODEL

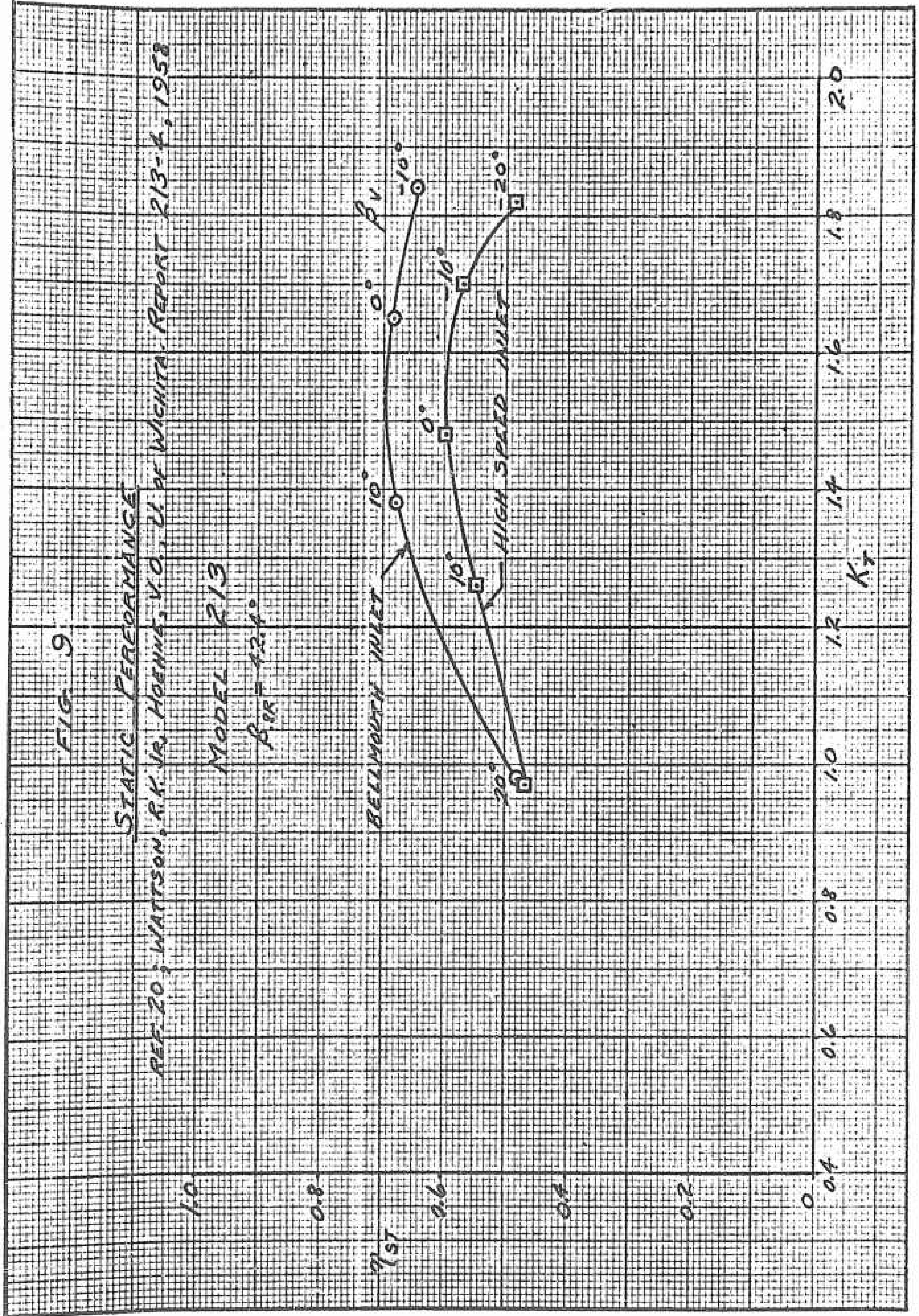

PREPARED JBS 2-1-60 PAGE 140
CHECKED REPORT NO.
REVISED MODEL

REPUBLIC AVIATION

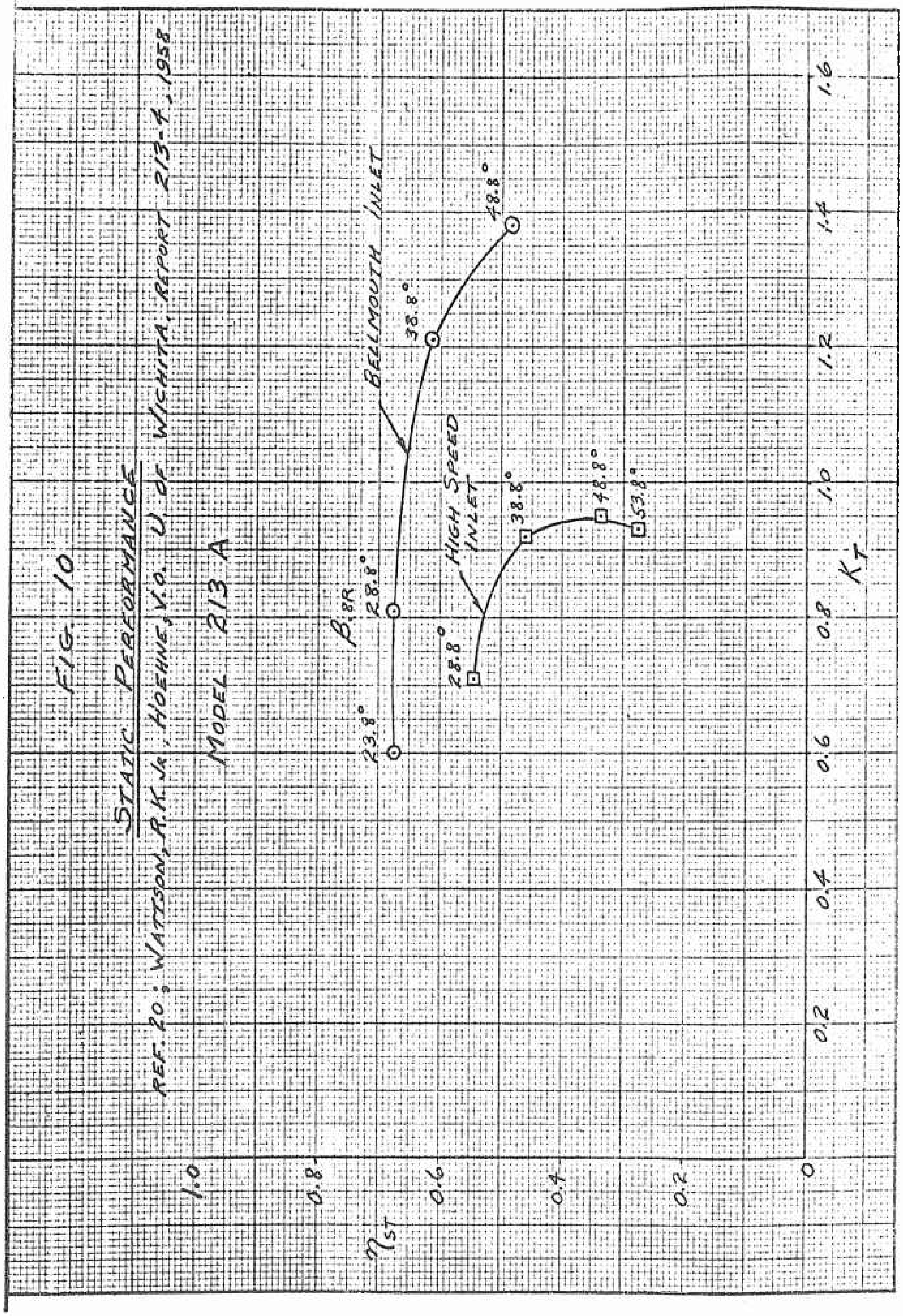

PREPARED JBS 2-3-60

CHECKED

REVISED

REPUBLIC AVIATION

REPORT NO.

MODEL

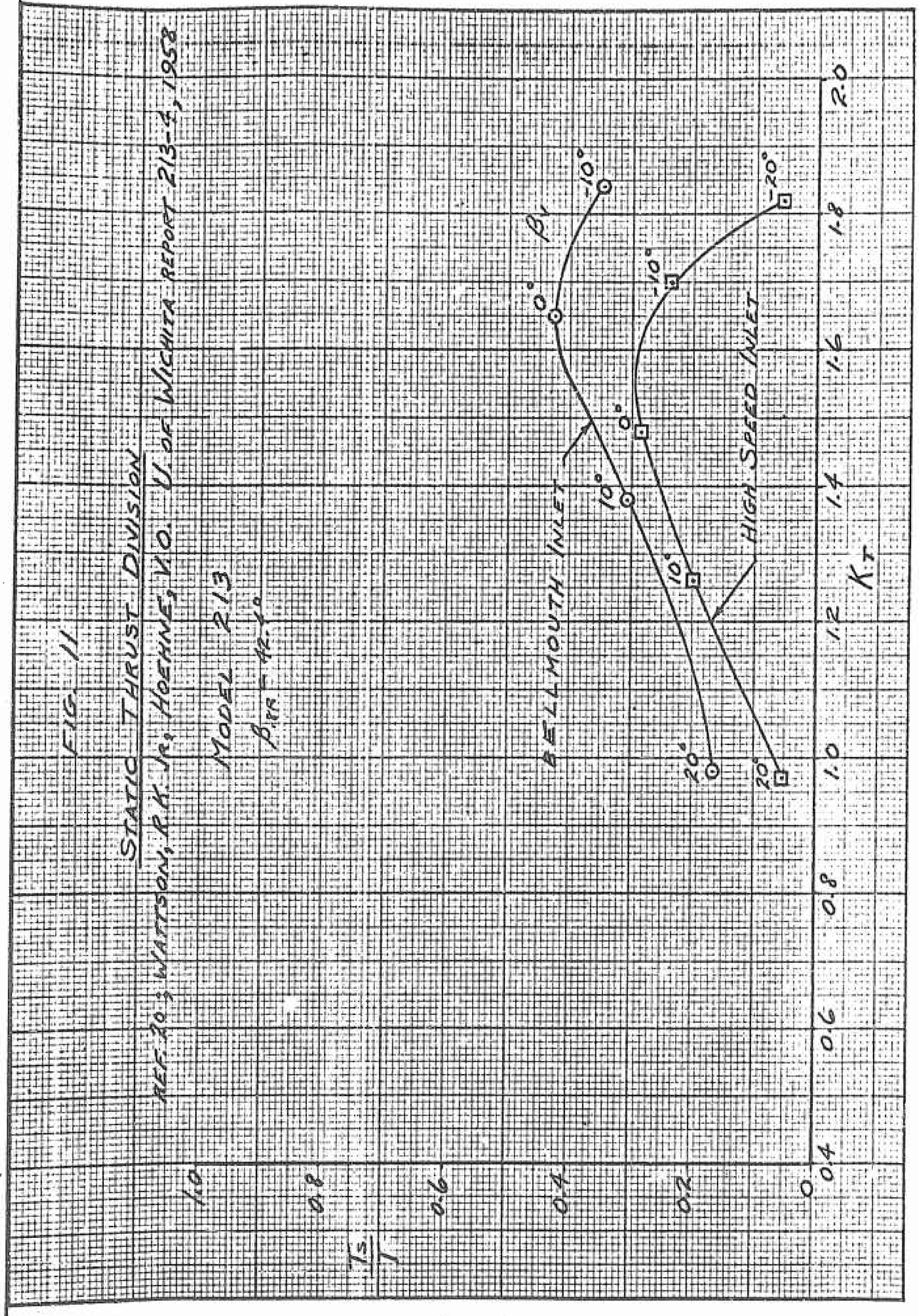

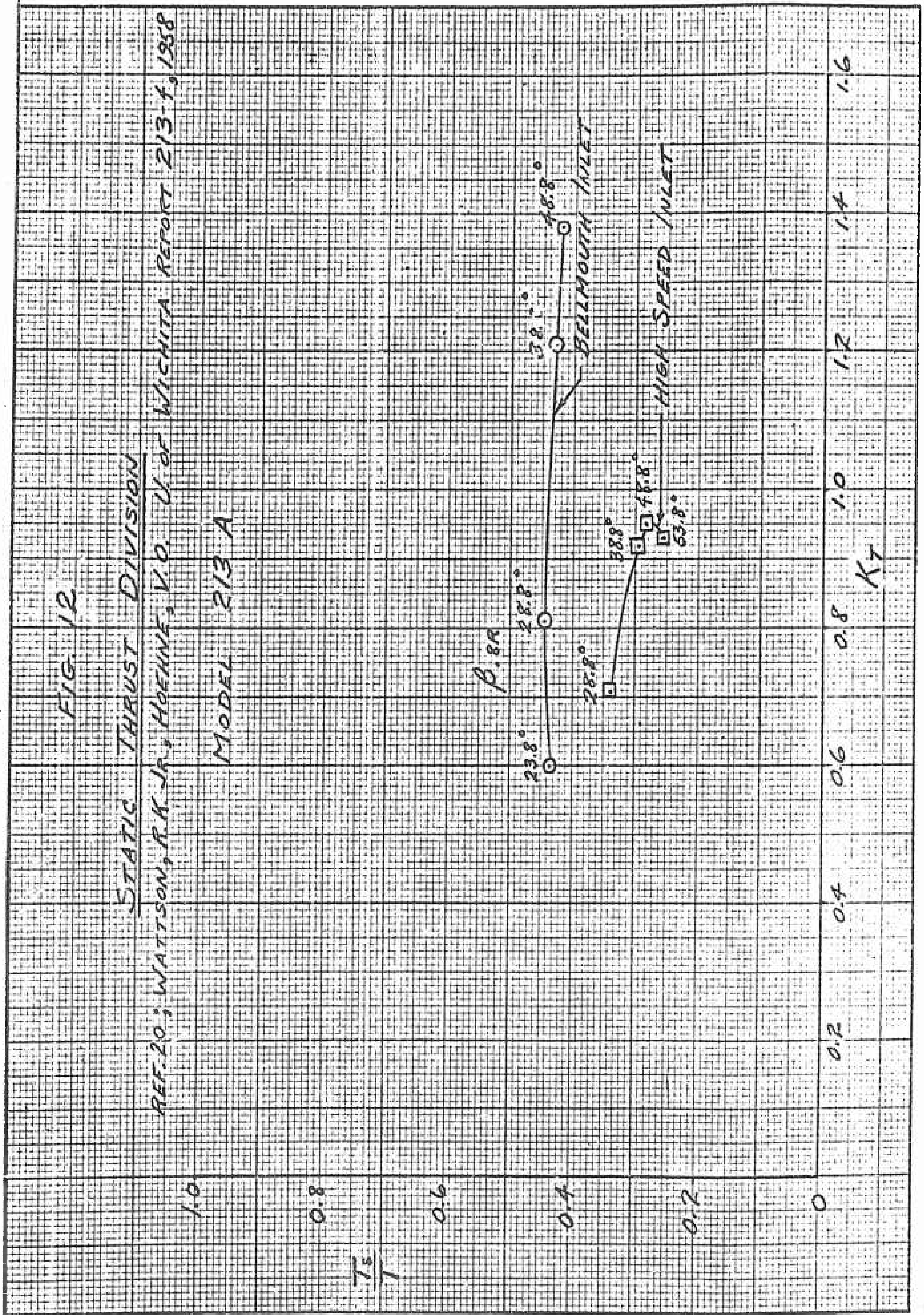
FIG. 12
STATIC THRUST DIVISION
REF. 20; WATTSON, R.K. JR., HOEHNE, V.O. U. of WICHITA REPORT 213-4, 1958
MODEL 213 A
β 8R
BELLMOUTH INLET
HIGH SPEED INLET
23.8°
28.8°
38.8°
48.8°
28.8°
38.8°
48.8°
63.8°
Ts/T
1.0
0.8
0.6
0.4
0.2
0
K_T
0.2
0.4
0.6
0.8
1.0
1.2
1.4
1.6

FIG. 13

AXIAL PERFORMANCE

REF. 18; WATTSON, R.K. JR, HOEHNE, V.O.
U. OF WICHITA REPORT 213-2, 1958

MODEL 213
WITH BELLMOUTH INLET

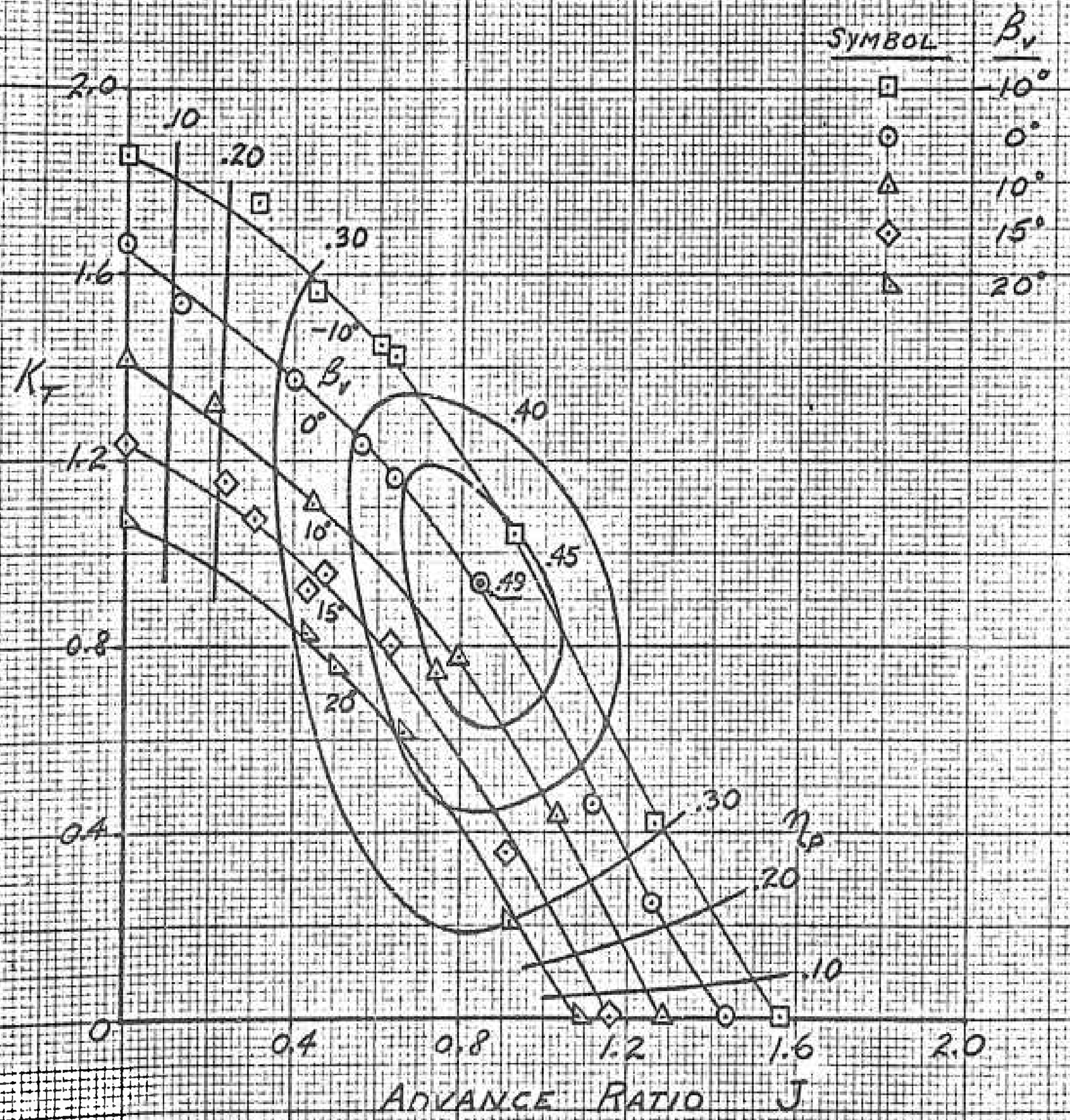

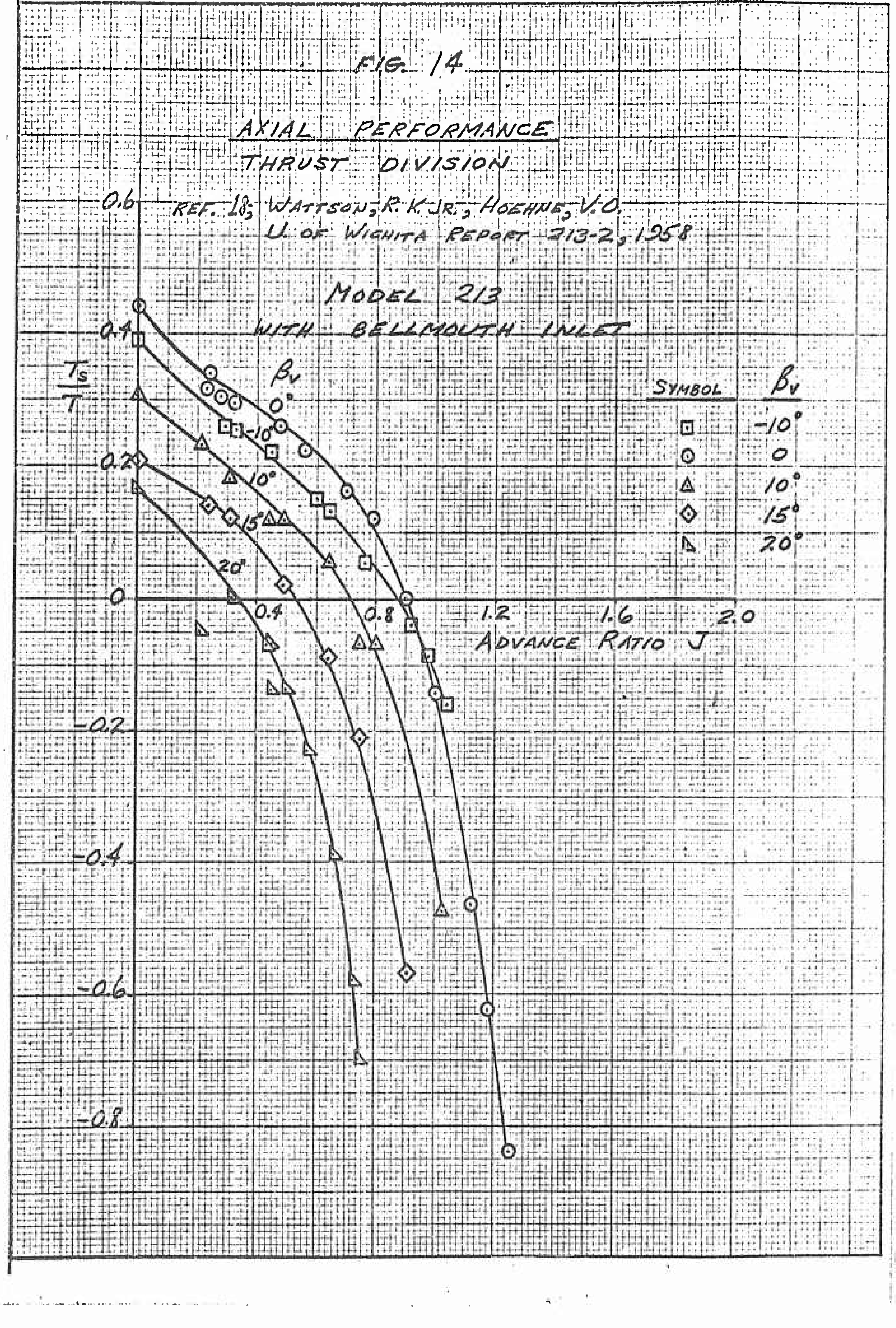
FIG. 14
AXIAL PERFORMANCE
THRUST DIVISION
REF. 18, WATTSON, R.K.JR., HOEHNE, V.O.
U. OF WICHITA REPORT 213-2, 1958
MODEL 213
WITH BELLMOUTH INLET
$\frac{T_S}{T}$
β_V
0°
-10°
10°
15°
20°
SYMBOL
β_V
-10°
0
10°
15°
20°
0.6
0.4
0.2
0
-0.2
-0.4
-0.6
-0.8
0.4
0.8
1.2
1.6
2.0
ADVANCE RATIO J

FIG. 15

AXIAL PERFORMANCE

REF. 17; WATTSON, R.K. JR., HOEHNE, V.O.
U. OF WICHITA REPORT 213-1, 1958

MODEL 213
WITH HIGH SPEED INLET

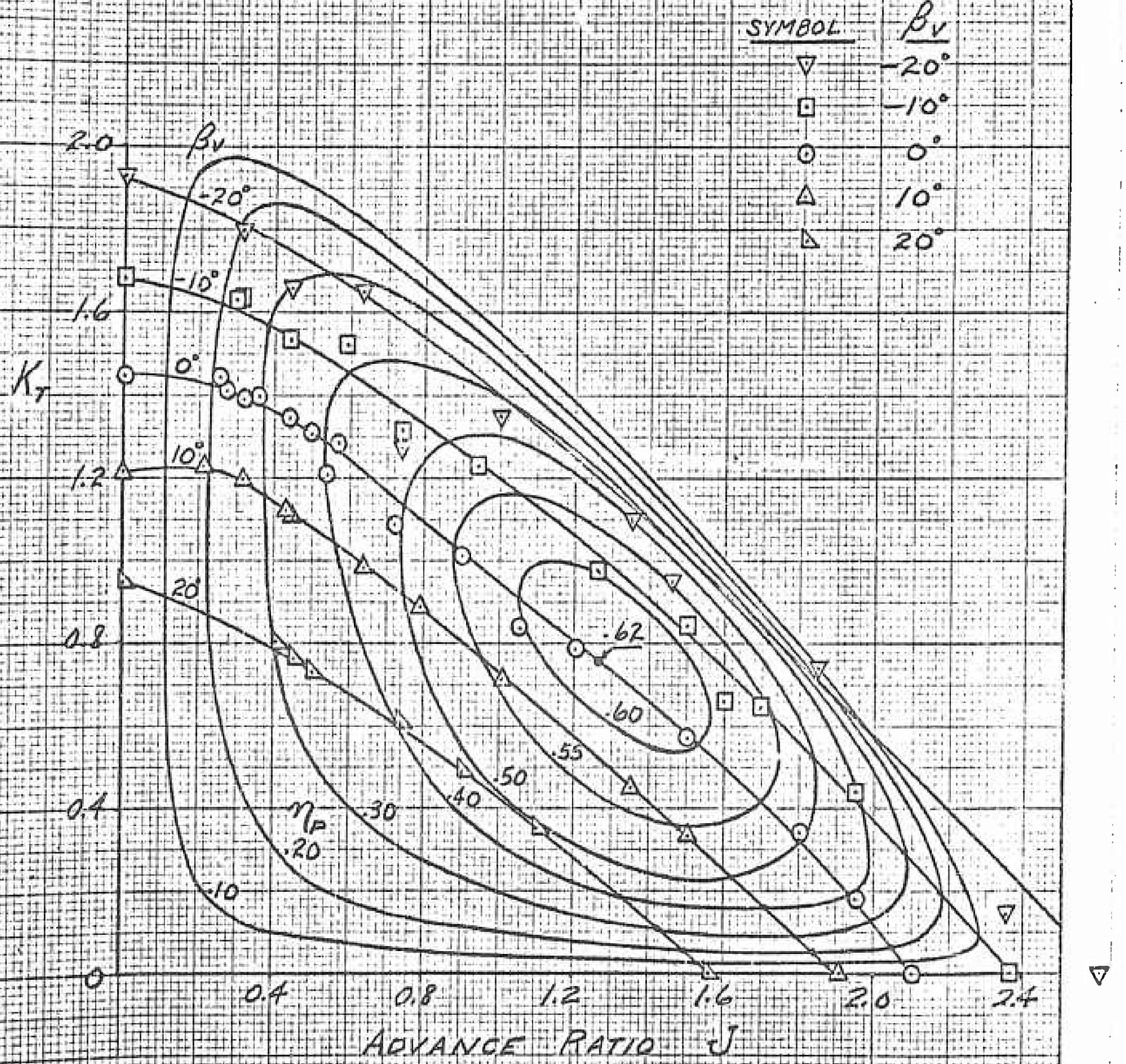

FIG. 16

AXIAL PERFORMANCE
THRUST DIVISION

REF. 17; WATTSON, R.K. JR.; HOEHNE, V.O.
U. OF WICHITA REPORT 213-1, 1958

MODEL 213
WITH HIGH SPEED INLET

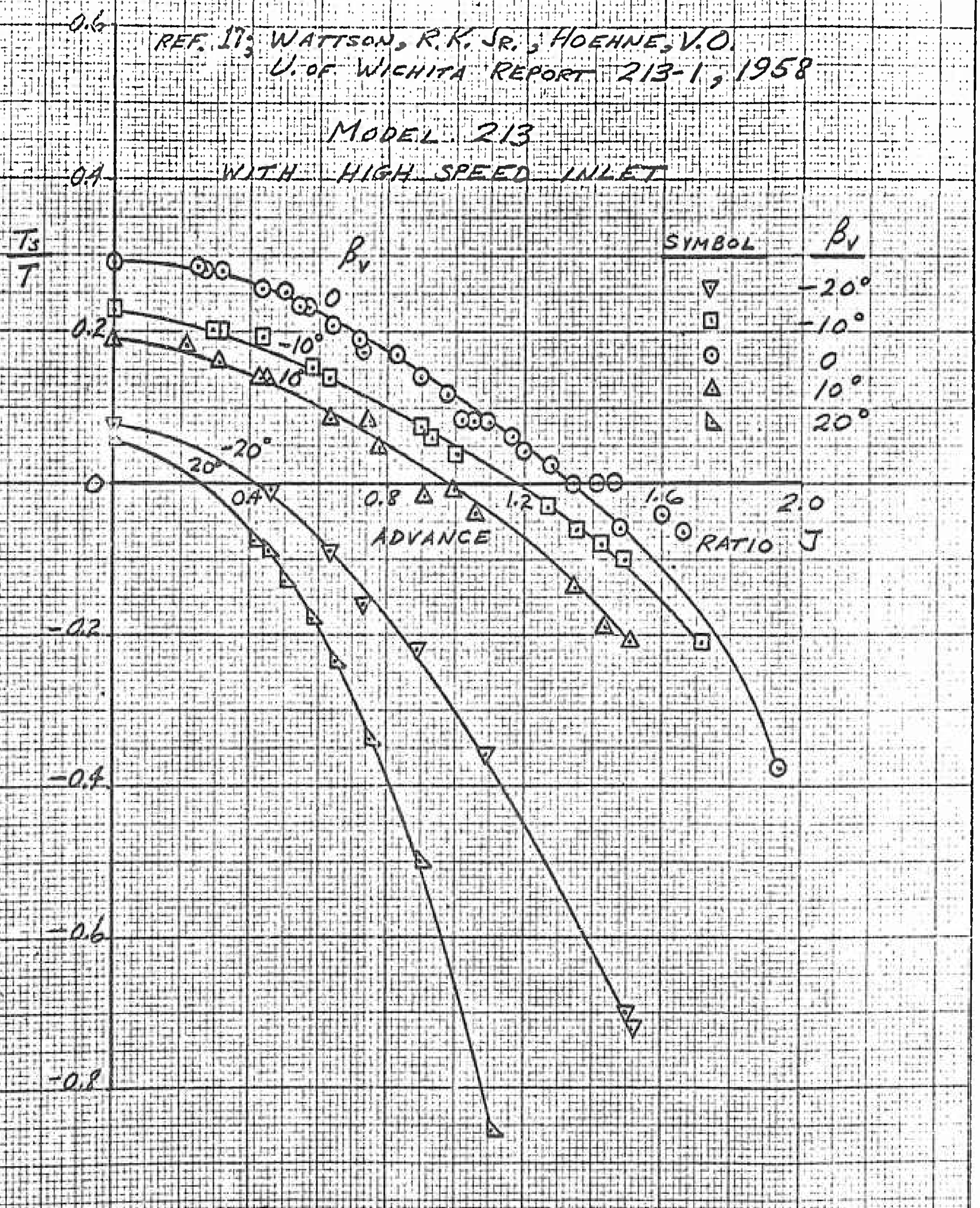

FIG 17

AXIAL PERFORMANCE

REF. 22; HOEHNE, V.O., U. OF WICHITA REP. 213-6, 1959

MODEL 213 A WITH
BELLMOUTH INLET

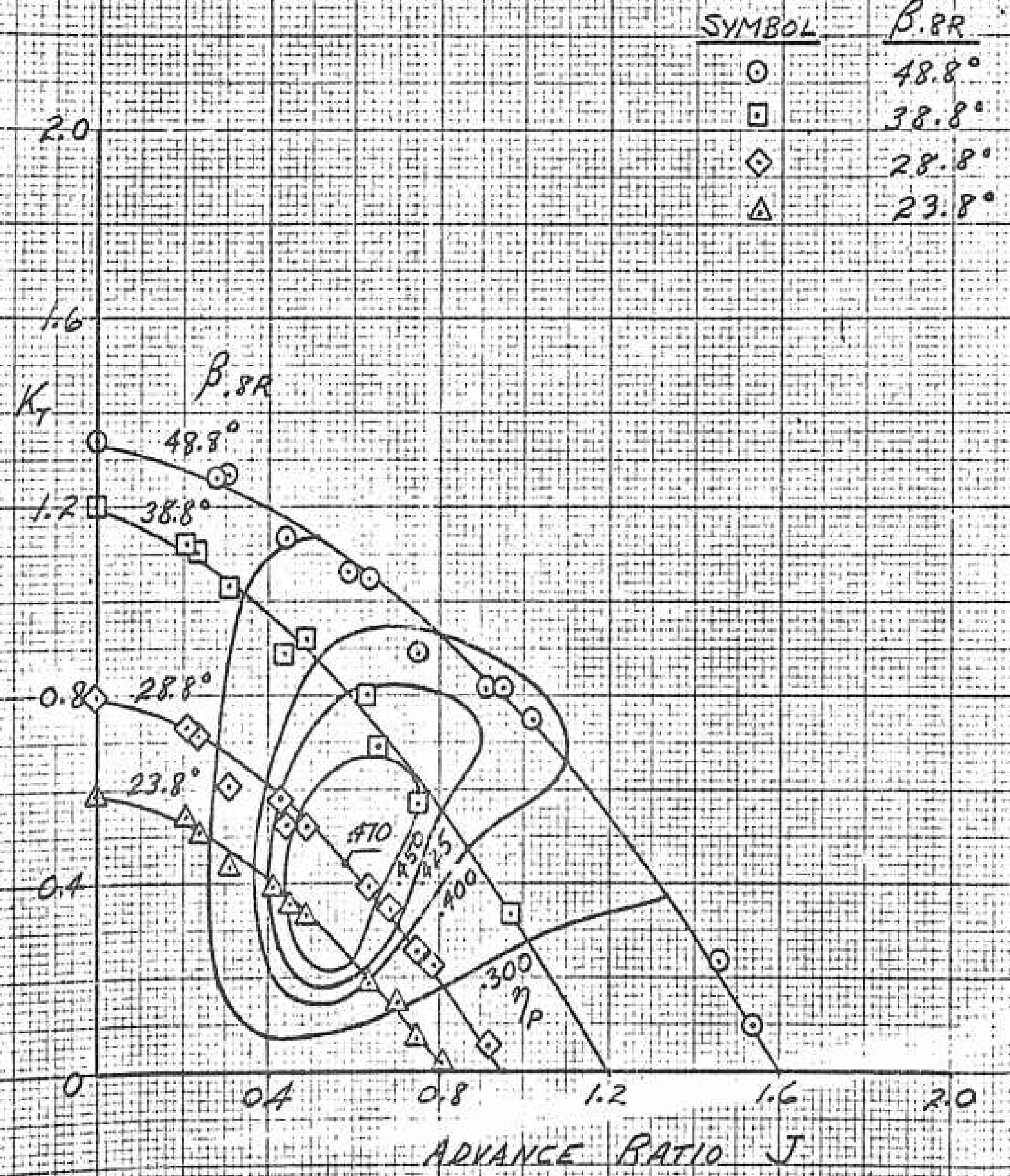

PREPARED [initials] 4-4-60 PAGE 154

CHECKED REPORT NO

REVISED MODEL

REPUBLIC AVIATION

FIG. 18

AXIAL PERFORMANCE

THRUST DIVISION

REF. 22; HOENNE, V.O., U. OF WICHITA REP. 213-6, 1959

MODEL 213 A WITH BELLMOUTH INLET

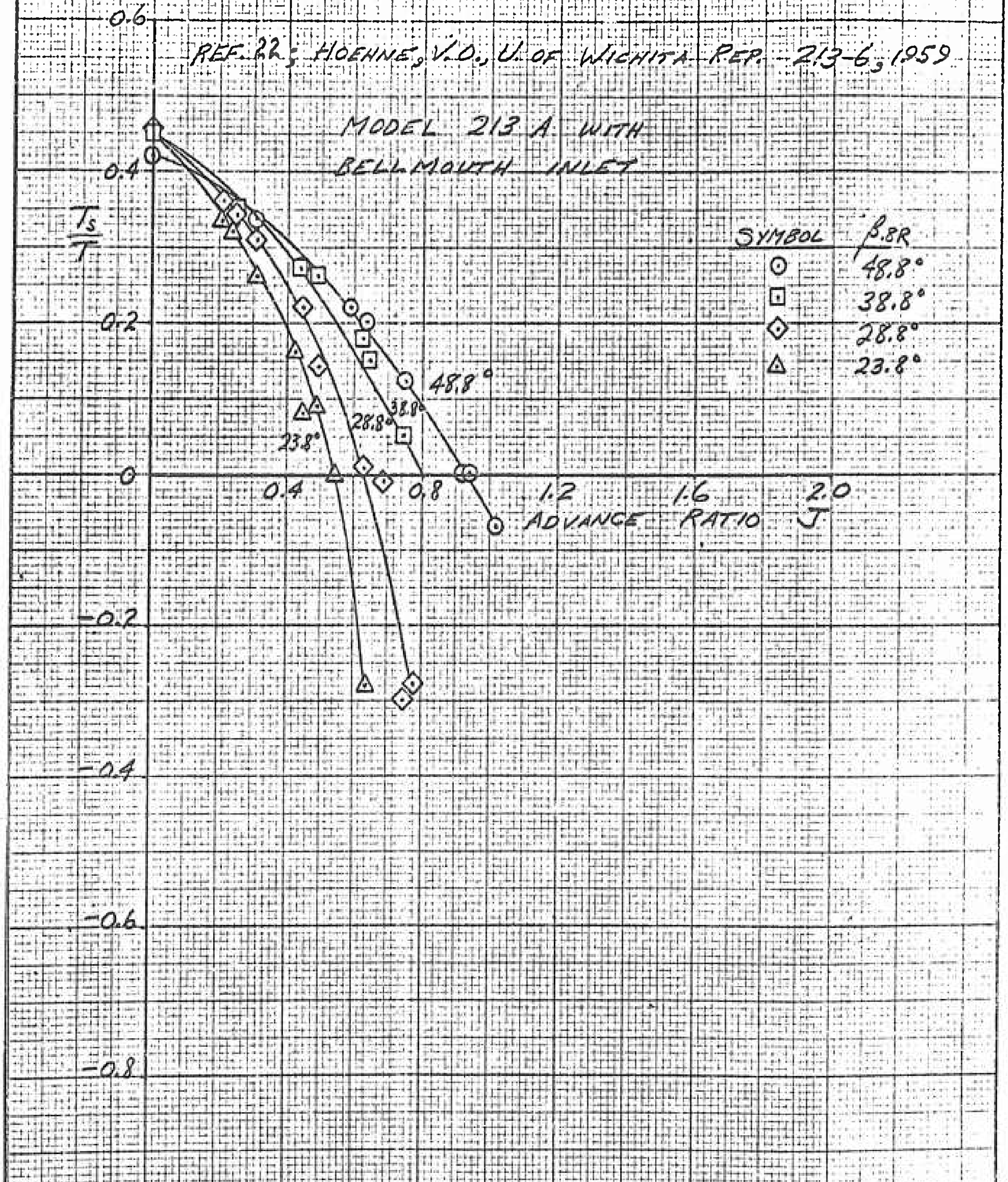

PREPARED JBL 7-31-60
CHECKED
REVISED

REPUBLIC AVIATION

REPORT NO.
MODEL

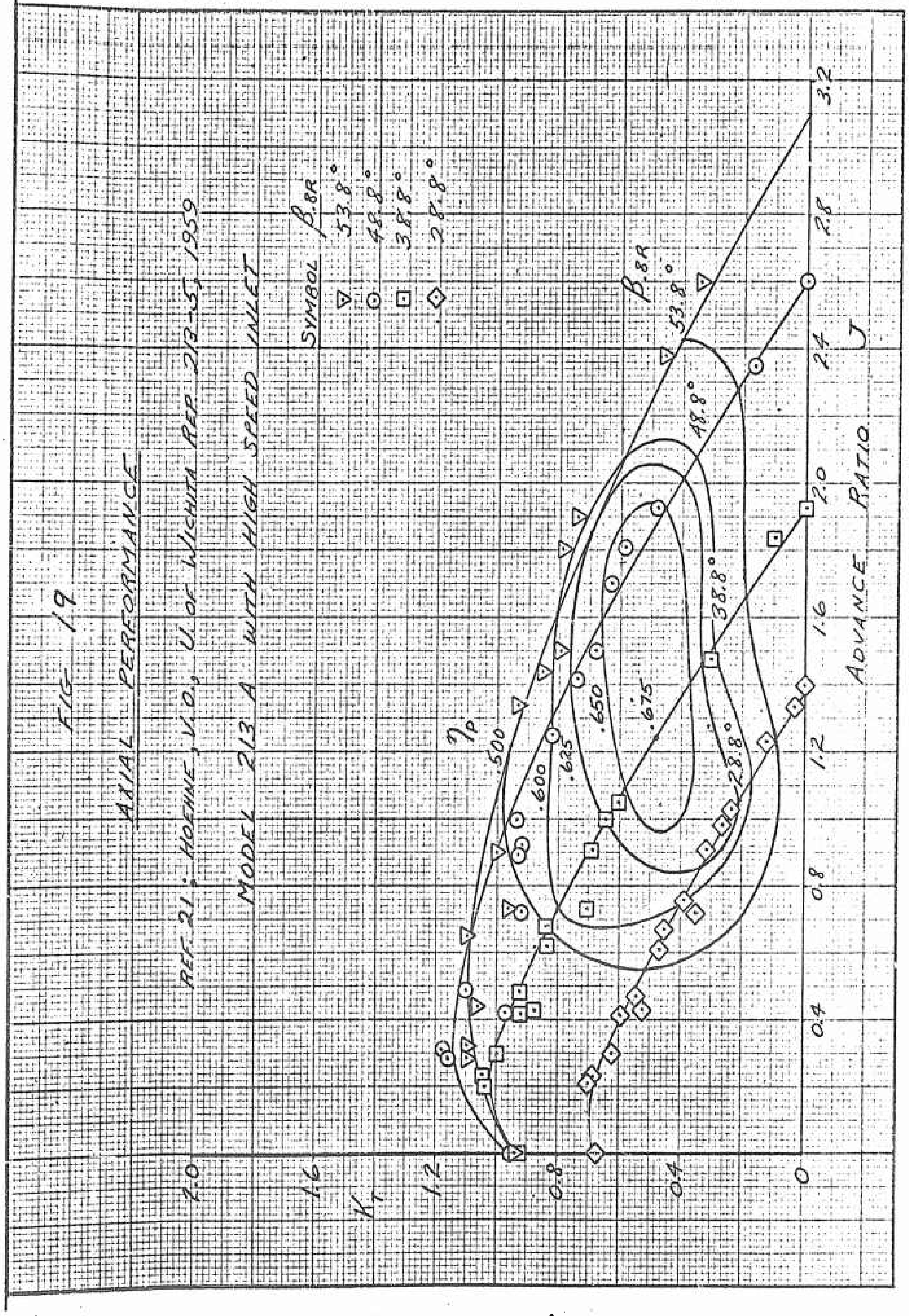

PREPARED JBL 3-31-60 PAGE 156
CHECKED REPORT NO.
REVISED MODEL

REPUBLIC AVIATION

FIG 20

AXIAL PERFORMANCE
THRUST DIVISION

REF. 21; HOEHNE, V.O., U. OF WICHITA REP. 213-5, 1959

MODEL 213 A WITH
HIGH SPEED INLET

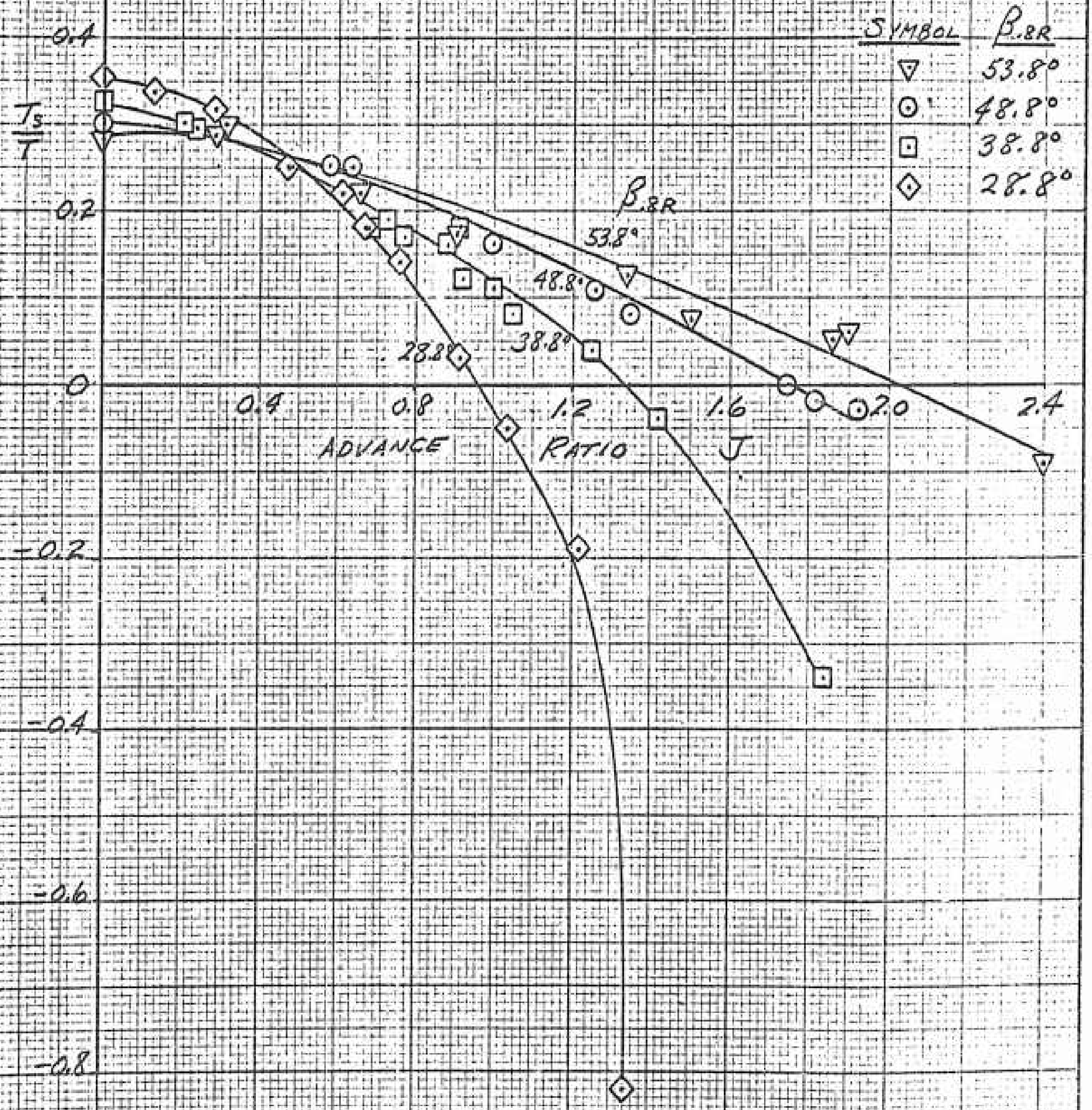

E-1-10A
REV. 2/49

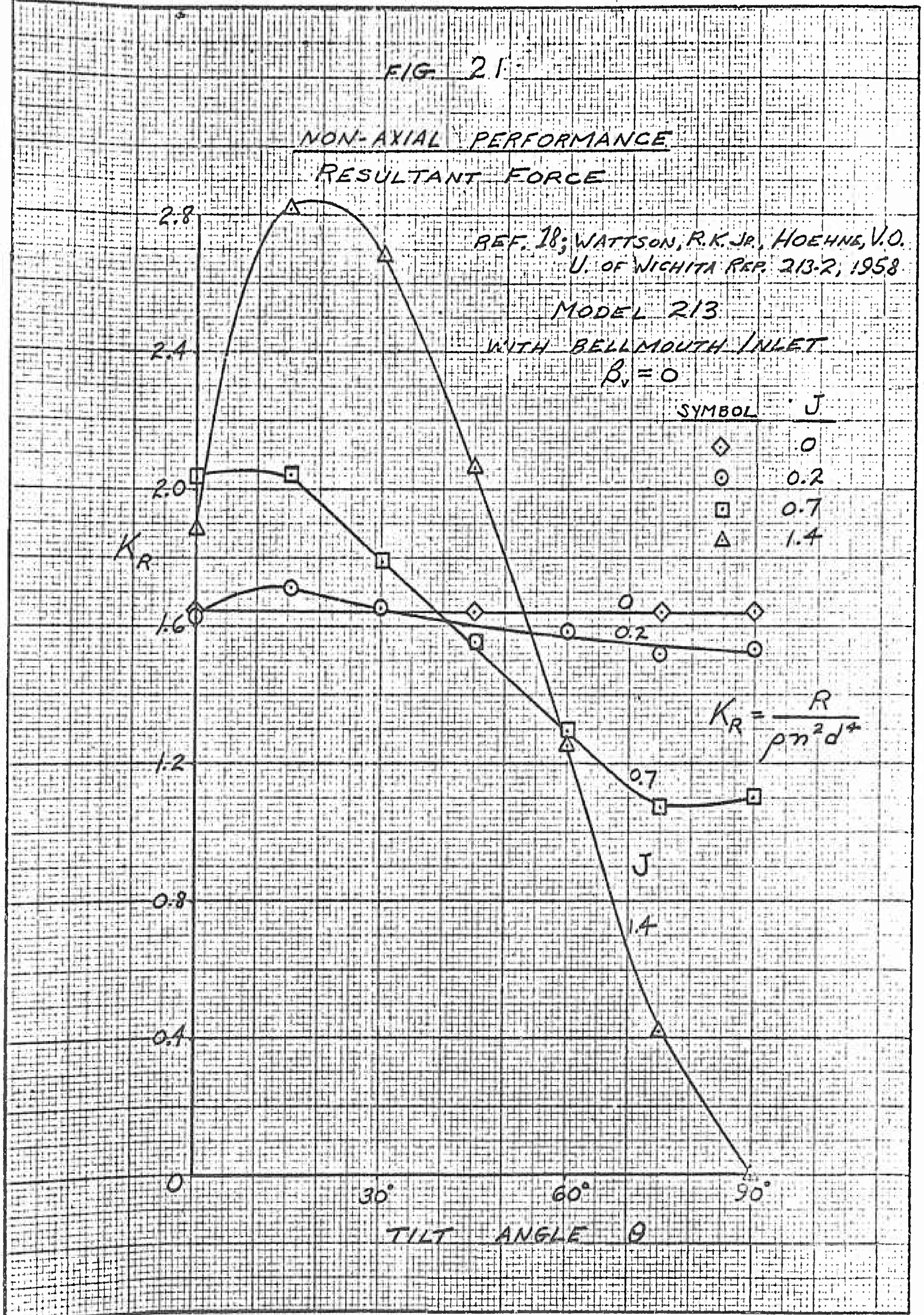
FIG. 21
NON-AXIAL PERFORMANCE
RESULTANT FORCE
REF. 18; WATTSON, R.K. JR., HOEHNE, V.O.
U. OF WICHITA REP. 213-2, 1958
MODEL 213
WITH BELLMOUTH INLET
$\beta_v = 0$
SYMBOL J
◇ 0
⊙ 0.2
□ 0.7
△ 1.4
$K_R = \frac{R}{\rho n^2 d^4}$
K_R
2.8
2.4
2.0
1.6
1.2
0.8
0.4
0
30°
60°
90°
0
0.2
0.7
J
1.4
TILT ANGLE θ

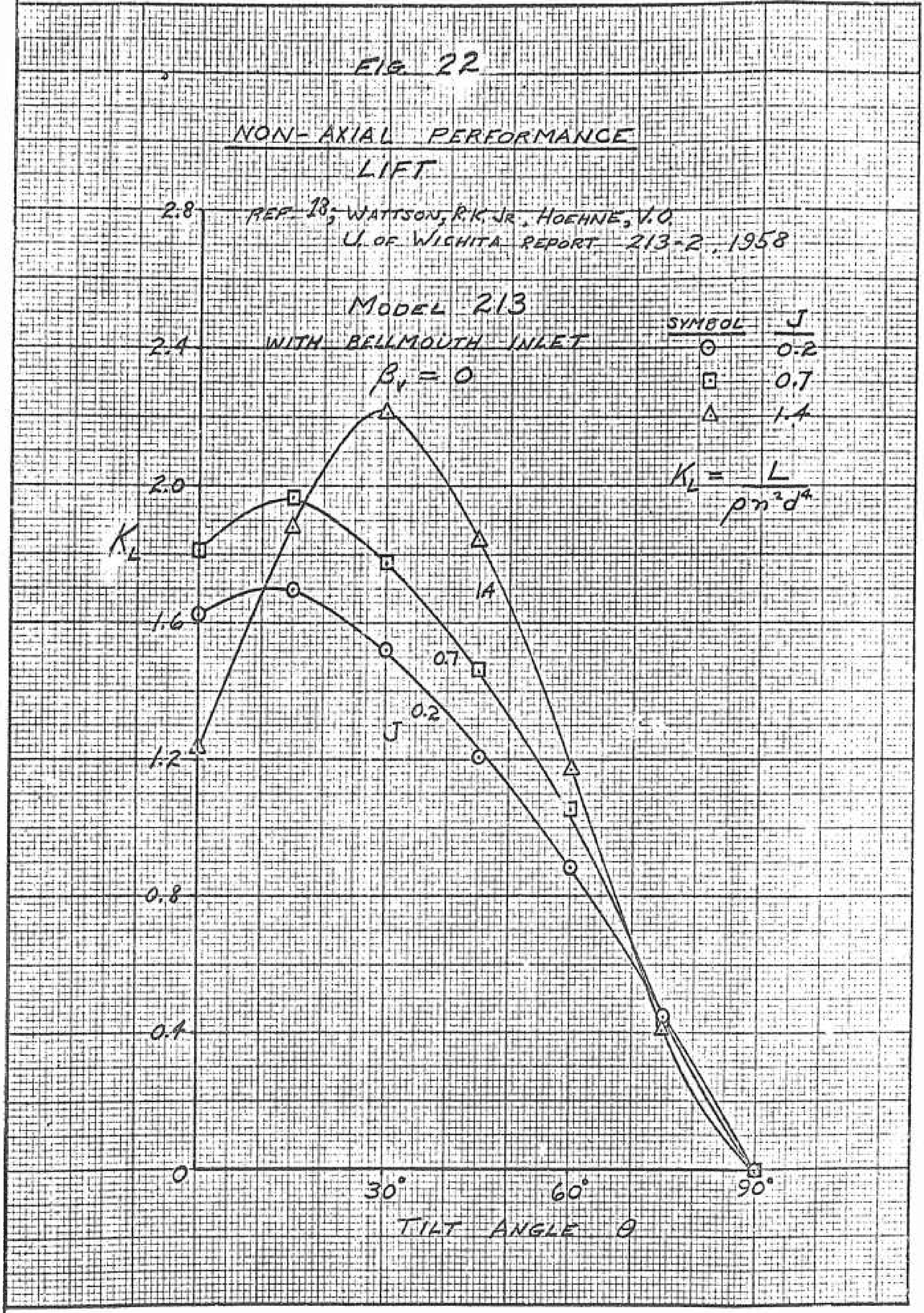
FIG. 22
NON-AXIAL PERFORMANCE
LIFT
REF. 13; WATTSON, R.K. JR., HOEHNE, V.O.
U. OF WICHITA REPORT 213-2, 1958
MODEL 213
WITH BELLMOUTH INLET
$\beta_v = 0$
SYMBOL J
0.2
0.7
1.4
$K_L = \frac{L}{\rho n^2 d^4}$
K_L
2.8
2.4
2.0
1.6
1.2
0.8
0.4
0
1.4
0.7
0.2
J
30°
60°
90°
TILT ANGLE θ

FIG. 23

NON-AXIAL PERFORMANCE

DRAG

REF. 18; WATTSON, R.K. JR., HOEHNE, V.O.
U. OF WICHITA REPORT 213-2, 1958

MODEL 213
WITH BELLMOUTH INLET

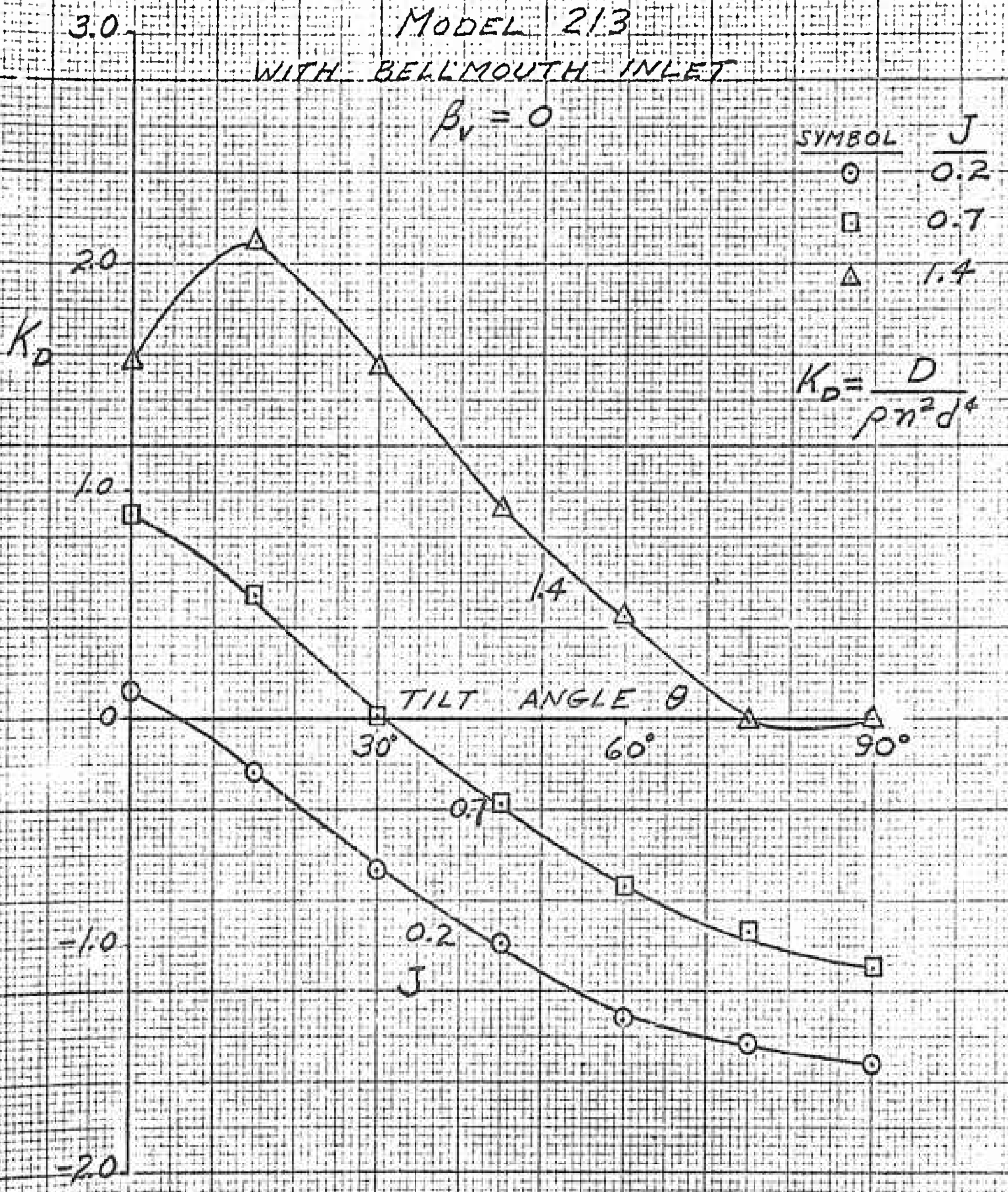

FIG 24

NON-AXIAL PERFORMANCE

POWER

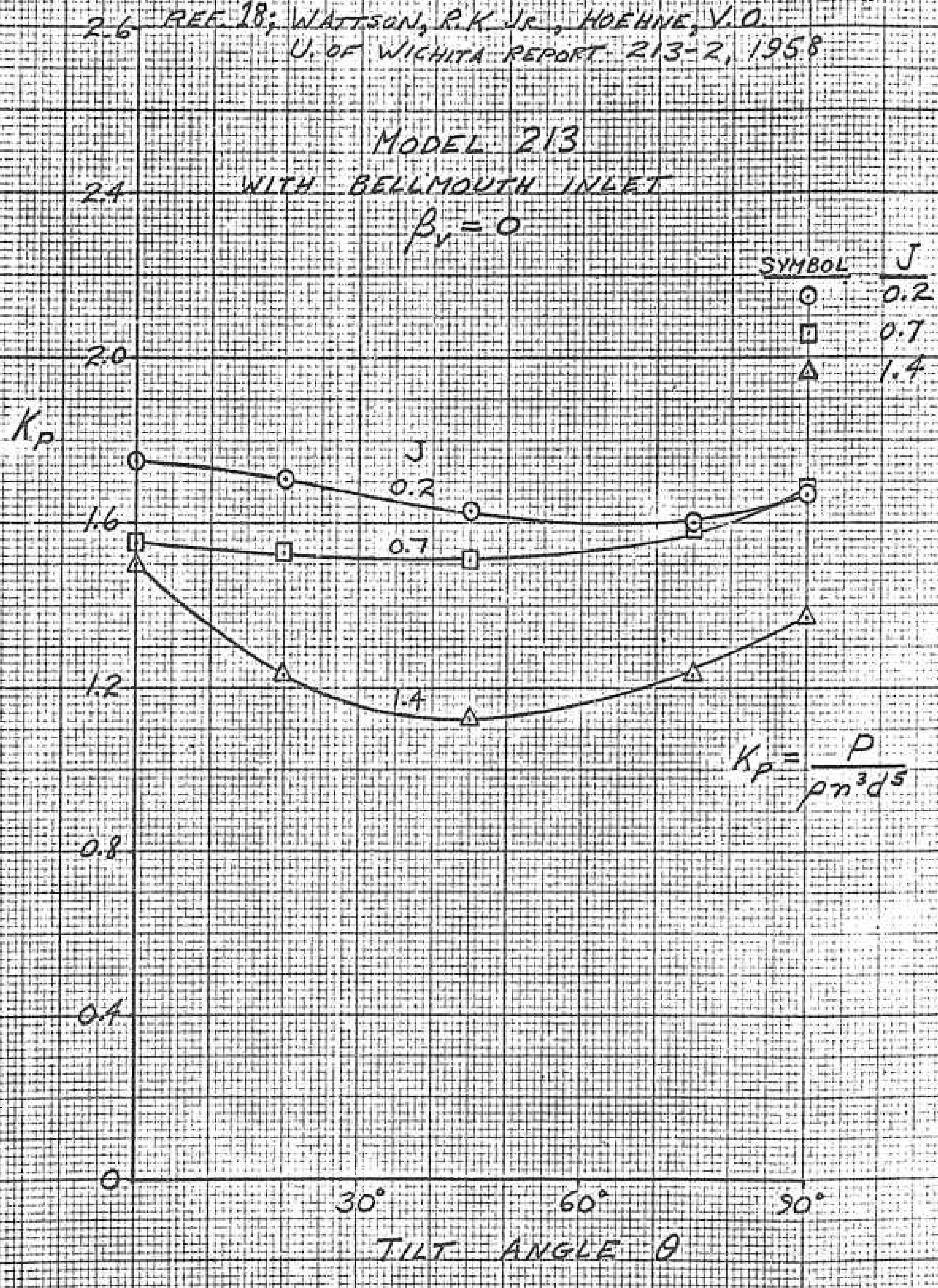

FIG 25

NON-AXIAL PERFORMANCE
SHROUD LIFT

REF. 18: WATTSON, R.K. JR., HOEHNE, V.O.
U. OF WICHITA REPORT 213-2, 1958

MODEL 213
WITH BELLMOUTH INLET
$\beta_v = 0$

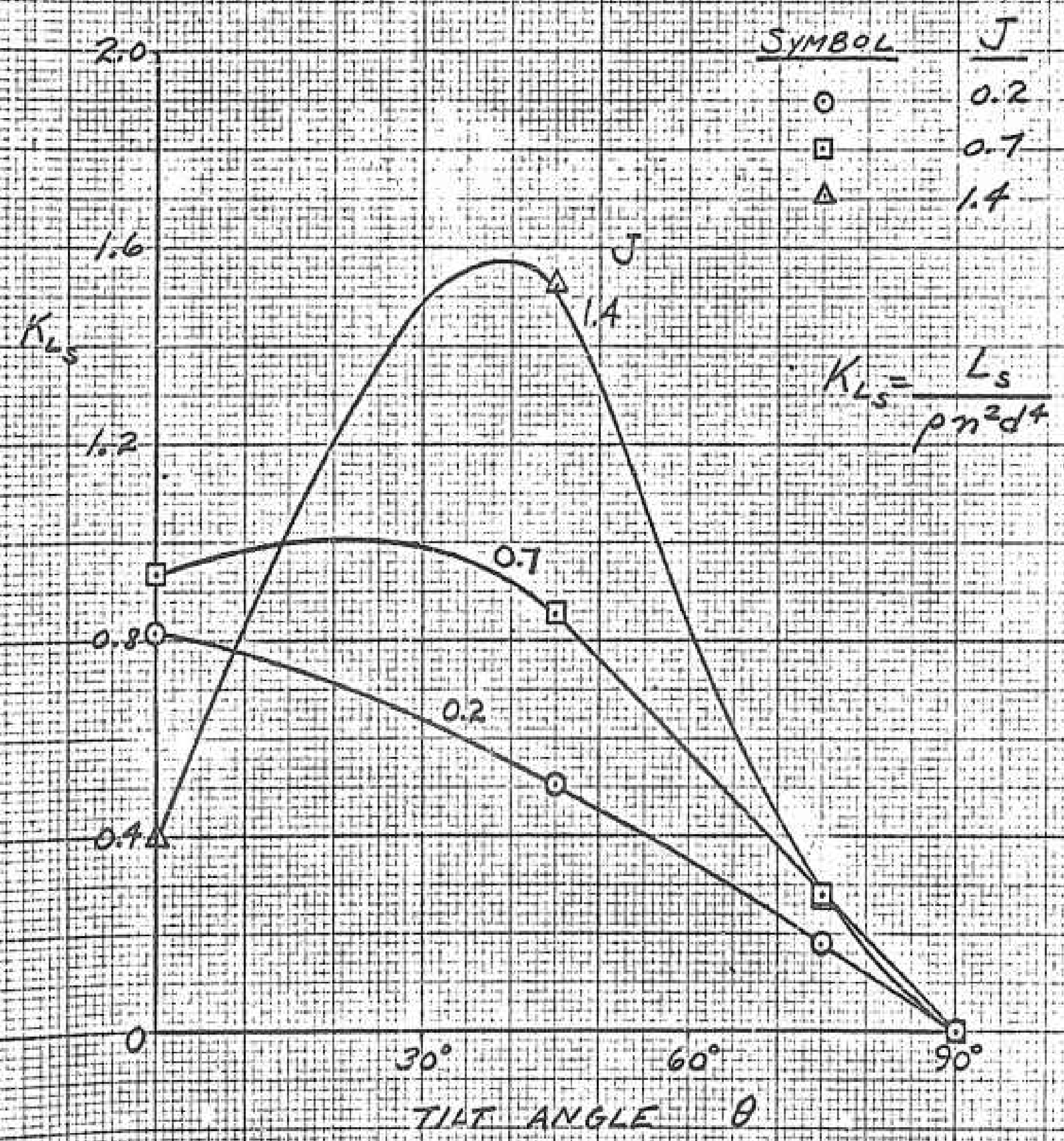

FIG. 26

NON-AXIAL PERFORMANCE

SHROUD DRAG

REF. 18; WATTSON, R.K. JR., HOEHNE, V.O.
U OF WICHITA REPORT 213-2, 1958

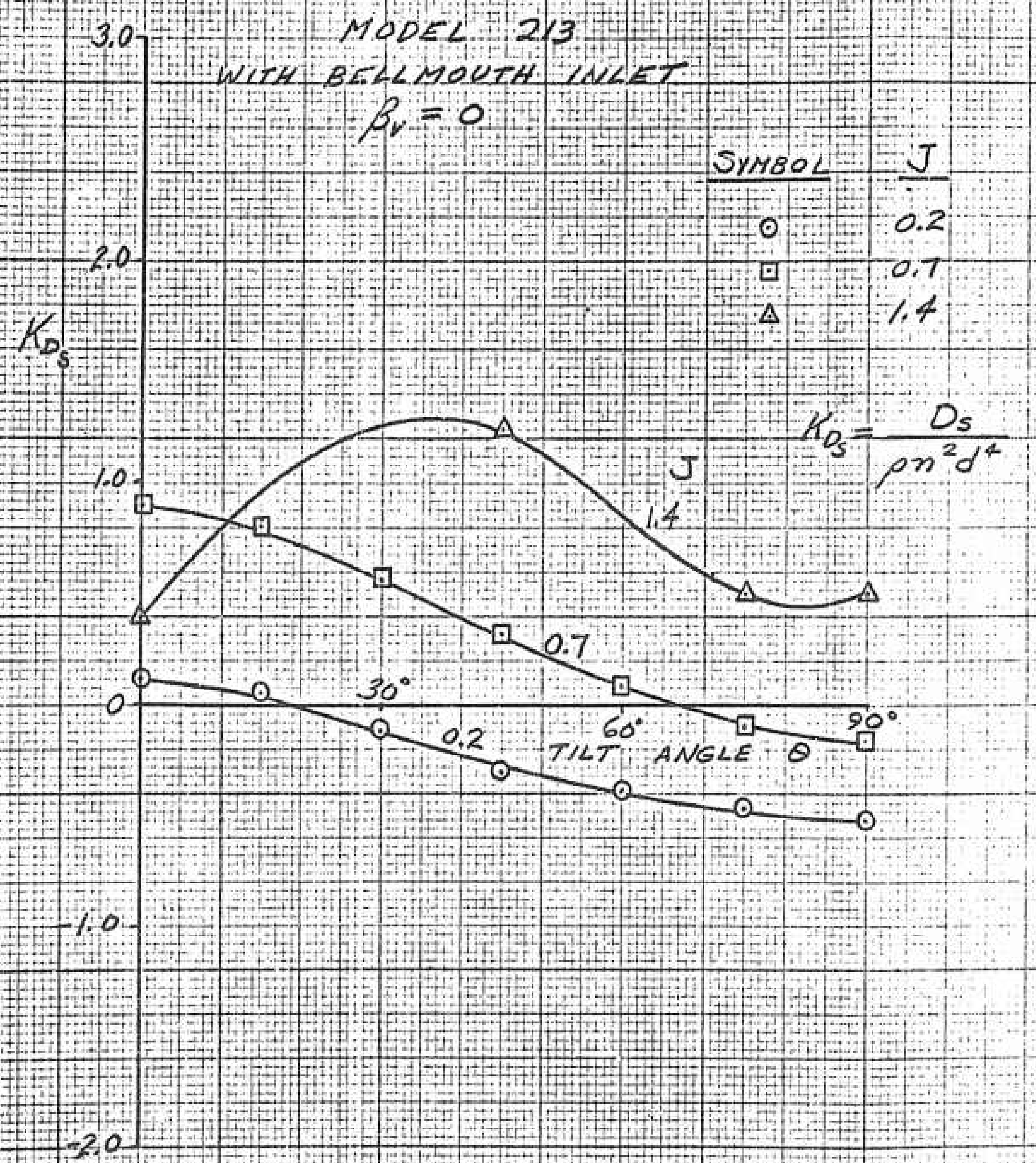

FIG. 27

NON-AXIAL PERFORMANCE
LIFT DIVISION

REF. 18; WATTSON, R.K. JR., HOEHNE, V.O.
U. OF WICHITA REPORT 213-2, 1958

MODEL 213
WITH BELLMOUTH INLET
$\beta_V = 0$

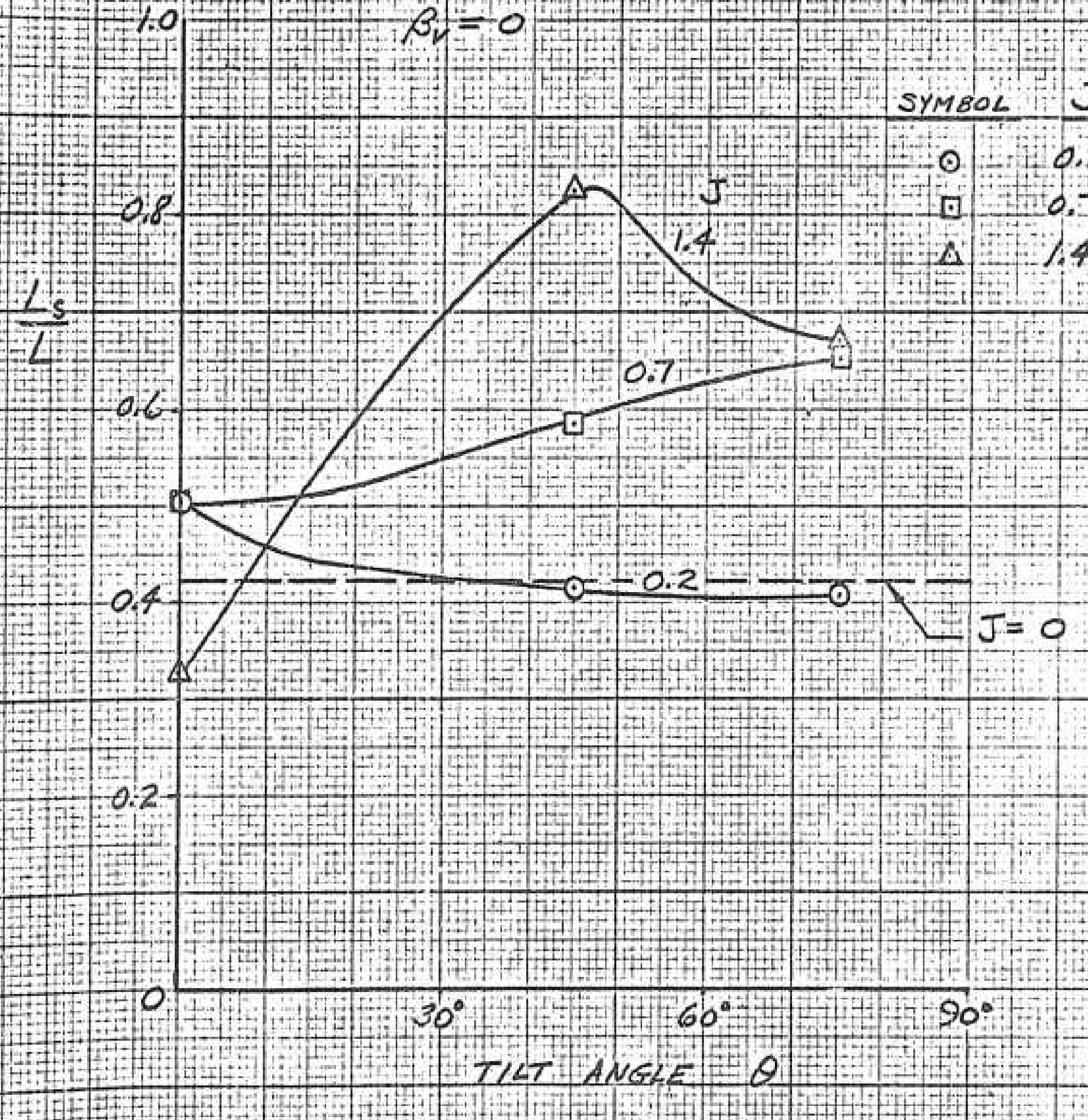

FIG. 28

NON-AXIAL PERFORMANCE
MOMENTS

REF. 18; WATTSON, R.K. JR.; HOEHNE, V.O.
U. OF WICHITA REPORT 213-2, 1958

MODEL 213 WITH BELLMOUTH INLET

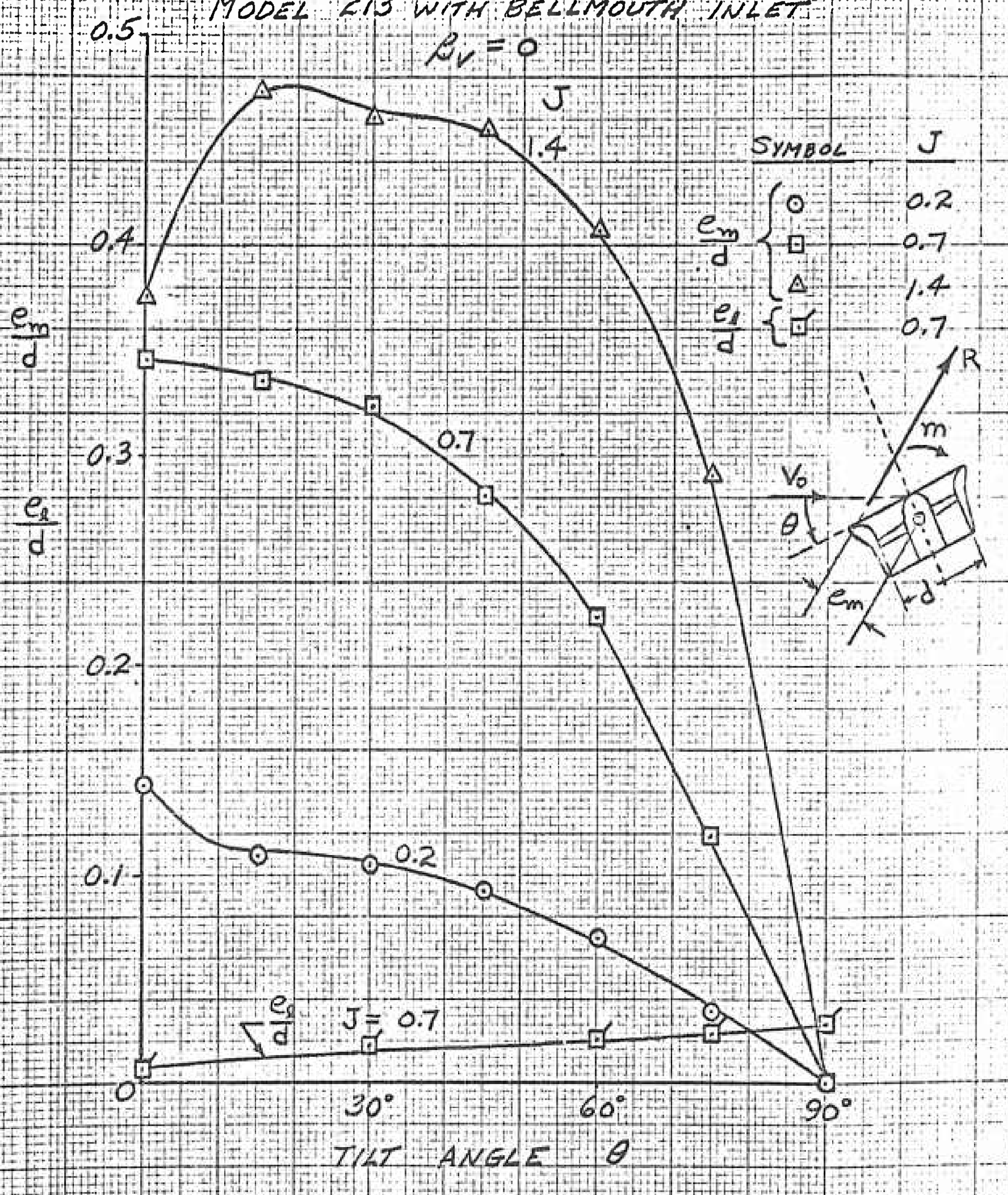

PREPARED gsl 3-24-60
CHECKED
REVISED

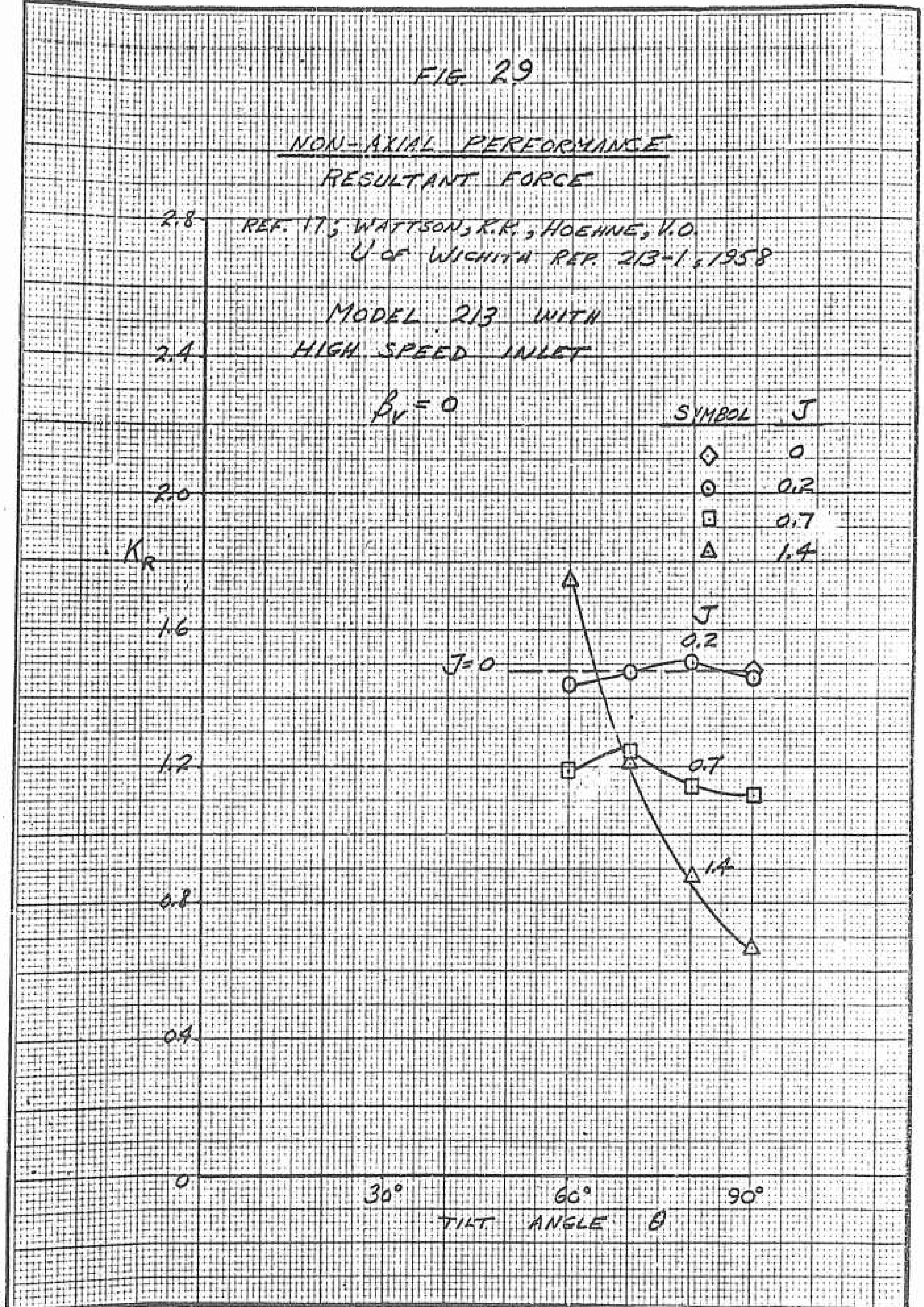

FIG. 30

NON-AXIAL PERFORMANCE
LIFT

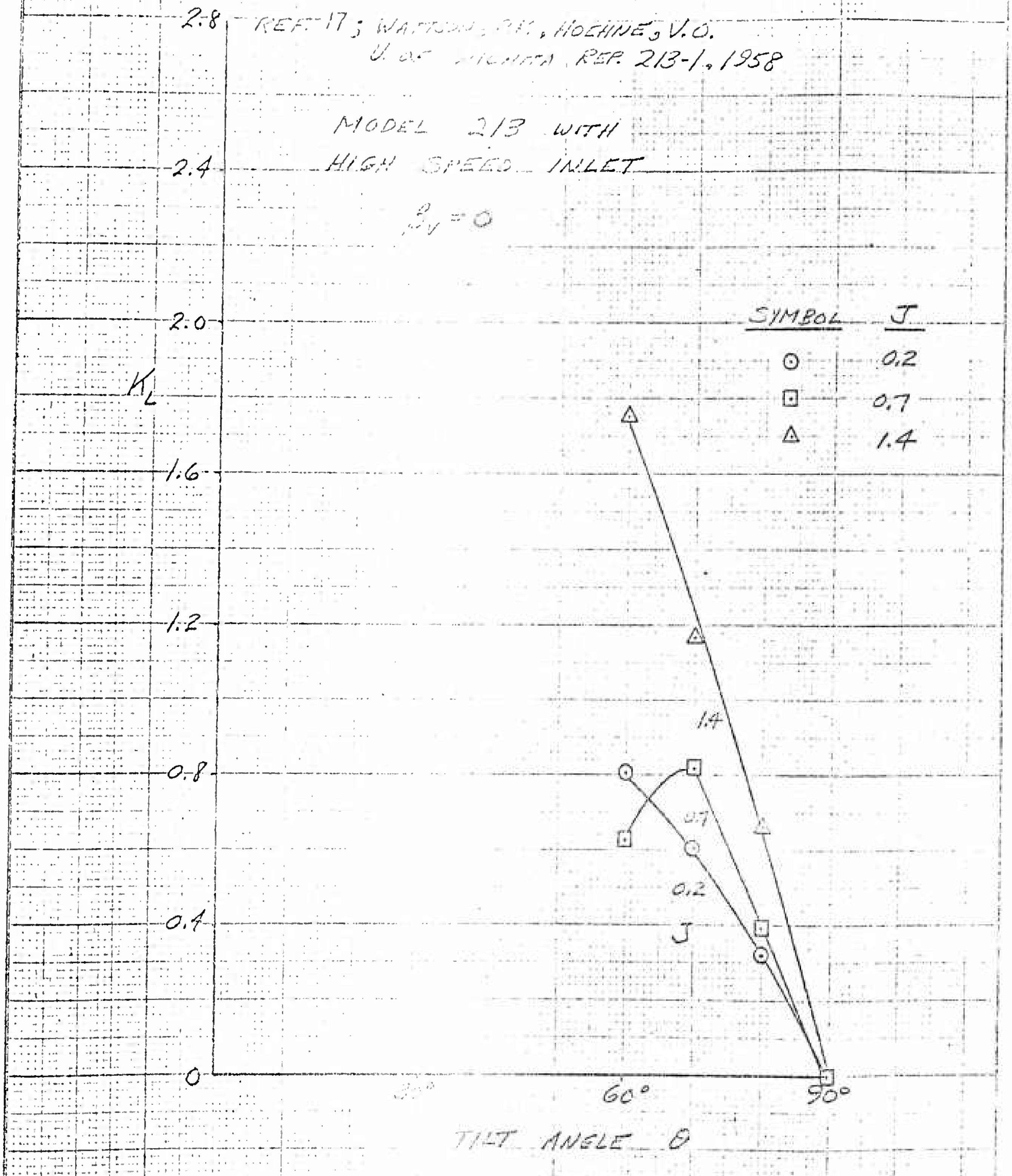

E-1-10A
REV. 8/49

FIG. 31

NON-AXIAL PERFORMANCE

DRAG

REF. 17; WATTSON, R.K., HOEHNE, V.O.,
U. OF WICHITA REP. 213-1, 1958

MODEL 213 WITH
HIGH SPEED INLET
$\beta_V = 0$

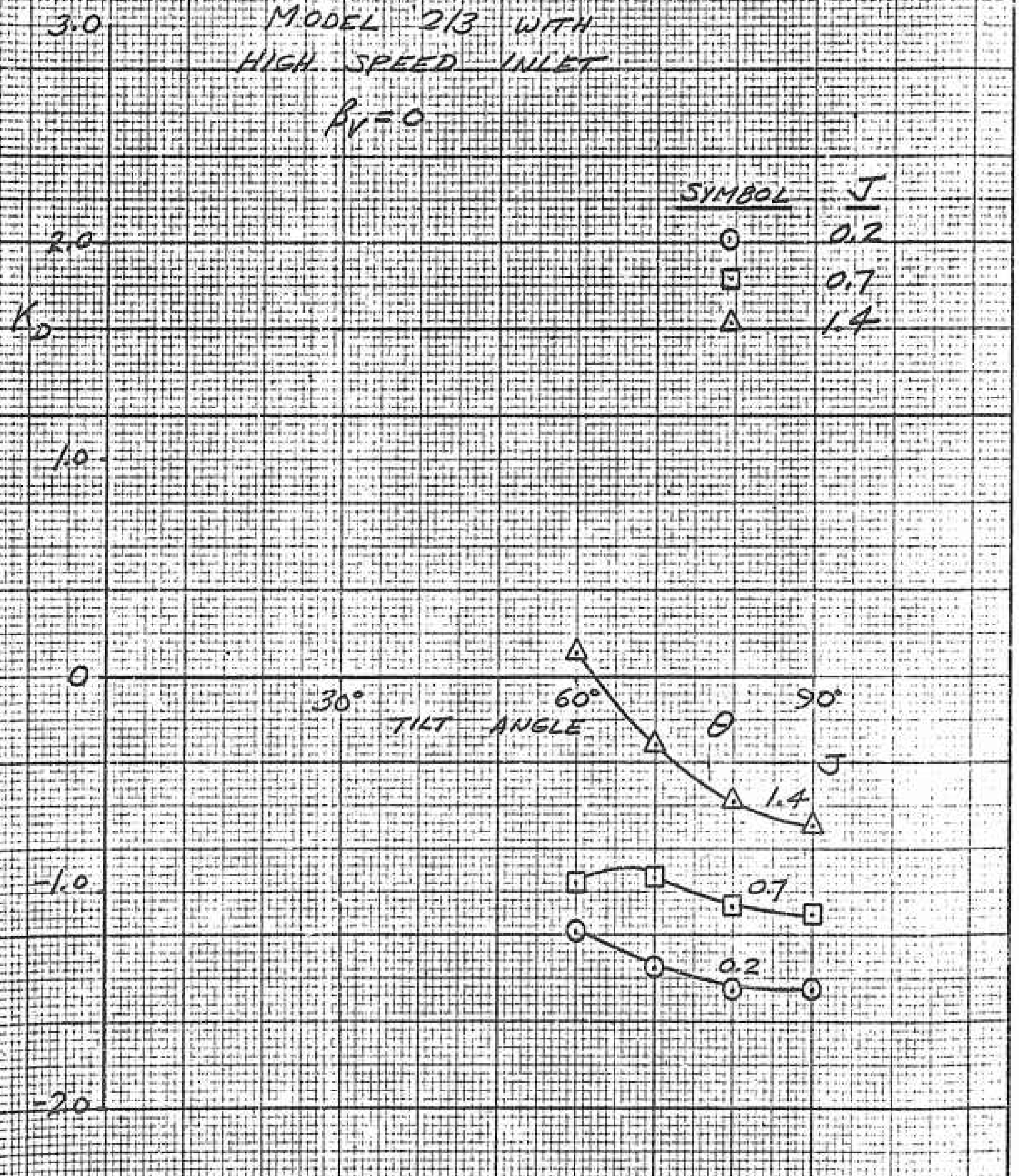

FIG. 32

NON-AXIAL PERFORMANCE

POWER

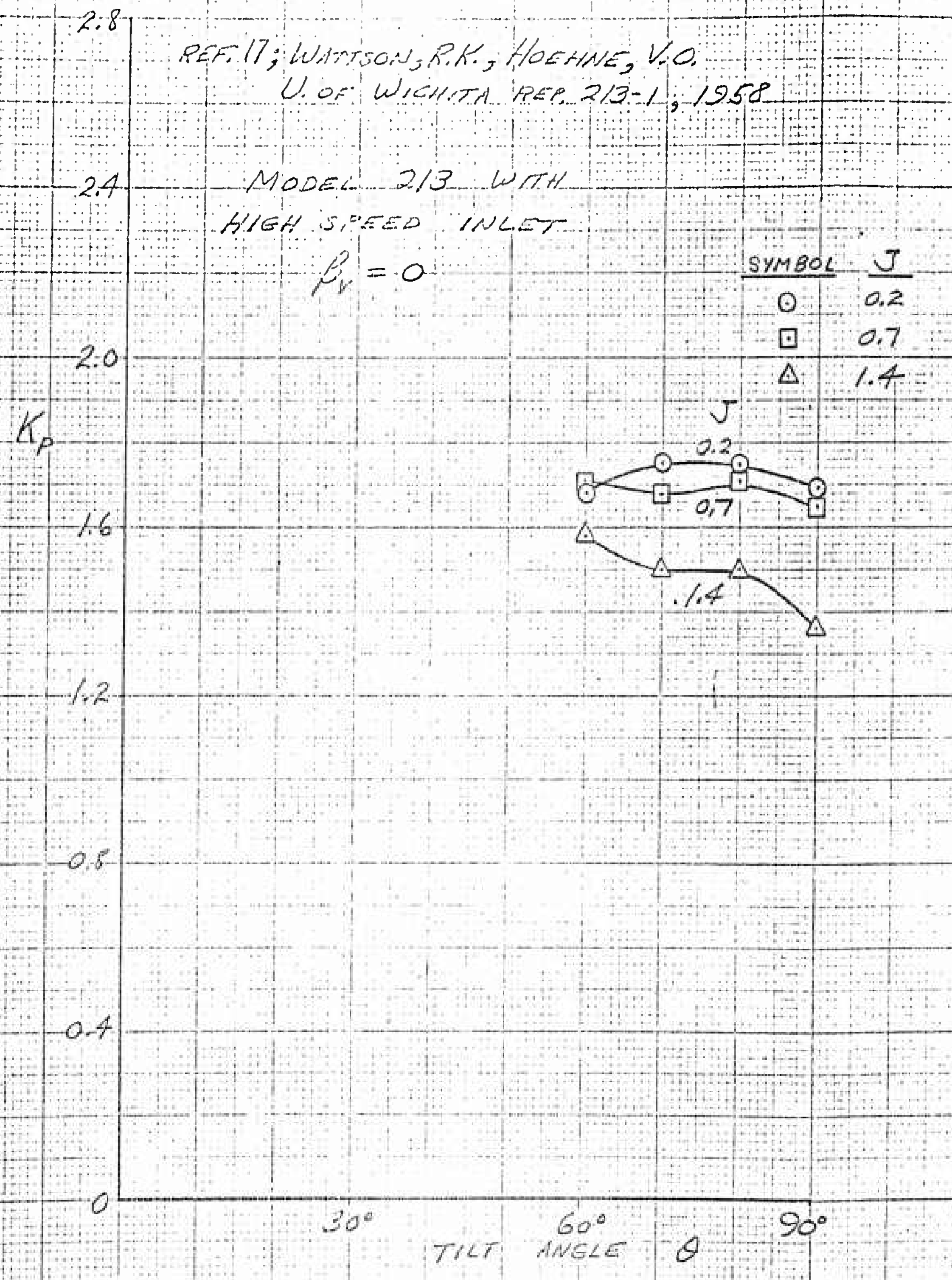

FIG. 33

NON-AXIAL PERFORMANCE
LIFT DIVISION

REF. 17; WATTSON, R.K., HOEHNE, V.O.
U. OF WICHITA REP. 213-1, 1958

MODEL 213
WITH HIGH SPEED INLET

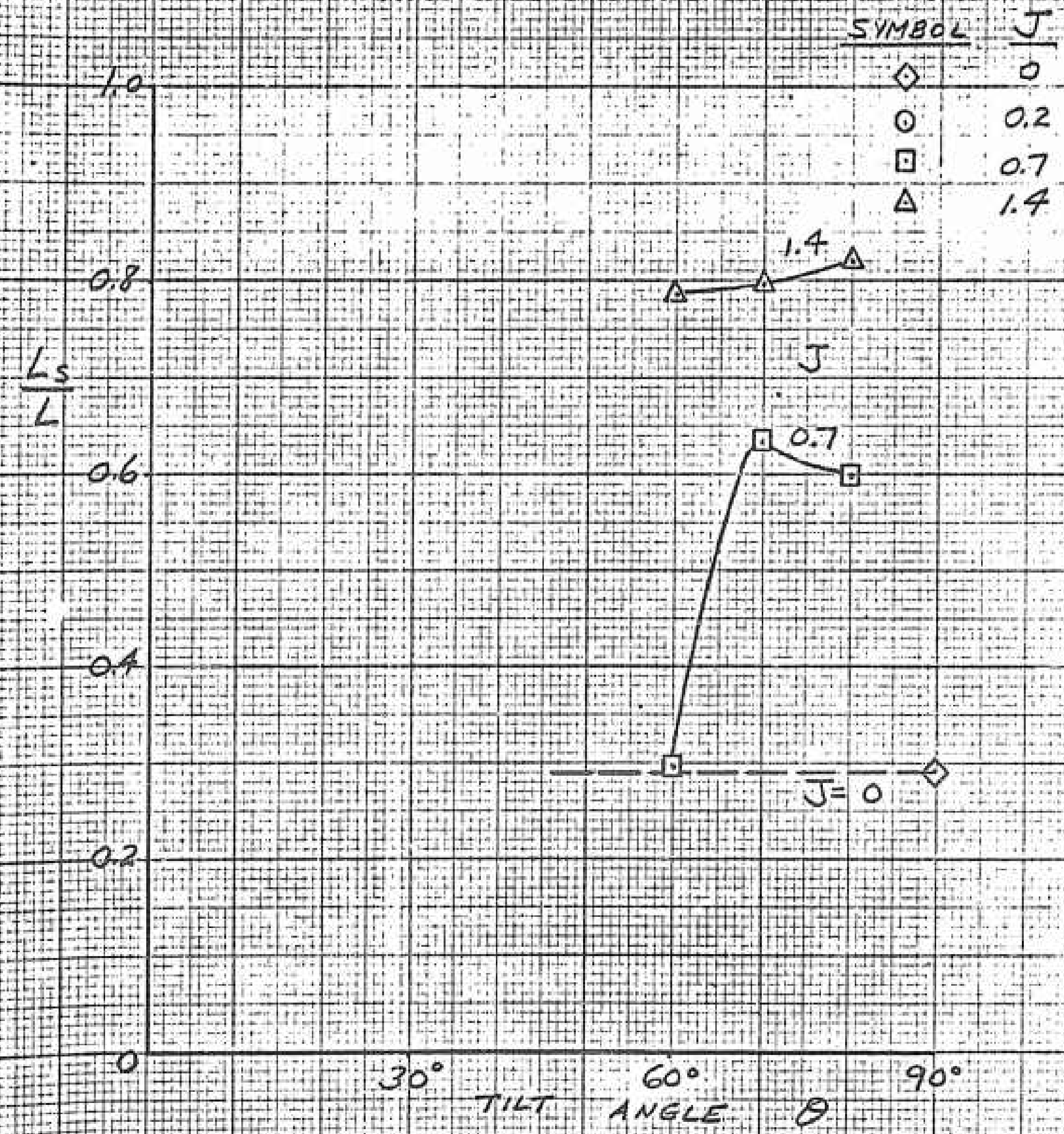

FIG. 34

NON-AXIAL PERFORMANCE
SHROUD DRAG

REF. 17; WATTSON, R.K.; HOEHNE, V.O.
U. OF WICHITA REP. 213-1, 1958

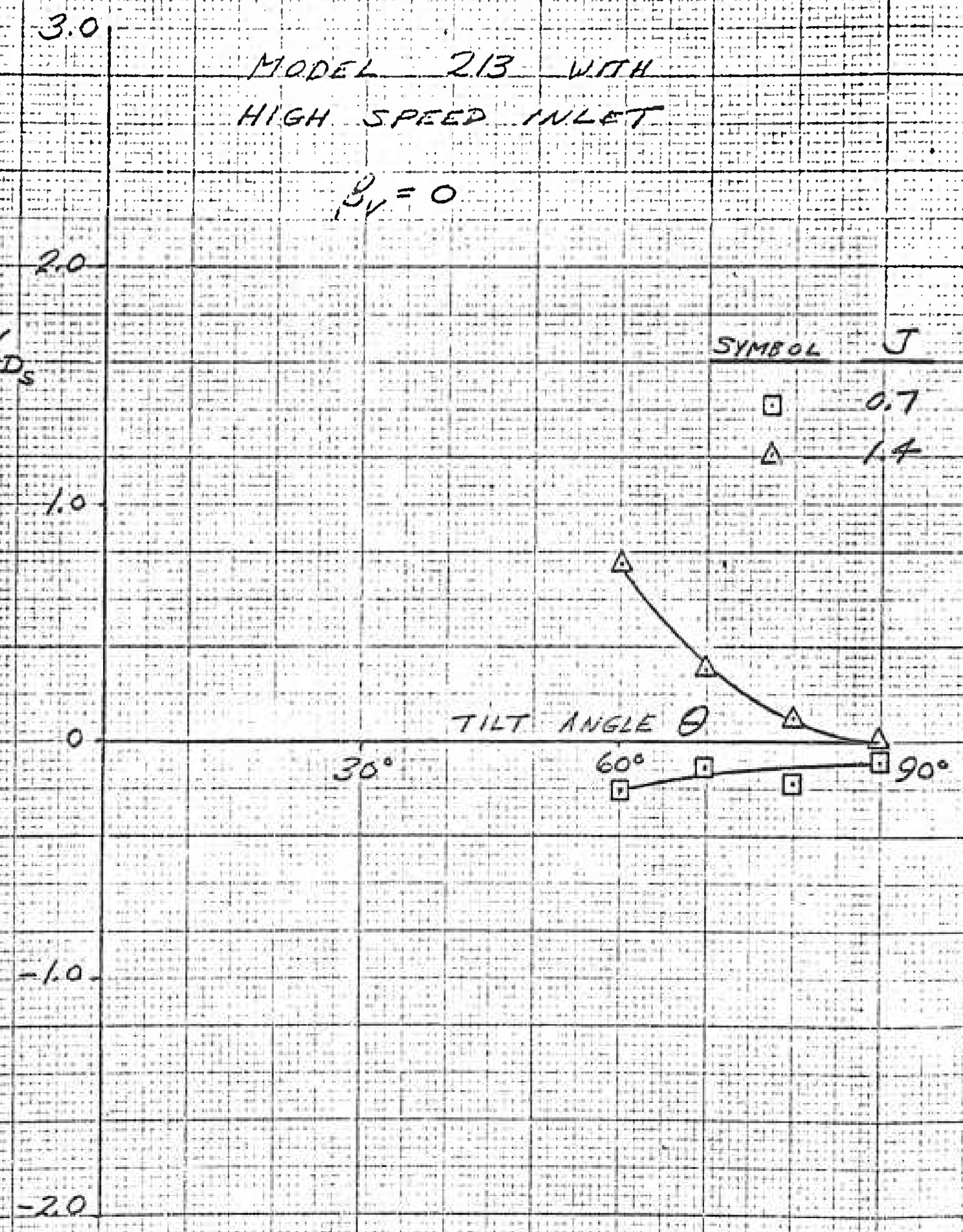

FIG. 35

NON-AXIAL PERFORMANCE
MOMENTS

REF. 17; WATTSON, R.K.; HOEHNE, V.O.
U. OF WICHITA REP. 213-1, 1958

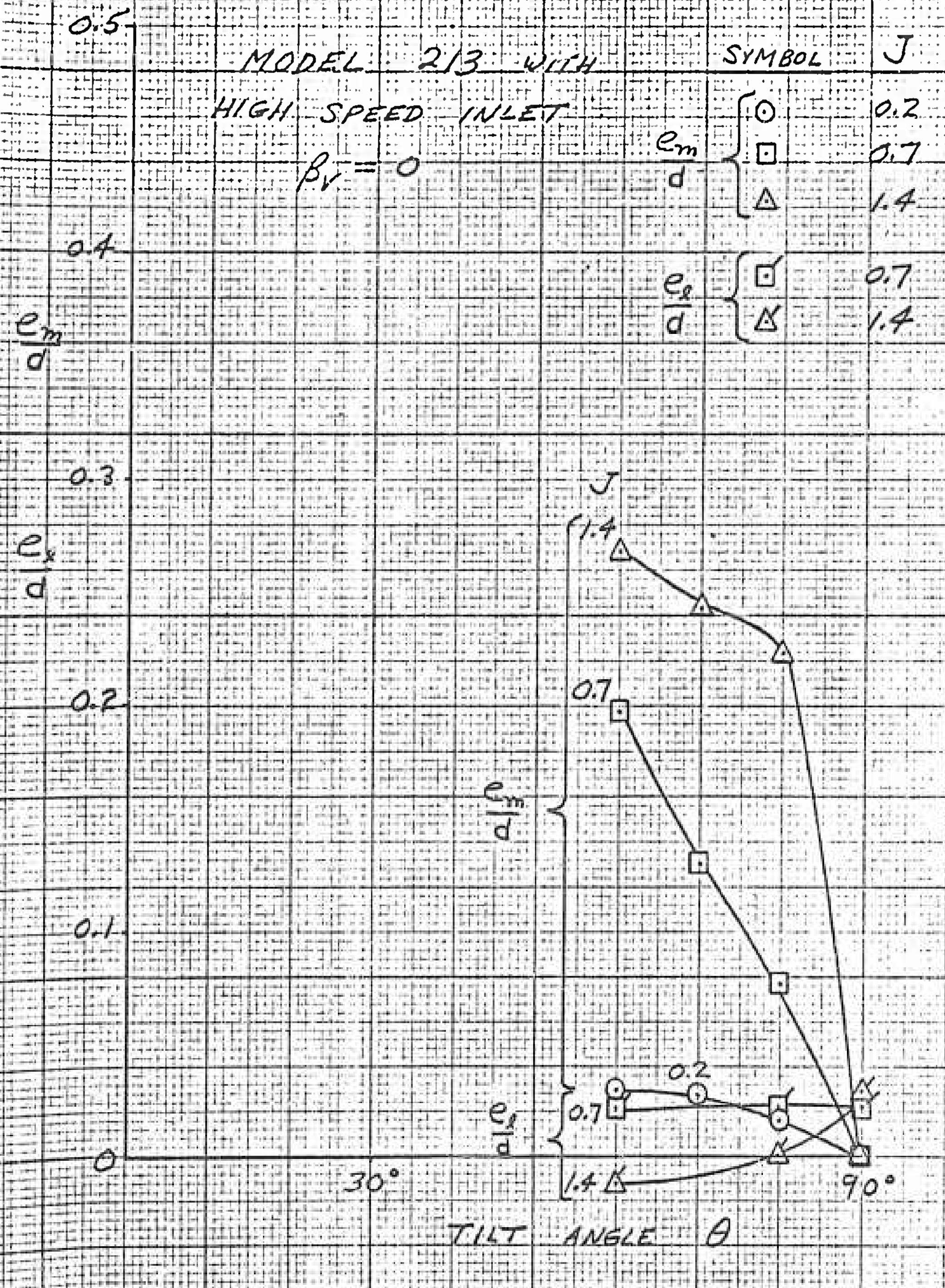

PREPARED JEL 3-25-60

CHECKED

REVISED

REPUBLIC AVIATION

REPORT NO

MODEL

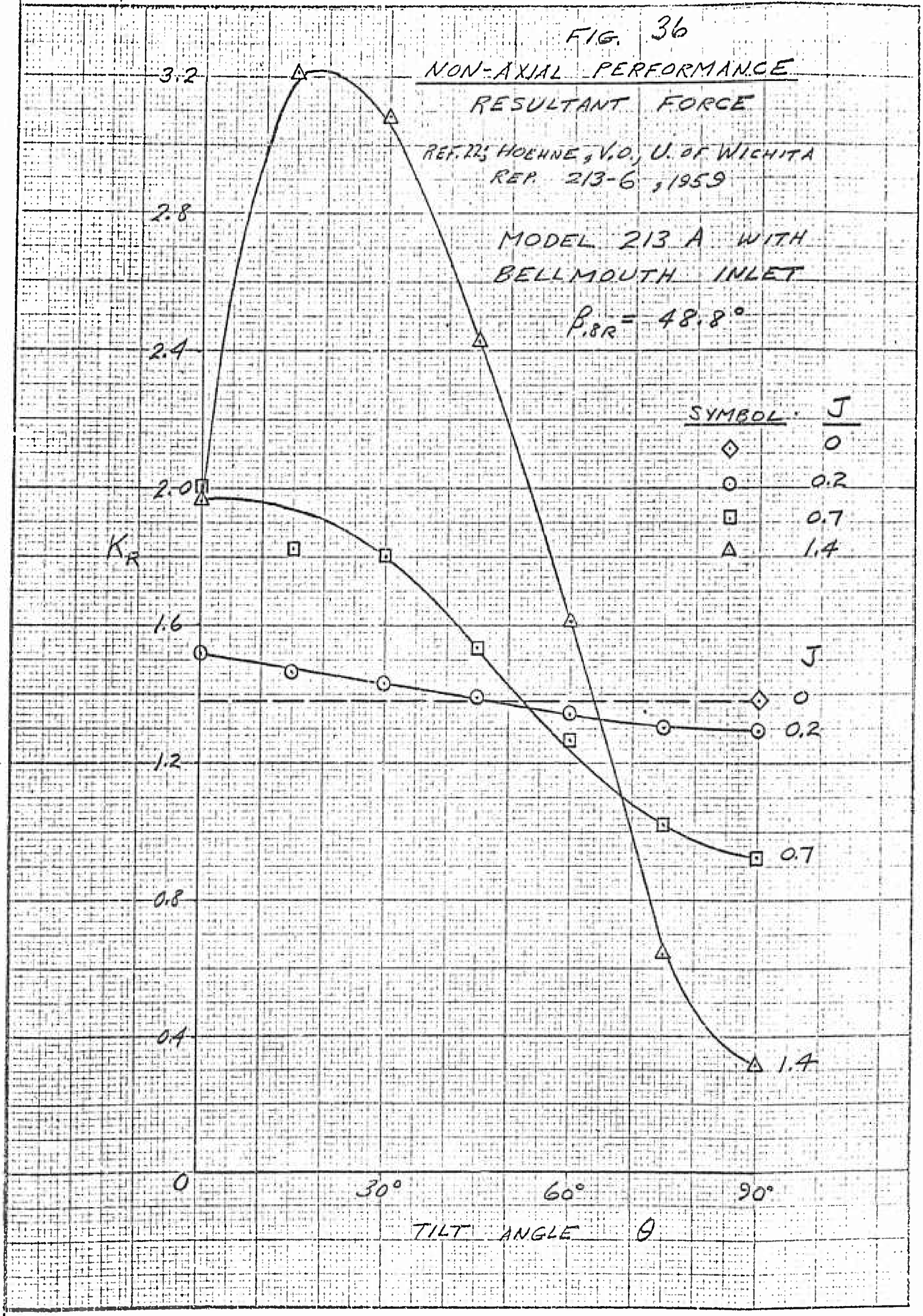

E-1-10A
REV. 2/49

FIG. 37
NON-AXIAL PERFORMANCE
LIFT
REF. 22; HOEHNE, V.O., U. OF WICHITA REP. 213-6, 1959

MODEL 213 A WITH BELLMOUTH INLET

$\beta_{.8R} = 48.8°$

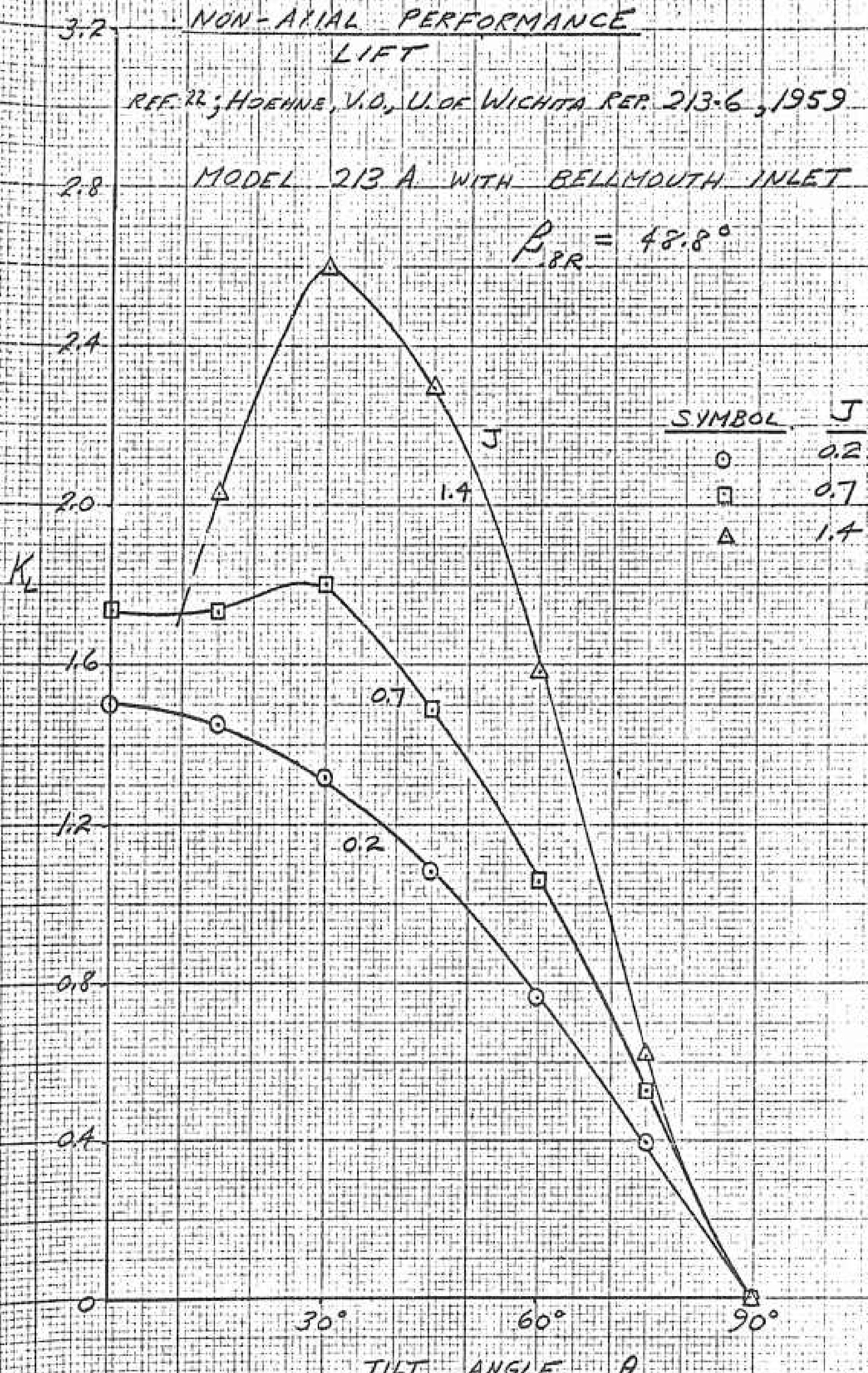

FIG. 38

NON-AXIAL PERFORMANCE
DRAG

REF. 22; HOEHNE, V.O., U. of WICHITA REP. 213-6, 1959

MODEL 213 A WITH
BELL MOUTH INLET

$\beta_{.8R} = 48.8°$

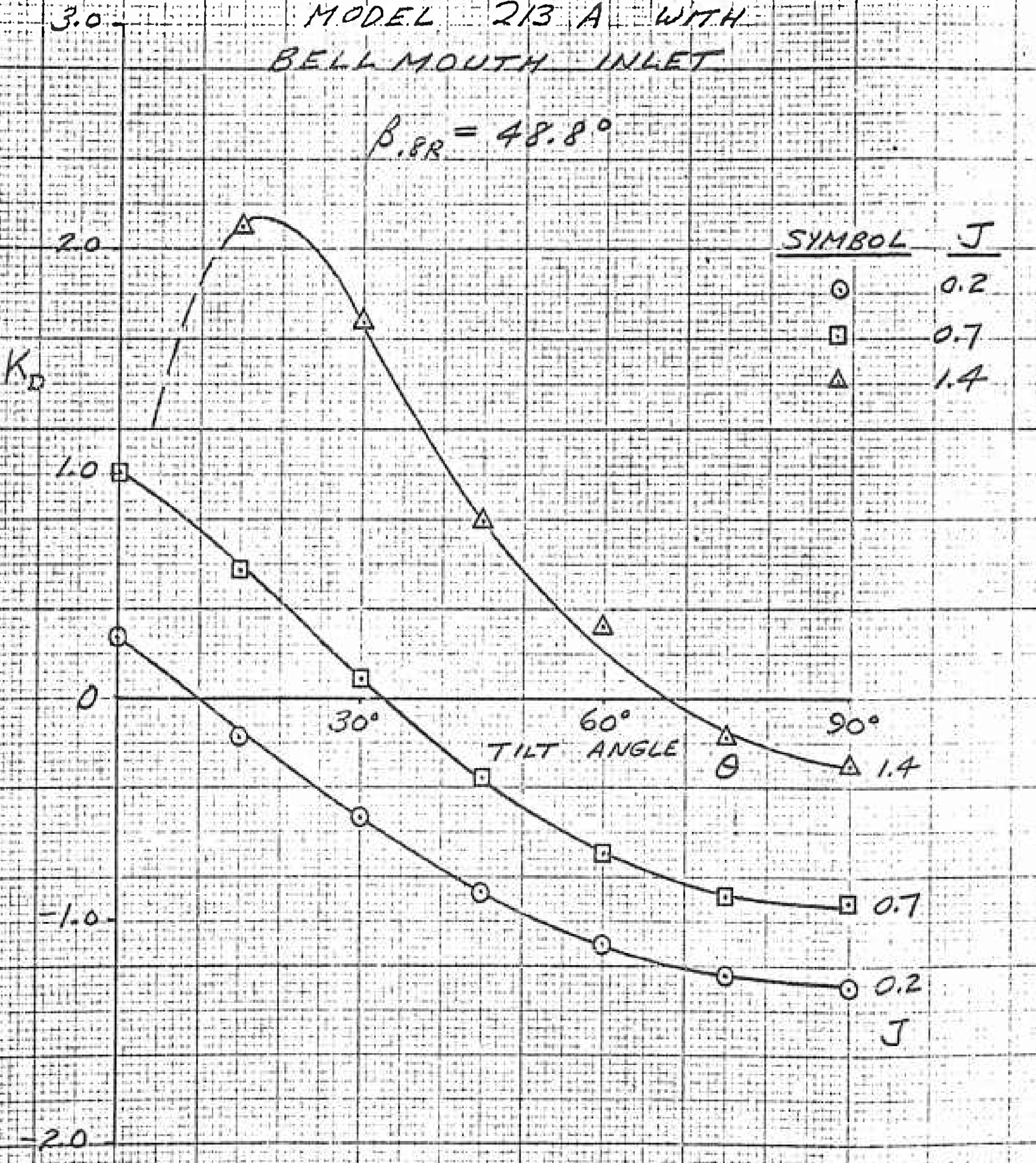

PREPARED JSS 3-25-60
CHECKED
REVISED

REPUBLIC AVIATION

REPORT NO.
MODEL

FIG. 39

NON-AXIAL PERFORMANCE
POWER

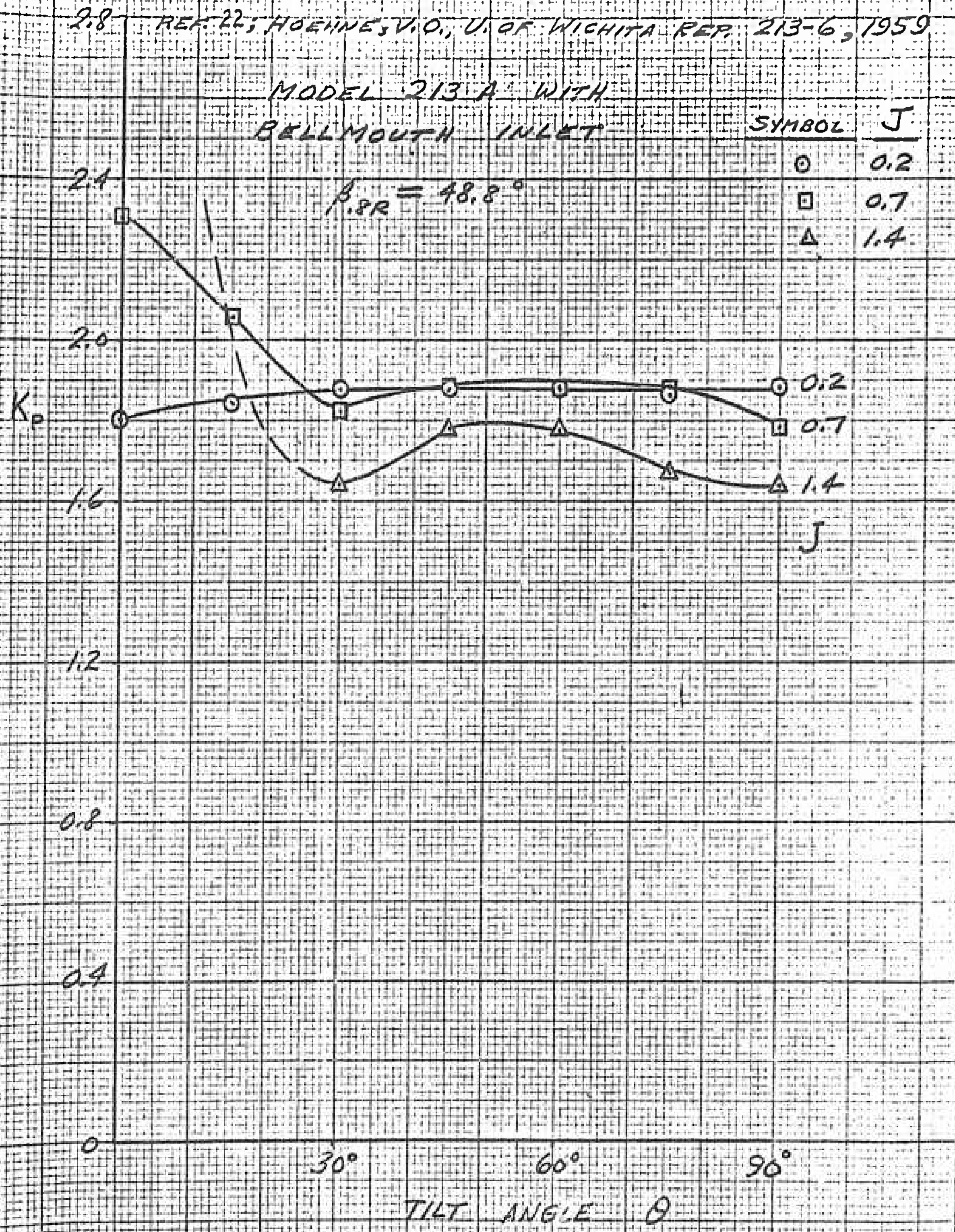

FIG. 40

NON-AXIAL PERFORMANCE
LIFT DIVISION

REF. 22, HOEHNE, V.O. U. OF WICHITA REP. 213-6, 1959

MODEL 213 A WITH
BELLMOUTH INLET

$\beta_{.8D} = 48.8°$

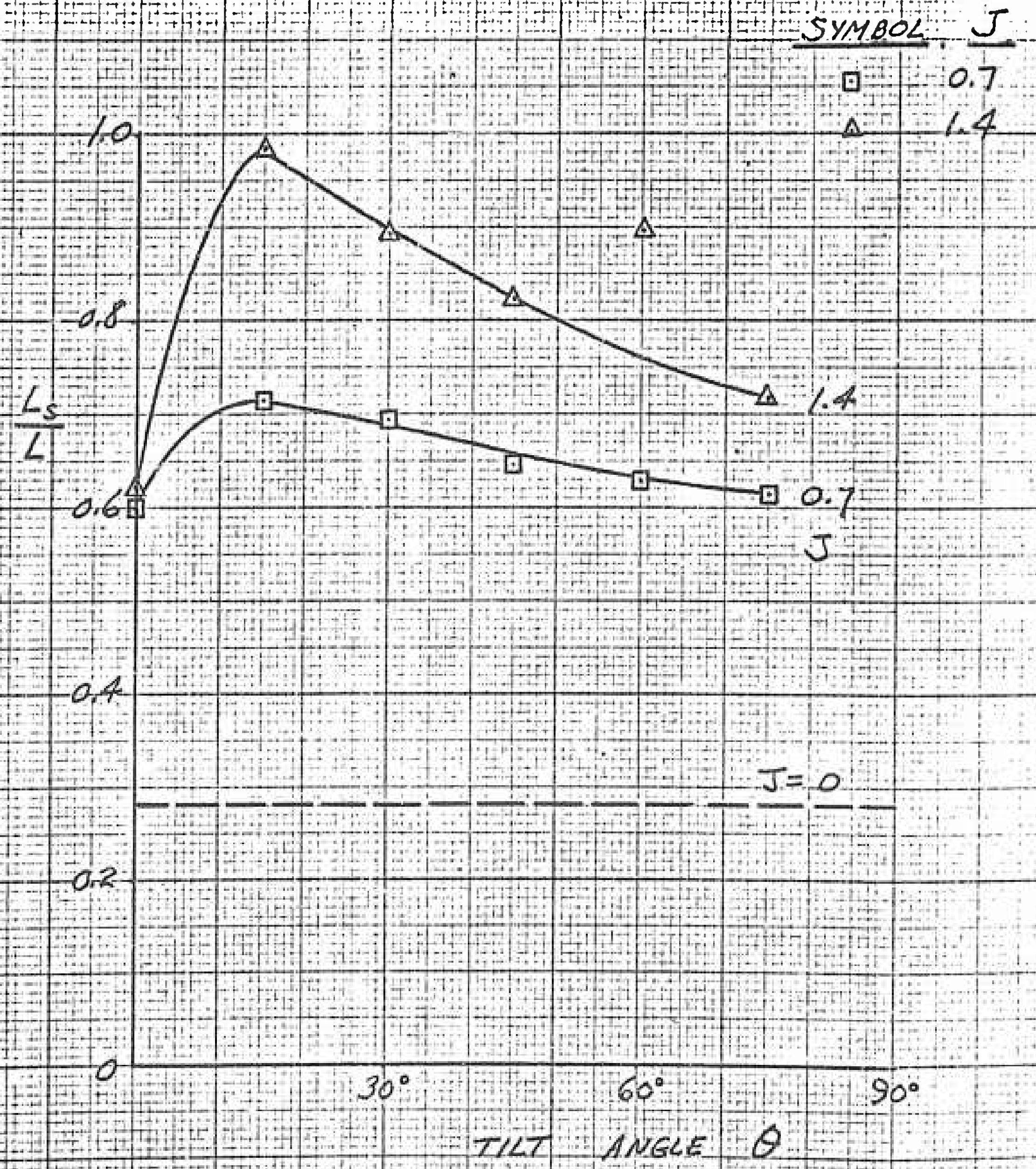

FIG 41

NON-AXIAL PERFORMANCE
SHROUD DRAG

REF. 22; HOEHNE, V. O., U. OF WICHITA REP. 213-6, 1959

MODEL 213 A WITH
BELLMOUTH INLET

$\beta_{.8R} = 48.8°$

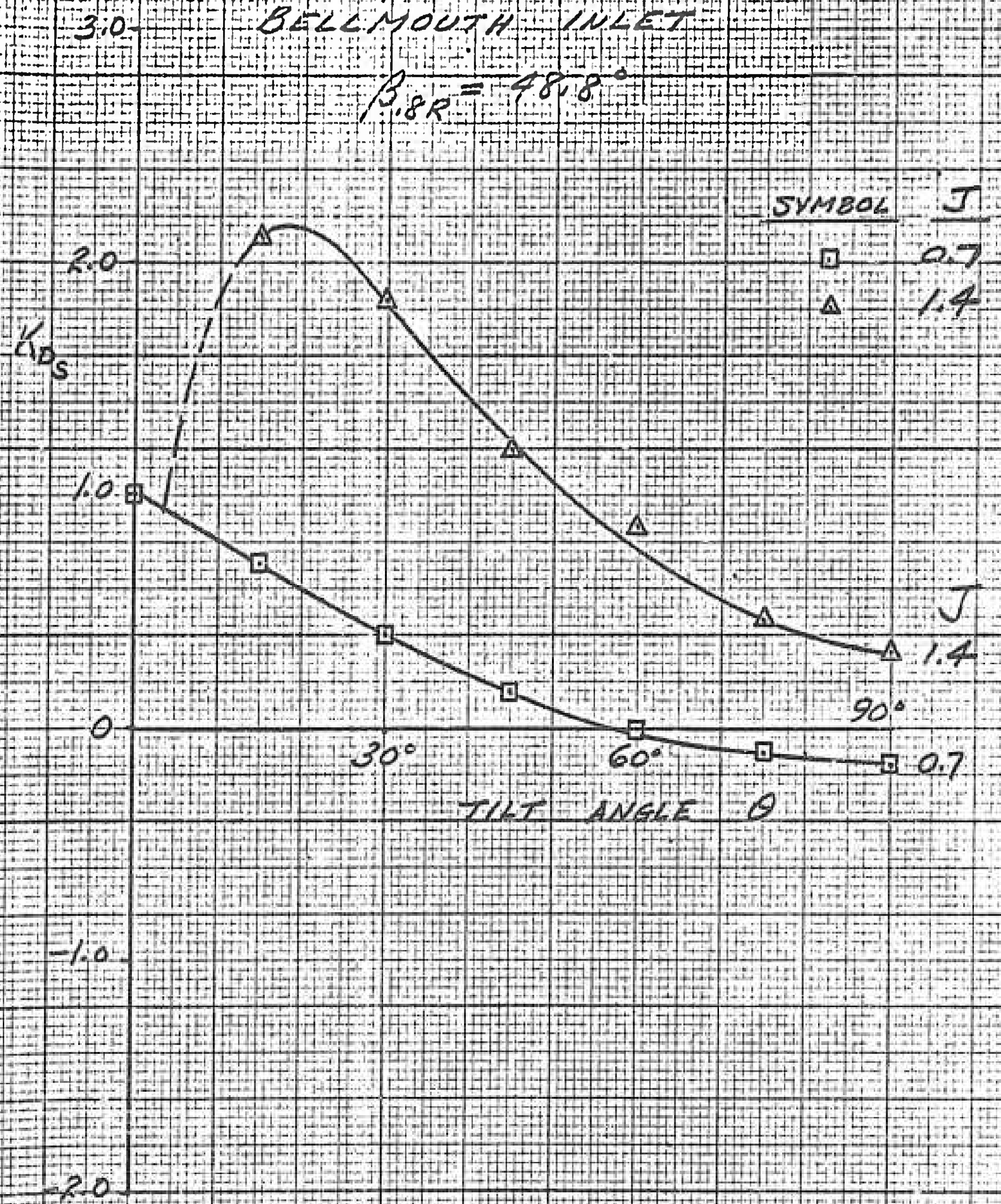

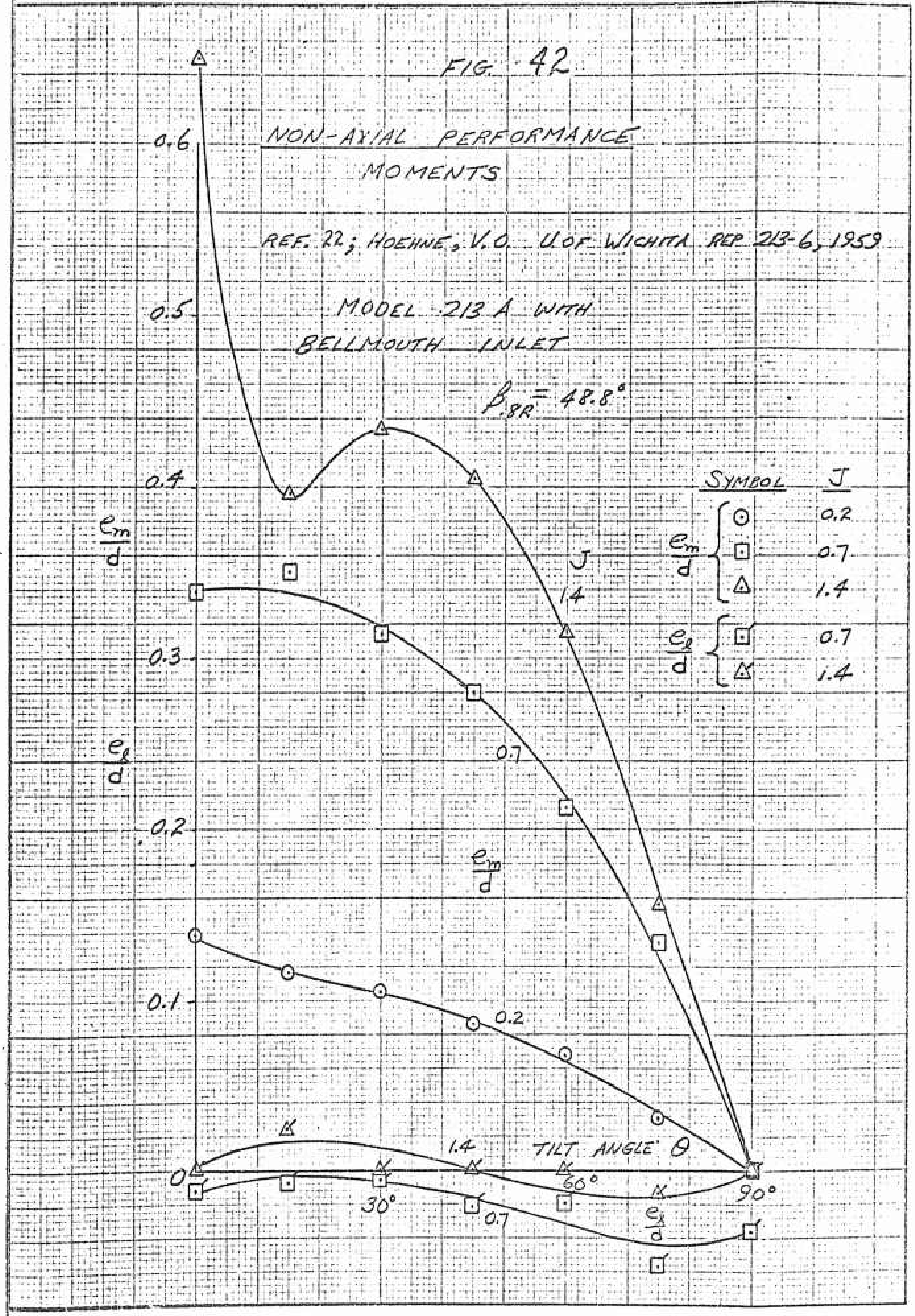
FIG. 42
NON-AXIAL PERFORMANCE
MOMENTS
REF. 22; HOEHNE, V.O. U OF WICHITA REP 213-6, 1959
MODEL 213 A WITH
BELLMOUTH INLET
$\beta_{.8R} = 48.8°$
SYMBOL J
$\frac{e_m}{d}$ 0.2
0.7
1.4
$\frac{e_l}{d}$ 0.7
1.4
0.6
0.5
0.4
0.3
0.2
0.1
0
$\frac{e_m}{d}$
$\frac{e_l}{d}$
J
1.4
0.7
0.2
TILT ANGLE θ
30°
60°
90°

FIG. 43

NON-AXIAL PERFORMANCE
RESULTANT FORCE

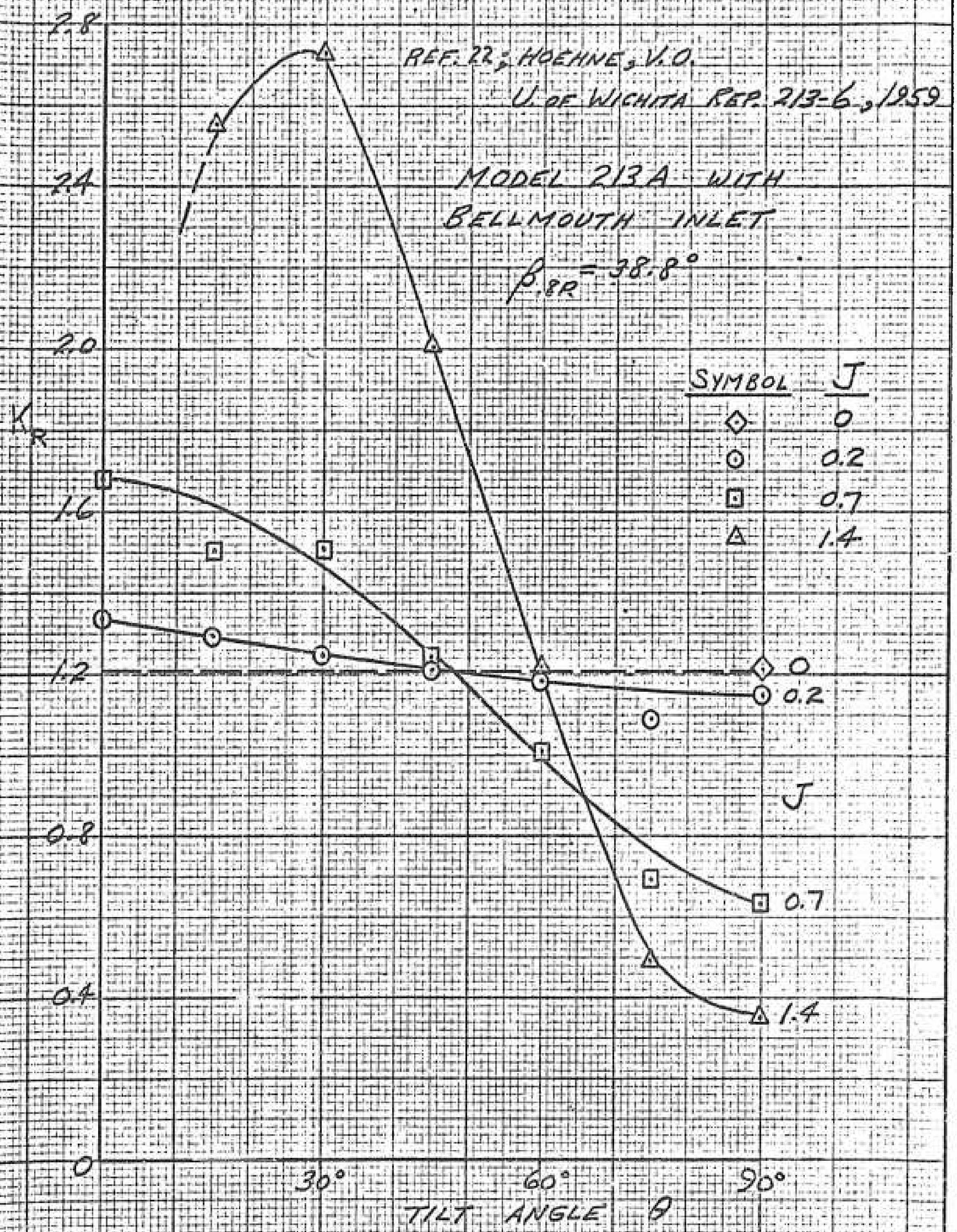

FIG. 44

NON-AXIAL PERFORMANCE
LIFT

REF. 22; HOEHNE, V.O., U. OF WICHITA REP. 213-6, 1958

MODEL 213 A WITH
BELLMOUTH INLET
$\beta_{.8R} = 38.8°$

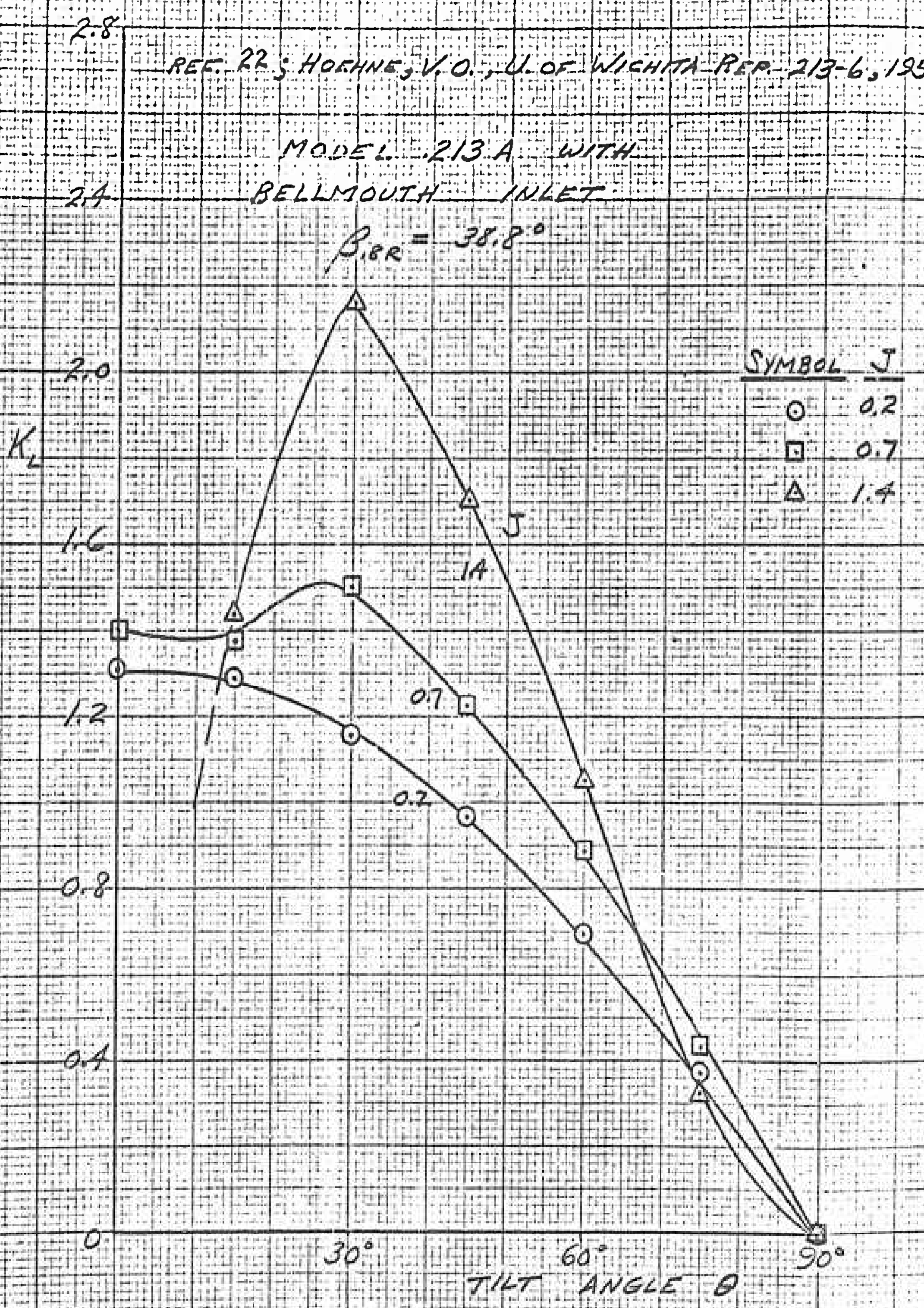

FIG 45

NON-AXIAL PERFORMANCE
DRAG

REF. 22; HOEHNE, V.O., U. OF WICHITA REP. 213-6, 1959

MODEL 213 A WITH BELLMOUTH INLET

$\beta_{.8R} = 38.8°$

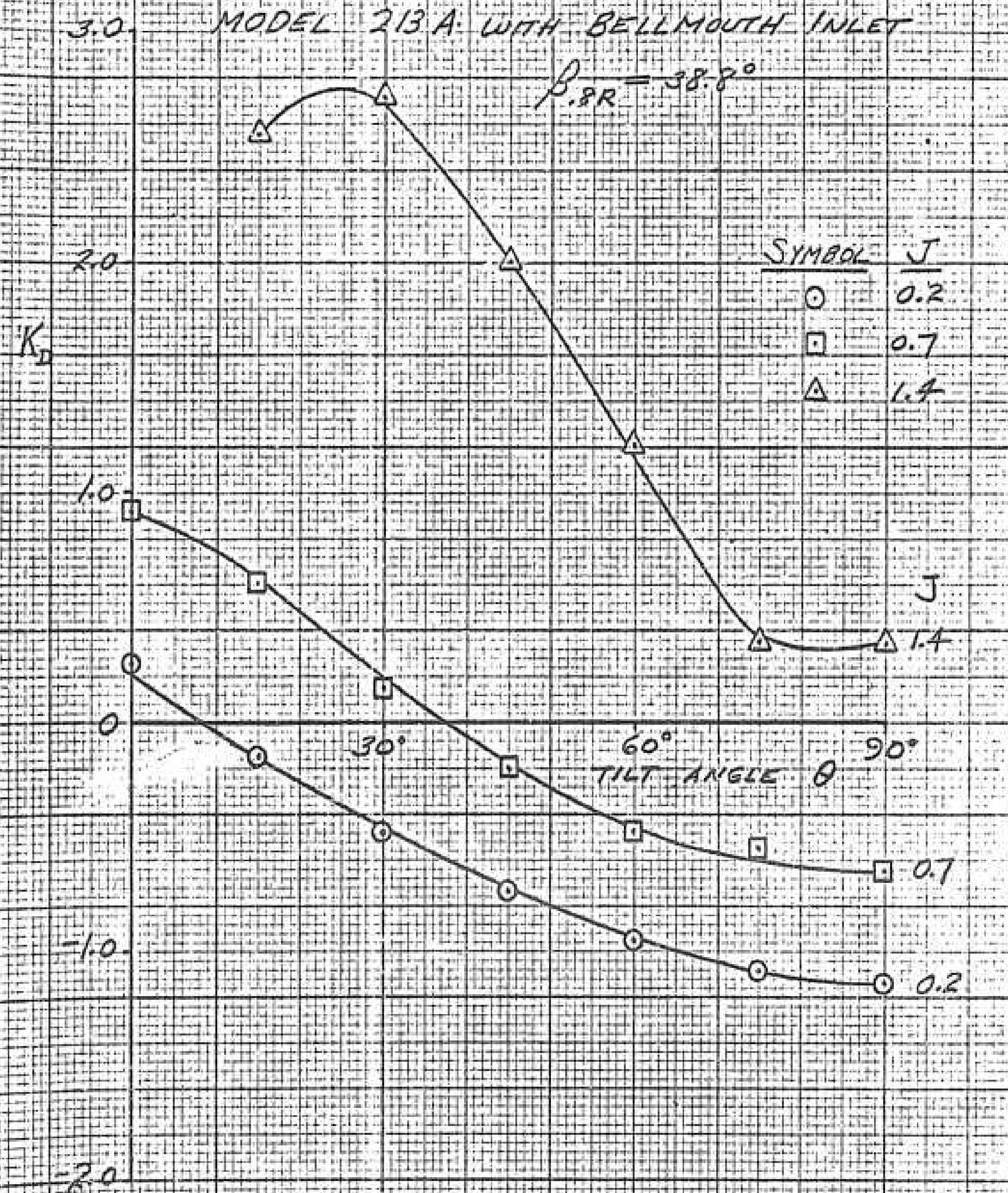

FIG. 46

NON-AXIAL PERFORMANCE
POWER

REF. 22; HOEHNE, V. O., U. OF WICHITA REP. 213-6, 1959

MODEL 213 A WITH
BELLMOUTH INLET

$\beta_{.8R} = 38.8°$

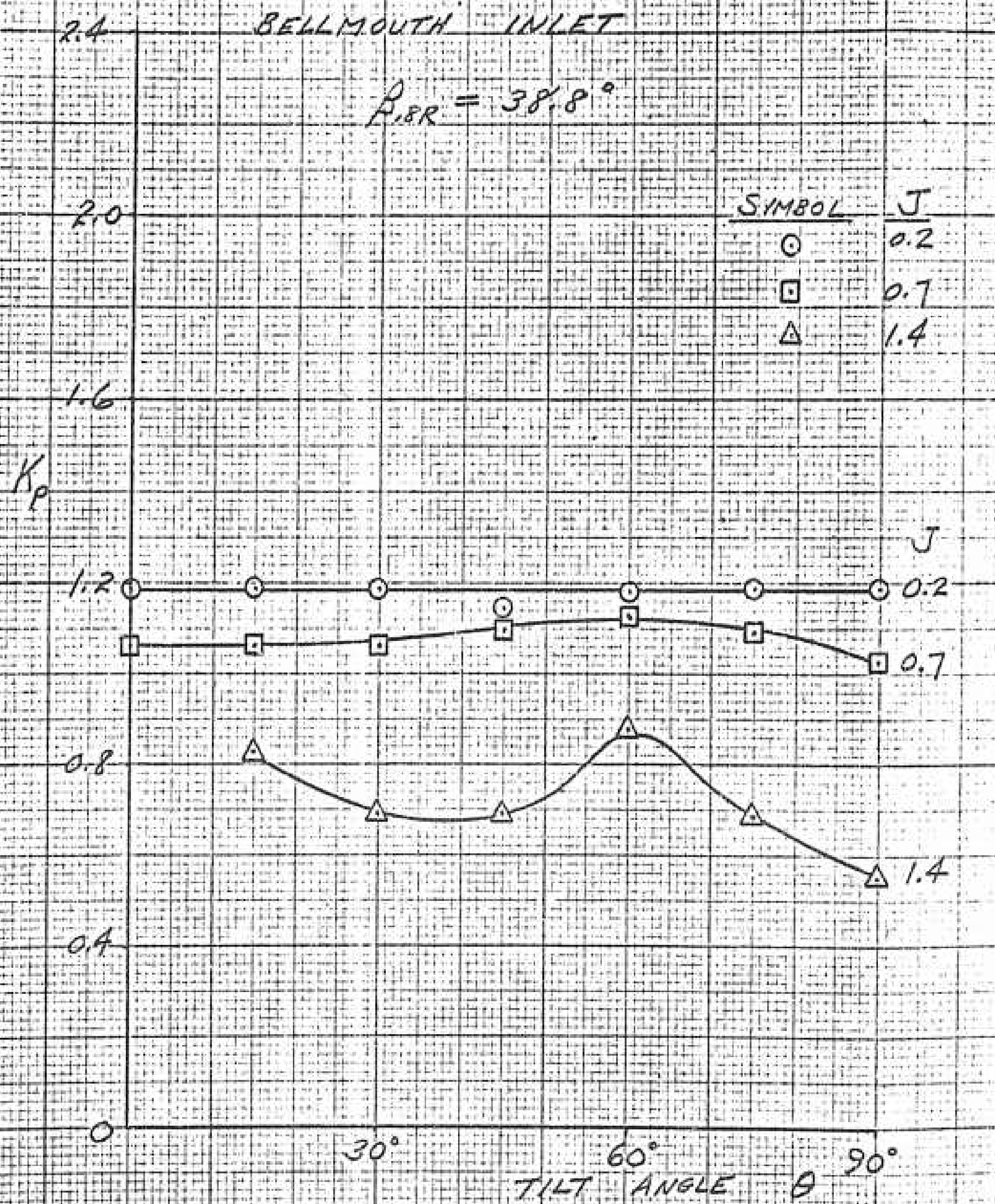

PREPARED JRL 3-30-60
CHECKED
REVISED

57

REPORT NO.
MODEL

FIG 47

NON-AXIAL PERFORMANCE
LIFT DIVISION

REF. 22; HOEHNE, V.O.; U. OF WICHITA REP. 213-6, 1958

MODEL 213 A WITH
BELLMOUTH INLET

$\beta_{.8R} = 38.8°$

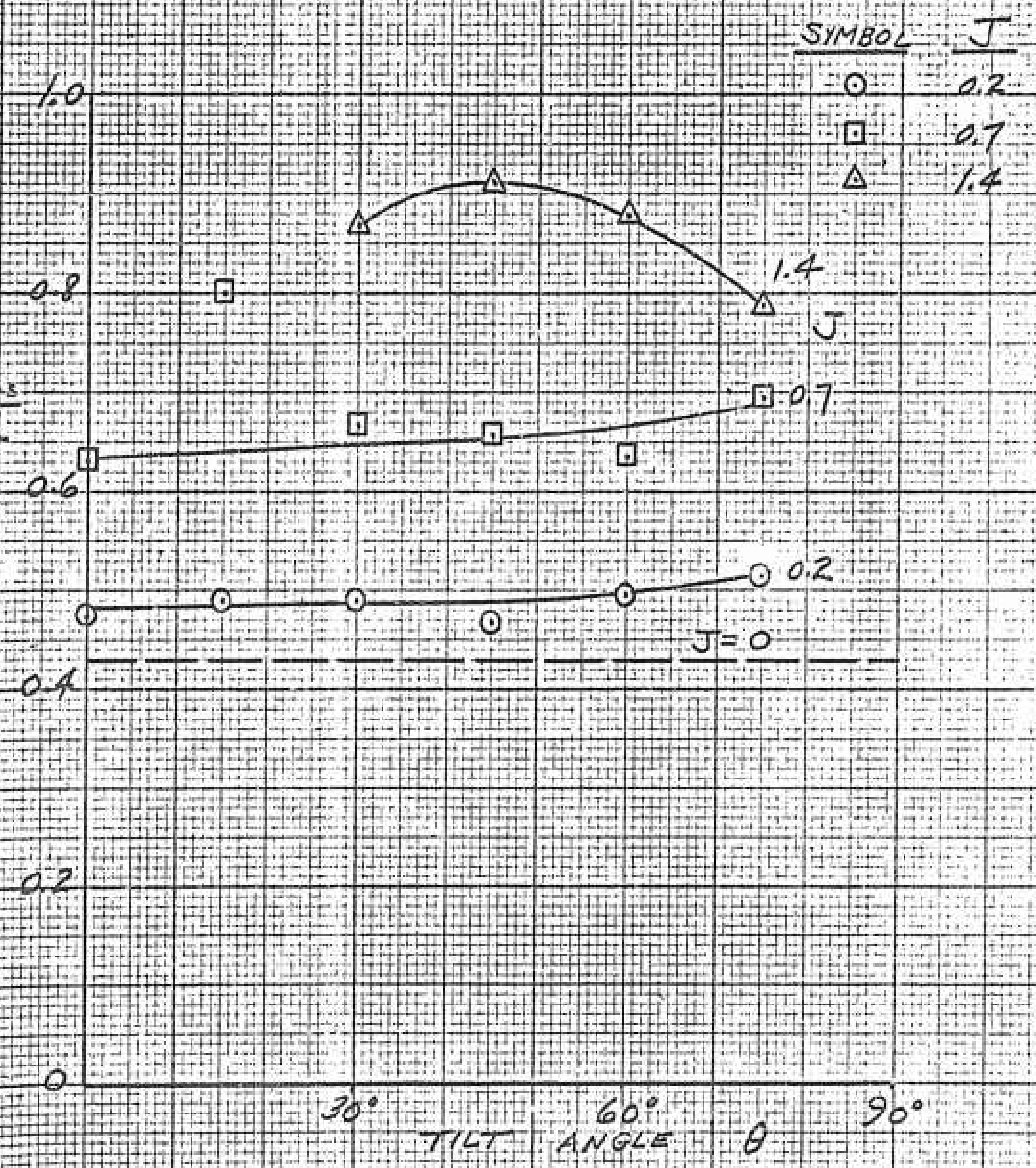

FIG. 48

NON-AXIAL PERFORMANCE
SHROUD DRAG

REF. 22; HOEHNE, V.O., U. OF WICHITA REP. 213-6, 1959

MODEL 213 A WITH
BELLMOUTH INLET

$\beta_{.8R} = 38.8°$

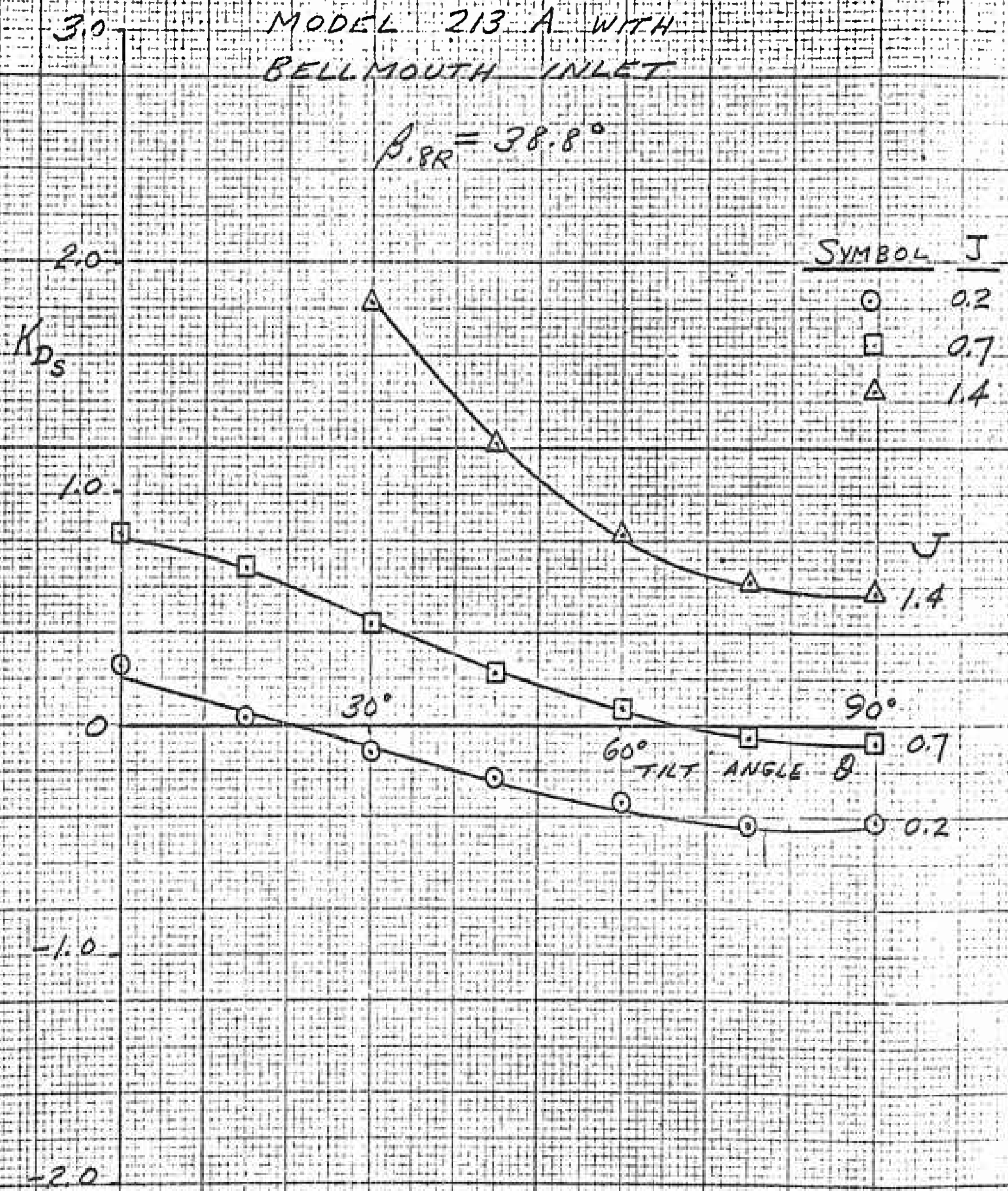

REPUBLIC AVIATION

FIG 49
NON-AXIAL PERFORMANCE
MOMENTS

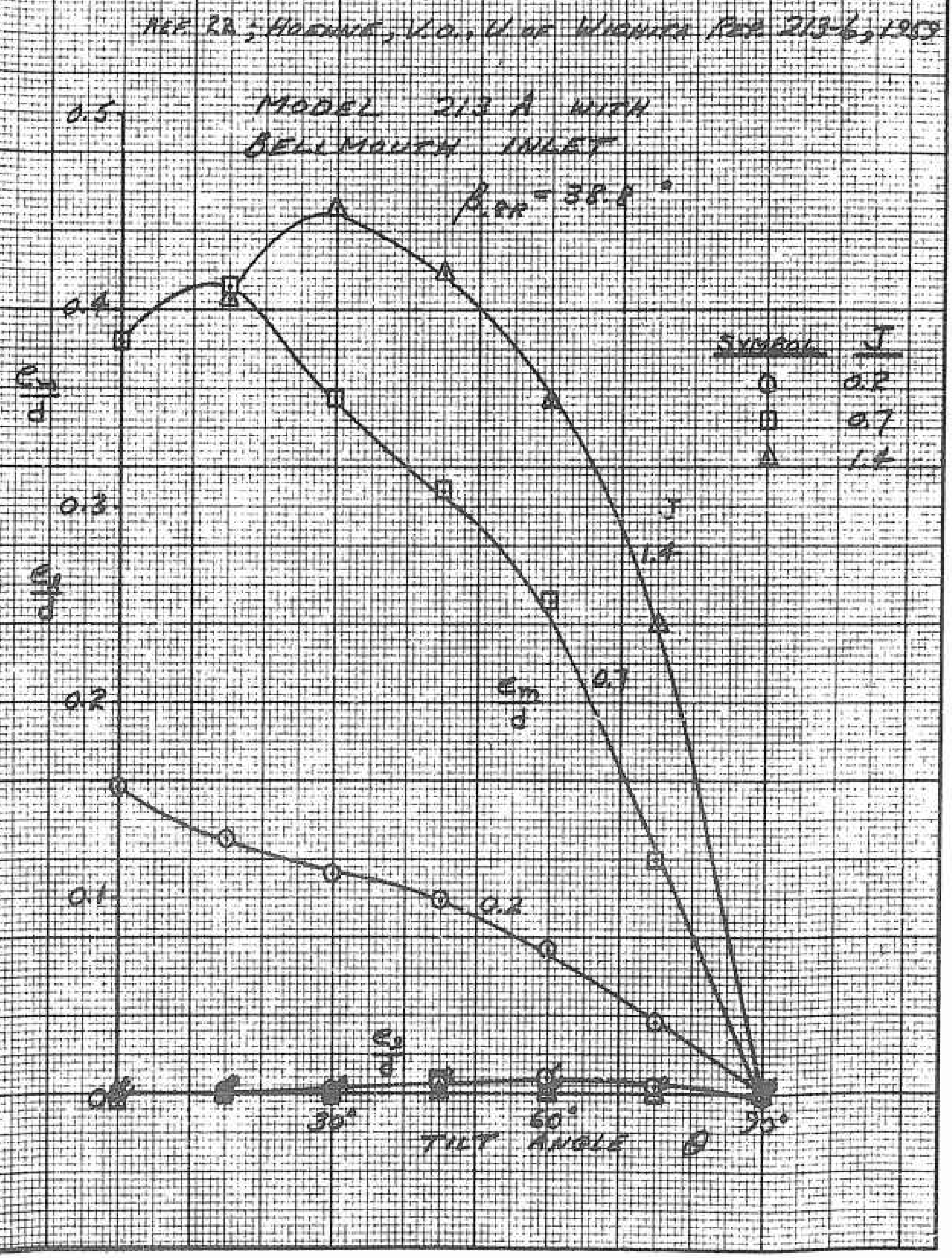

Reference	7
Author	Gill, W. J.
Source	Hiller Aircraft Corporation
Figs.	50-108

FIG. 50

DUCT CONFIGURATIONS

REF. 7; GILLY, W. J., HILLER AIRCRAFT CORP. ARD-224, 1959

DUCT 1

MODIFIED NACA 6421 SECTION

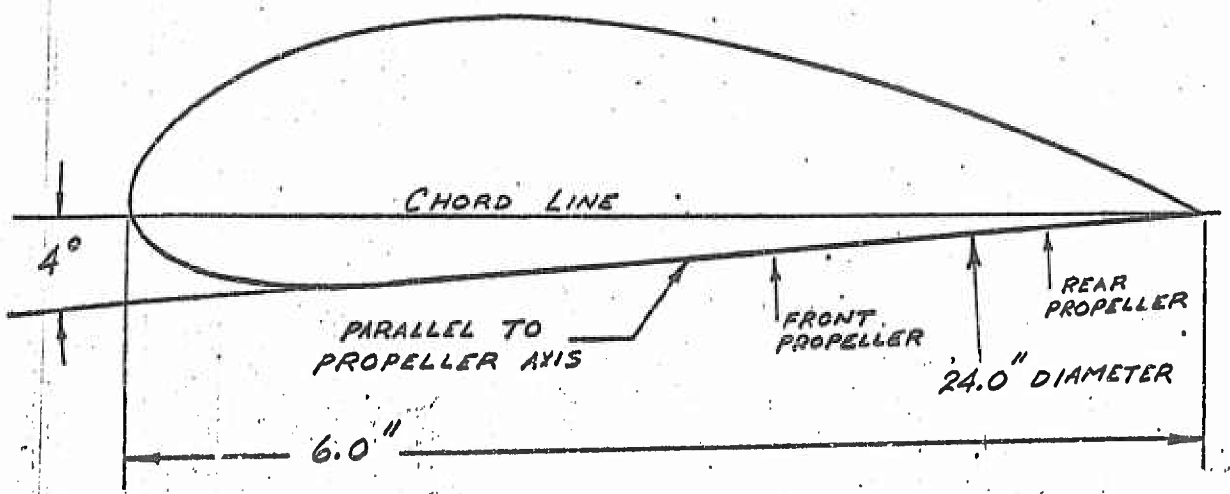

DUCT 2

NACA 0018 SECTION

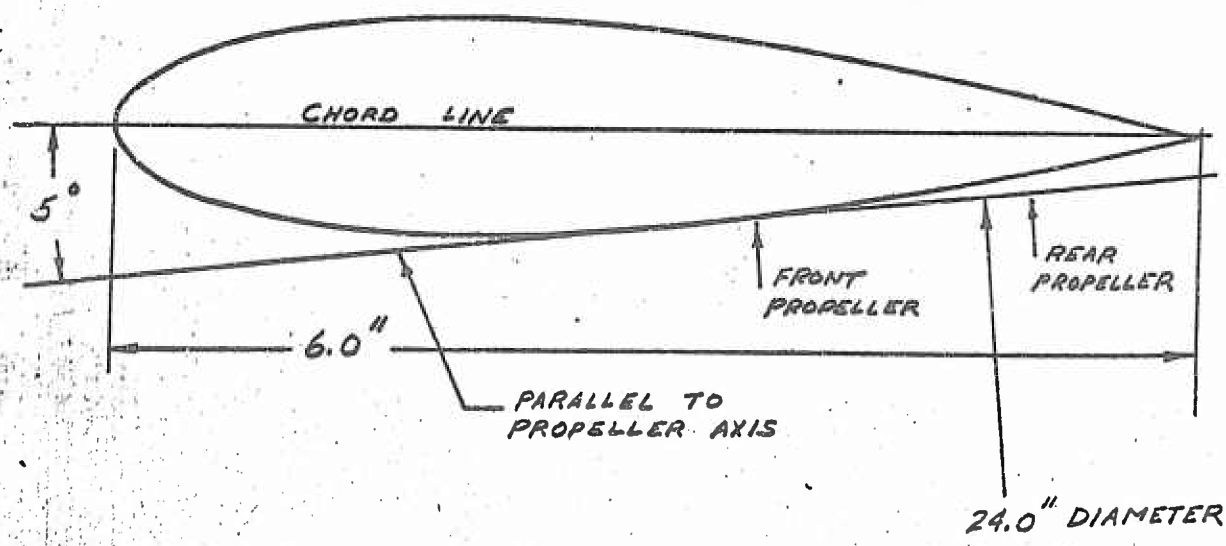

FIG. 51

DUCT CONFIGURATIONS

REF. 7 ; GILL, W.J., HILLER AIRCRAFT CORP. ARD-224, 1959

DUCT 3

MODIFIED LEMNISCATE CURVE

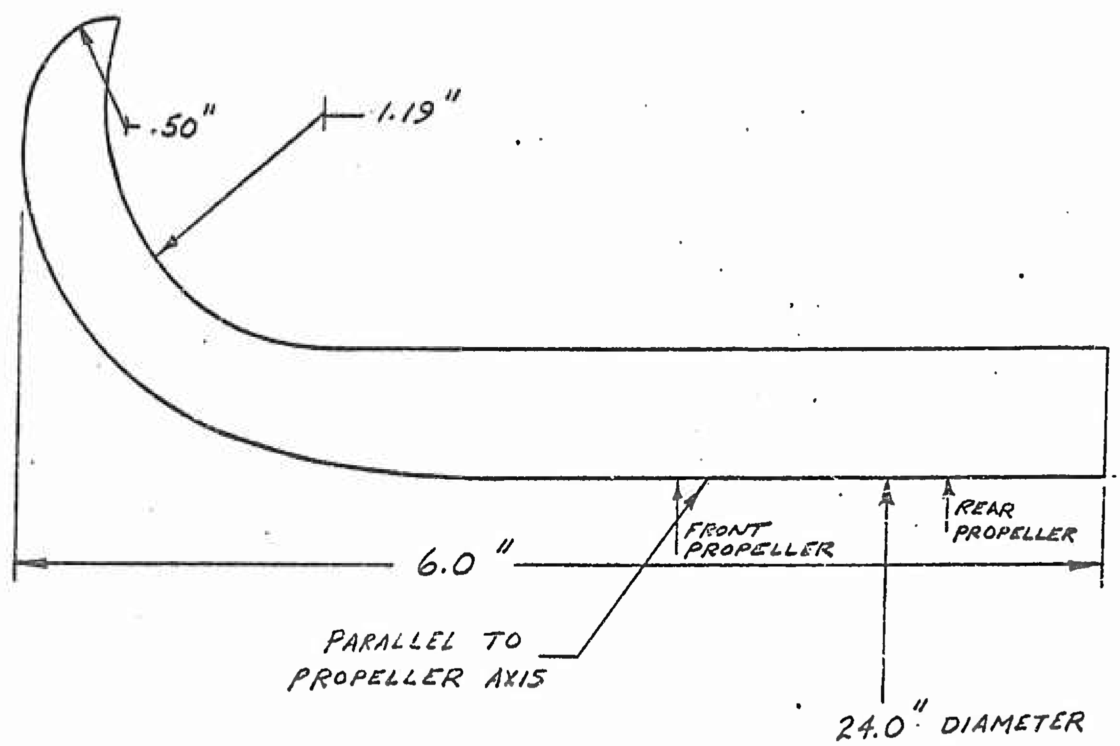

DUCT 4

MODIFIED NACA 6421 SECTION

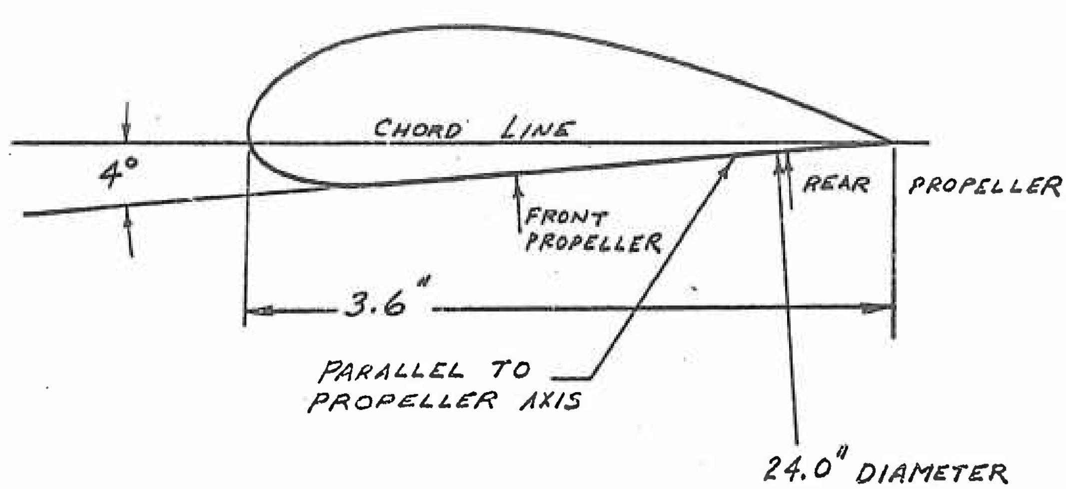

PREPARED Jol 1-21-60 | PAGE 189
CHECKED | REPORT NO.
REVISED | MODEL

REPUBLIC AVIATION

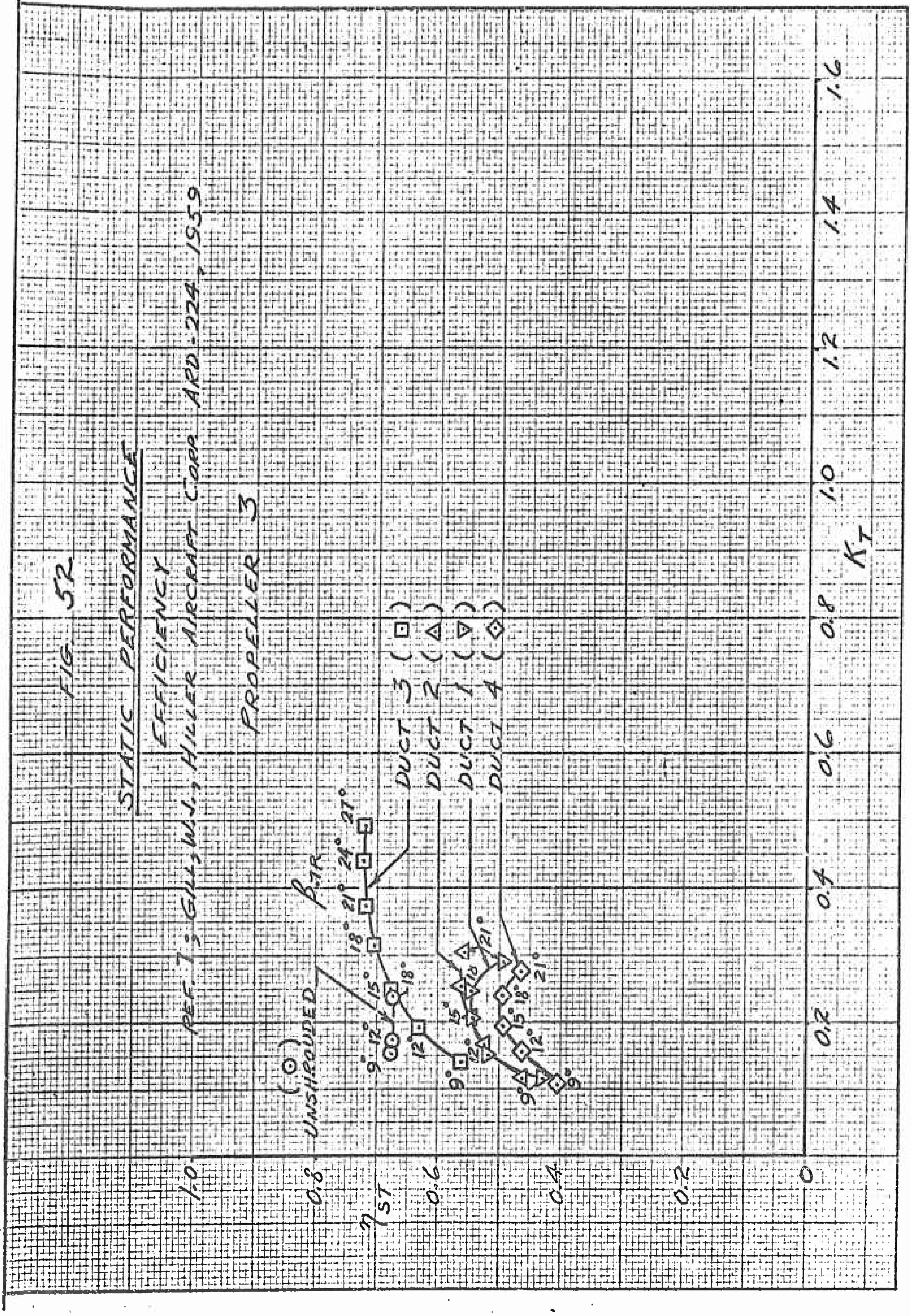

-1-10A
v. 2/49

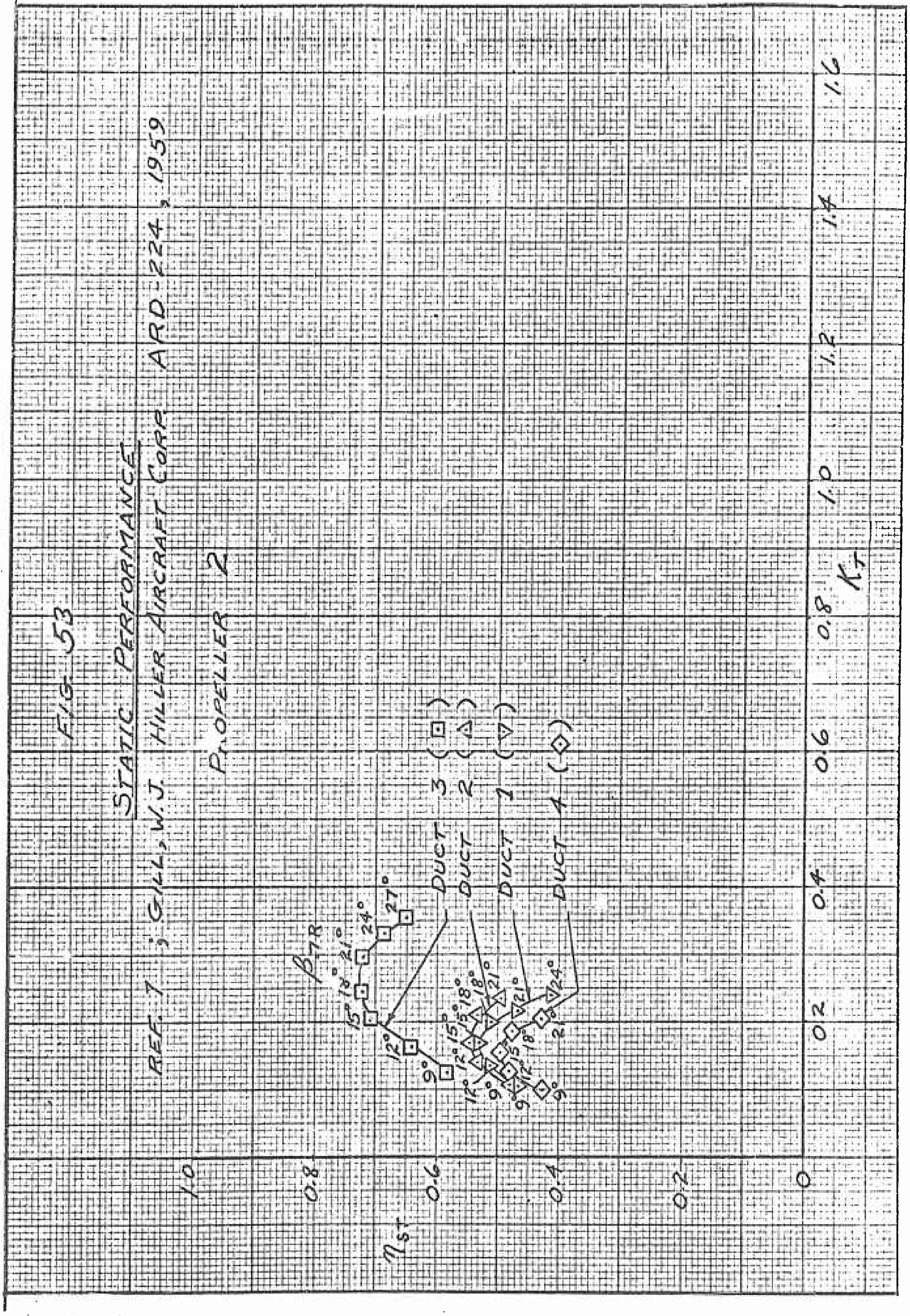
FIG. 53
STATIC PERFORMANCE
REF. 7; GILL, W.J. HILLER AIRCRAFT CORP. ARD-224, 1959
PROPELLER 2
DUCT 3 (□)
DUCT 2 (△)
DUCT 1 (▽)
DUCT 4 (◇)
$\beta_{.7R}$
9°
12°
15°
18°
21°
24°
27°
η_{ST}
1.0
0.8
0.6
0.4
0.2
0
0.2
0.4
0.6
0.8
1.0
1.2
1.4
1.6
K_T

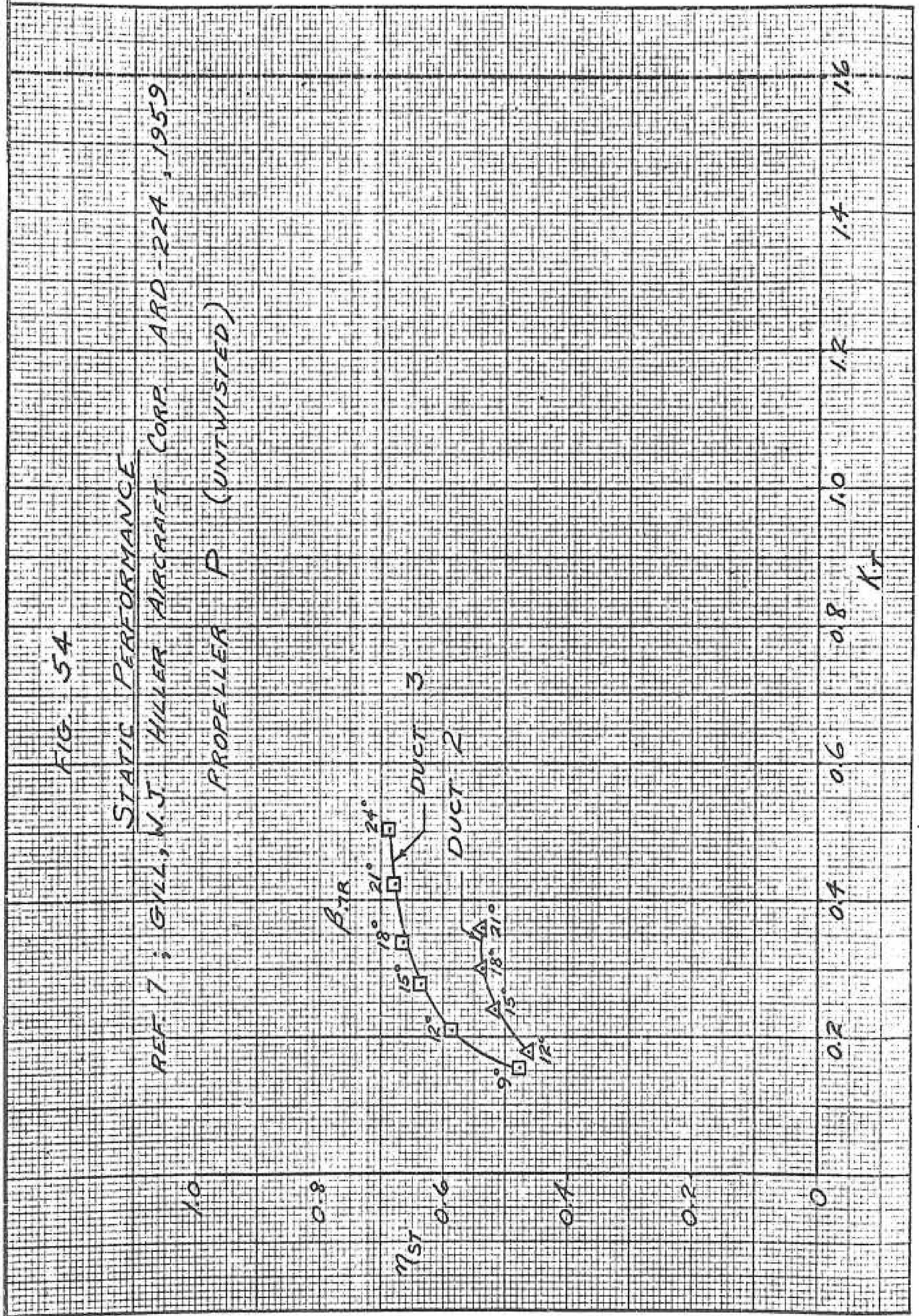
FIG. 54
STATIC PERFORMANCE
REF. 7; GILL, W.J. HILLER AIRCRAFT CORP. ARD-224, 1959
PROPELLER P (UNTWISTED)
DUCT 3
DUCT 2
β.7R
9°
12°
15°
18°
21°
24°
η ST
1.0
0.8
0.6
0.4
0.2
0
K T
0.2
0.4
0.6
0.8
1.0
1.2
1.4
1.6

PREPARED JBS 1-22-60 | PAGE 192

CHECKED | REPORT NO.

REVISED | MODEL

REPUBLIC AVIATION

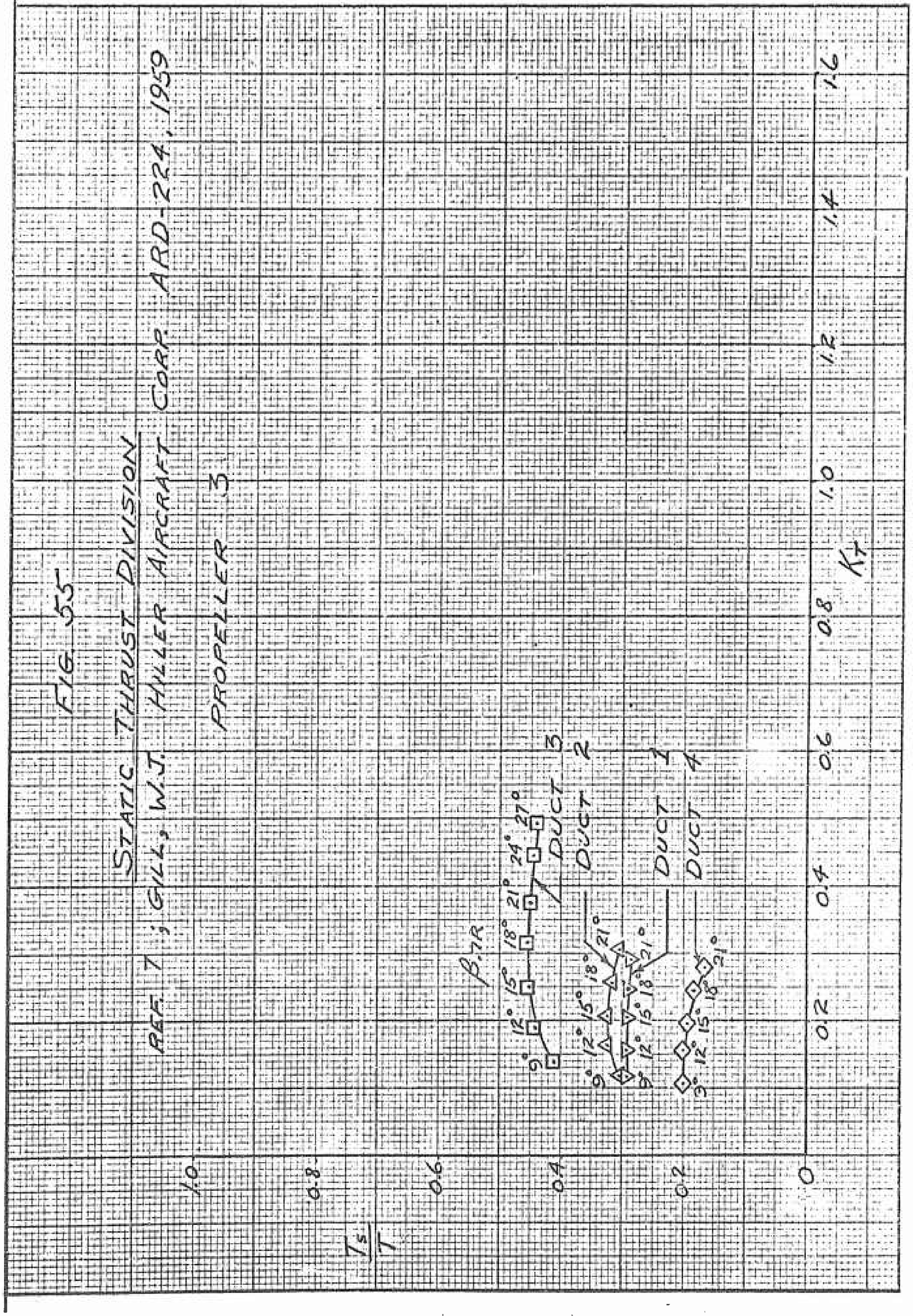

•1•10A
V. 8/40

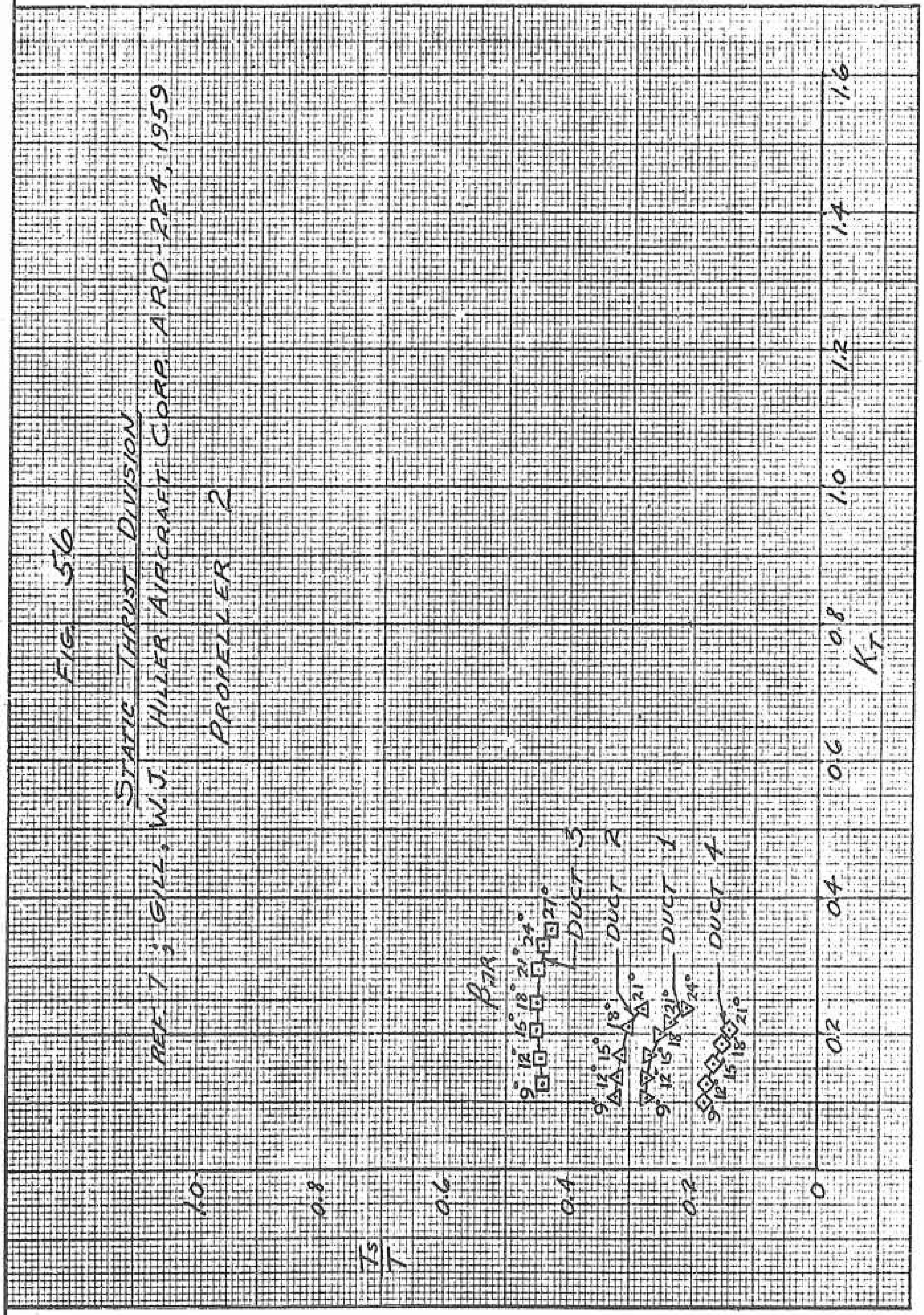
FIG. 56
STATIC THRUST DIVISION
REF 7; GILL, W.J.; HILLER AIRCRAFT CORP. ARD-224, 1959
PROPELLER 2
$\beta_{.7R}$
DUCT 3
DUCT 2
DUCT 1
DUCT 4
T_S/T
K_T
0
0.2
0.4
0.6
0.8
1.0
1.2
1.4
1.6

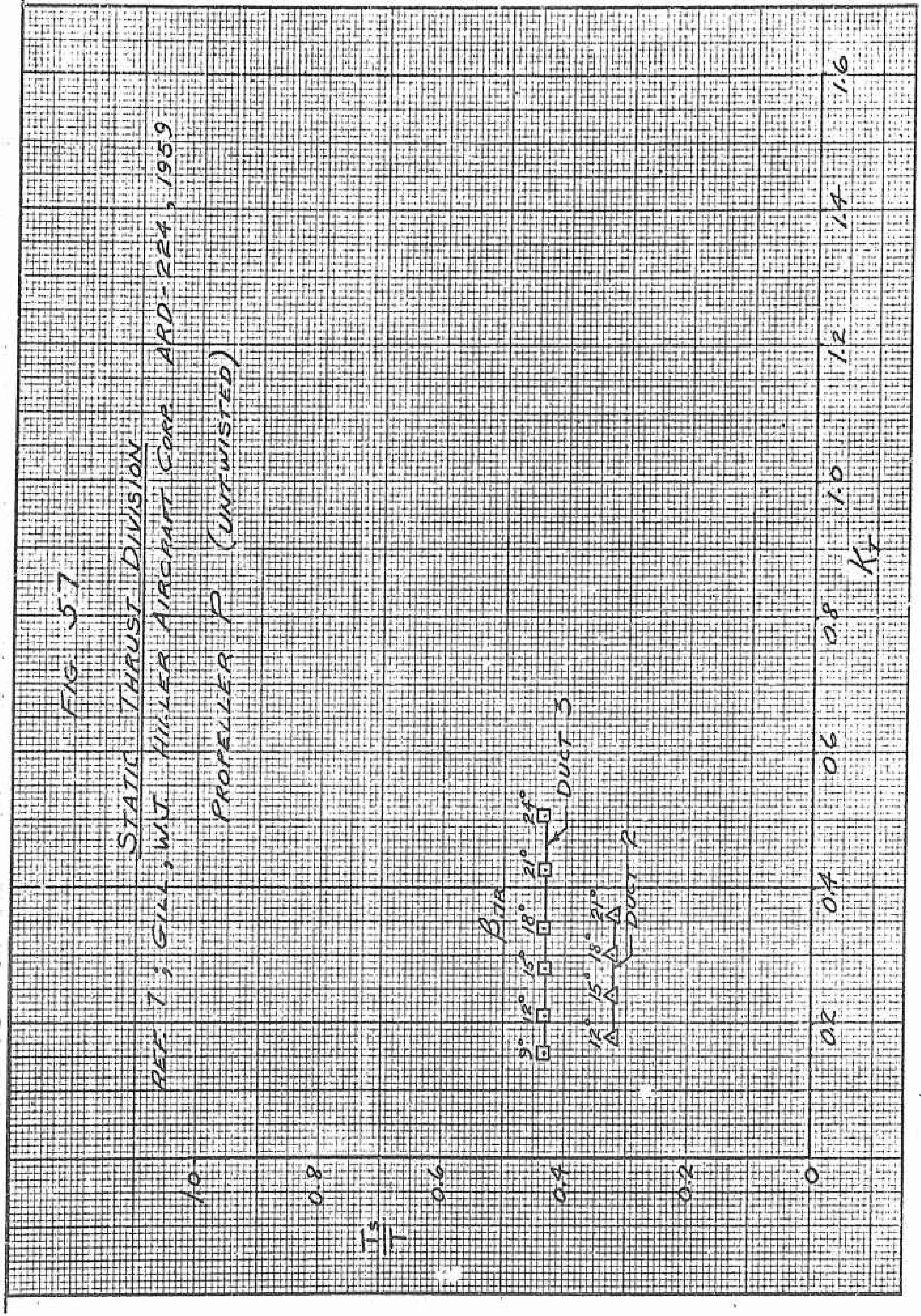
FIG. 57
STATIC THRUST DIVISION
REF. 7; GILL, W.J. HILLER AIRCRAFT CORP. ARD-224, 1959
PROPELLER P (UNTWISTED)
$\beta_{.7R}$
9° 12° 15° 18° 21° 24°
DUCT 3
12° 15° 18° 21°
DUCT 2
K_T
0 0.2 0.4 0.6 0.8 1.0 1.2 1.4 1.6
$\frac{T_s}{T}$
0 0.2 0.4 0.6 0.8 1.0

FIG. 58

STATIC VELOCITY SURVEY

REF. 7; GILL, W.J. HILLER AIRCRAFT CORP. ARD-224, 1959

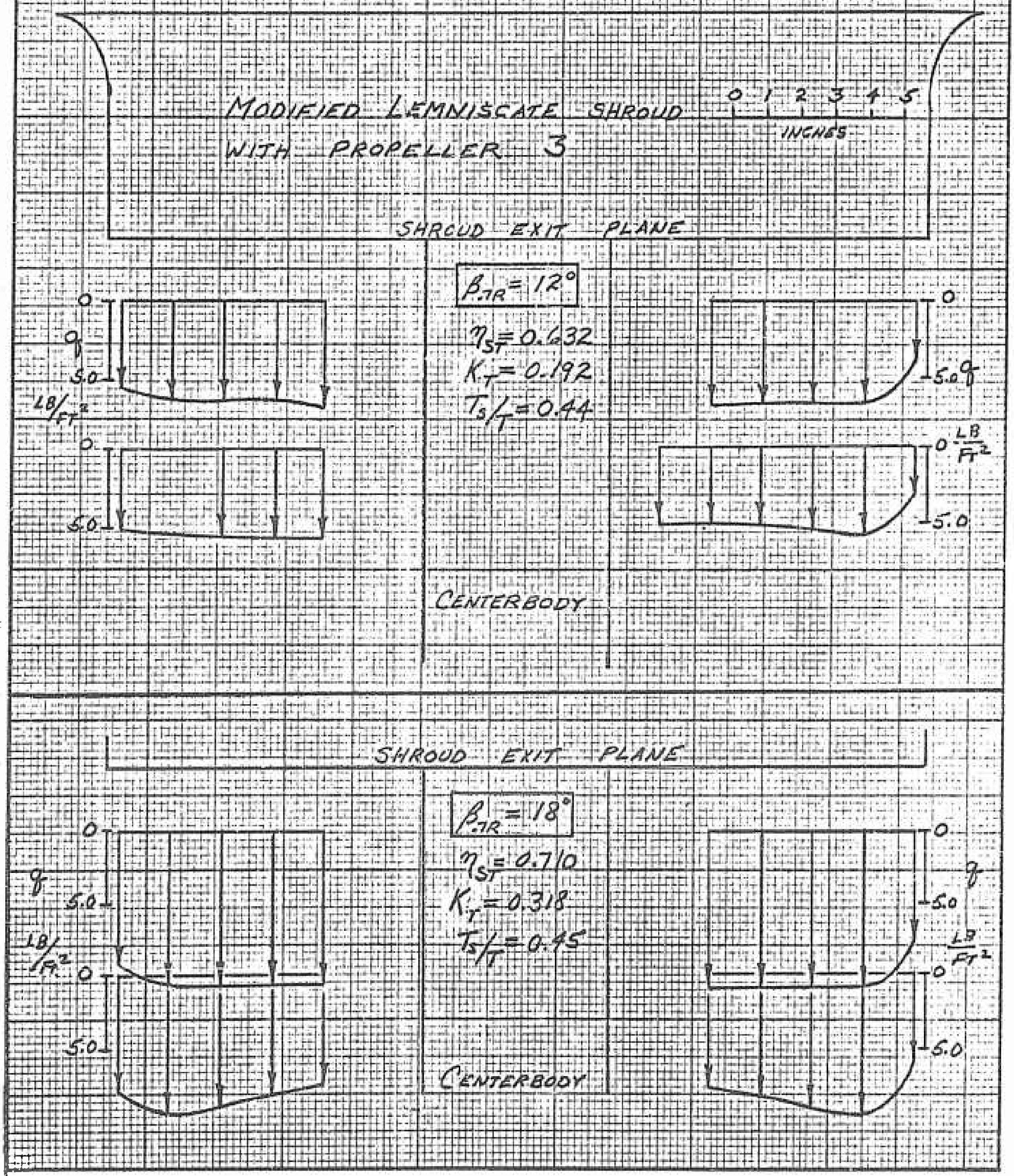

FIG 59

AXIAL PERFORMANCE

REF 7; GILL, W.J. HILLER AIRCRAFT CORP. ARD-224 1959

PROPELLER 3

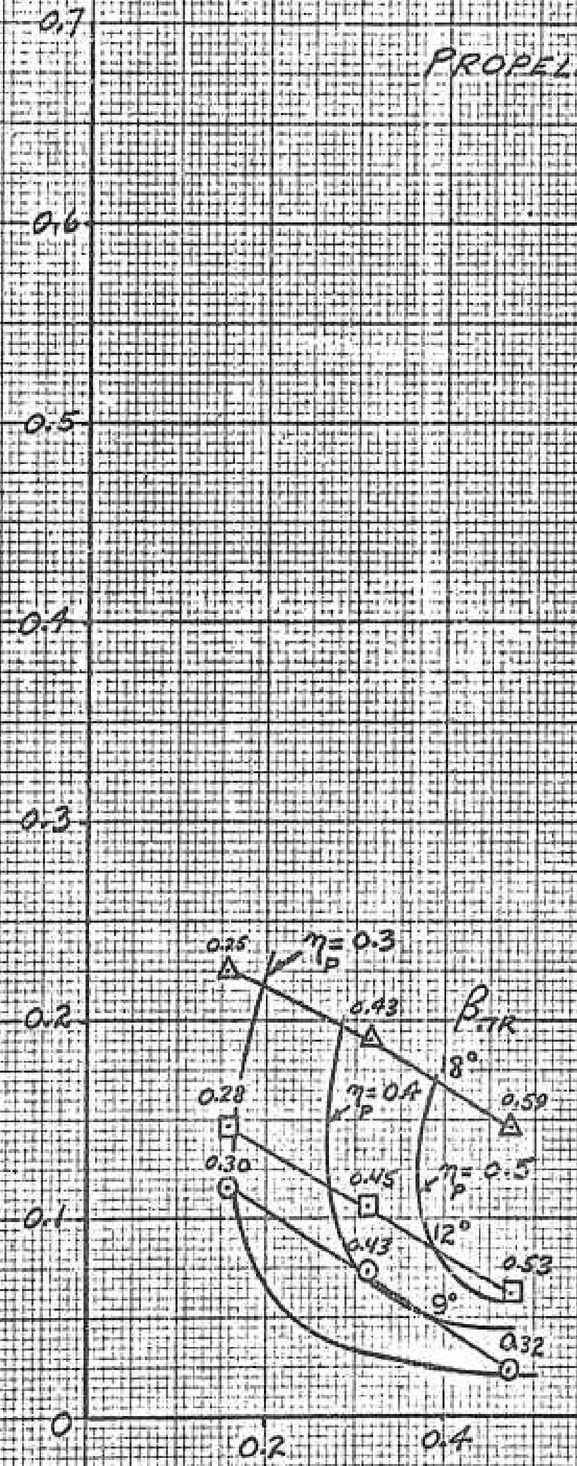

FIG. 60

AXIAL PERFORMANCE

REF. 7; GILL, W.T. HILLER AIRCRAFT CORP. ARD-224, 1959

PROPELLER 3 WITH DUCT 4

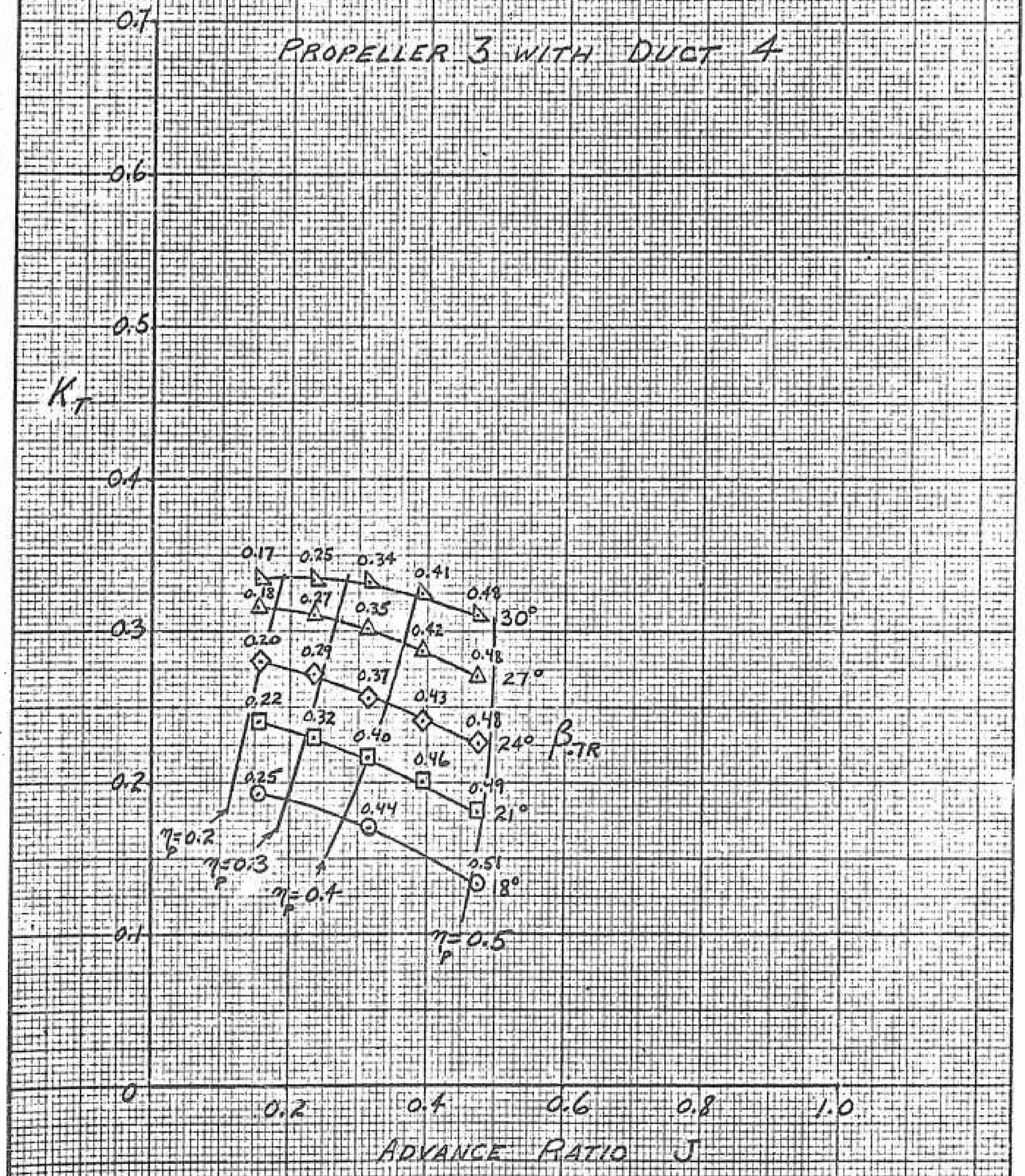

FIG. 61

NON-AXIAL PERFORMANCE
RESULTANT FORCE

REF. 7; GILL, W.J. HILLER AIRCRAFT CORP. ARD-224, 1959

PROPELLER 3 UNSHROUDED
$\beta_{.7R} = 12°$

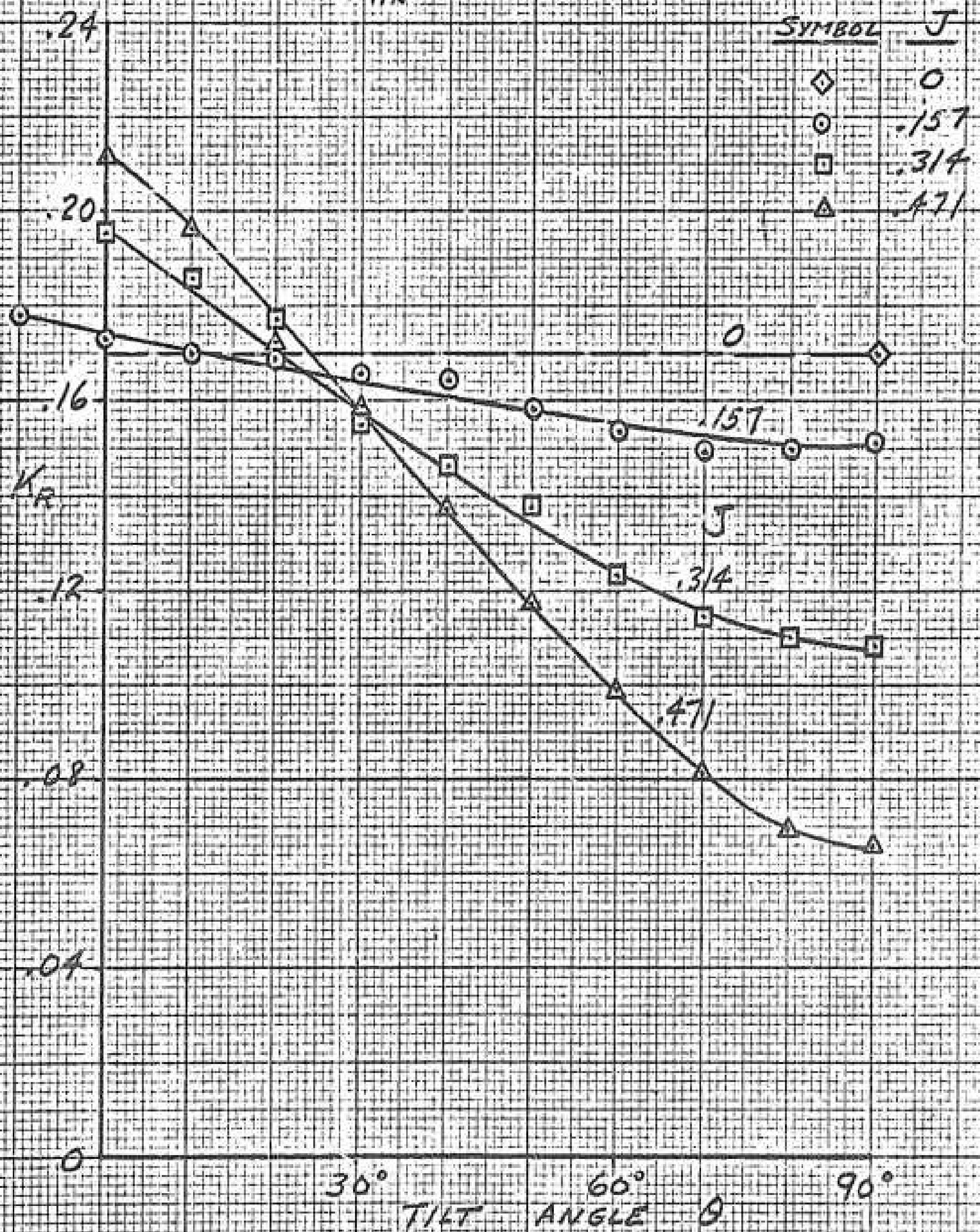

FIG. 62

NON-AXIAL PERFORMANCE
LIFT

REF. 7; GILL, W.J., HILLER AIRCRAFT CORP. ARD-224, 1959

PROPELLER 3 UNSHROUDED

$\beta_{.7R} = 12°$

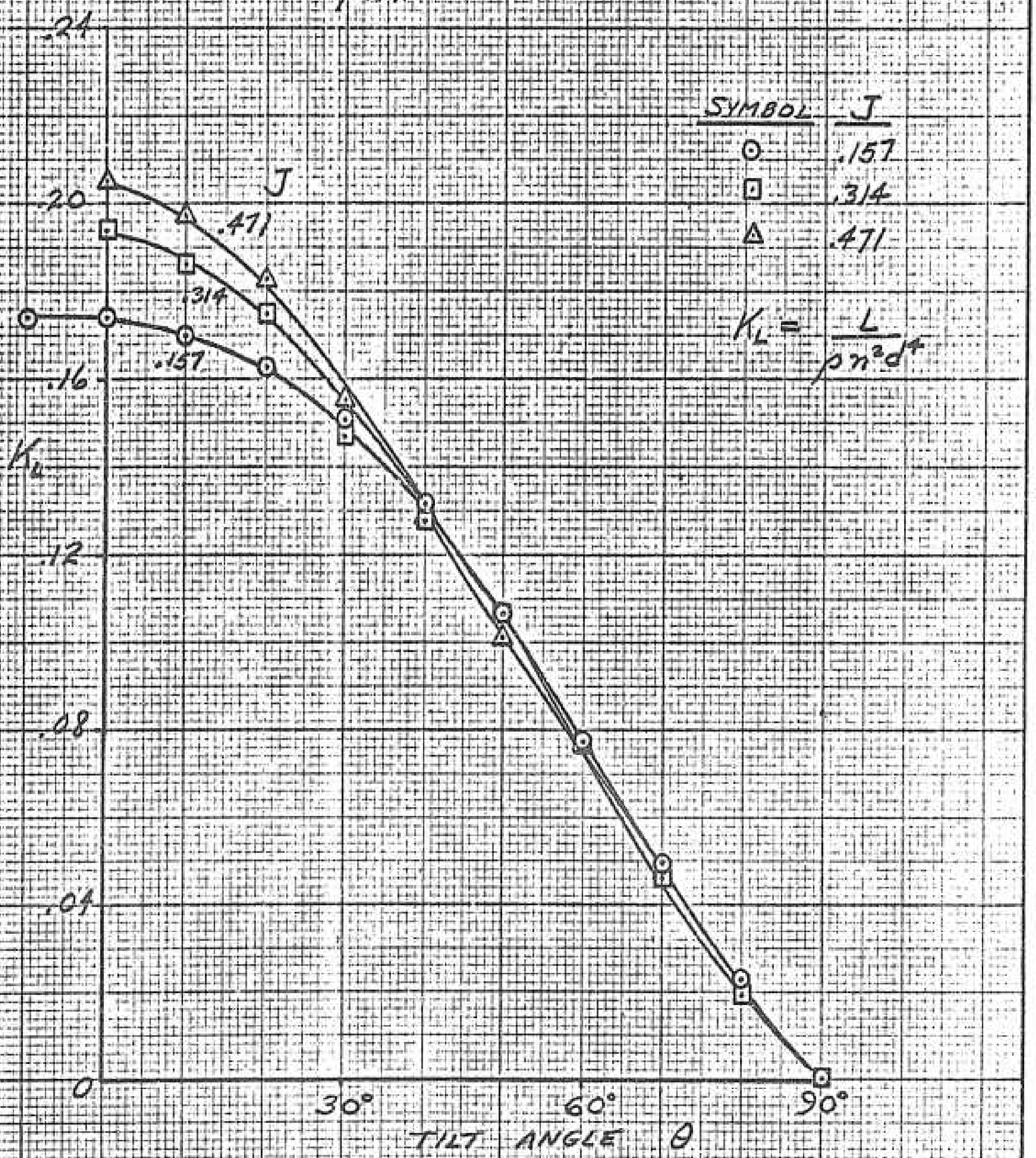

PREPARED GBL 2-25-60 PAGE 200
CHECKED REPORT NO.
REVISED MODEL

REPUBLIC AVIATION

FIG. 63

NON-AXIAL PERFORMANCE

DRAG

REF. 7; GILL, W.J., HILLER AIRCRAFT CORP. ARD-224, 1959

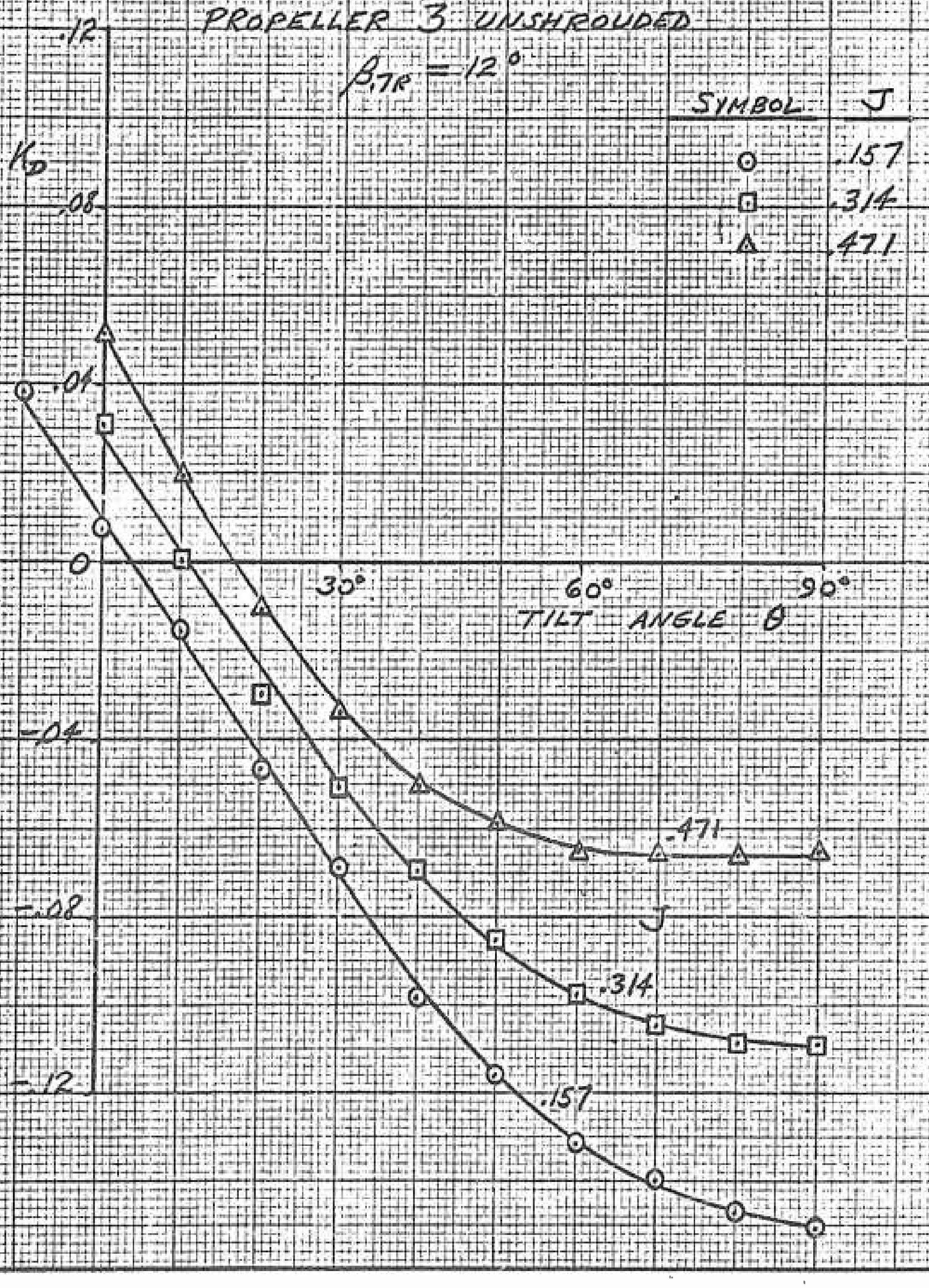

FIG. 64

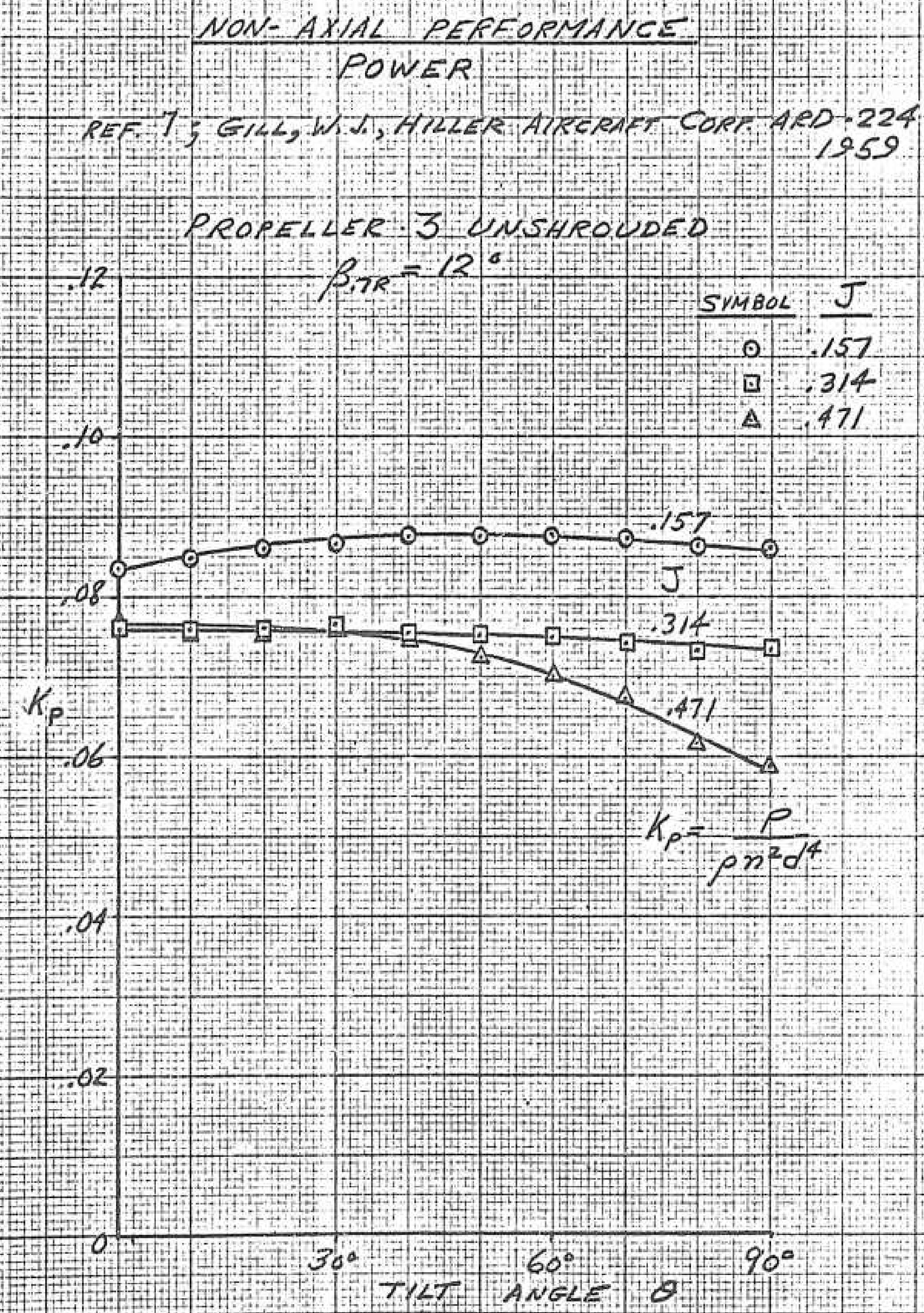

1-10A
2/49

FIG 65

NON-AXIAL PERFORMANCE
MOMENT

REF. 7 ; GILL, W.J., HILLER AIRCRAFT CORP. ARD-224, 1959

PROPELLER 3 UNSHROUDED
$\beta_{.7R} = 12°$

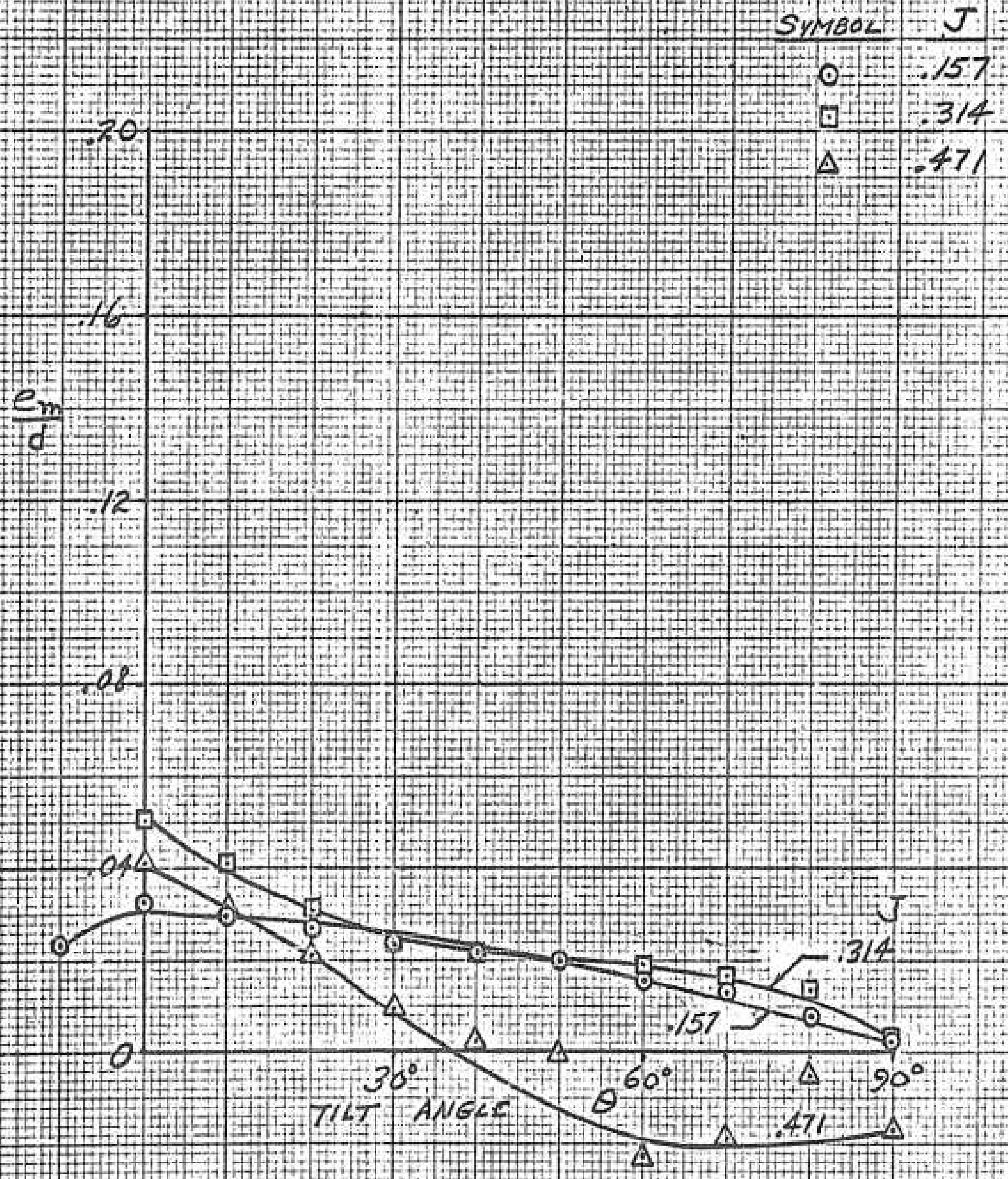

FIG. 66

NON-AXIAL PERFORMANCE

RESULTANT FORCE

REF 7: GILL, W. J., HILLER AIRCRAFT CORP. ARD-224, 1959

PROPELLER 3 UNSHROUDED

$\beta_m = 18°$

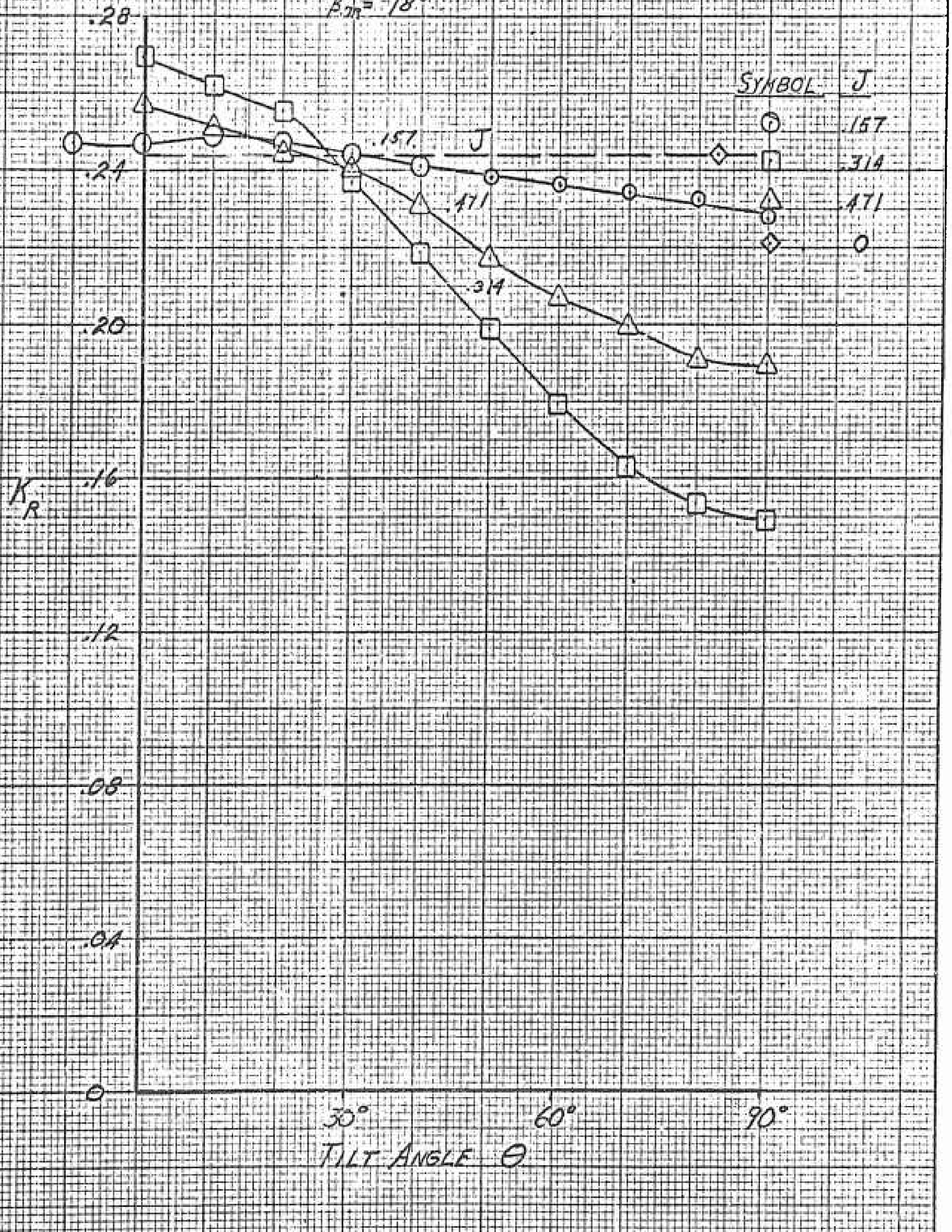

FIG. 67
NON-AXIAL PERFORMANCE
LIFT
PROPELLER 3 UNSHROUDED
REF. 7: GILL, W.J., HILLER AIRCRAFT CORP. ARD-224, 1959

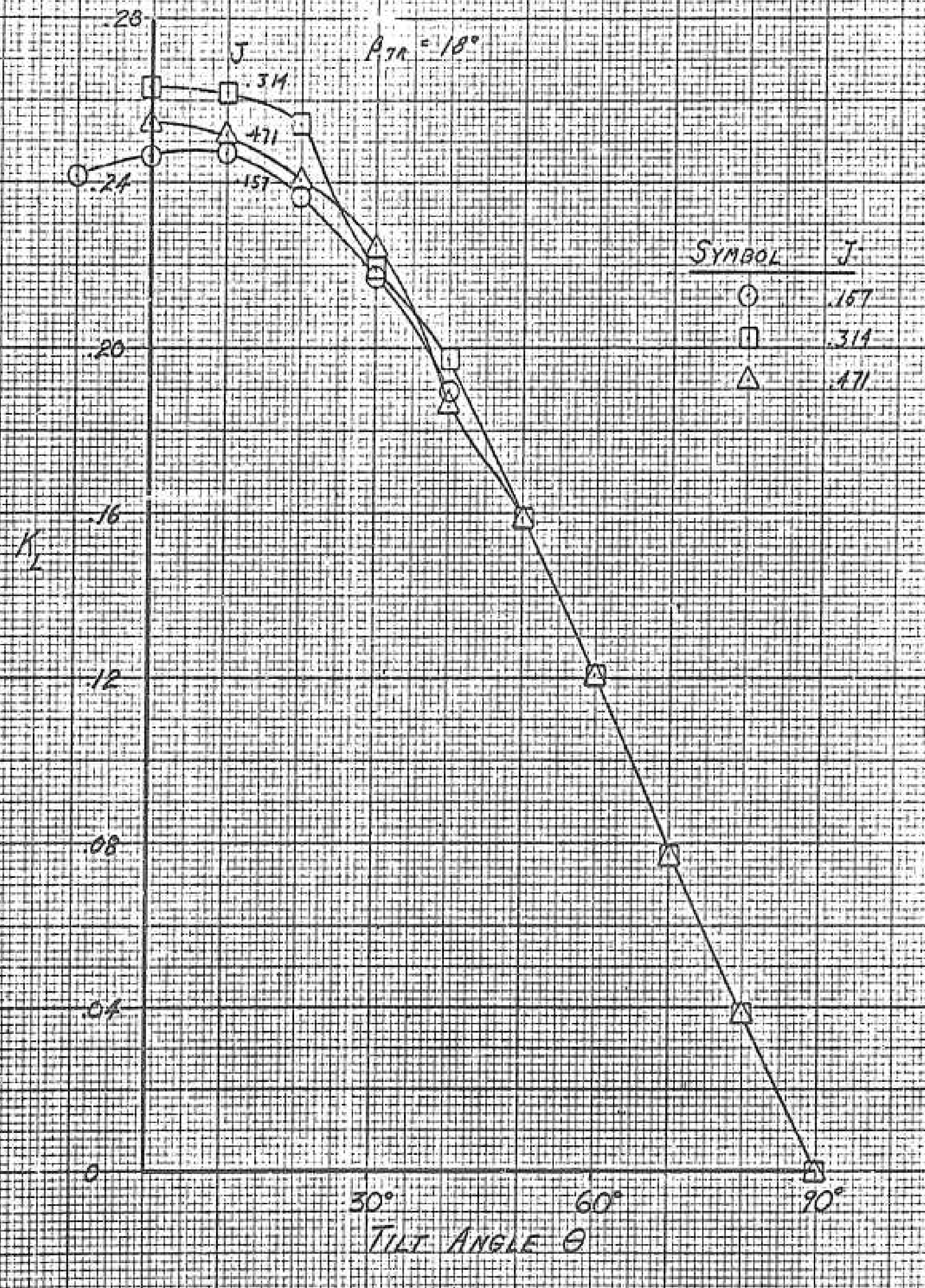

FIG. 68

NON-AXIAL PERFORMANCE

DRAG

REF. 7; GILL, W.J., HILLER AIRCRAFT CORP. ARD-224, 1959

PROPELLE 3 UNSHROUDED

$\beta_{.7R} = 18°$

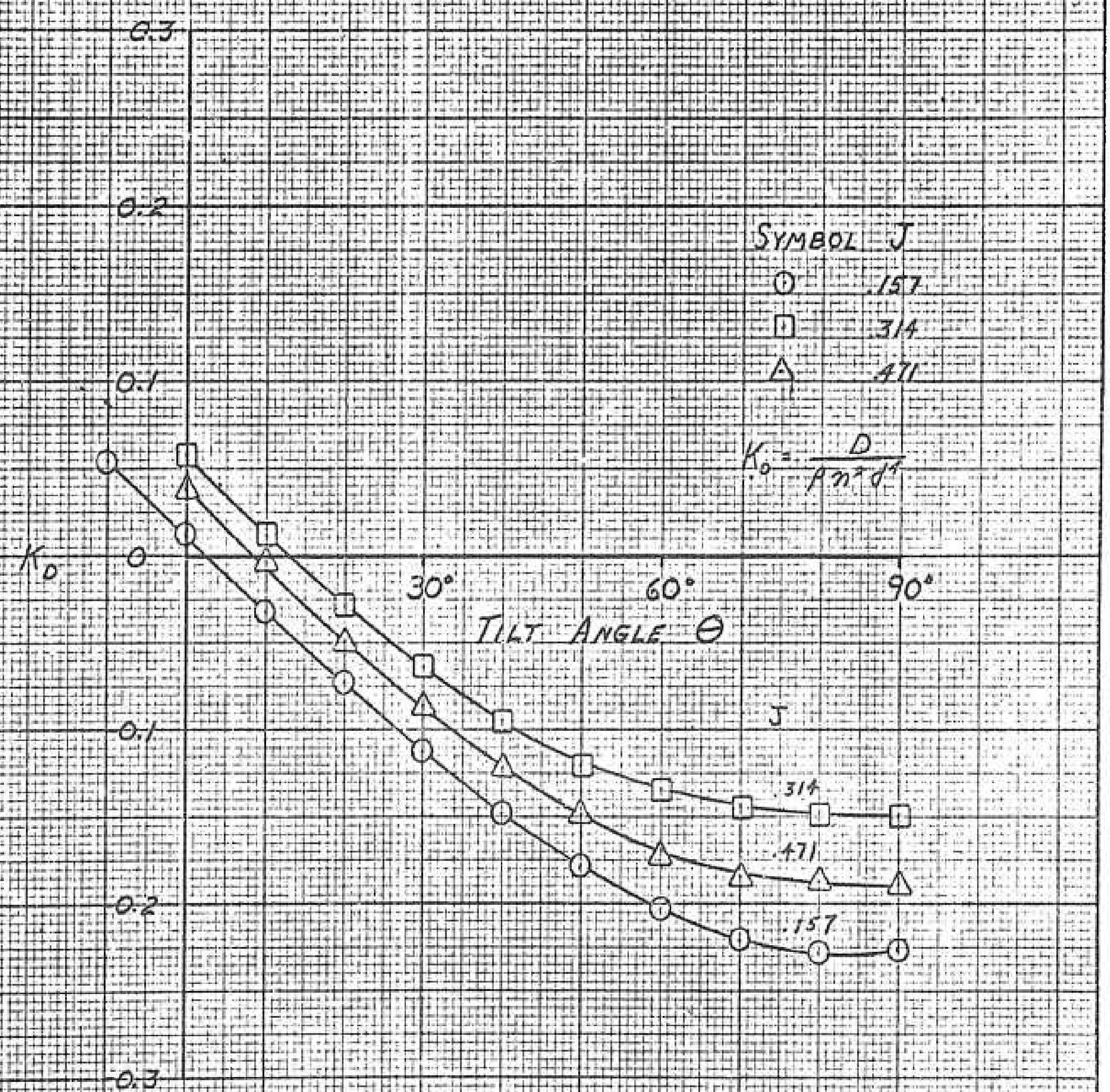

FIG. 69

NON-AXIAL PERFORMANCE

POWER

REF. 7; GILL, W. J., HILLER AIRCRAFT CORP. ARD-224, 1959

PROPELLER 3 UNSHROUDED

$\beta_{.75} = 18°$

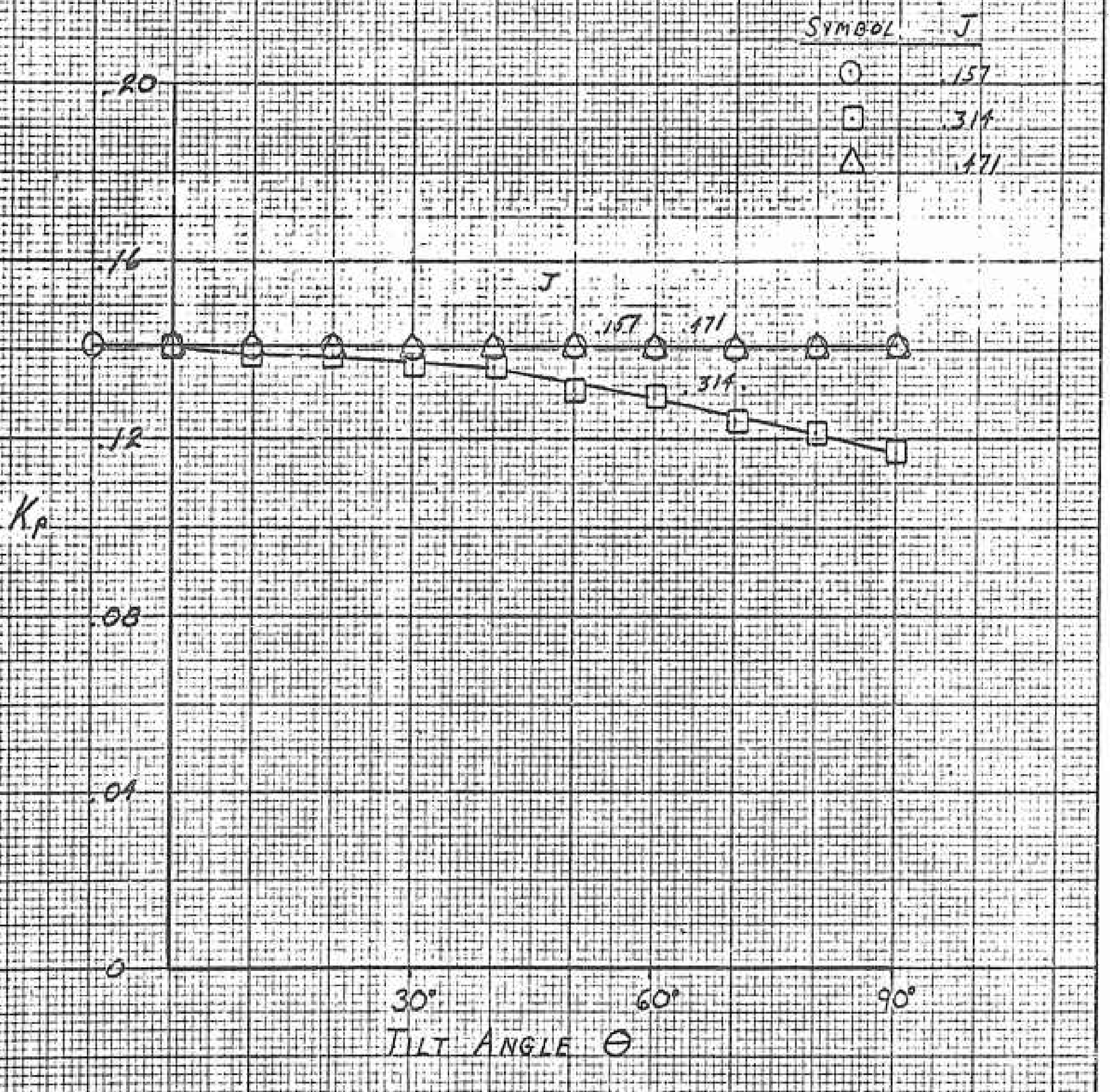

FIG. 70

NON-AXIAL PERFORMANCE

MOMENTS

REF. 7, GILL, W.J, HILLER AIRCRAFT CORP. ARD-221, 1959

PROPELLER 3 UNSHROUDED

$\beta_{.7R} = 18°$

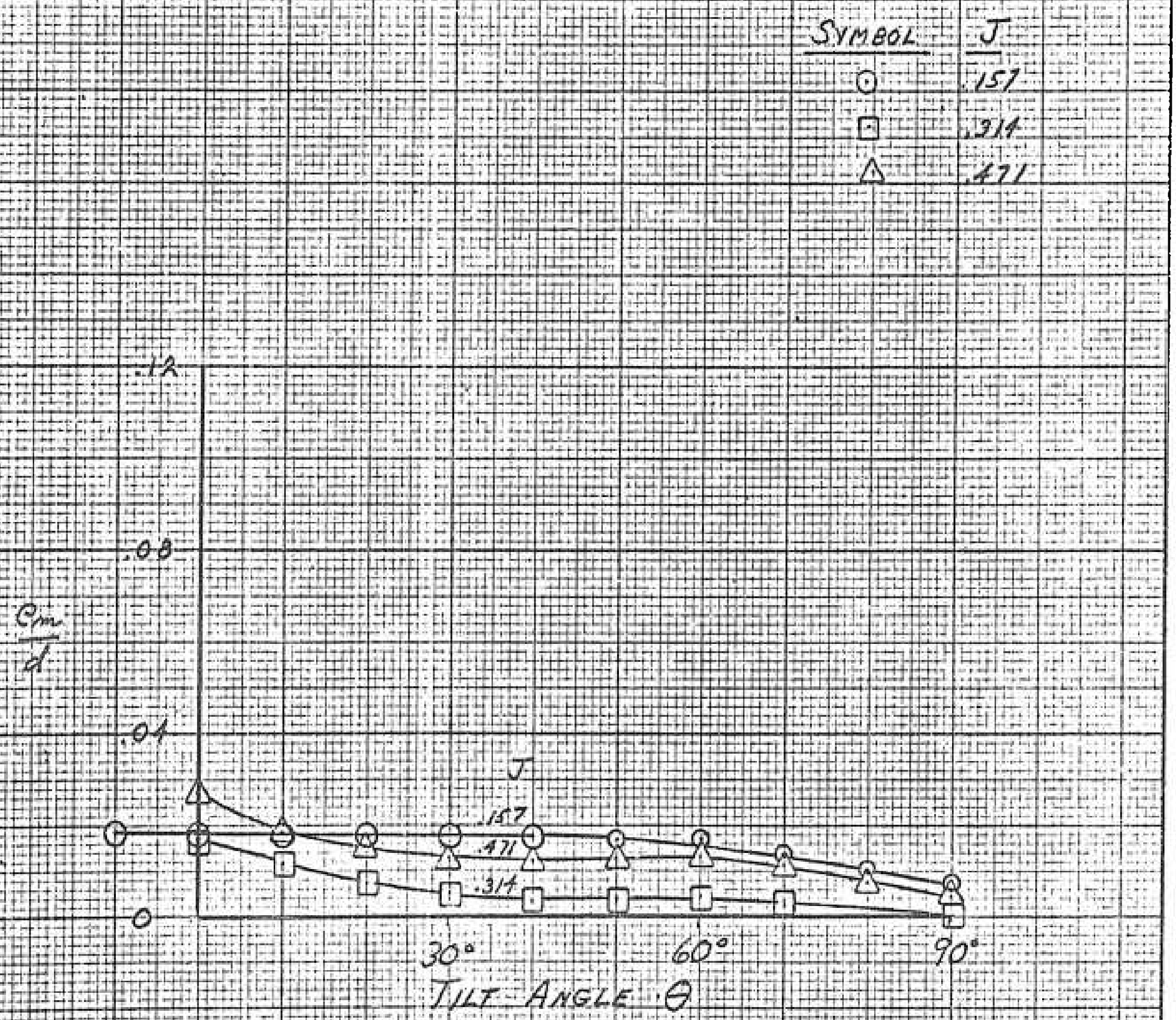

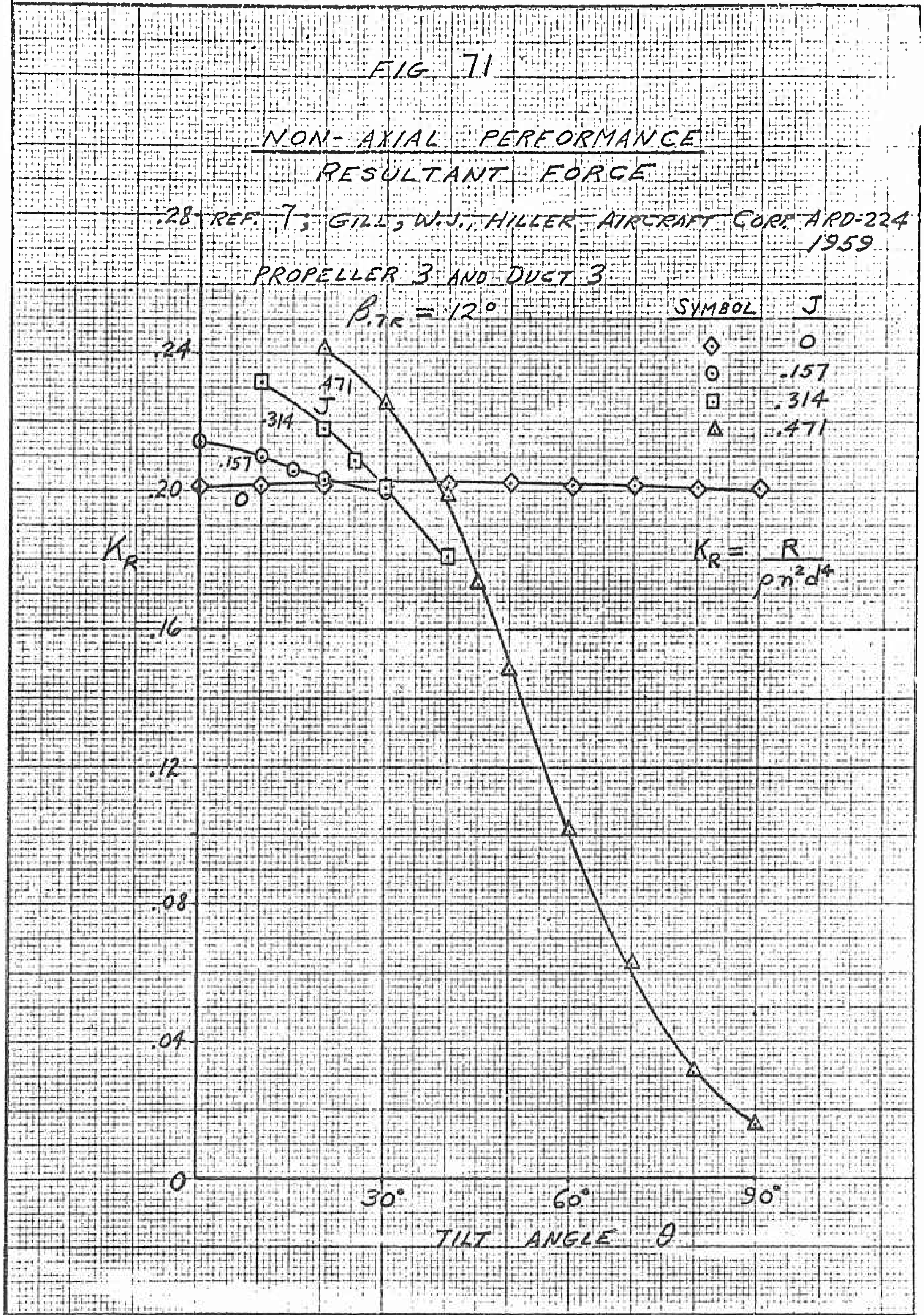
FIG 71
NON-AXIAL PERFORMANCE
RESULTANT FORCE
REF. 7; GILL, W.J., HILLER AIRCRAFT CORP. ARD-224 1959
PROPELLER 3 AND DUCT 3
$\beta_{.7R} = 12°$
SYMBOL J
0
.157
.314
.471
$K_R = \frac{R}{\rho n^2 d^4}$
K_R
.28
.24
.20
.16
.12
.08
.04
0
30°
60°
90°
TILT ANGLE θ

FIG. 72

NON-AXIAL PERFORMANCE
LIFT

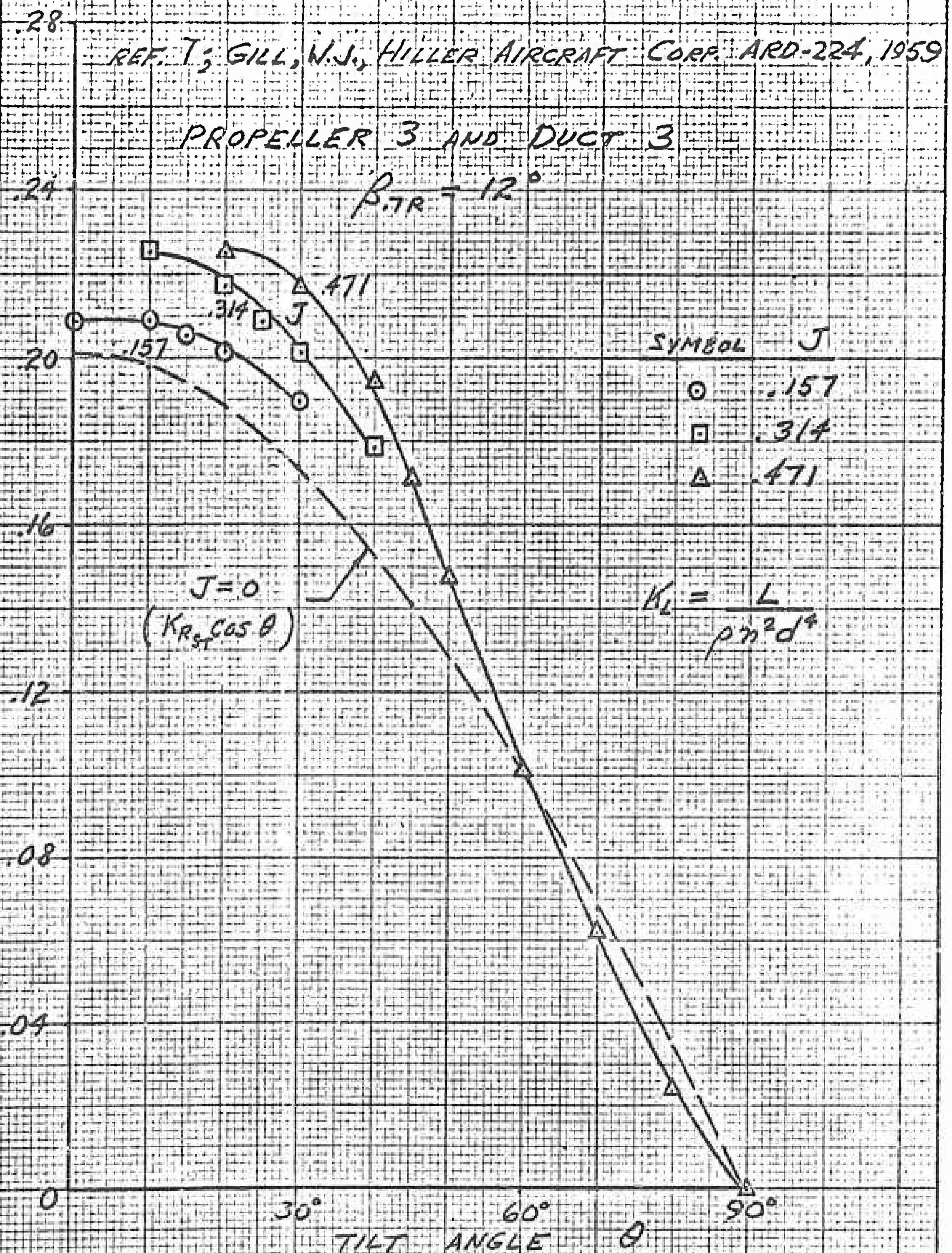

FIG. 73

NON-AXIAL PERFORMANCE
DRAG

REF. 7; GILL, W.J., HILLER AIRCRAFT CORP. ARD-224, 1959

PROPELLER 3 AND DUCT 3

$\beta_{.7R} = 12°$

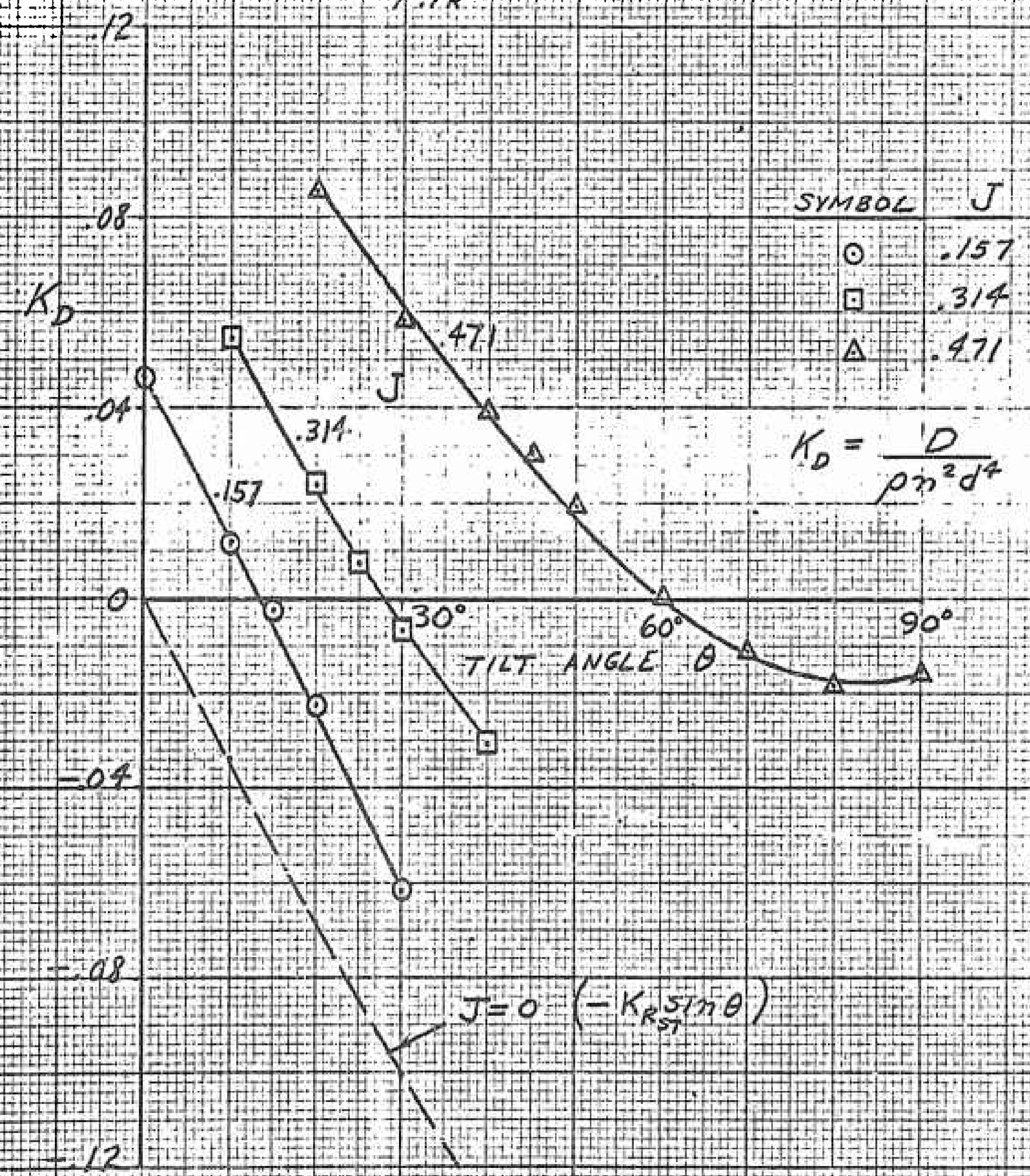

REPUBLIC AVIATION

FIG. 74

NON-AXIAL PERFORMANCE
SHROUD LIFT

REF. 7; GILL, W.J., HILLER AIRCRAFT CORP., ARD-224, 1959

PROPELLER 3 AND DUCT 3
$\beta_{.7R} = 12°$

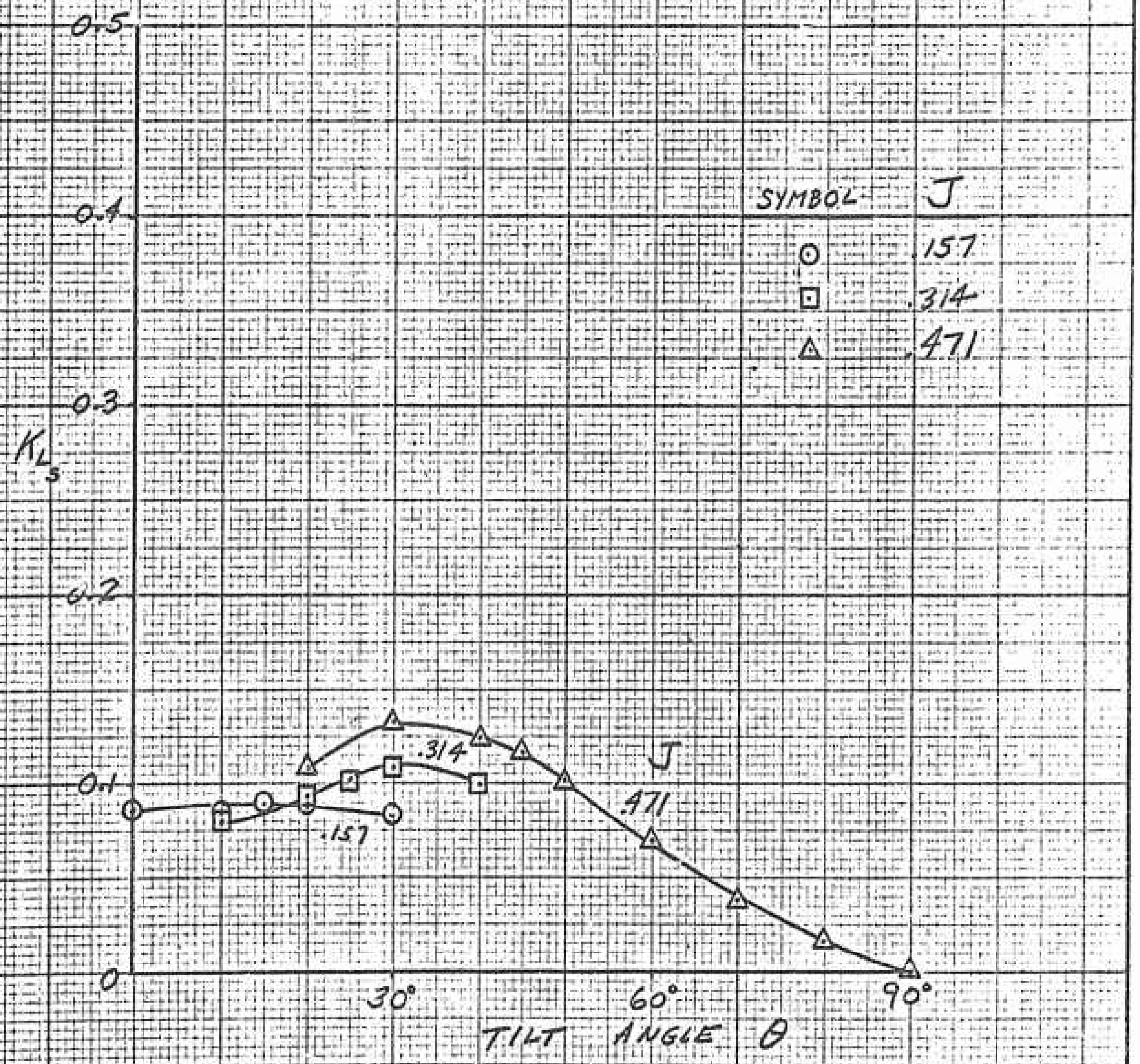

FIG. 75

NON-AXIAL PERFORMANCE
LIFT DIVISION

REF. 7; GILL, W.J., HILLER AIRCRAFT CORP. ARD-224, 1959

PROPELLER 3 AND DUCT 3

$\beta_{.7R} = 12°$

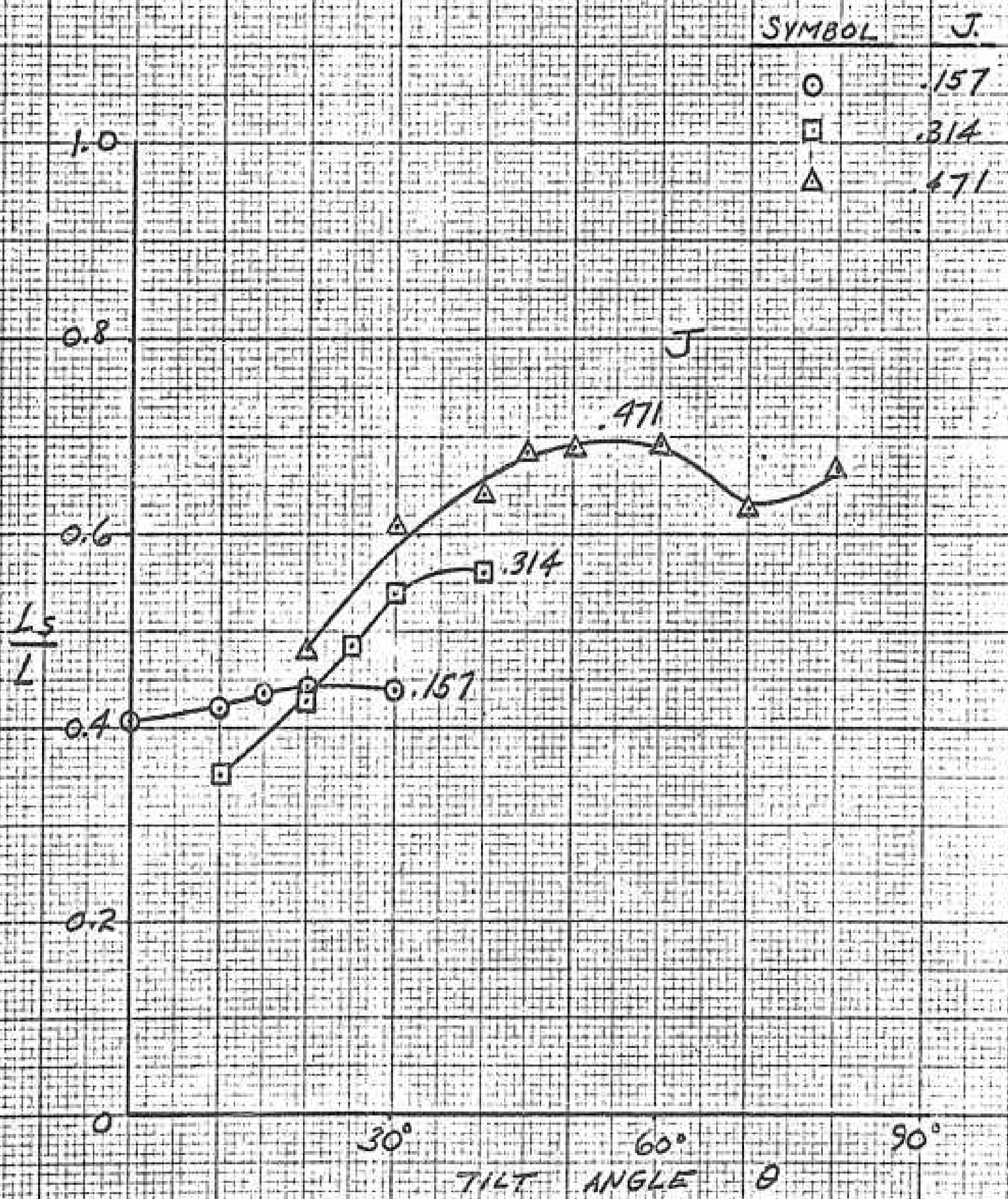

FIG. 76

NON-AXIAL PERFORMANCE
SHROUD DRAG

REF. 7; GILL, W.J., HILLER AIRCRAFT CORP., ARD-224, 1959

PROPELLER 3 AND DUCT 3

$\beta_{.7R} = 12°$

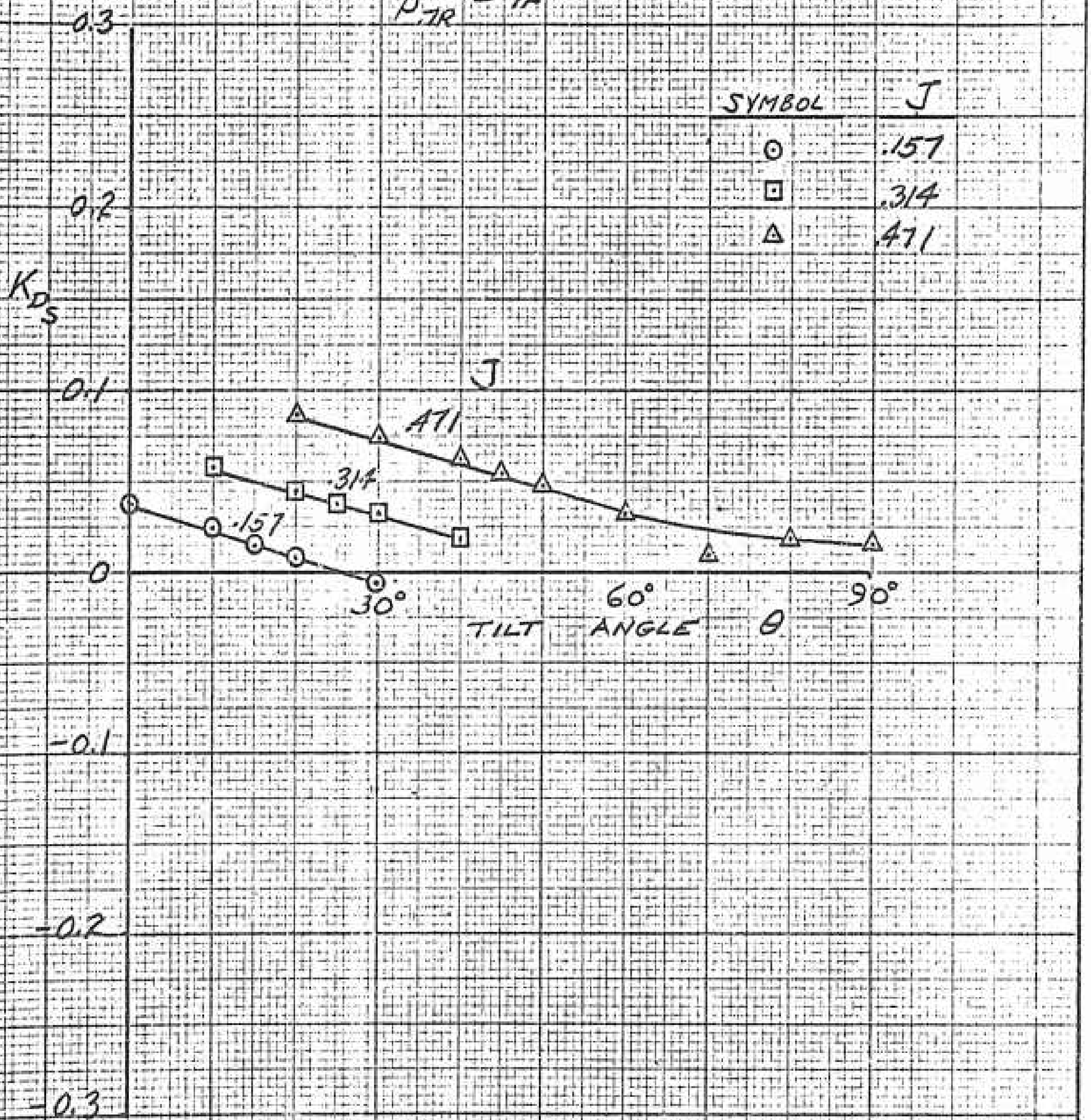

FIG 77

NON-AXIAL PERFORMANCE
POWER

REF. 7; GILL; W.J. HILLER AIRCRAFT CORP. ARD-224, 1959

PROPELLER 3 AND DUCT 3

$\beta_{.7R} = 12°$

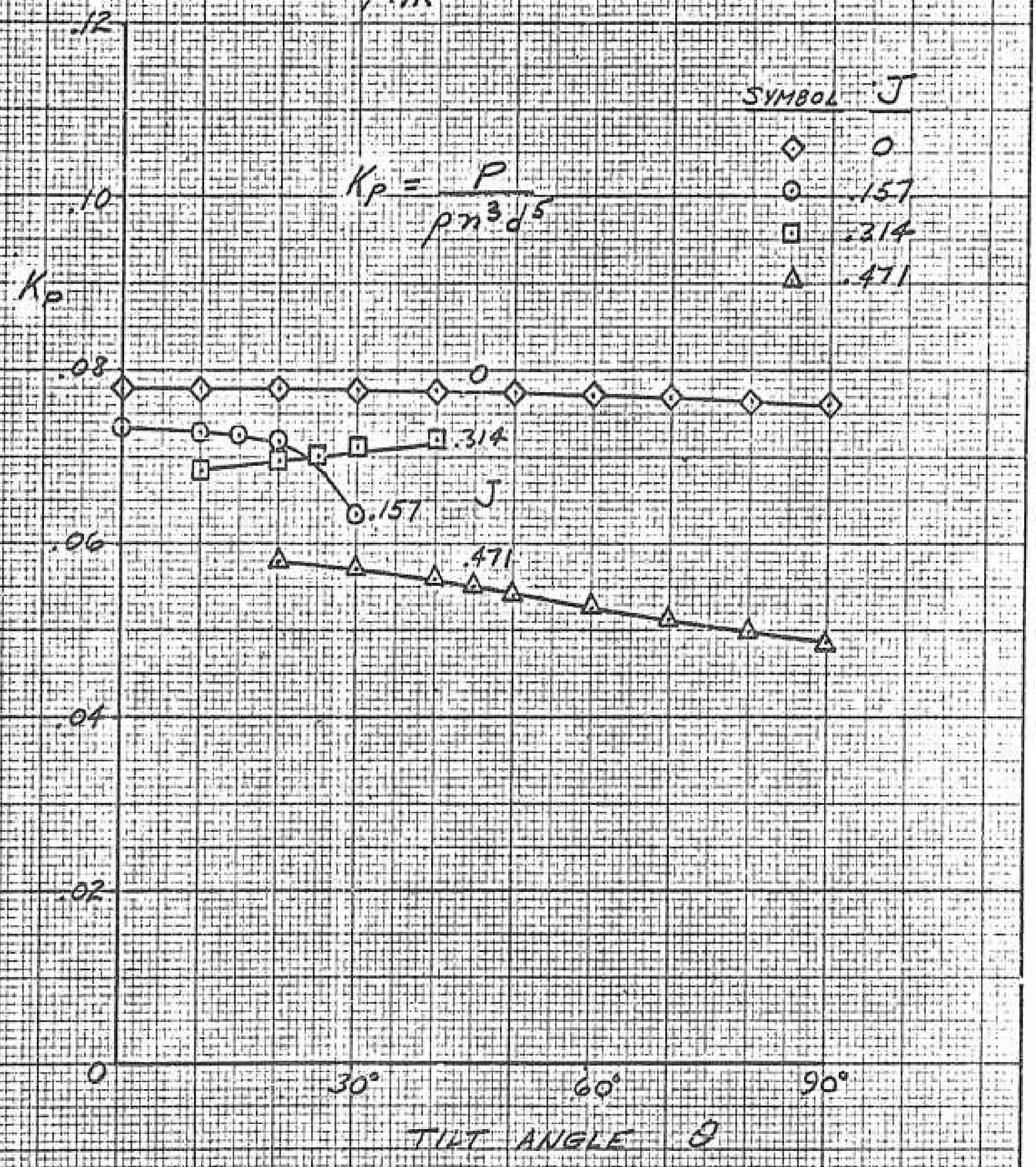

FIG 78

NON-AXIAL PERFORMANCE
MOMENTS

REF 7; GILL, W.J., HILLER AIRCRAFT CORP. ARD-224, 1959

PROPELLER 3 AND DUCT 3
$\beta_{.7R} = 12°$

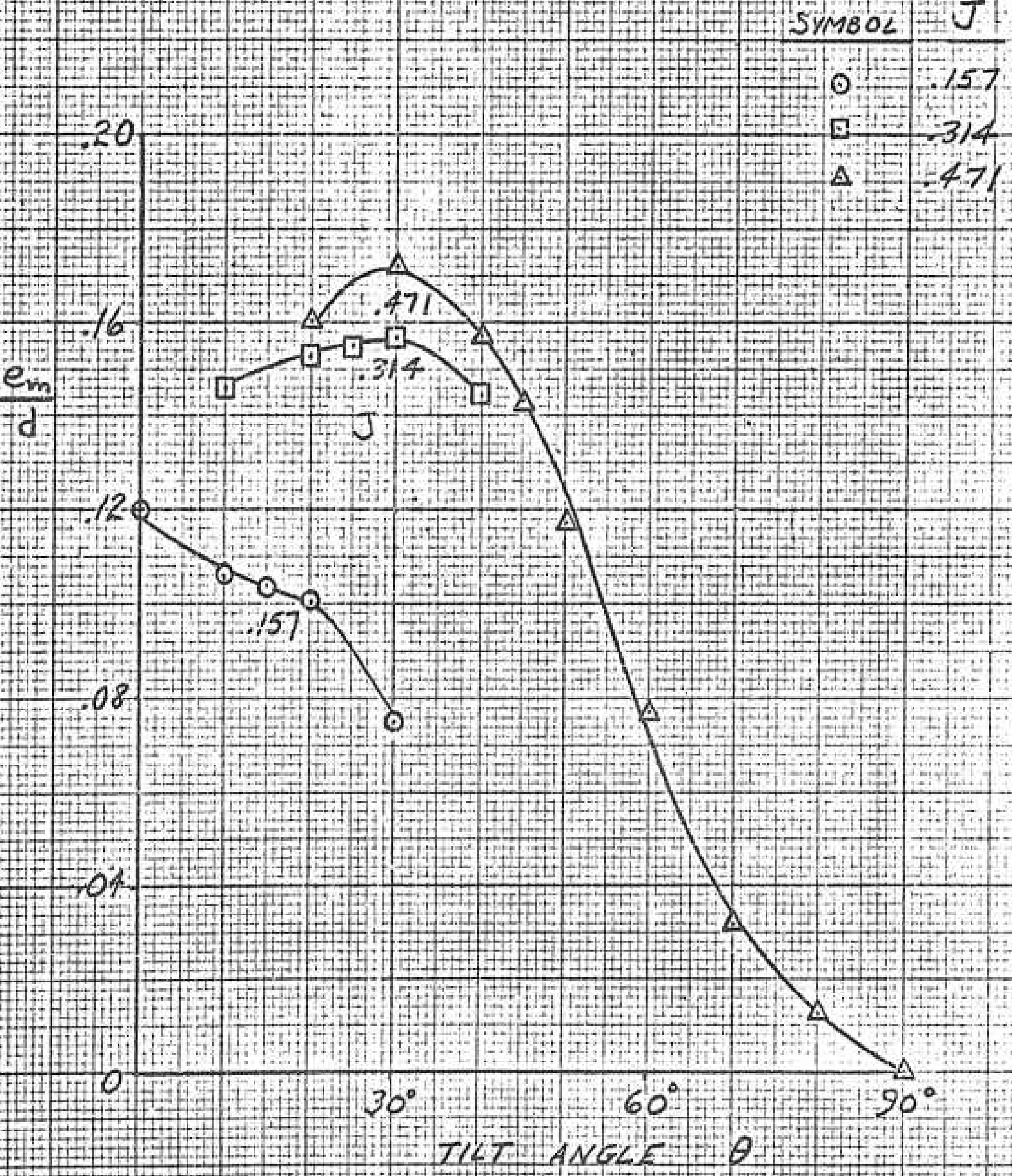

FIG 79

NON-AXIAL PERFORMANCE
PROPELLER MOMENT

REF. 7; GILL, W.J., HILLER AIRCRAFT CORP. ARD-224, 1959

PROPELLER 3 AND DUCT 3

$\beta_{.7R} = 12°$

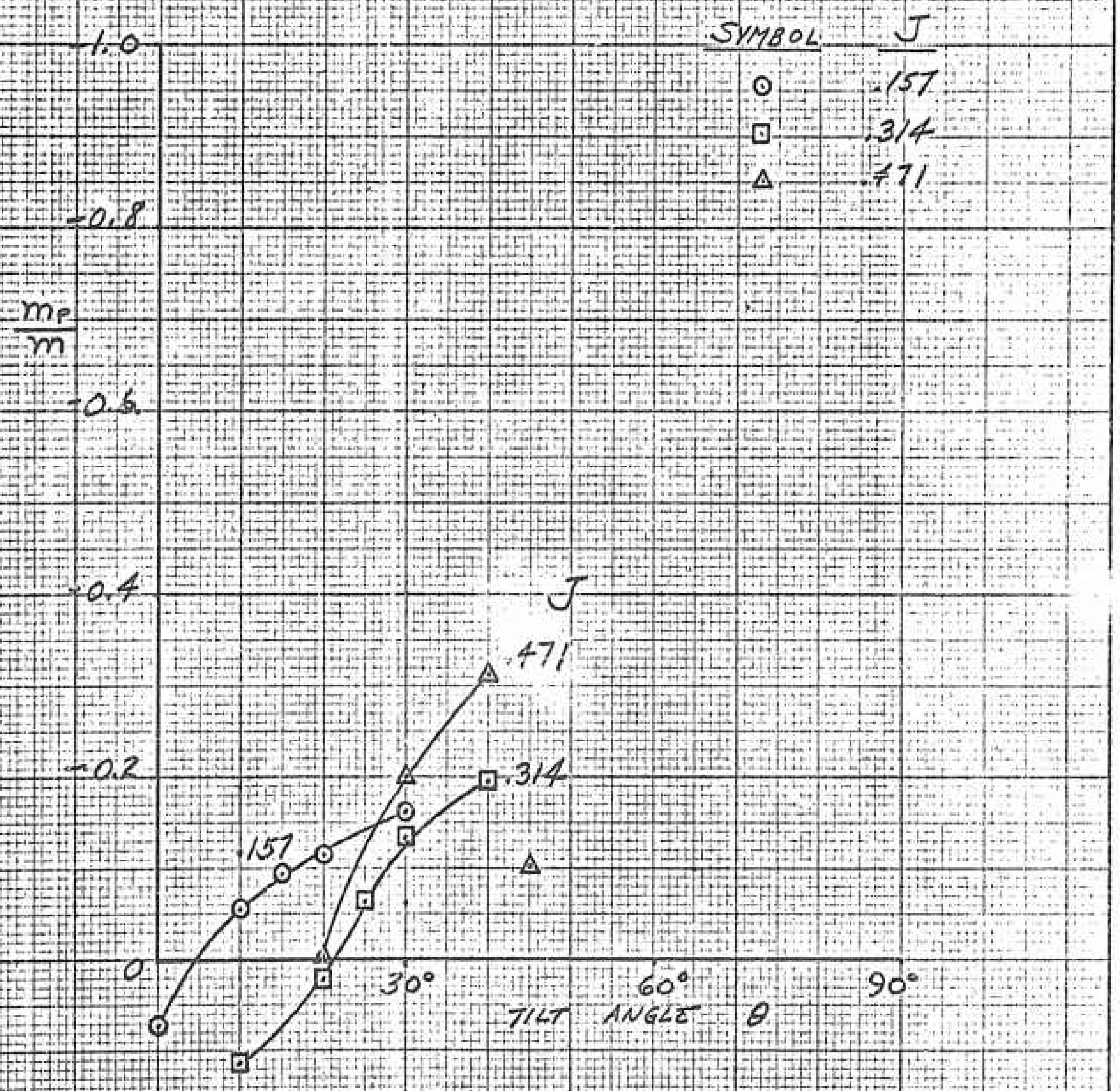

PREPARED J.B.L. 4-12-60

CHECKED

REVISED

REPORT NO.

MODEL

FIG. 80

NON-AXIAL PERFORMANCE

MEAN VELOCITY RATIOS AND DRAG

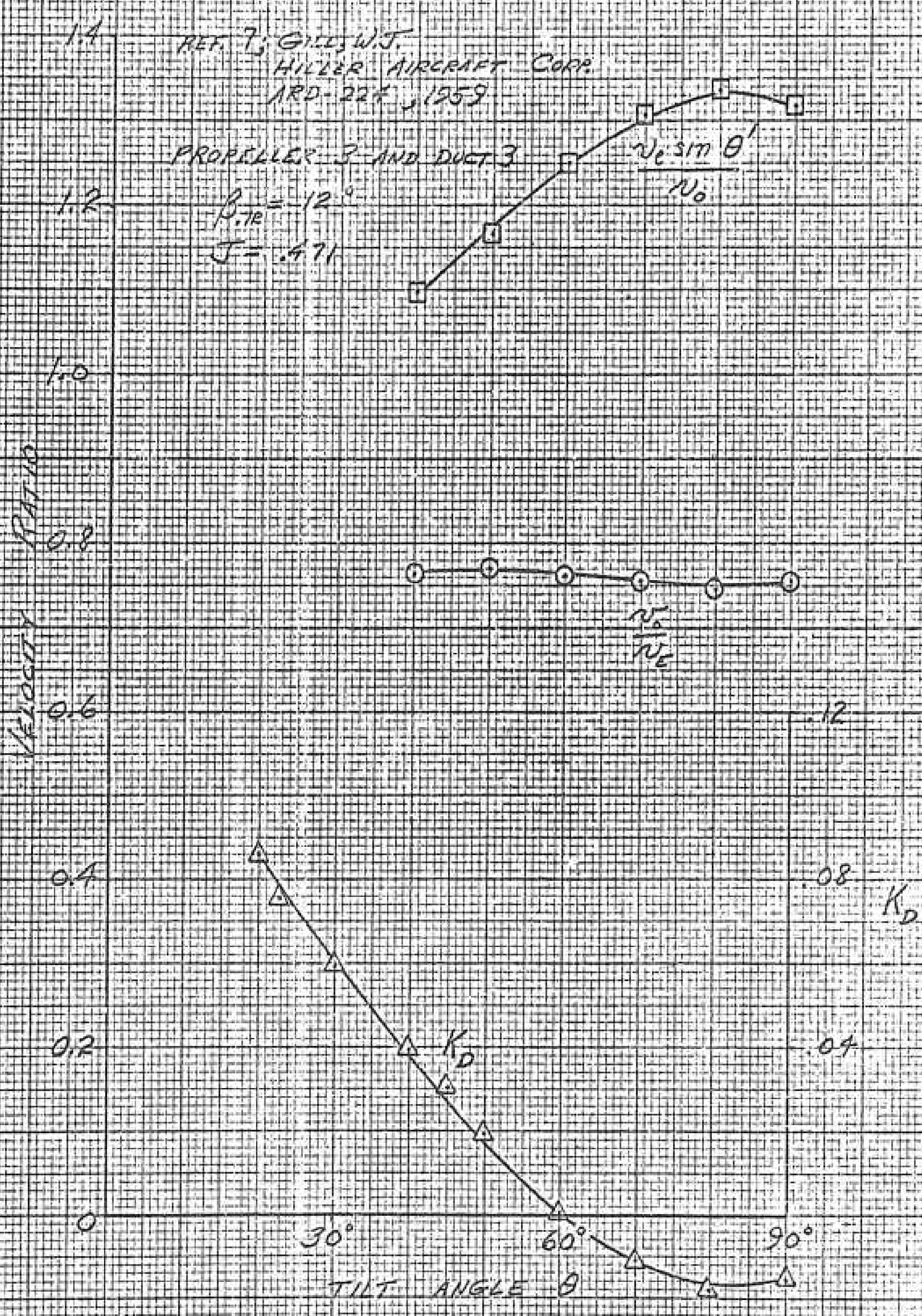

FIG 81

NON-AXIAL EXIT VELOCITY SURVEY

REF 7; GILL, W.J.
HILLER AIRCRAFT CORP
ARD-224, 1959

$\beta_{.7R} = 12°$ $J = .471$

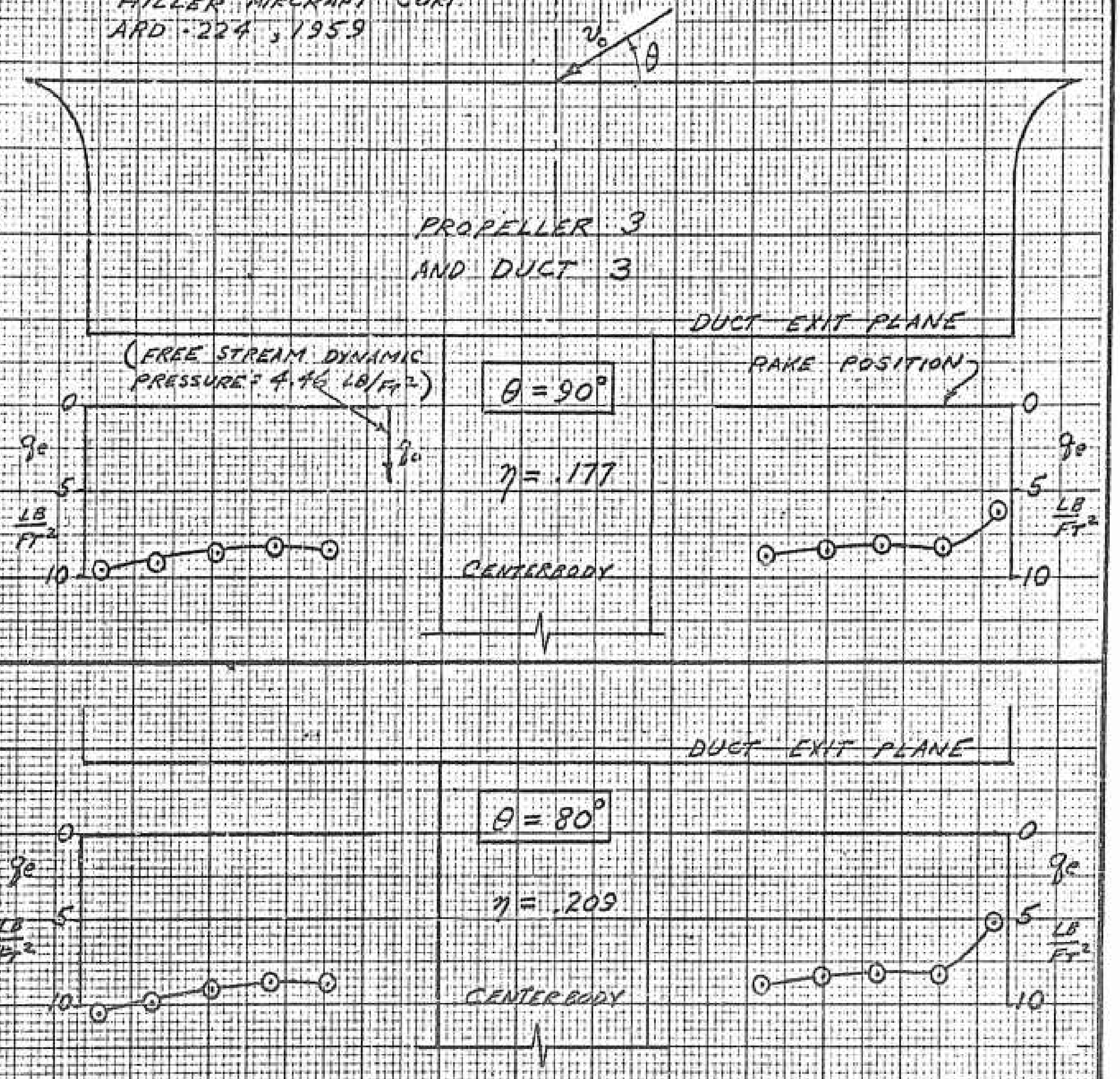

FIG. 81 (CONT.)

NON-AXIAL EXIT VELOCITY SURVEY

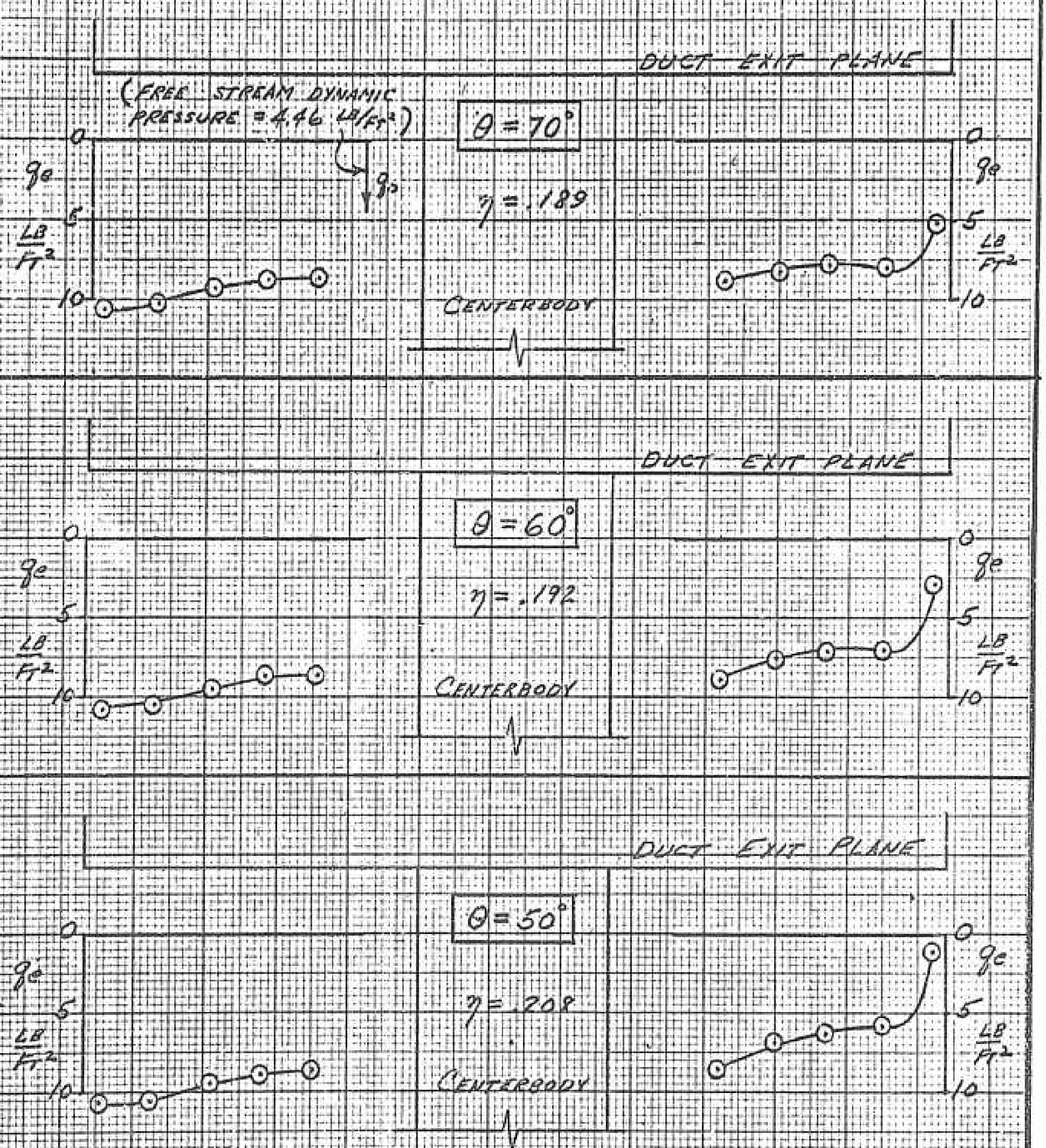

FIG. 81 (CONT.)

NON-AXIAL EXIT VELOCITY SURVEY

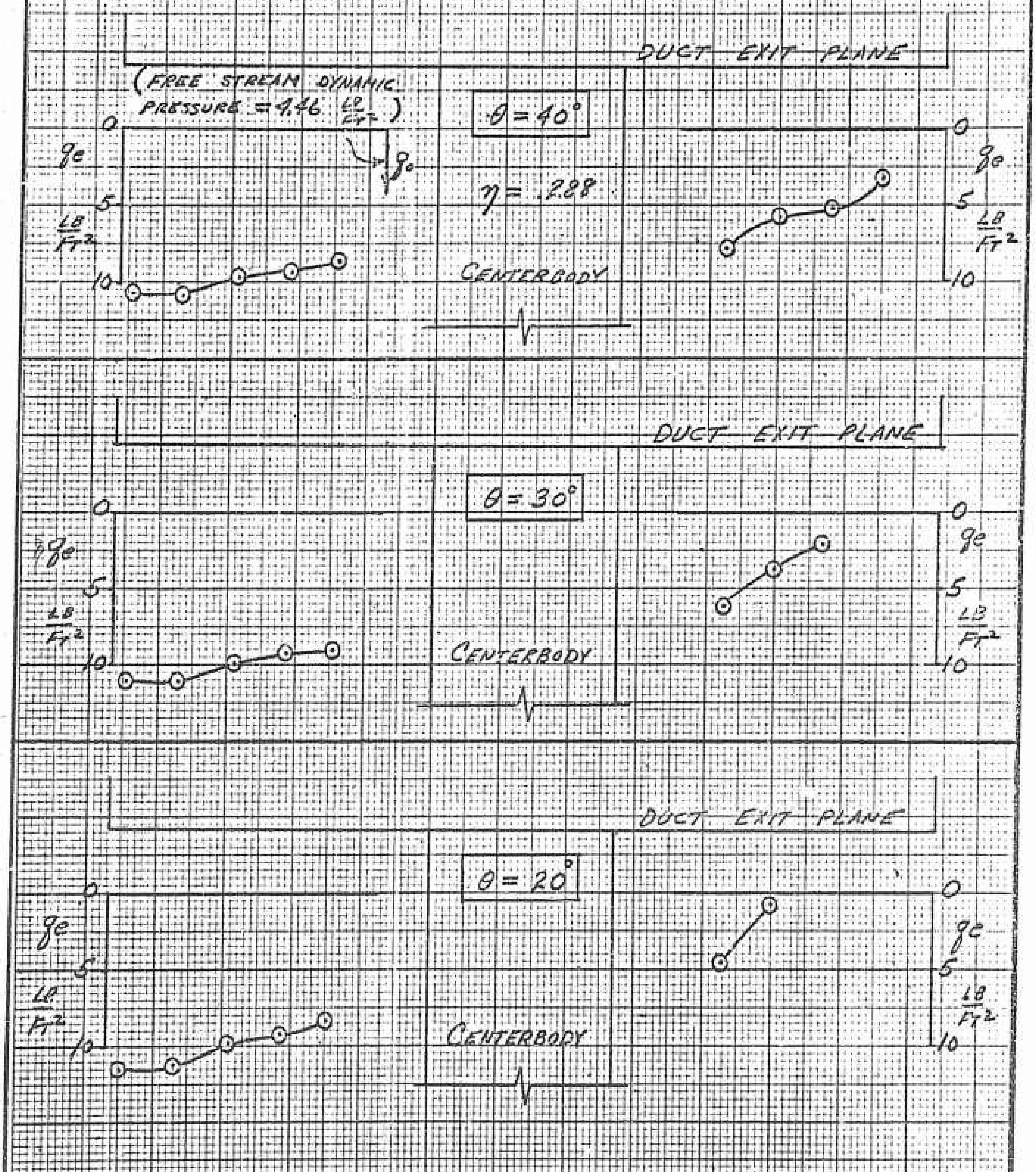

FIG. 82

NON-AXIAL PERFORMANCE

RESULTANT FORCE

REF. 7; GILL, W.J., HILLER AIRCRAFT CORP. ARD-224; 1959

PROPELLER 3 AND DUCT 3

$\beta_{.7R} = 18°$

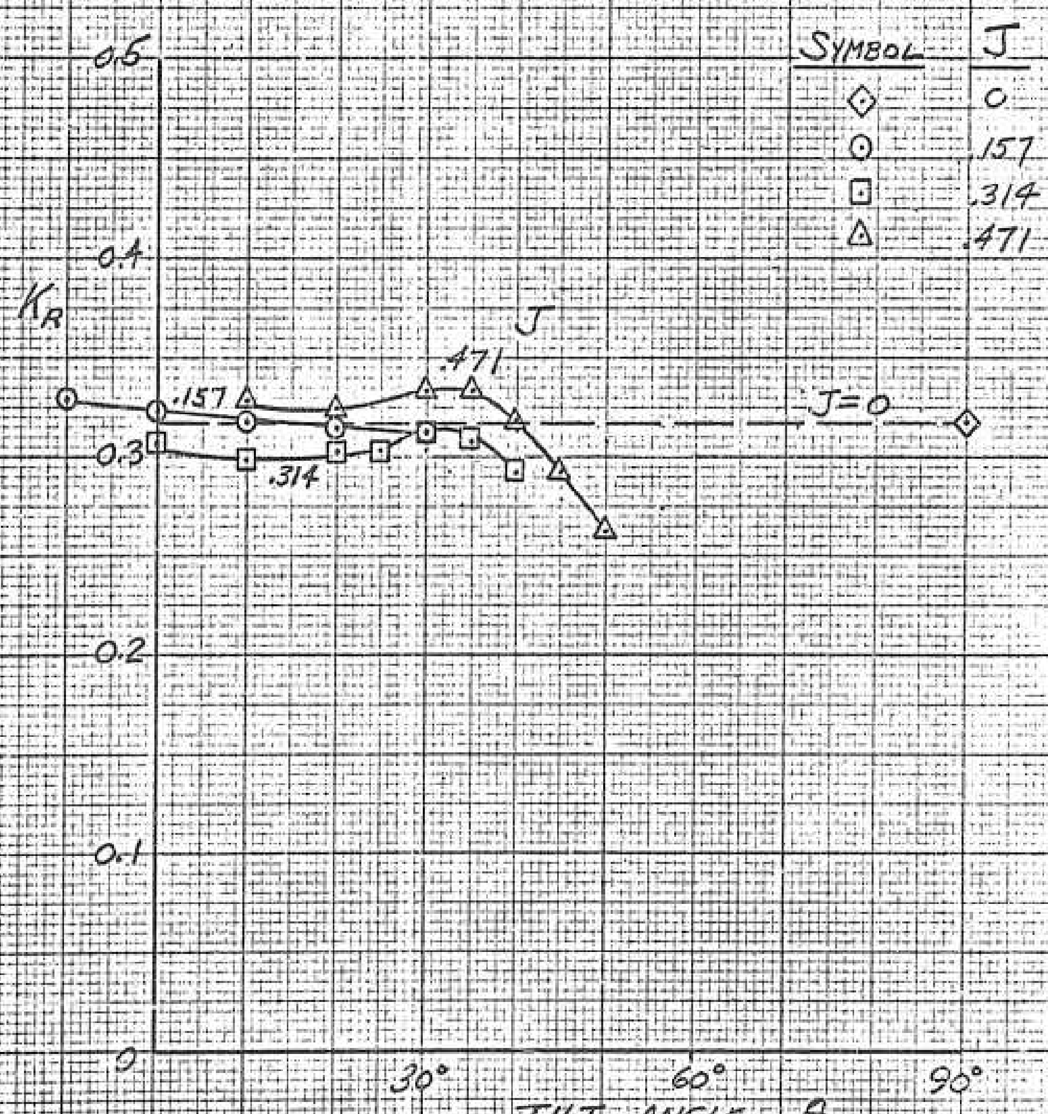

FIG. 83

NON-AXIAL PERFORMANCE
LIFT

REF. 7; GILL, W.J. HILLER AIRCRAFT CORP. ARD-224, 1959

PROPELLER 3 AND DUCT 3
$\beta_{.7R} = 18°$

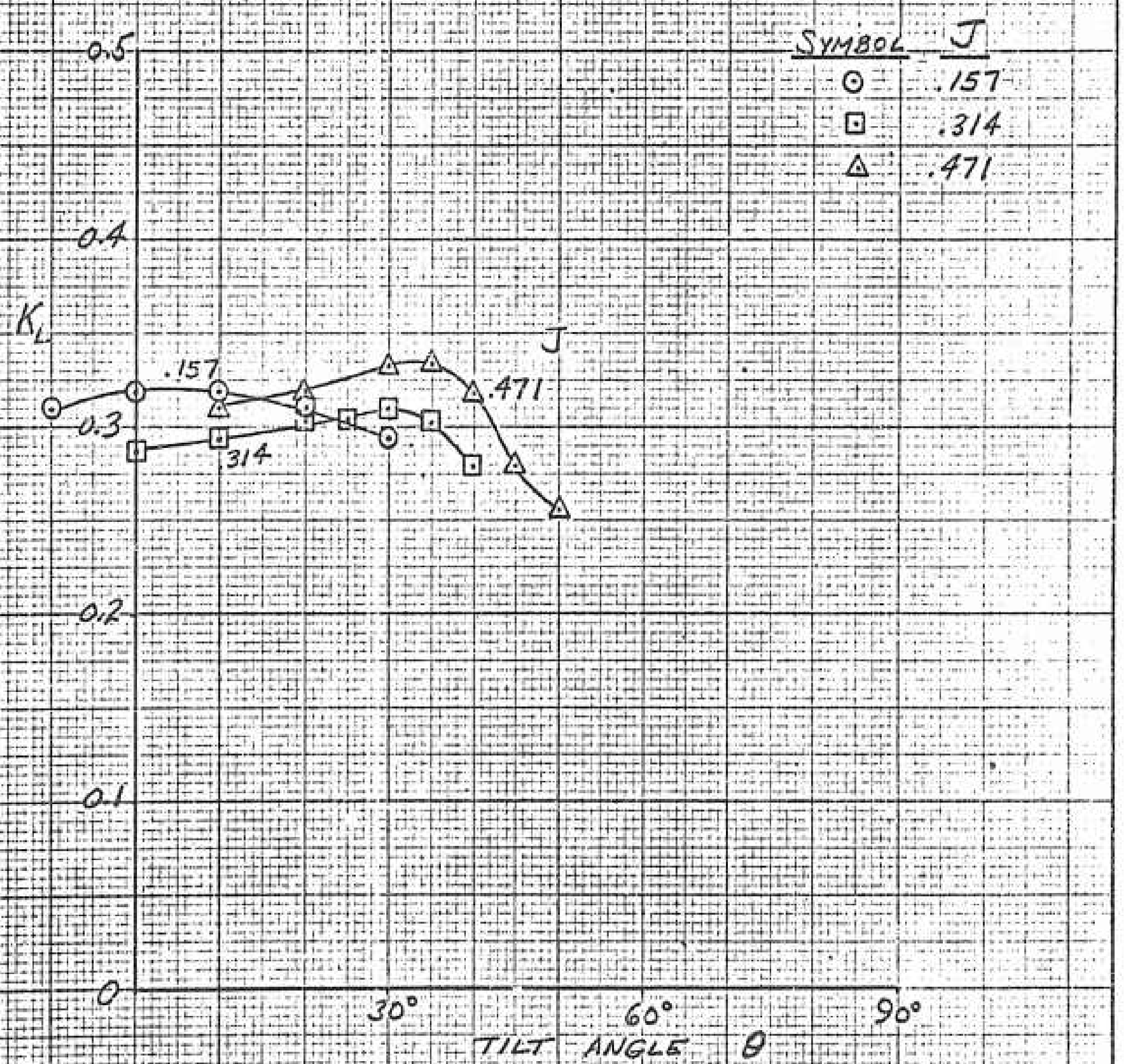

FIG. 84

NON-AXIAL PERFORMANCE
DRAG

REF. 7; GILL, W.J., HILLER AIRCRAFT CORP. ARD-224, 1959

PROPELLER 3 AND DUCT 3

$\beta_{.7R} = 18°$

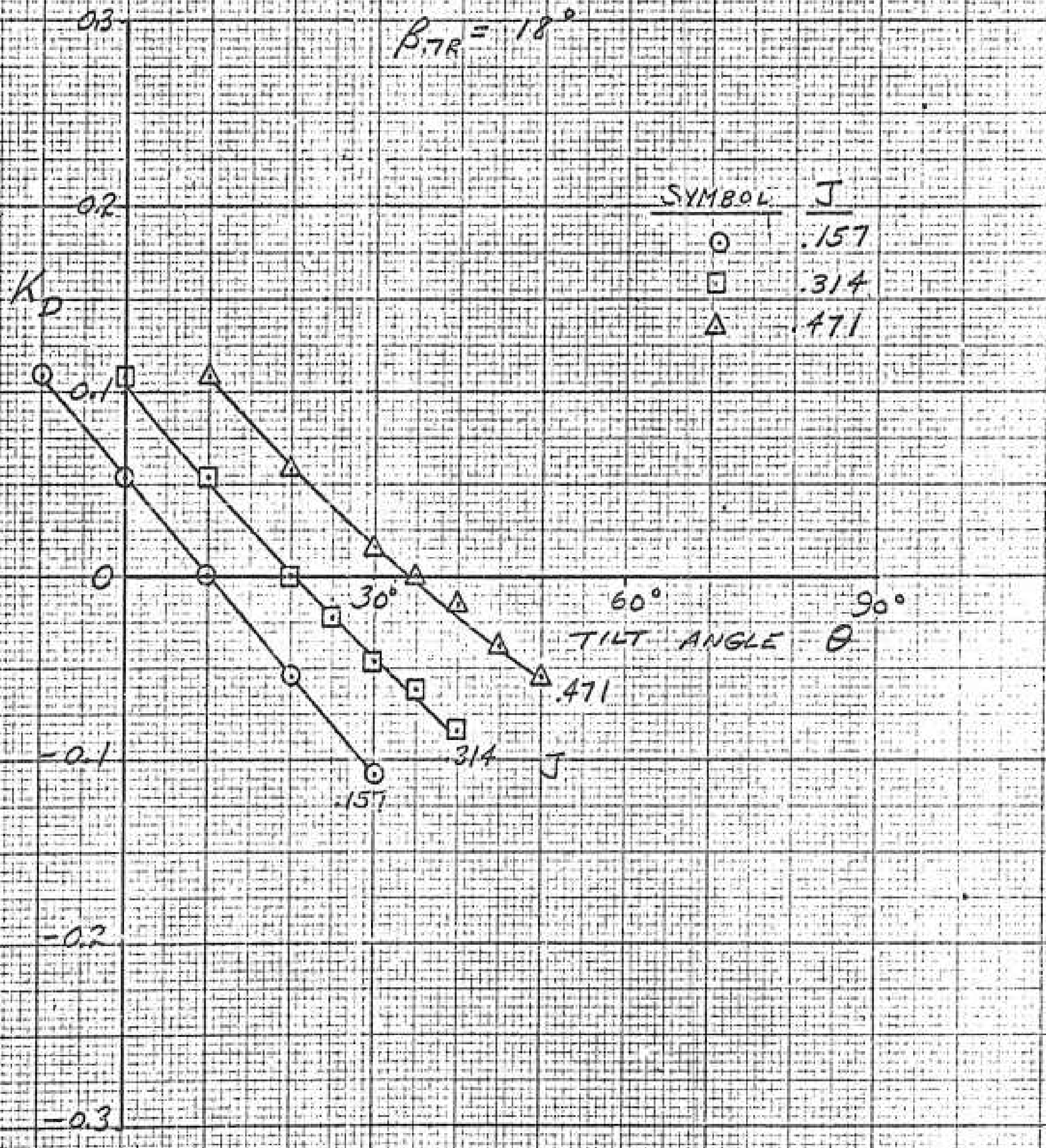

FIG. 85

NON-AXIAL PERFORMANCE
POWER

REF. 7; GILL, W.J., HILLER AIRCRAFT CORP. ARD-224, 1959

PROPELLER 3 AND DUCT 3

$\beta_{.7R} = 18°$

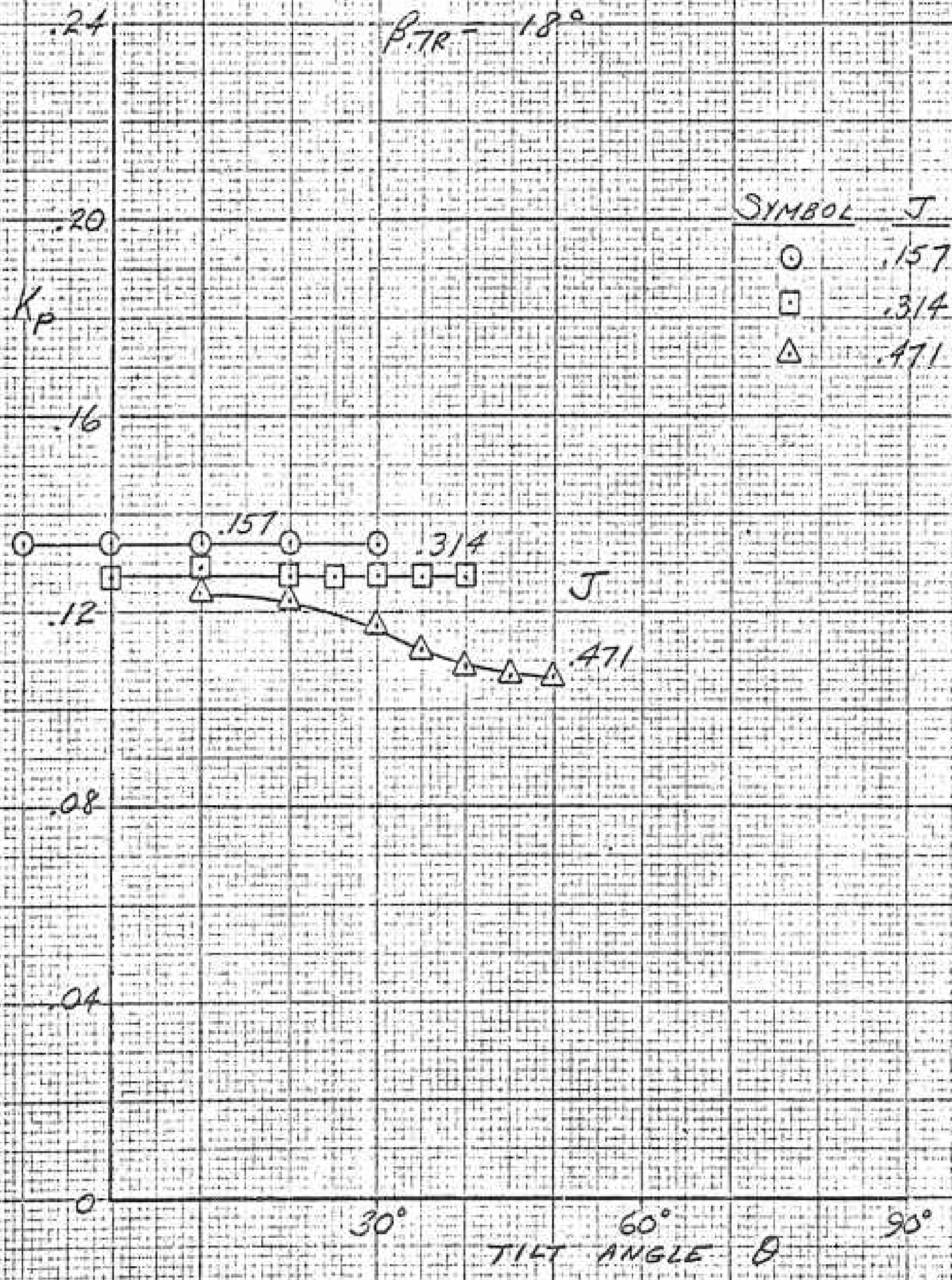

FIG. 86

NON-AXIAL PERFORMANCE
SHROUD LIFT

REF. 7; GILL, W.J., HILLER AIRCRAFT CORP. ARD-224, 1959

PROPELLER 3 AND DUCT 3

$\beta_{.7R} = 18°$

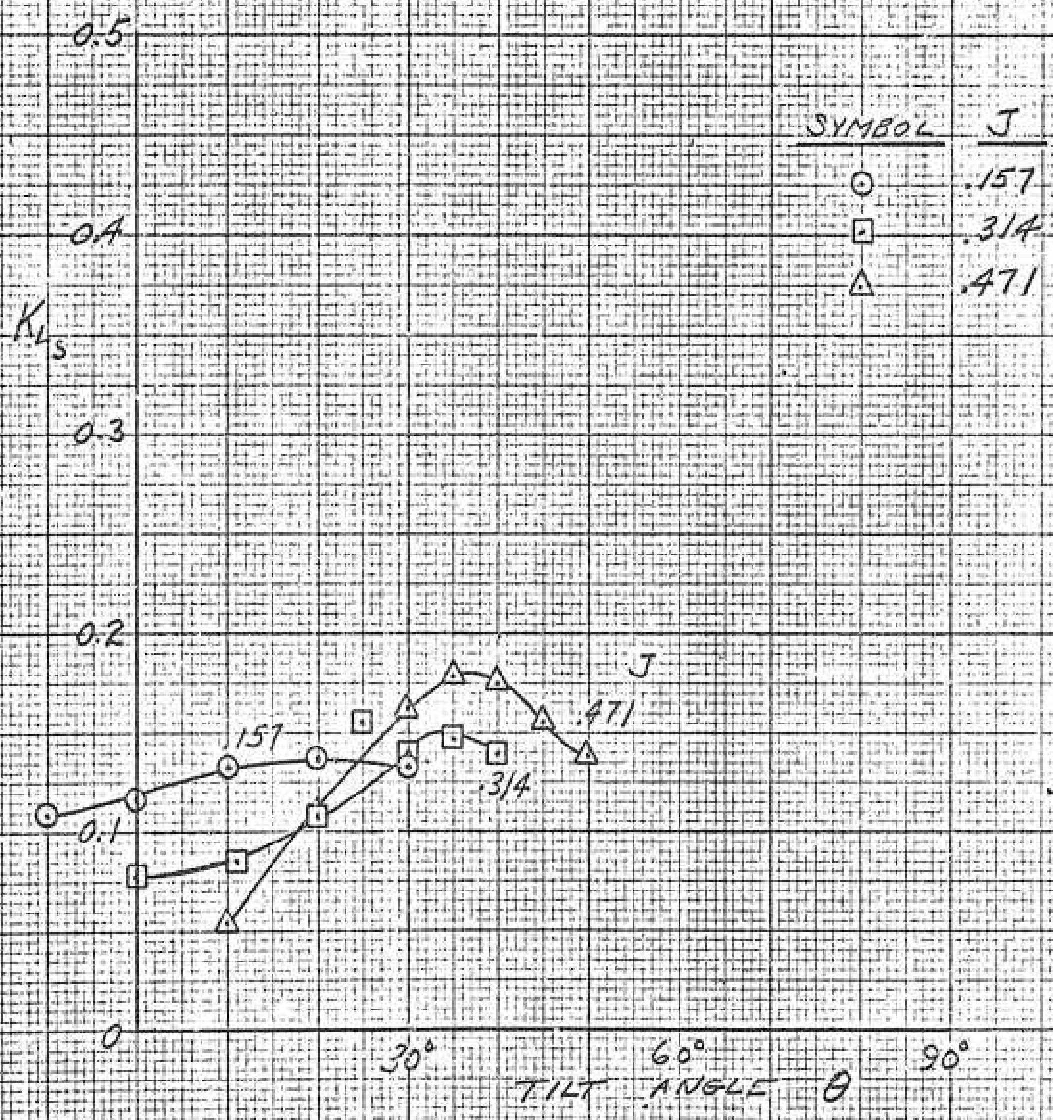

FIG. 87.

NON-AXIAL PERFORMANCE
LIFT DIVISION

REF. 7; GILL, W.J., HILLER AIRCRAFT CORP. ARD-224, 1959

PROPELLER 3 AND DUCT 3

$\beta_{.7R} = 18°$

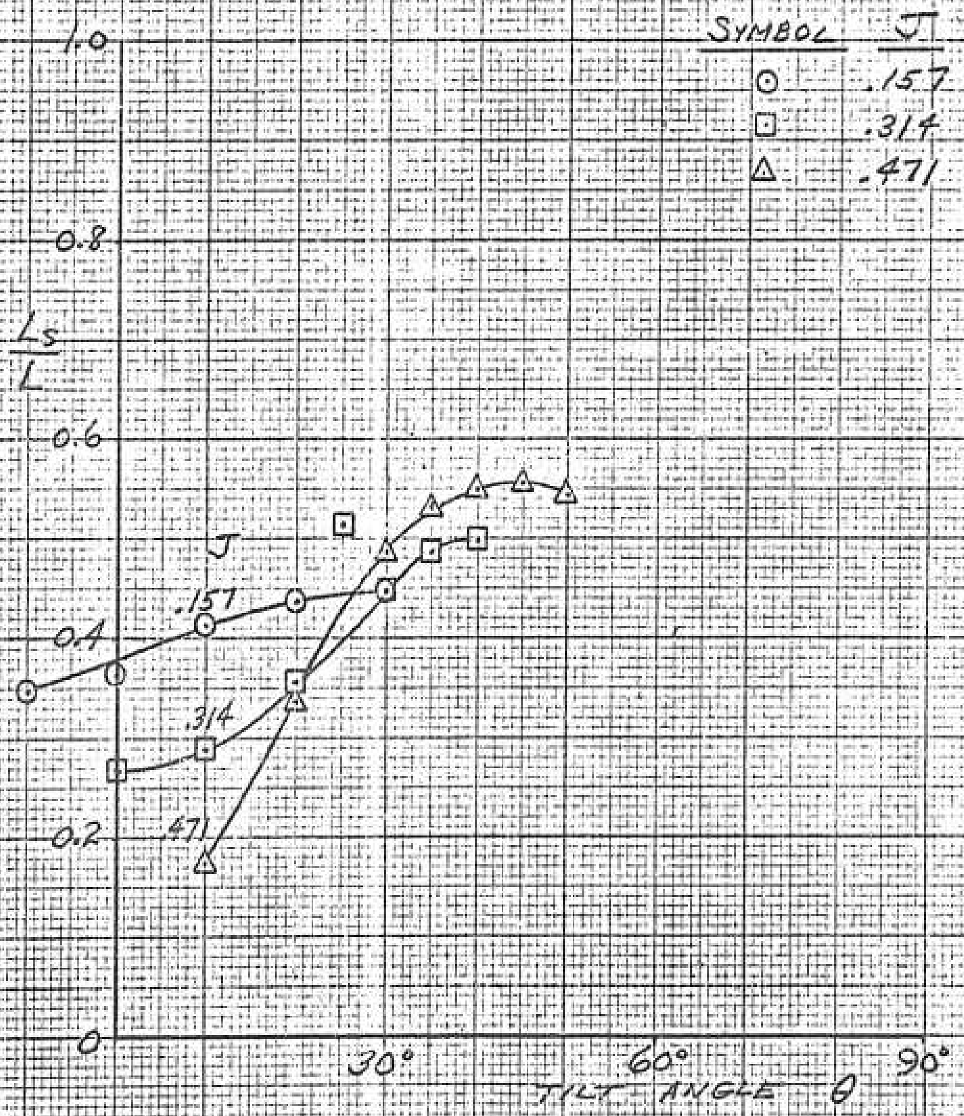

FIG. 88

NON-AXIAL PERFORMANCE

SHROUD DRAG

REF. 7; GILL, W.J., HILLER AIRCRAFT CORP. ARD-224, 1959

PROPELLER 3 AND DUCT 3

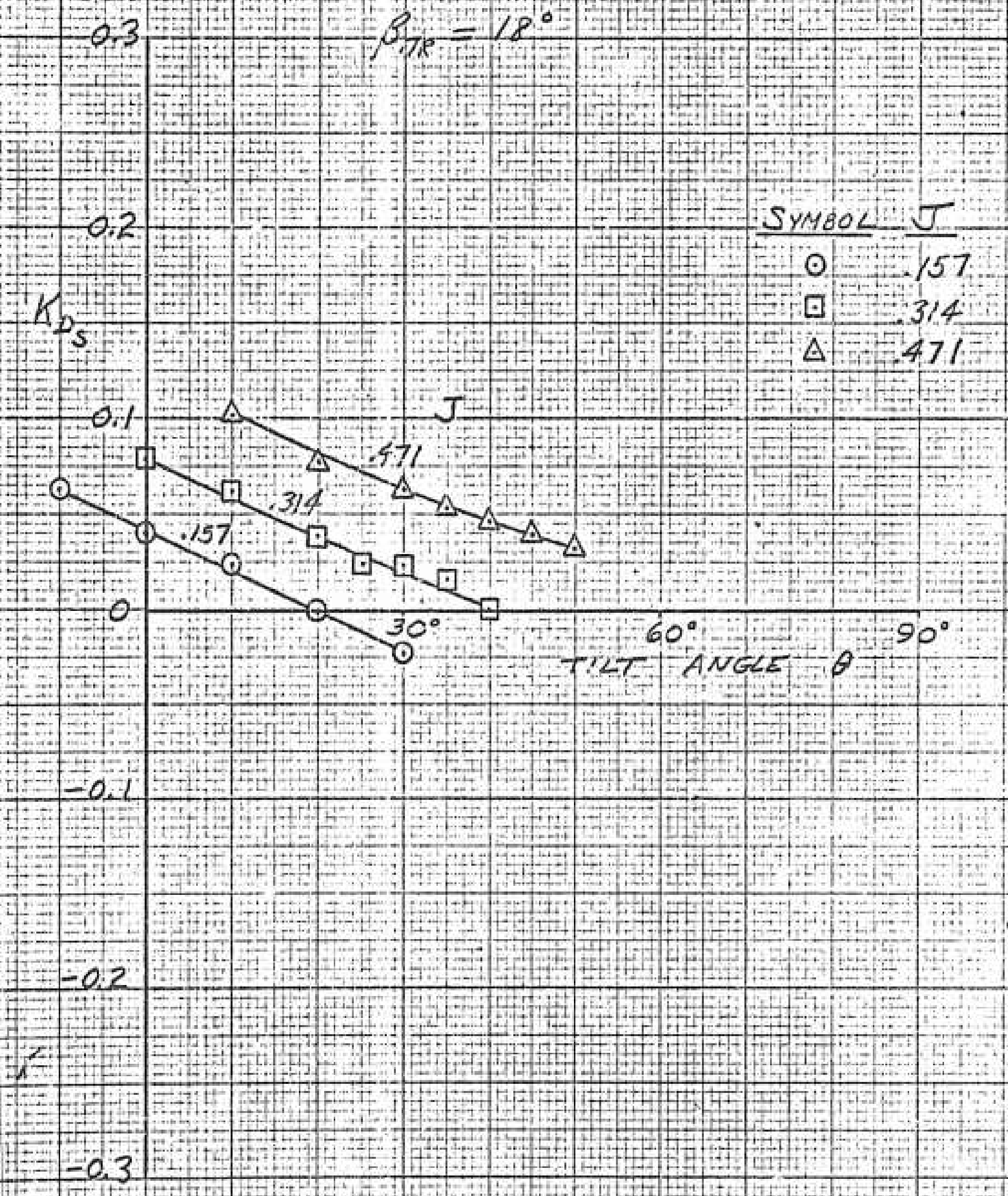

FIG 89

NON-AXIAL PERFORMANCE
MOMENTS

REF. 7; GILL, W.J.; HILLER AIRCRAFT CORP. ARD-224, 1959

PROPELLER 3 AND DUCT 3

$\beta_{.7R} = 18°$

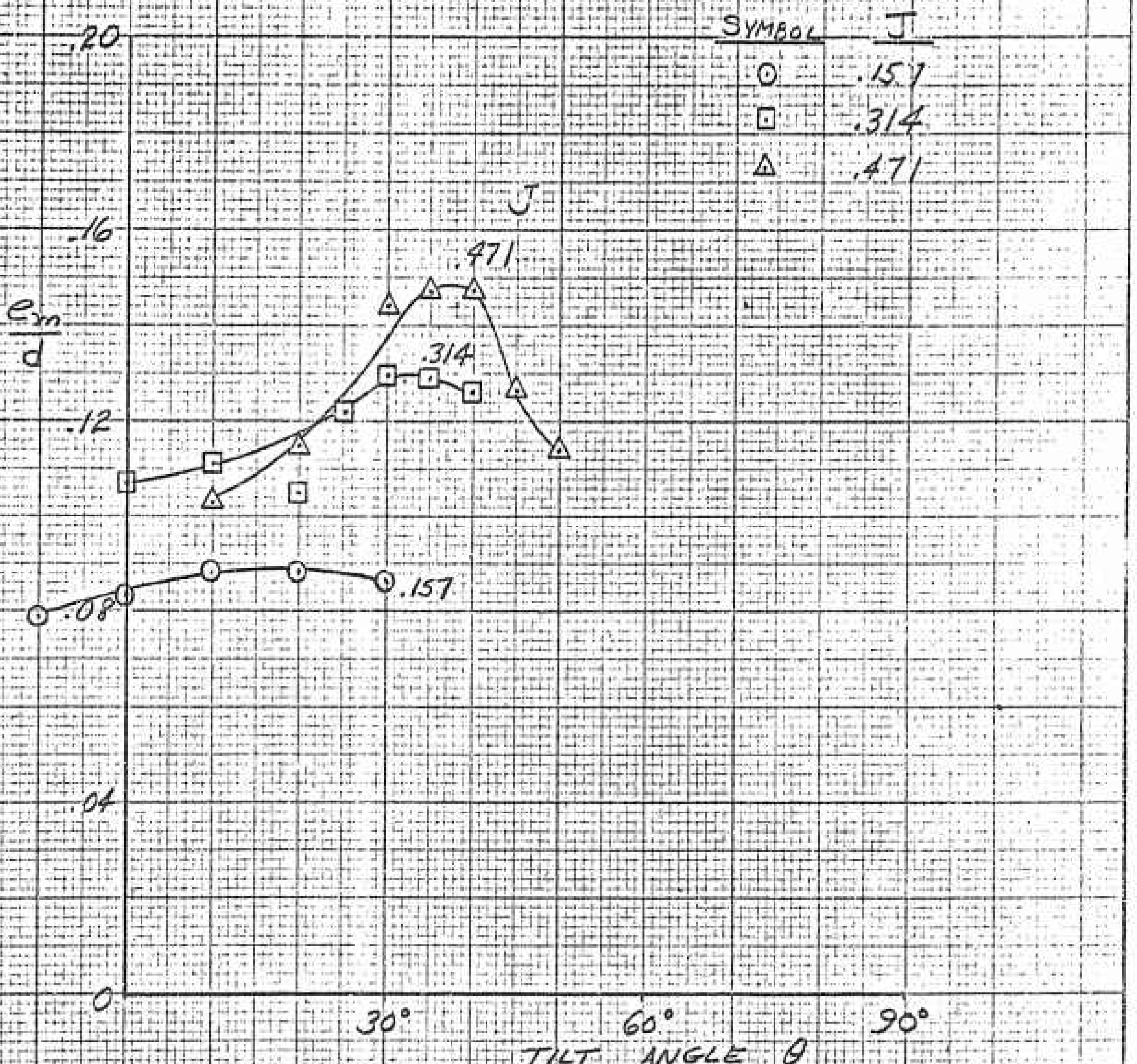

FIG. 90

NON-AXIAL PERFORMANCE
PROPELLER MOMENT

REF. 7; GILL, W.J., HILLER AIRCRAFT CORP. ARD-224, 1959

PROPELLER 3 AND DUCT 3

$\beta_{.7R} = 18°$

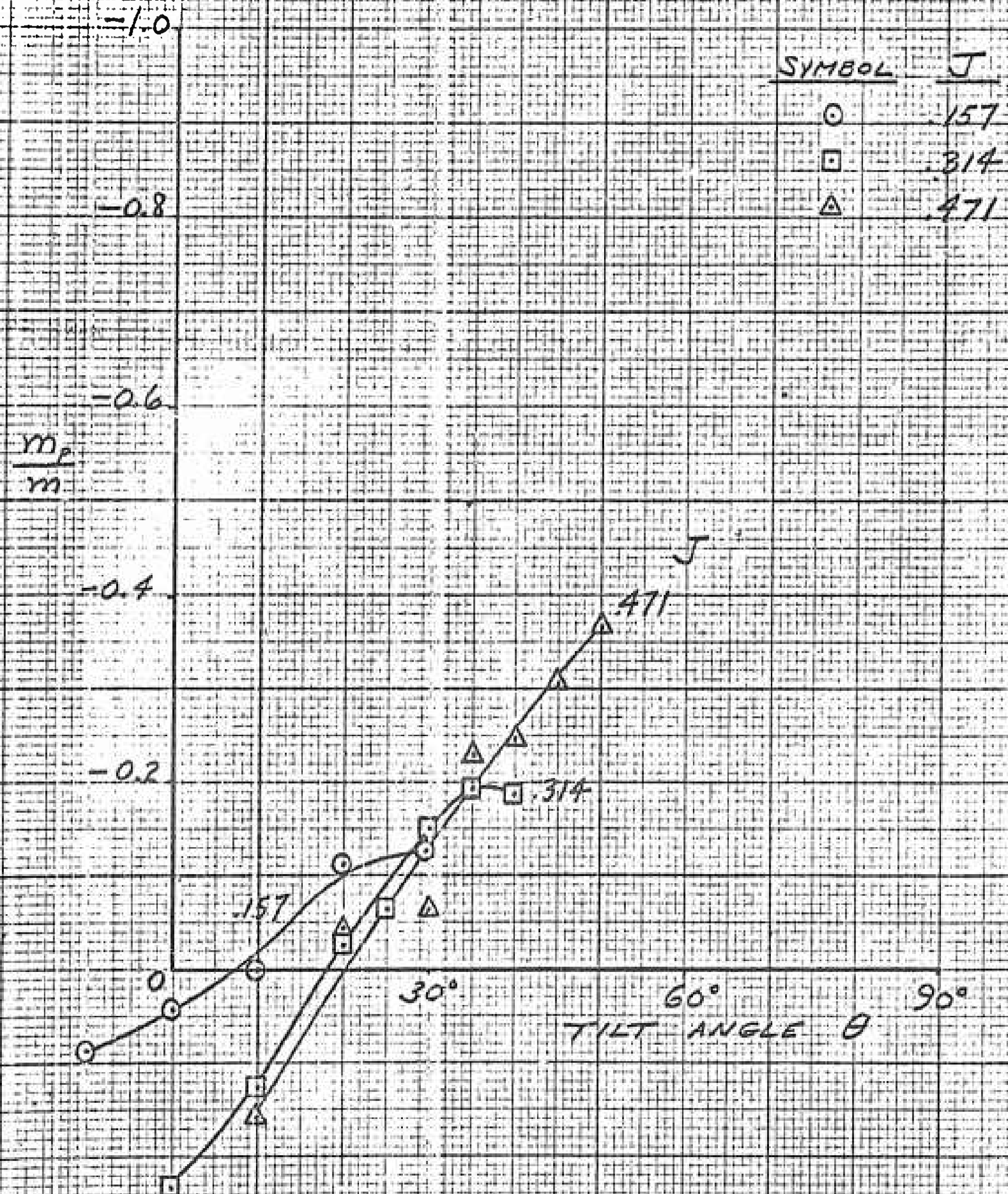

FIG. 91

NON-AXIAL PERFORMANCE

RESULTANT FORCE

REF. 7; GILL, W.J., HILLER AIRCRAFT CORP. ARD-224, 1959

PROPELLER 3 AND DUCT 3

$\beta_{.7R} = 24°$

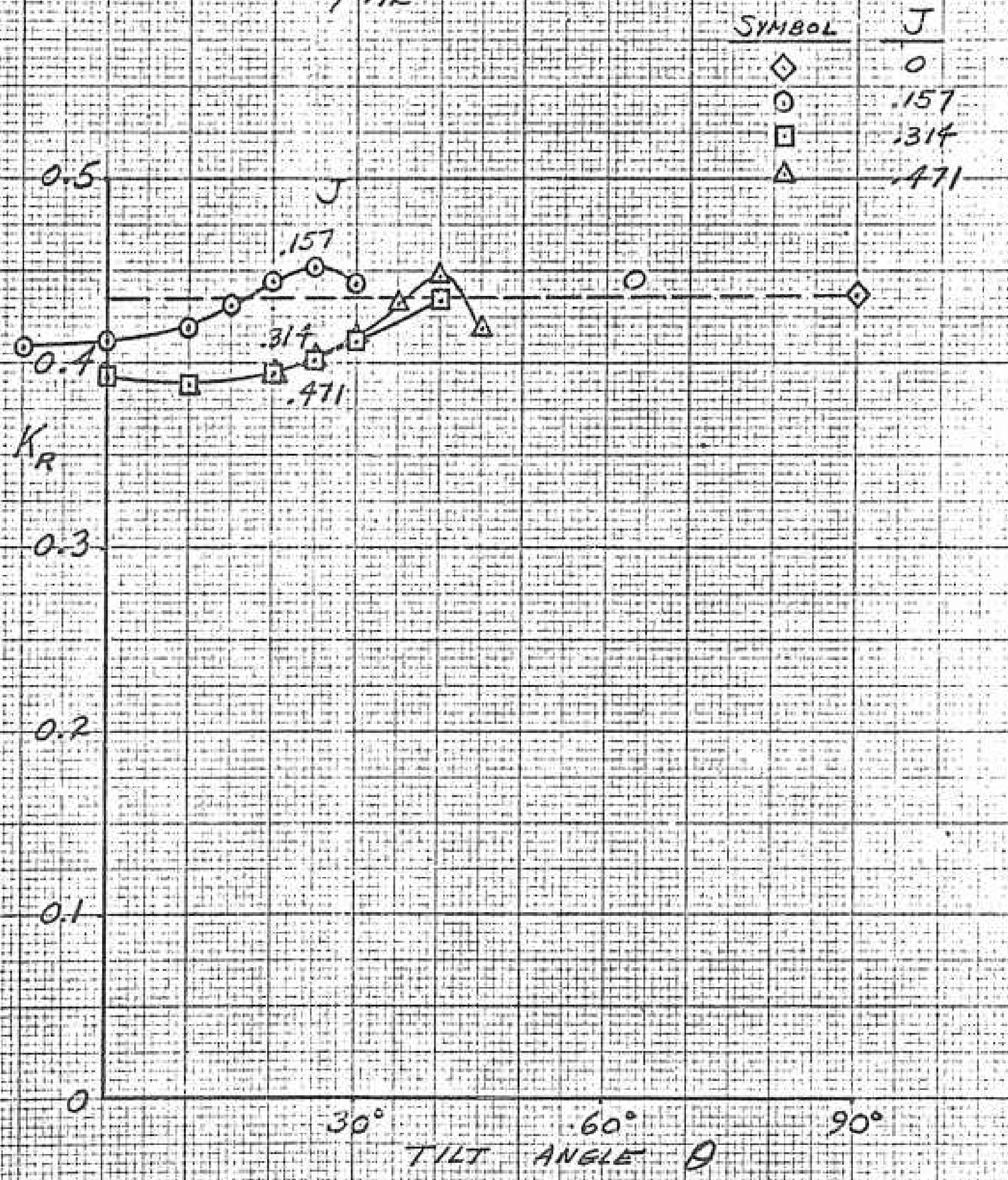

PREPARED ___ 2-29-60 PAGE 231

CHECKED ___ REPORT NO ___

REVISED ___ MODEL ___

REPUBLIC AVIATION

FIG. 92

NON-AXIAL PERFORMANCE

LIFT

REF. 7; GILL, W.J., HILLER AIRCRAFT CORP. ARD-224, 1959

PROPELLER 3 AND DUCT 3

$\beta_{.7R} = 24°$

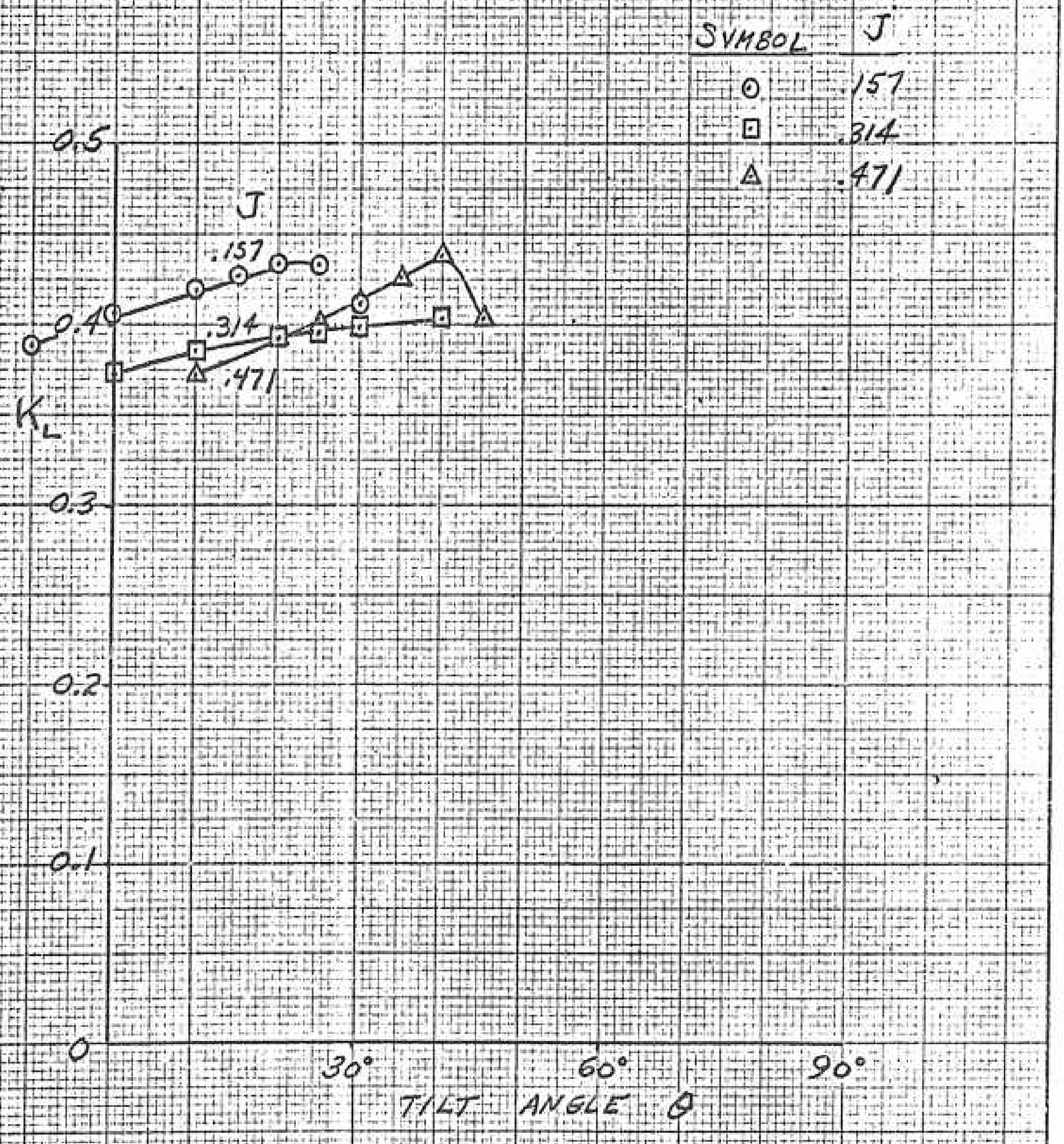

FIG. 93

NON-AXIAL PERFORMANCE

DRAG

REF. 7; GILL, W.J., HILLER AIRCRAFT CORP. ARD-224, 1959

PROPELLER 3 AND DUCT 3

$\beta_{7R} = 24°$

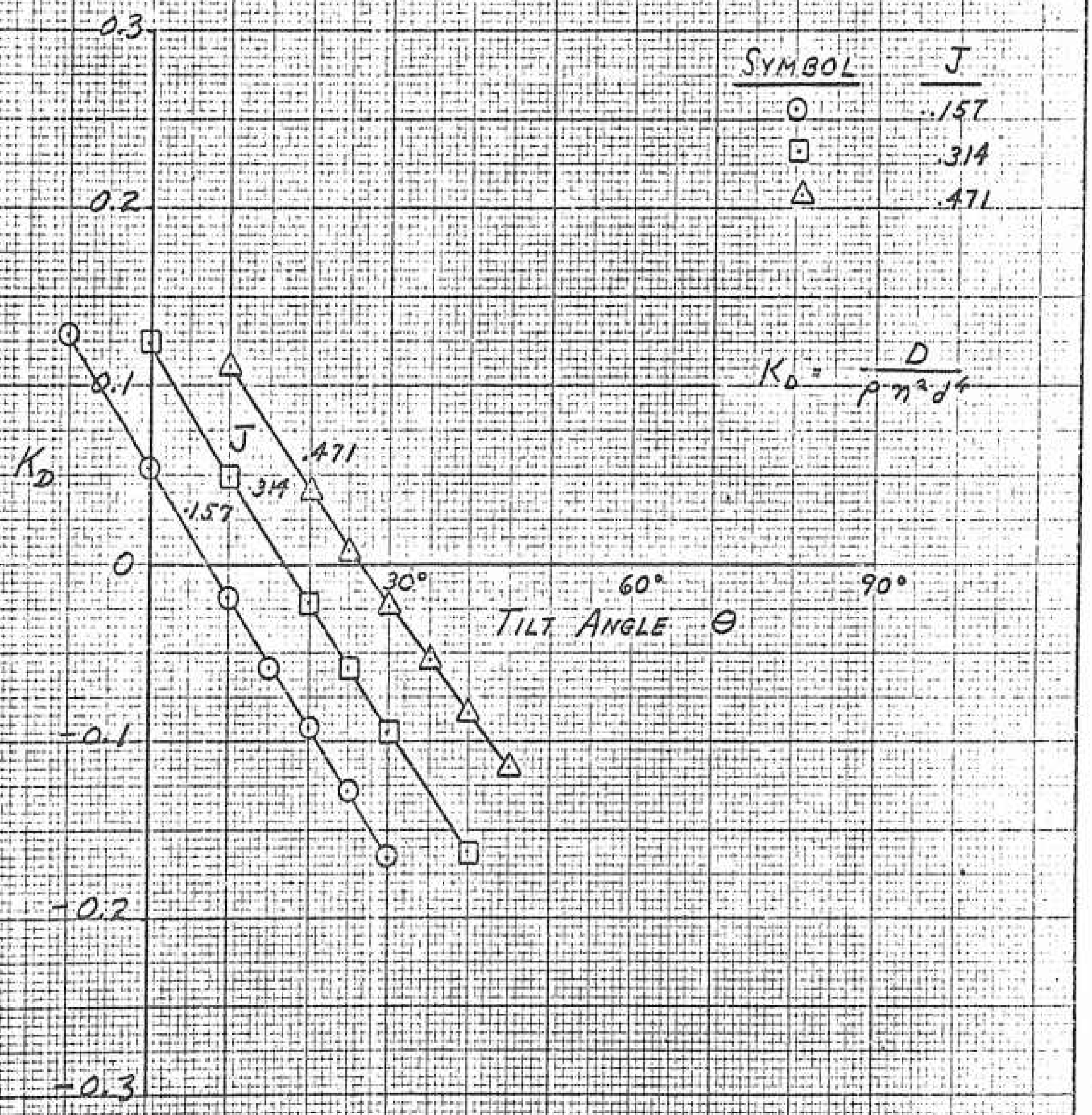

FIG. 94
NON-AXIAL PERFORMANCE
POWER
REF. 7; GILL, W.J., HILLER AIRCRAFT CORP., ARD-224, 1959.
PROPELLER 3 AND DUCT 3
$\beta_{.7R} = 24°$

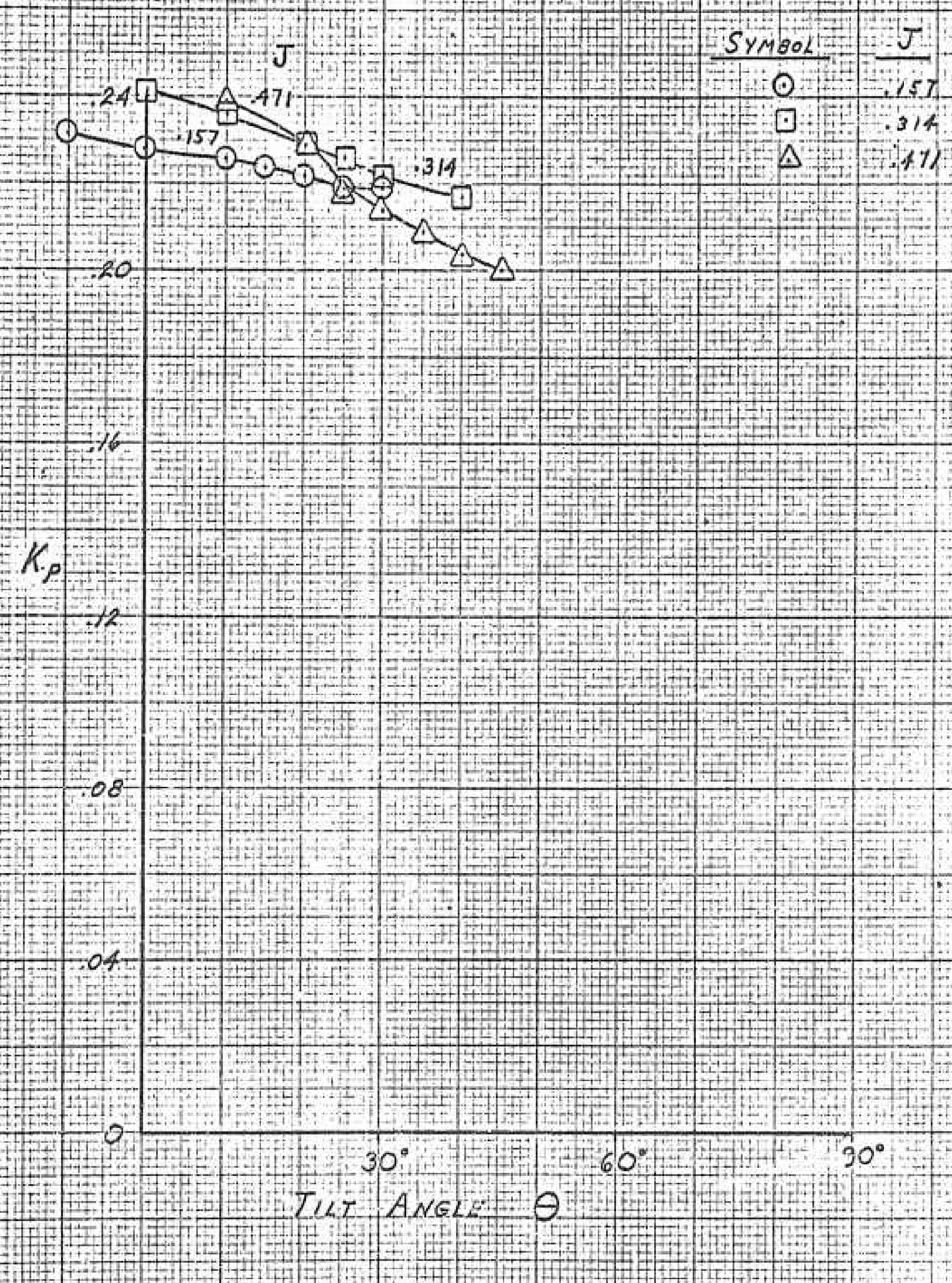

FIG. 95.

NON-AXIAL PERFORMANCE

SHROUD LIFT

REF. 7; GILL, W.J.; HILLER AIRCRAFT CORP. ARD-224, 1959

PROPELLER 3 AND DUCT 3

$\beta_{.7R} = 24°$

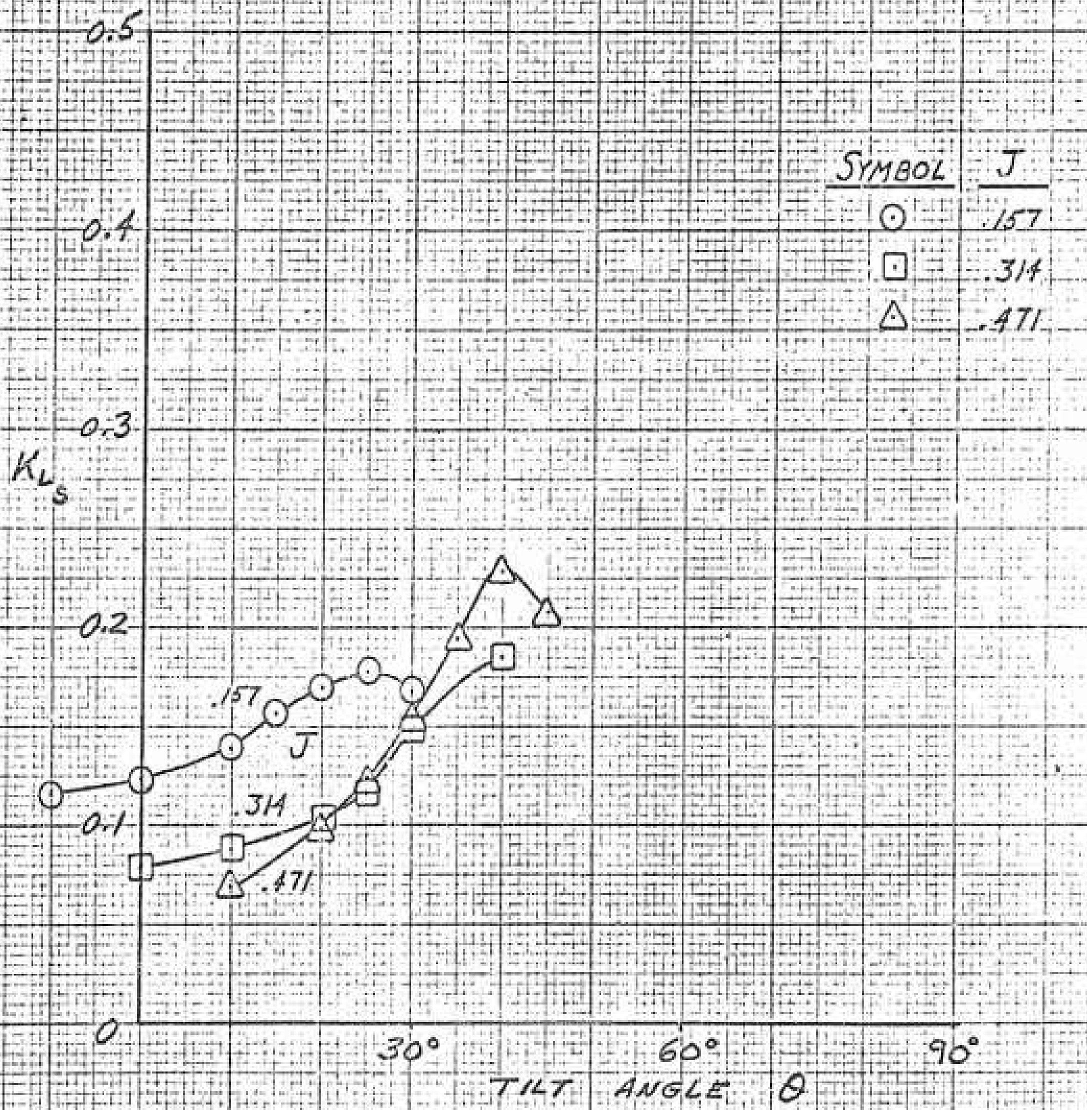

FIG. 96

NON-AXIAL PERFORMANCE

LIFT DIVISION

REF 7: GILL, W. J., HILLER AIRCRAFT CORP. ARD-224, 1959

PROPELLER 3 AND DUCT 3

$\beta_{TTR} = 24°$

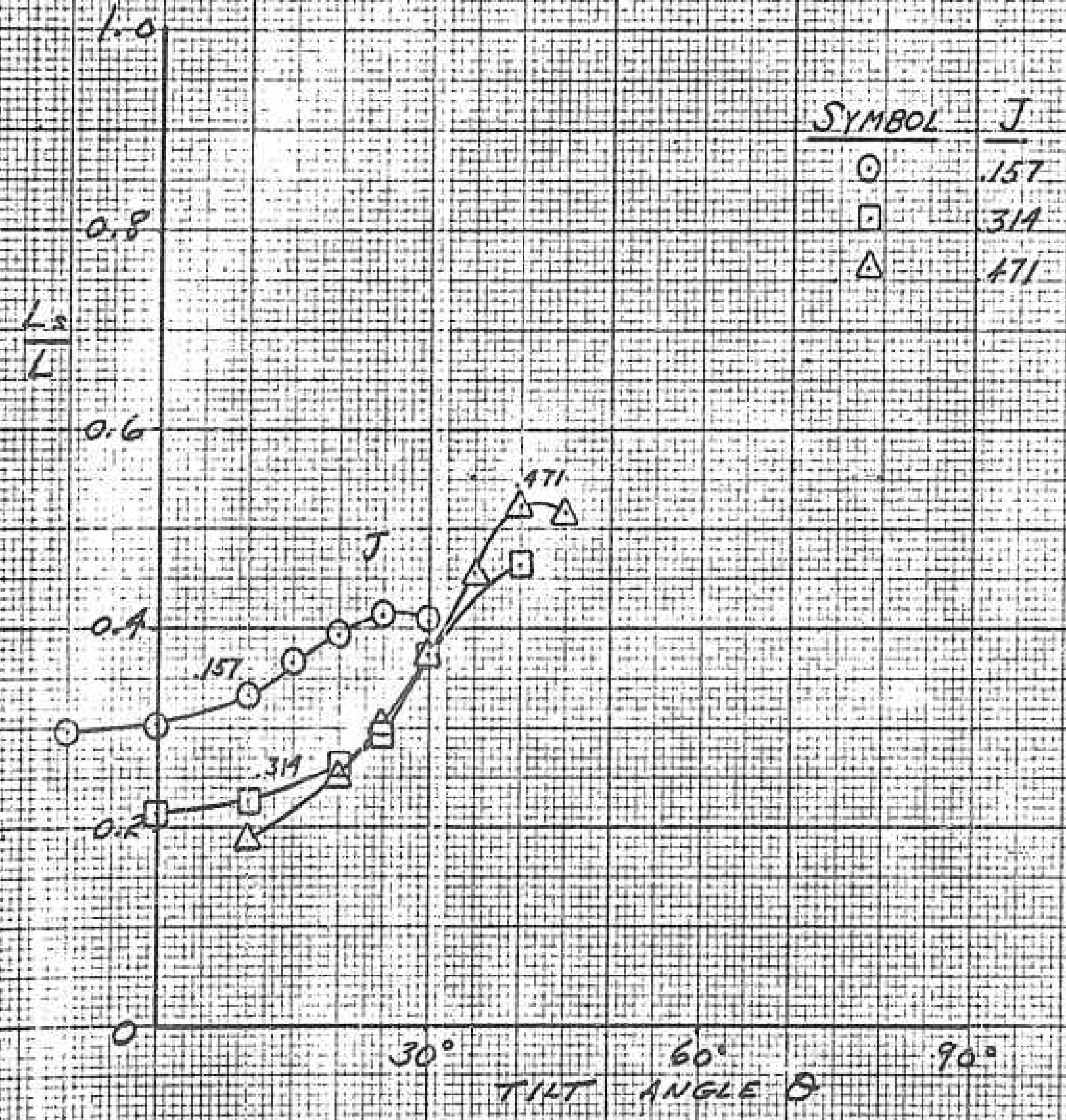

FIG. 97

NON-AXIAL PERFORMANCE

SHROUD DRAG

REF. 7; GILL, W. J., HILLER AIRCRAFT CORP. ARD-224, 1959

PROPELLER 3 AND DUCT 3

$\beta_{.7R} = 24°$

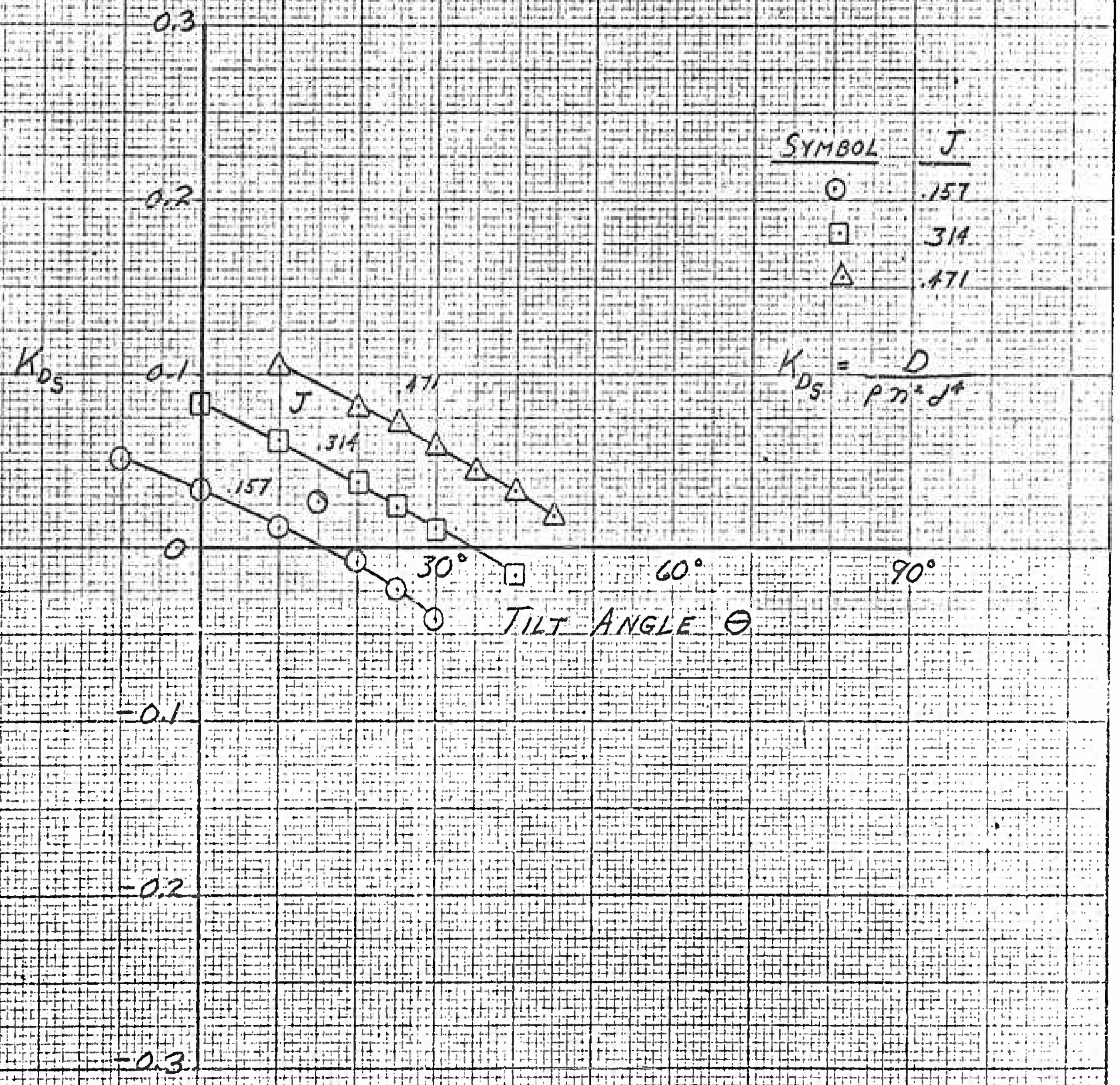

FIG. 98

NON-AXIAL PERFORMANCE
MOMENT

REF. 7; GILL, W. J., HILLER AIRCRAFT CORP., ARD-224, 1959

PROPELLER 3 AND DUCT 3

$\beta_{.7R} = 24°$

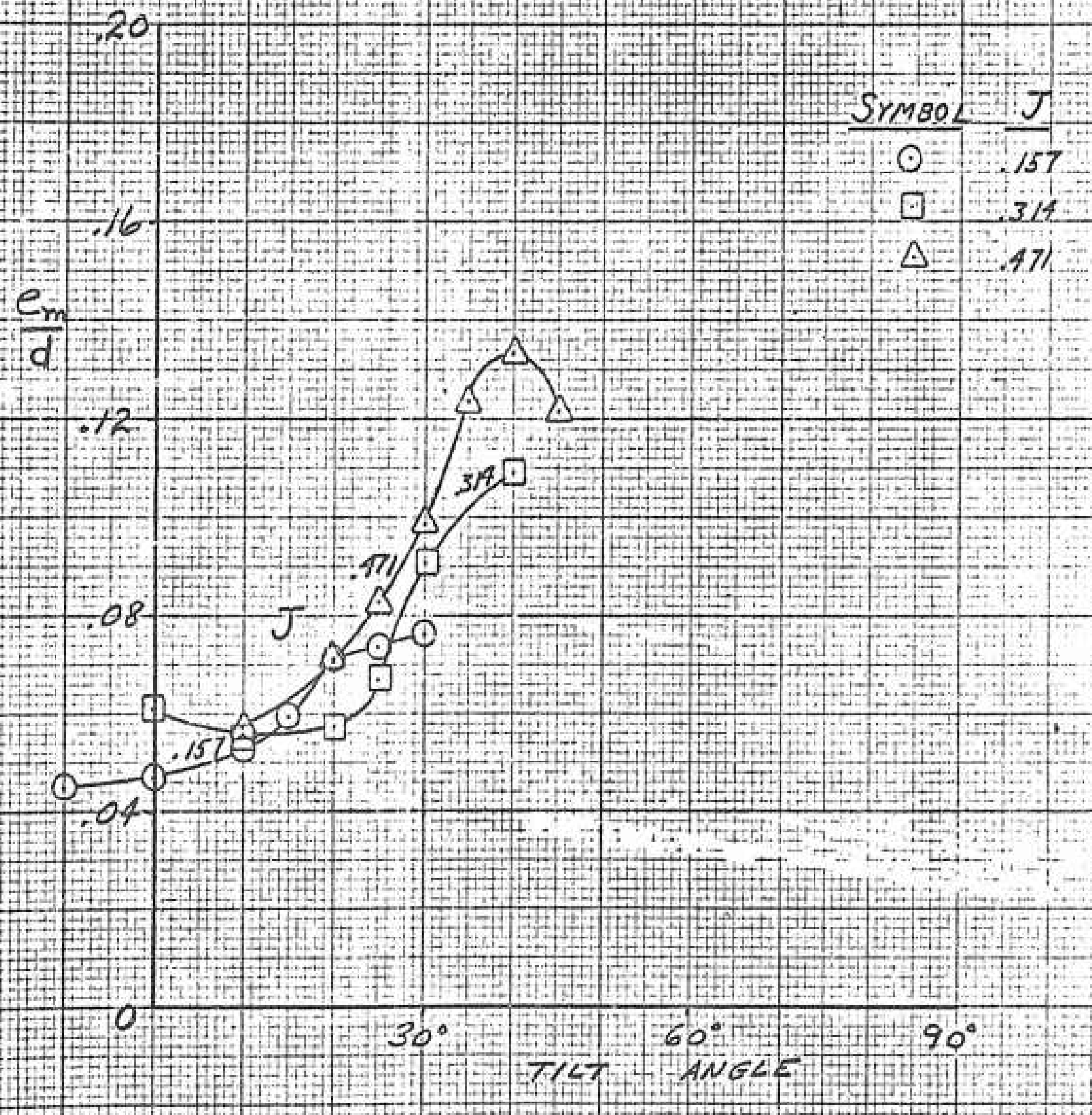

FIG. 99

NON-AXIAL PERFORMANCE

PROPELLER MOMENT

REF. 7: GILL, W.J., HILLER AIRCRAFT CORP. ARD-224, 1959

PROPELLER 3 AND DUCT 3

$\beta_{.7R} = 24°$

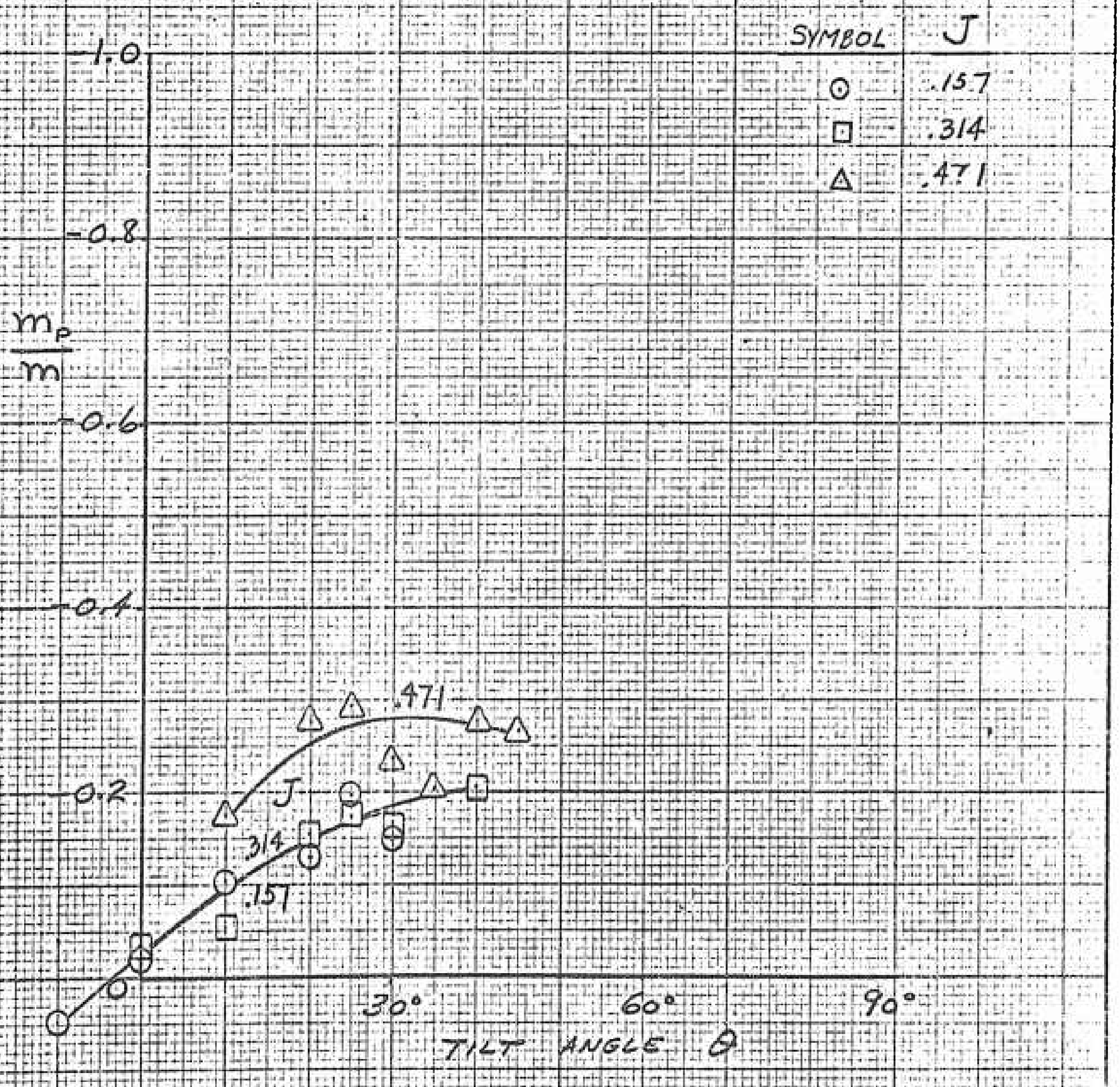

FIG. 100

NON-AXIAL PERFORMANCE
RESULTANT FORCE

REF. 7; GILL, W.J., HILLER AIRCRAFT CORP. ARD-224
1959

PROPELLER 3 AND DUCT 4
$\beta_{.7R} = 18°$

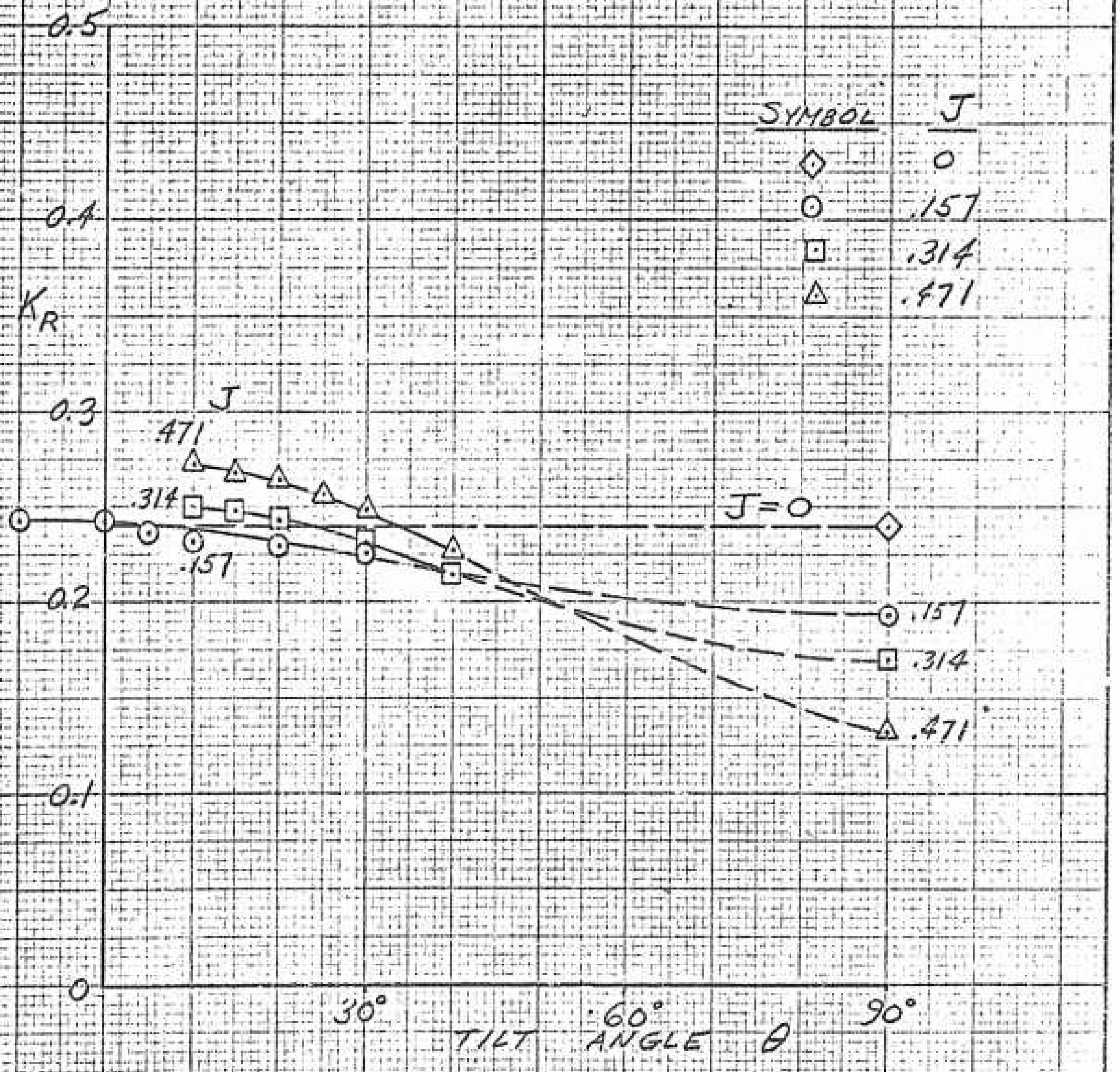

FIG. 101

NON-AXIAL PERFORMANCE
LIFT

REF. 7; GILL, W. J., HILLER AIRCRAFT CORP. ARD-224
1959

PROPELLER 3 AND DUCT 4
$\beta_{.7R} = 18°$

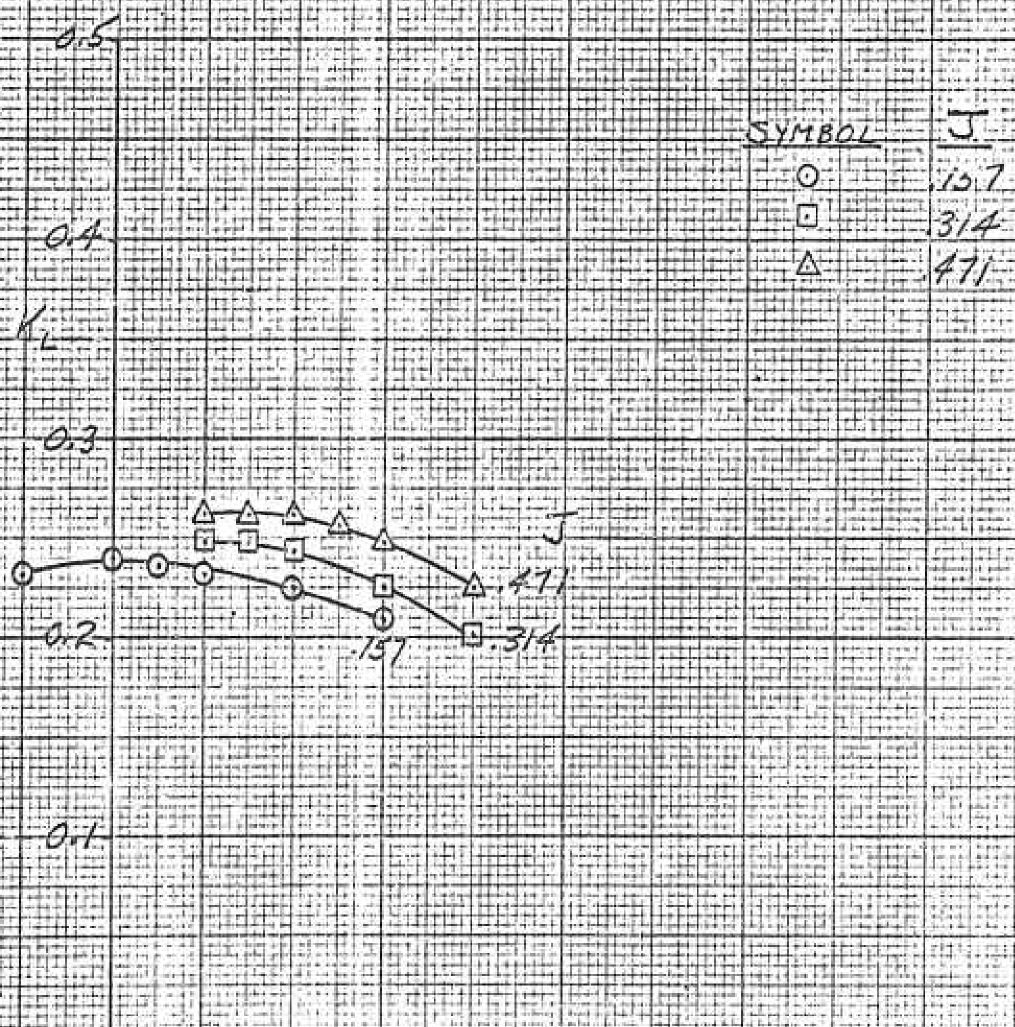

PREPARED JB 4-11-60 PAGE 241
CHECKED REPORT NO.
REVISED MODEL

FIG 102

NON-AXIAL PERFORMANCE
DRAG

REF 7; GILL, W.T., HILLER AIRCRAFT CORP. ARD-224, 1959

PROPELLER 3 AND DUCT 4

$\beta_{.7R} = 18°$

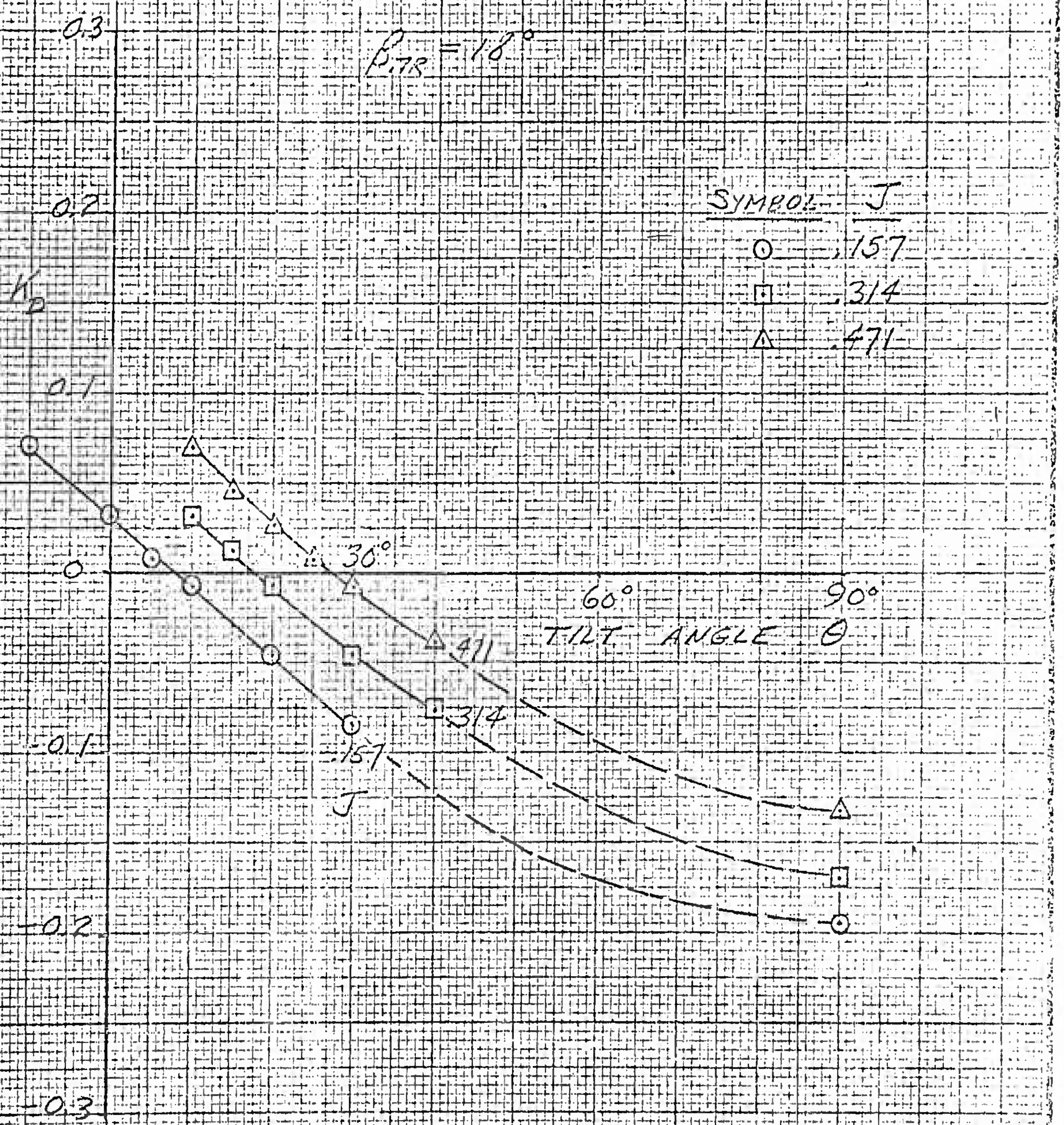

PREPARED JSL 4-11-60

CHECKED

REVISED

REPORT NO.

MODEL

FIG. 103

NON-AXIAL PERFORMANCE

POWER

REF 7; GILL, W.J., HILLER AIRCRAFT CORP. AKD-224 1959

PROPELLER 3 AND DUCT 4

$\beta_{.7R} = 18°$

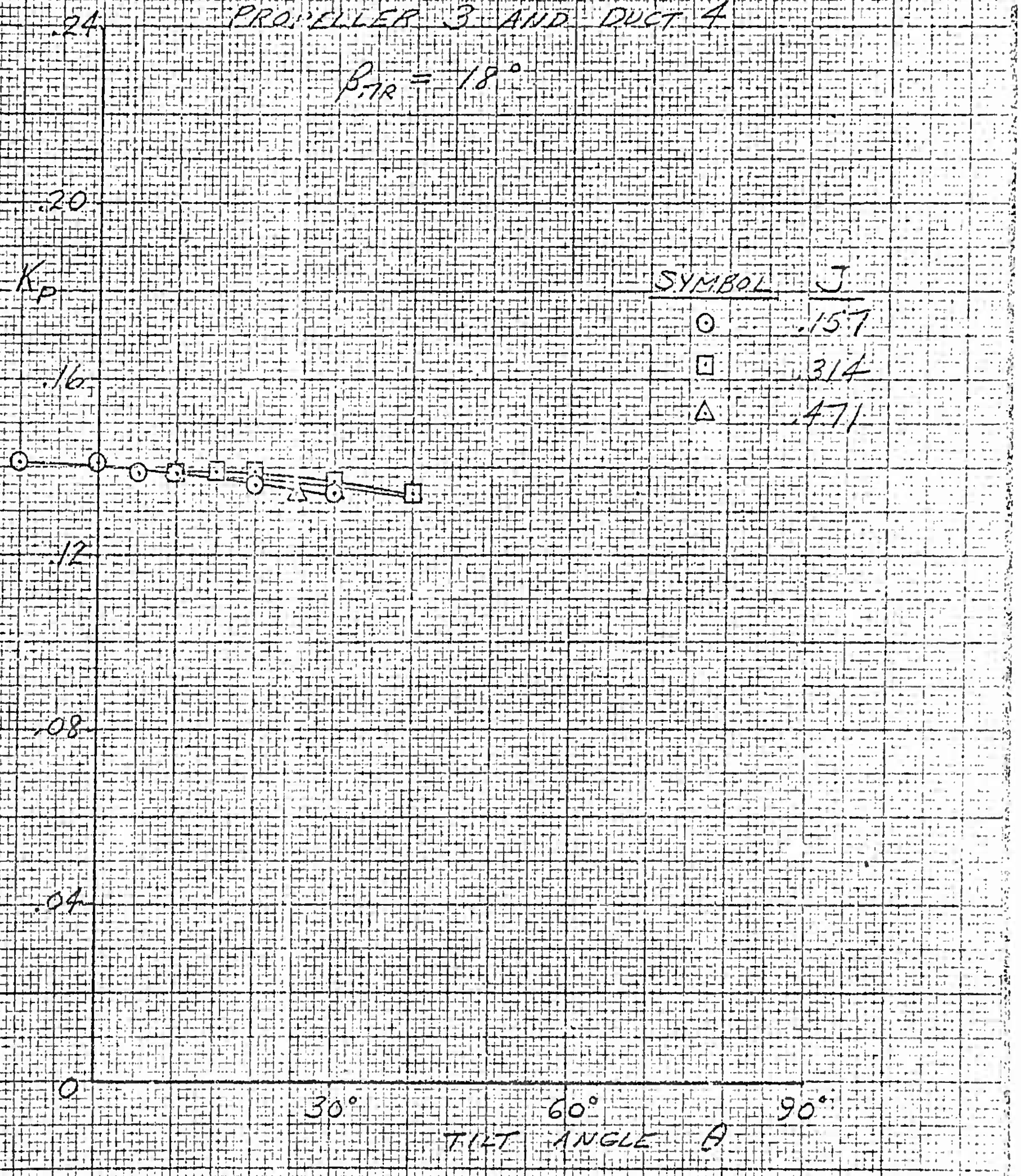

FIG. 104

NON-AXIAL PERFORMANCE
SHROUD LIFT

REF. 7; GILL, W.J., HILLER AIRCRAFT CORP. ARD-224, 1959

PROPELLER 3 AND DUCT 4
$\beta_{.7R} = 18°$

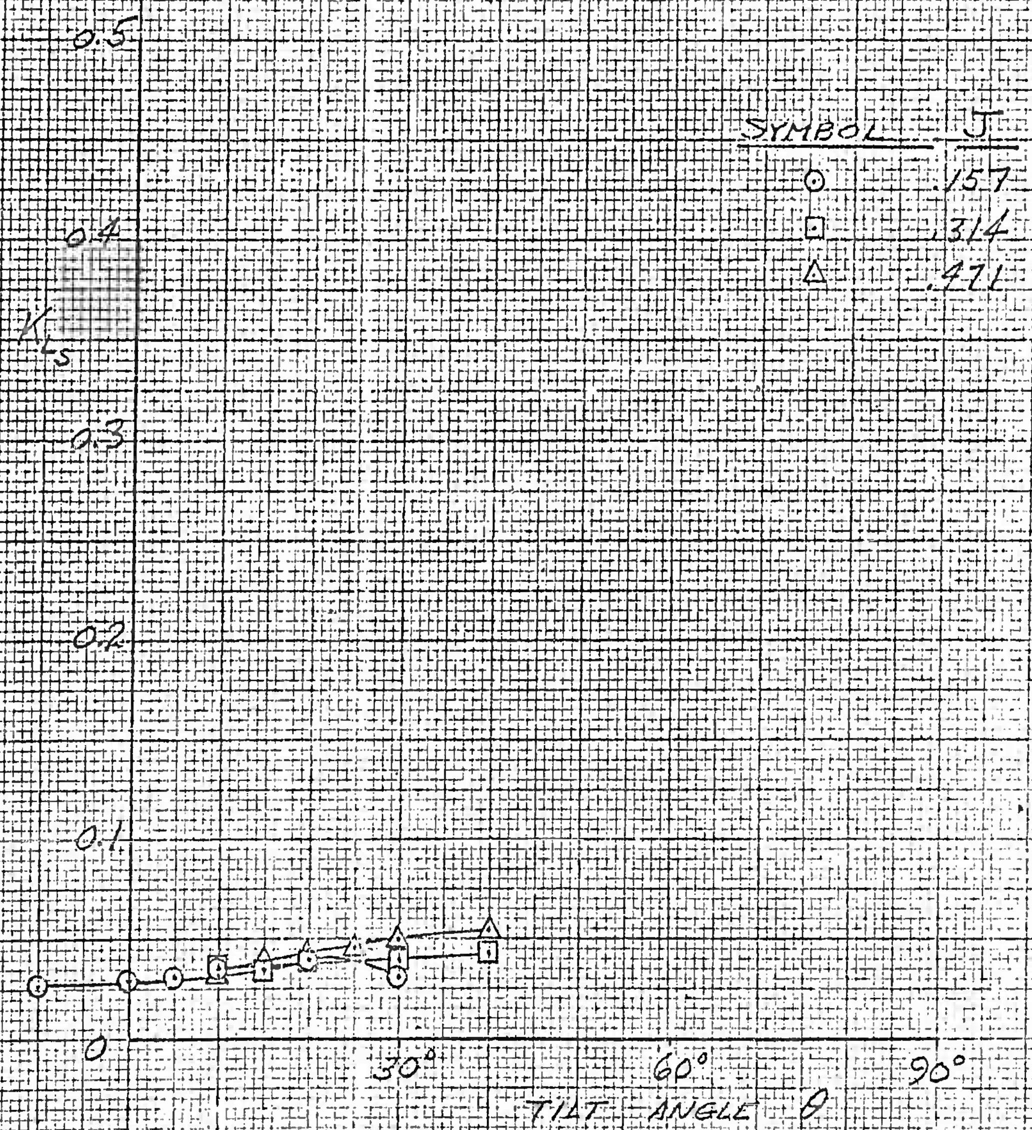

FIG. 105

NON-AXIAL PERFORMANCE

LIFT DIVISION

REF. 7; GILL, W.J., HILLER AIRCRAFT CORP. ARD-224, 1959

PROPELLER 3 AND DUCT 4

$\beta_{TR} = 18°$

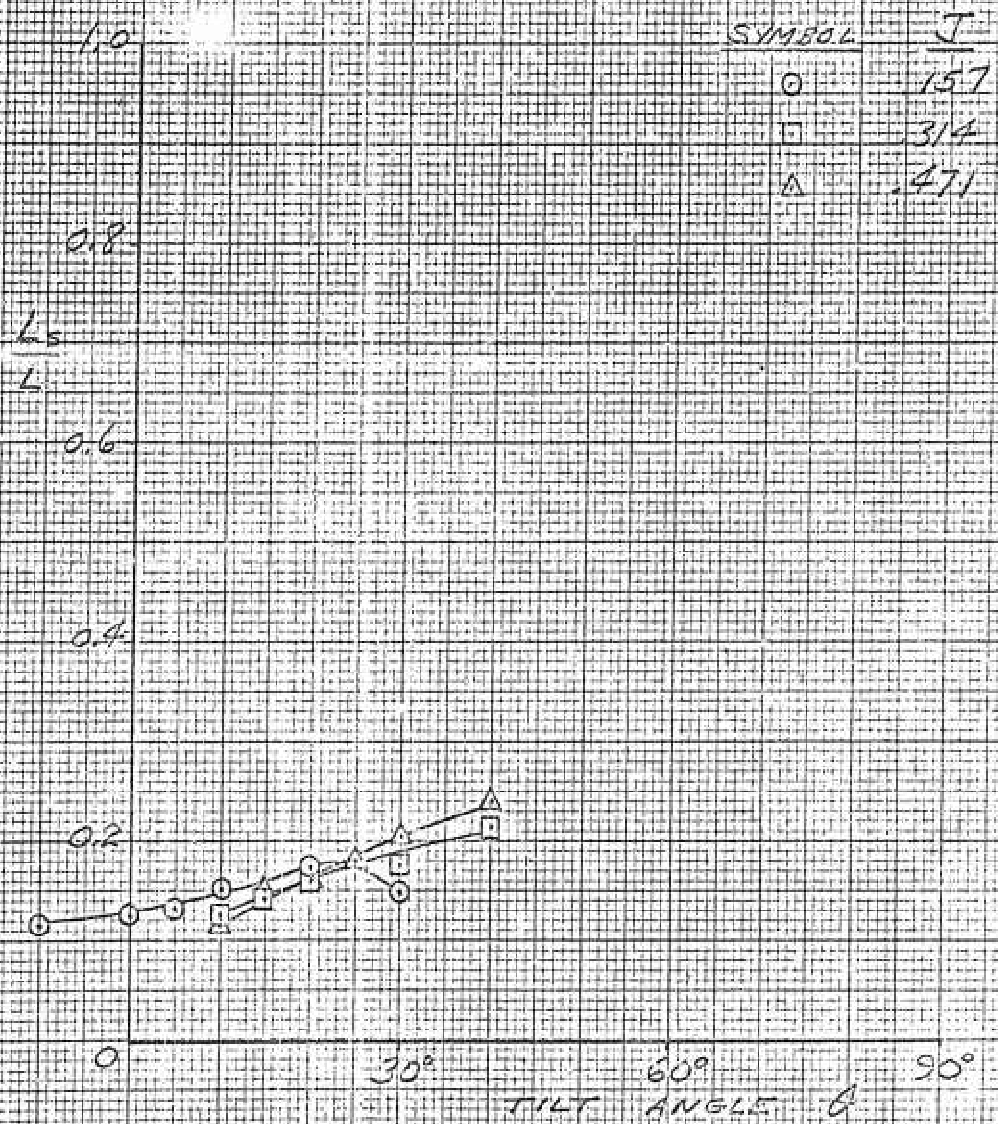

PREPARED JB 4-11-60
CHECKED
REVISED

PAGE 245
REPORT NO.
MODEL

FIG. 106

NON-AXIAL PERFORMANCE
SHROUD DRAG

REF. 7; GILL, W.J.; HILLER AIRCRAFT CORP. ARD-224, 1959

PROPELLER 3 AND DUCT 4

$\beta_{.7R} = 18°$

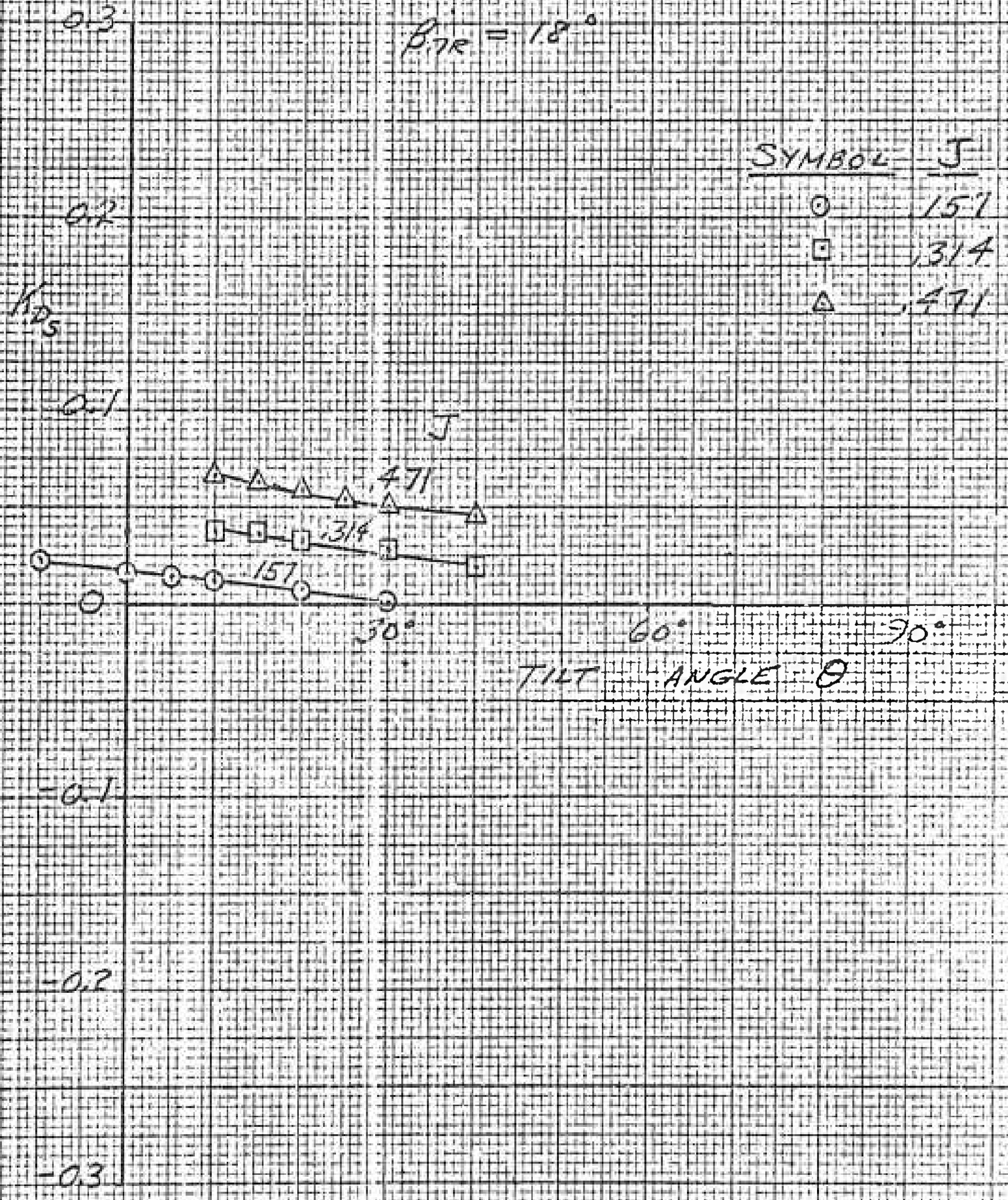

-10A
2/49

FIG. 107

NON-AXIAL PERFORMANCE
MOMENTS

REF 7; GILL, W.J., HILLER AIRCRAFT CORP ARD-224
1959

PROPELLER 3 AND DUCT 4

$\beta_{.7R} = 18°$

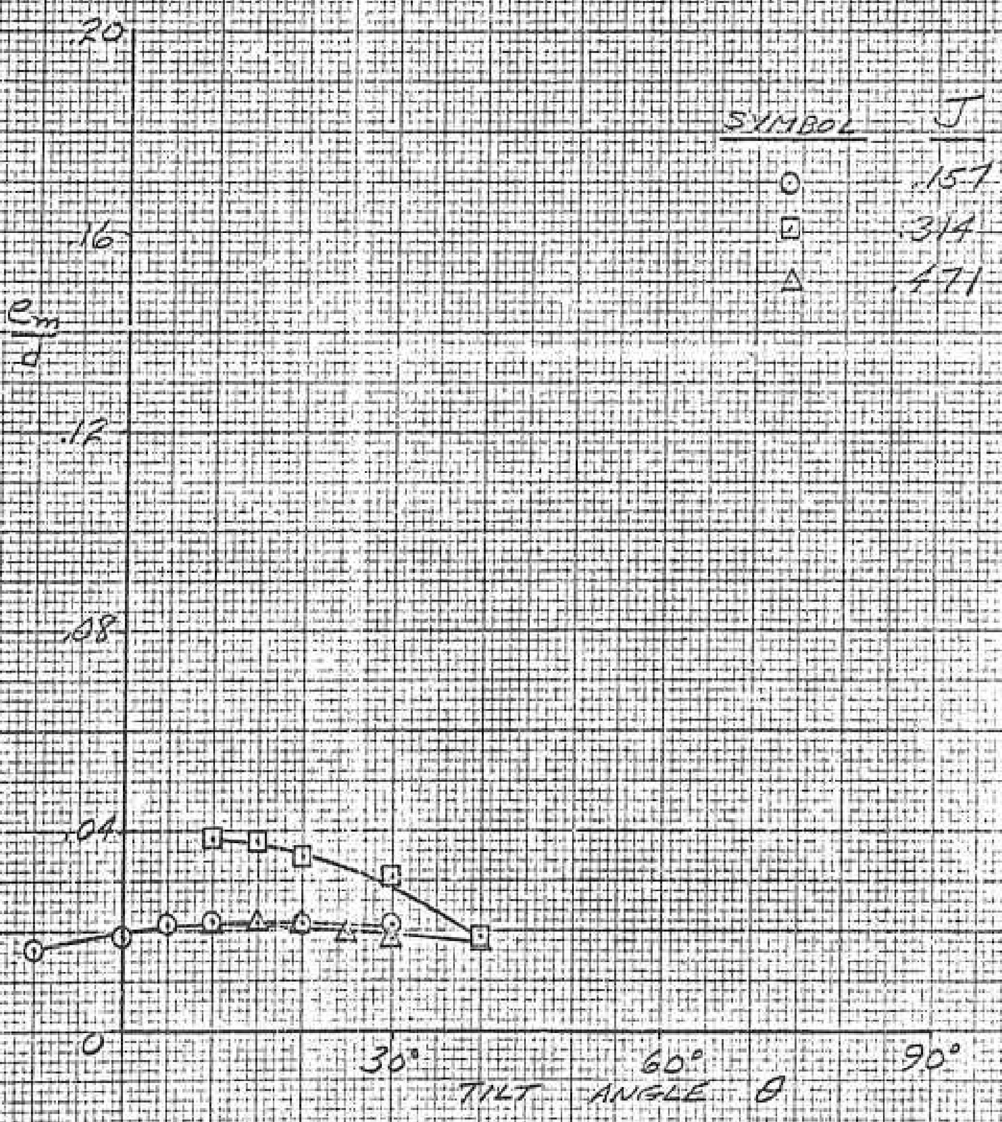

FIG. 108

NON-AXIAL PERFORMANCE

PROPELLER MOMENT

REF. 7; GILL, W.J., HILLER AIRCRAFT CORP. ARD-224, 1959

PROPELLER 3 AND DUCT 4

$\beta_{.75} = 13°$

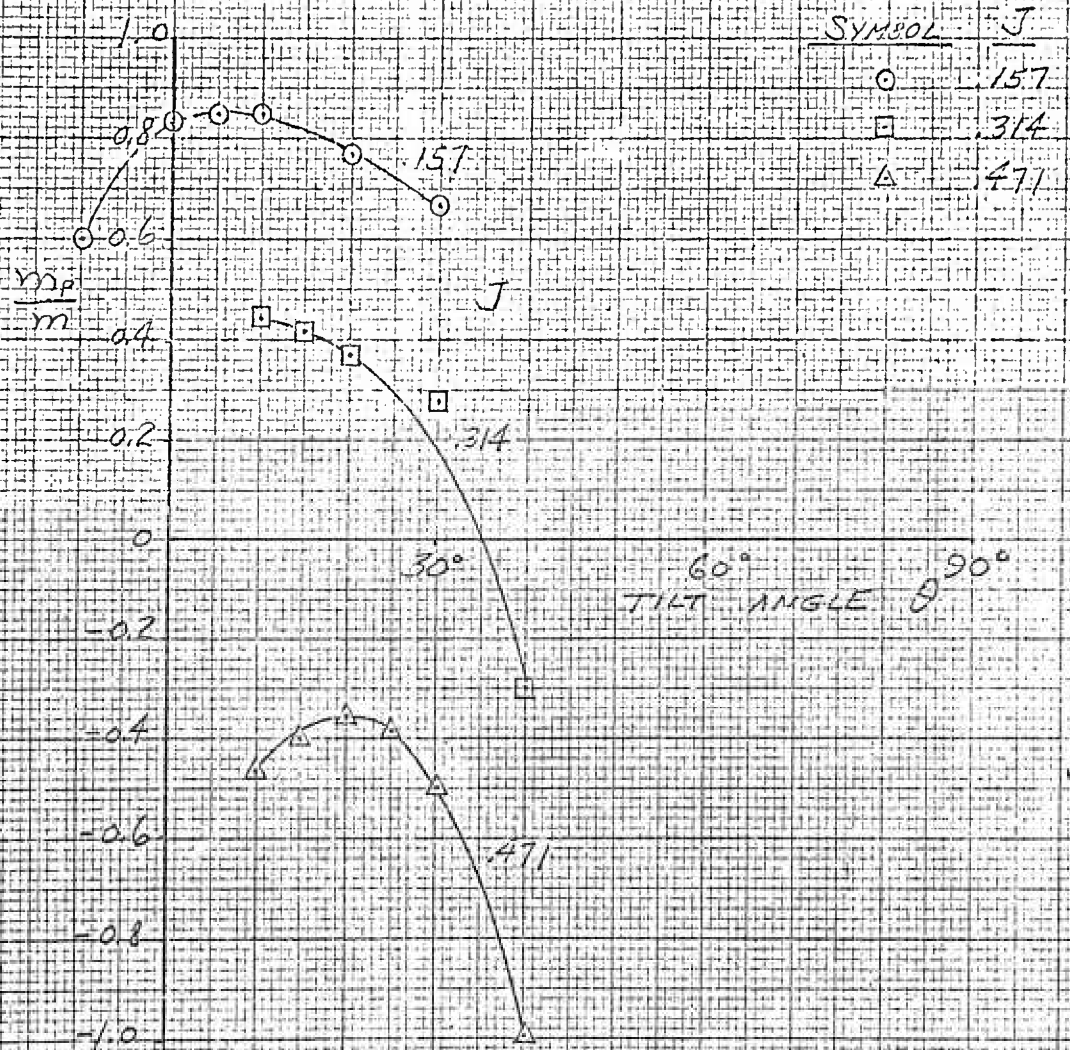

Reference	12
Author	Grose, R. M.
Source	United Aircraft Corporation
Figs.	109-114

FIG 109

CONFIGURATION

REF. 12 ; GROSE, R.M., UNITED AIRCRAFT CORP. (WADC TR 58-604, 1958)

$$\frac{A}{A_c} = .907$$

PROPELLER:- 4 BLADE SINGLE ROTATING
(HAMILTON STANDARD DIVISION MODEL SK-28175)

SHROUD :

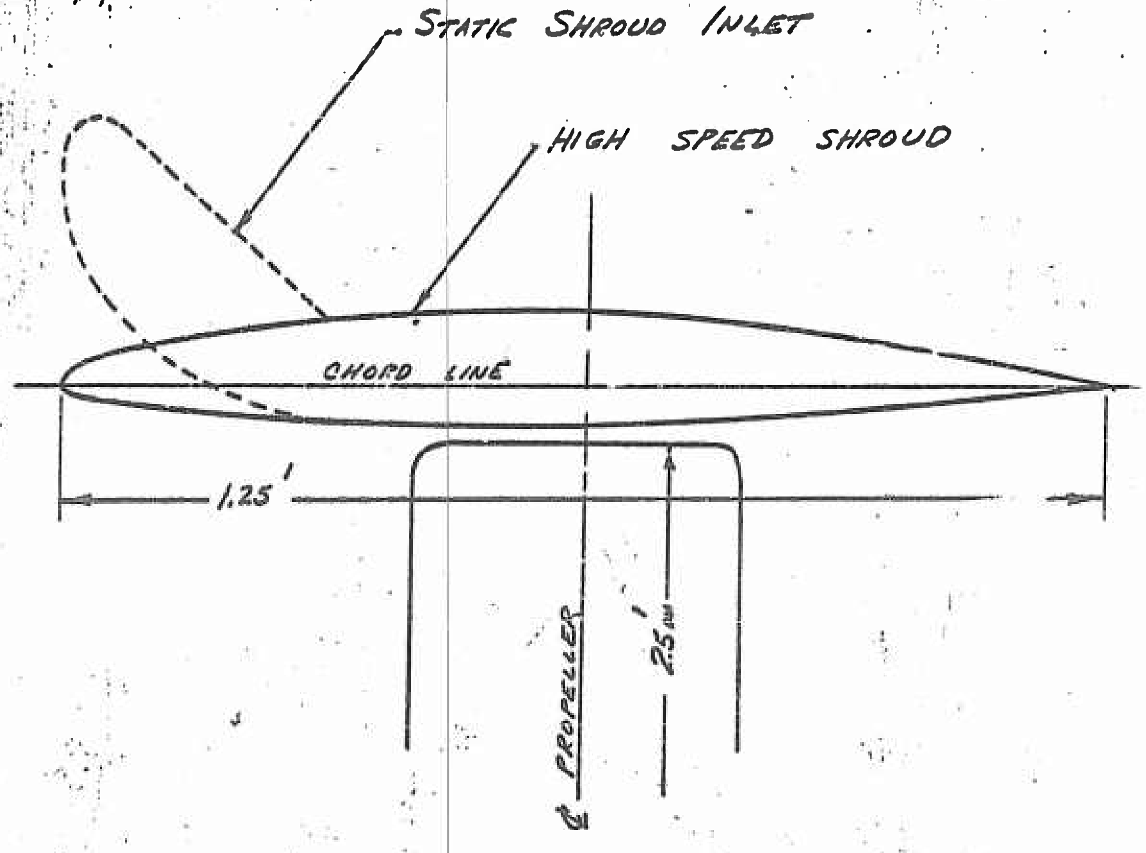

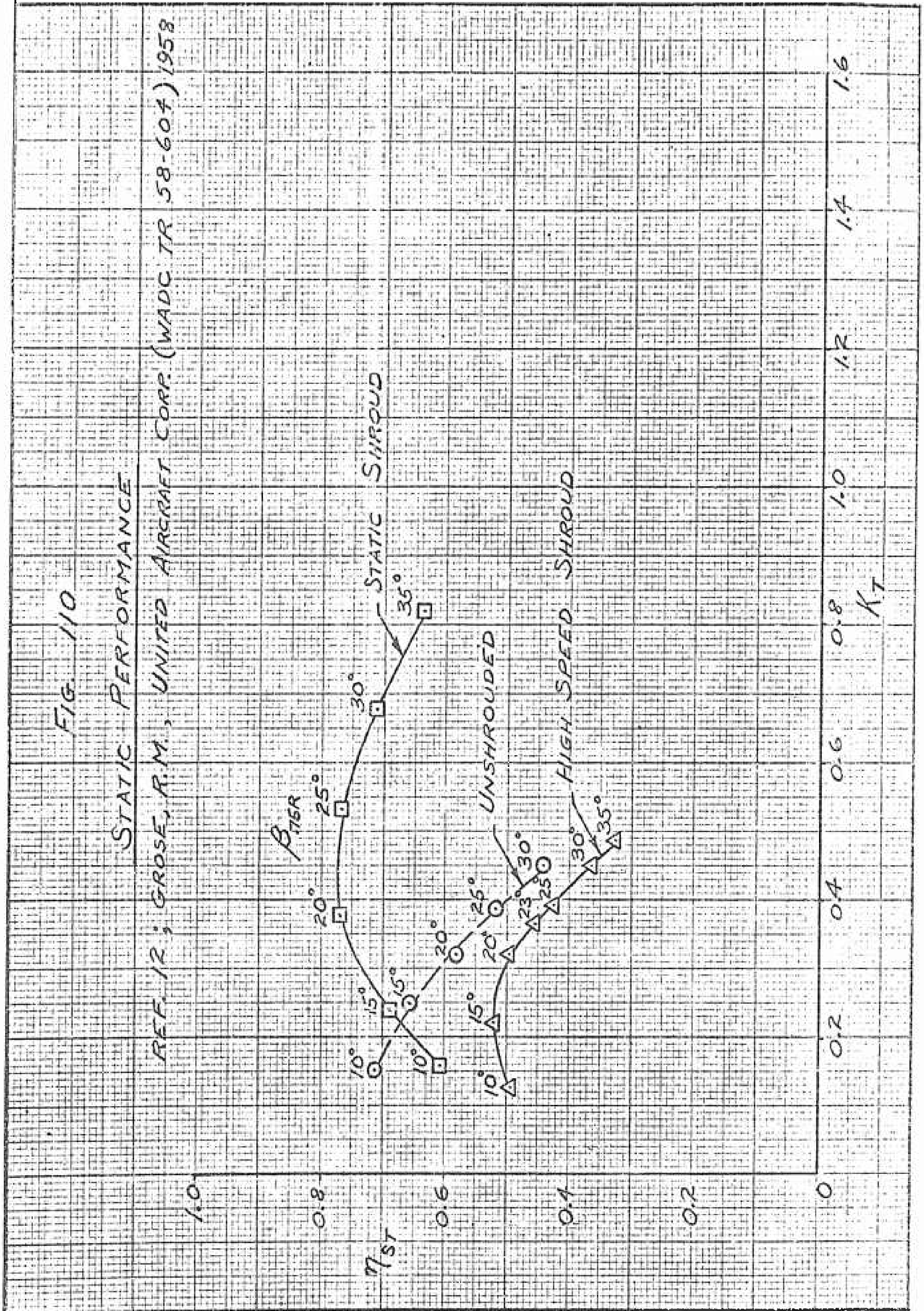
FIG. 110
STATIC PERFORMANCE
REF. 12; GROSE, R.M., UNITED AIRCRAFT CORP. (WADC TR 58-604) 1958
$\beta_{.75R}$
STATIC SHROUD
UNSHROUDED
HIGH SPEED SHROUD
10°
15°
20°
23°
25°
30°
35°
η_{ST}
1.0
0.8
0.6
0.4
0.2
0
K_T
1.2
1.4
1.6

PREPARED 6-27-60

CHECKED

REVISED

REPORT NO

MODEL

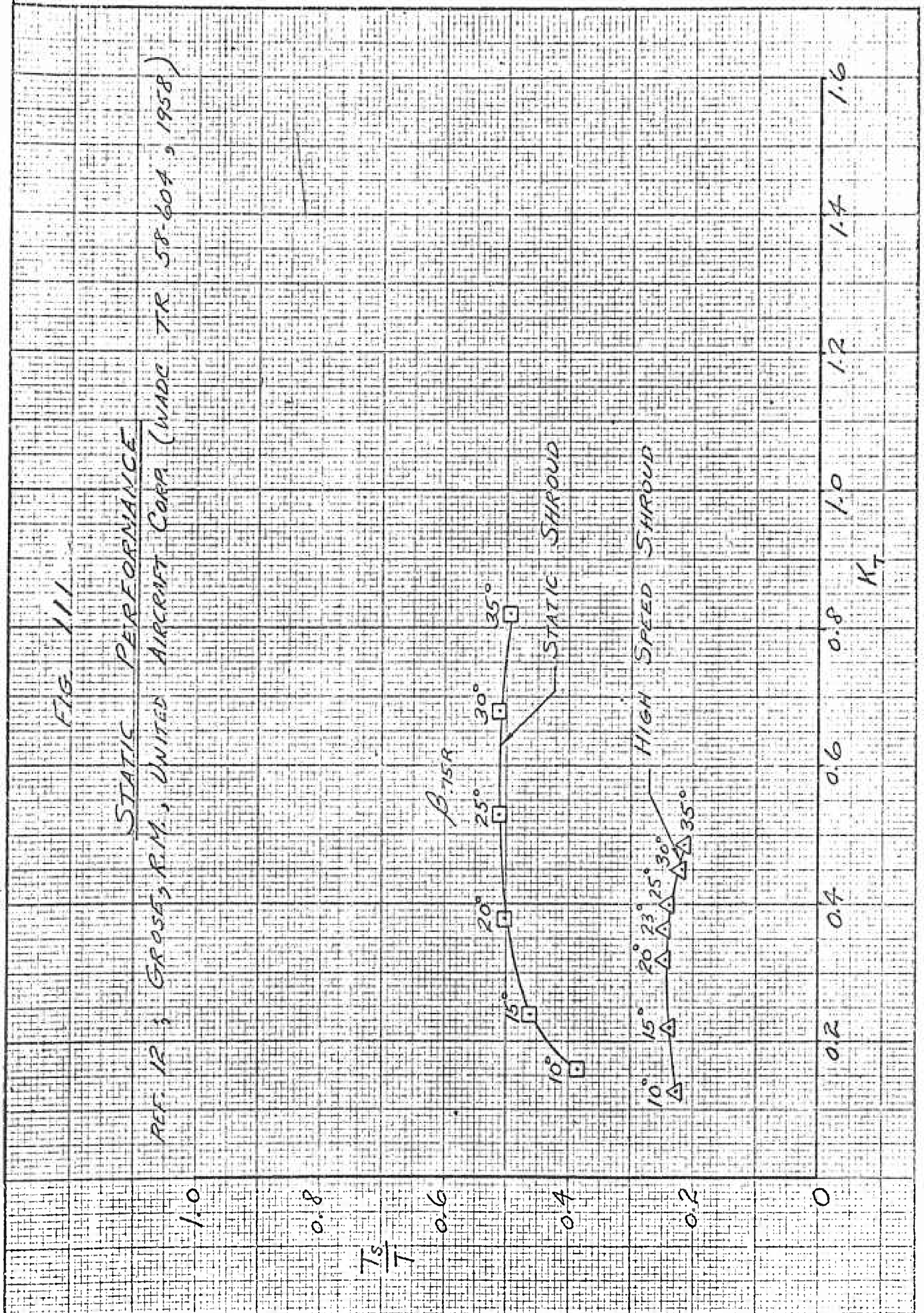

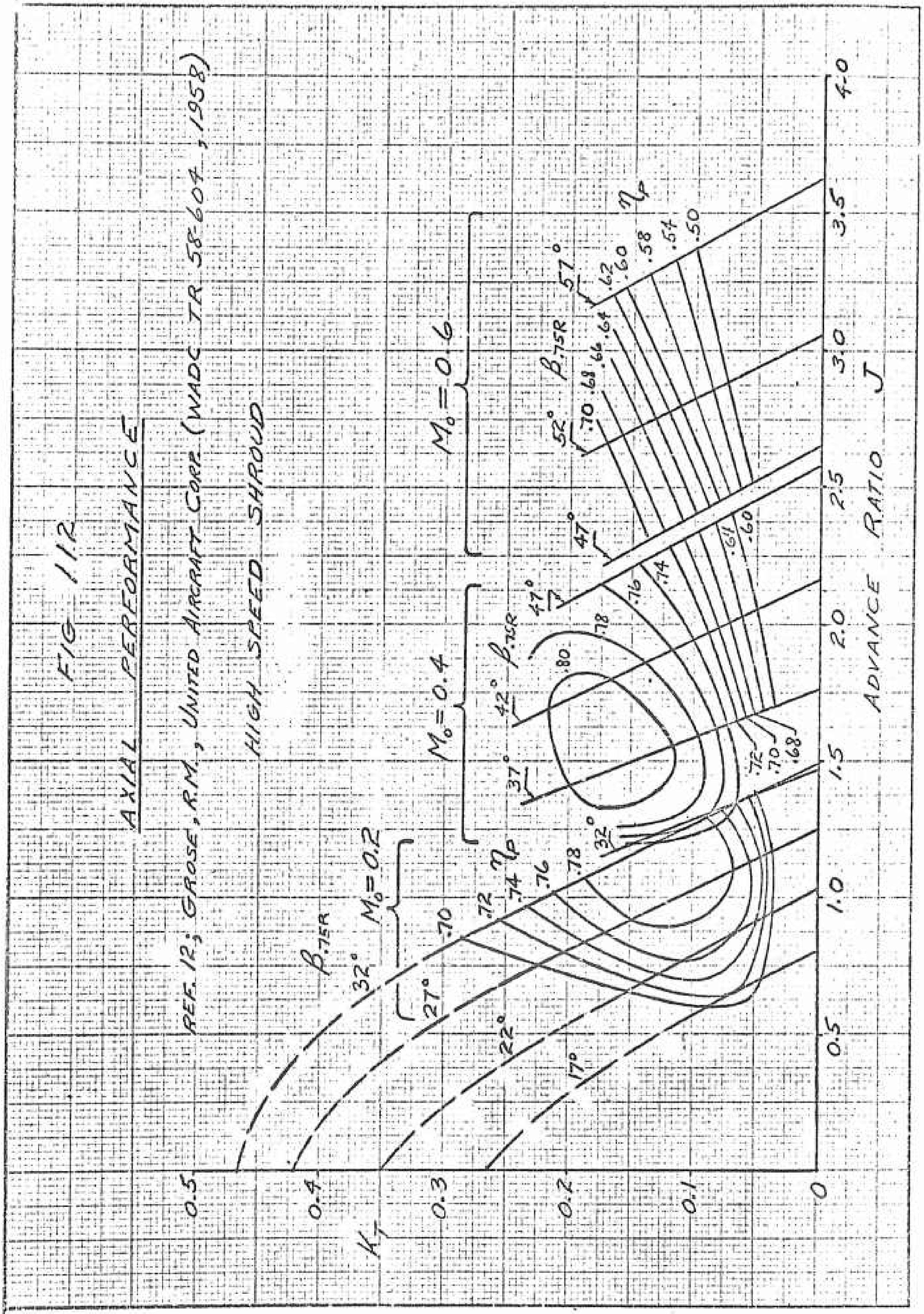
FIG 11.2
AXIAL PERFORMANCE
REF. 12; GROSE, R.M., UNITED AIRCRAFT CORP. (WADC TR 58-604, 1958)
HIGH SPEED SHROUD
K_T
ADVANCE RATIO J
$M_o = 0.2$
$M_o = 0.4$
$M_o = 0.6$
$\beta_{.75R}$
η_P
17°
22°
27°
32°
37°
42°
47°
52°
57°
.70
.72
.74
.76
.78
.80
.68
.61
.60
.66
.64
.62
.58
.54
.50
0
0.1
0.2
0.3
0.4
0.5
1.0
1.5
2.0
2.5
3.0
3.5
4.0

PREPARED ~~~~ 2-16-60

CHECKED

REVISED

REPUBLIC AVIATION

REPORT NO

MODEL

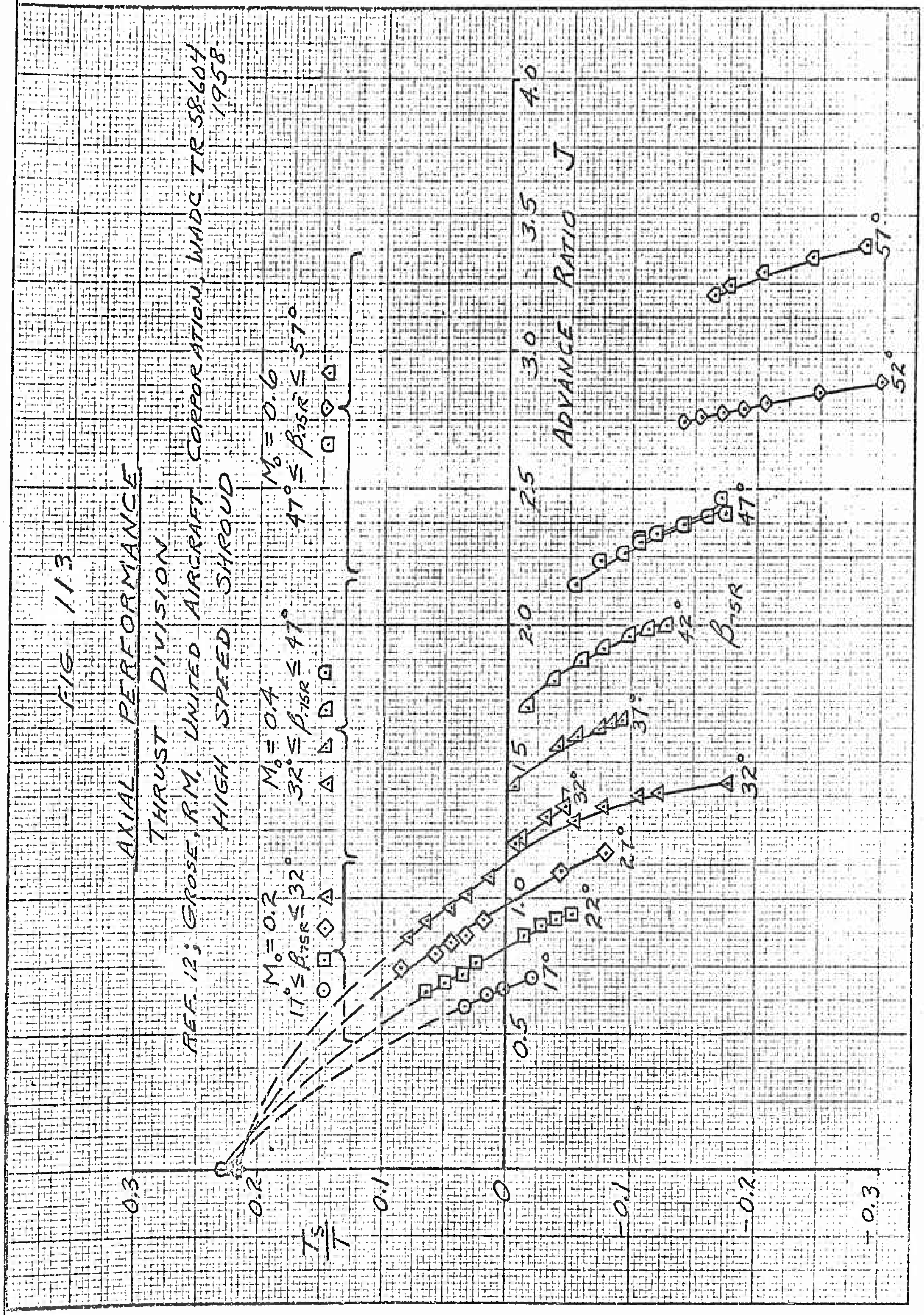

REPUBLIC AVIATION

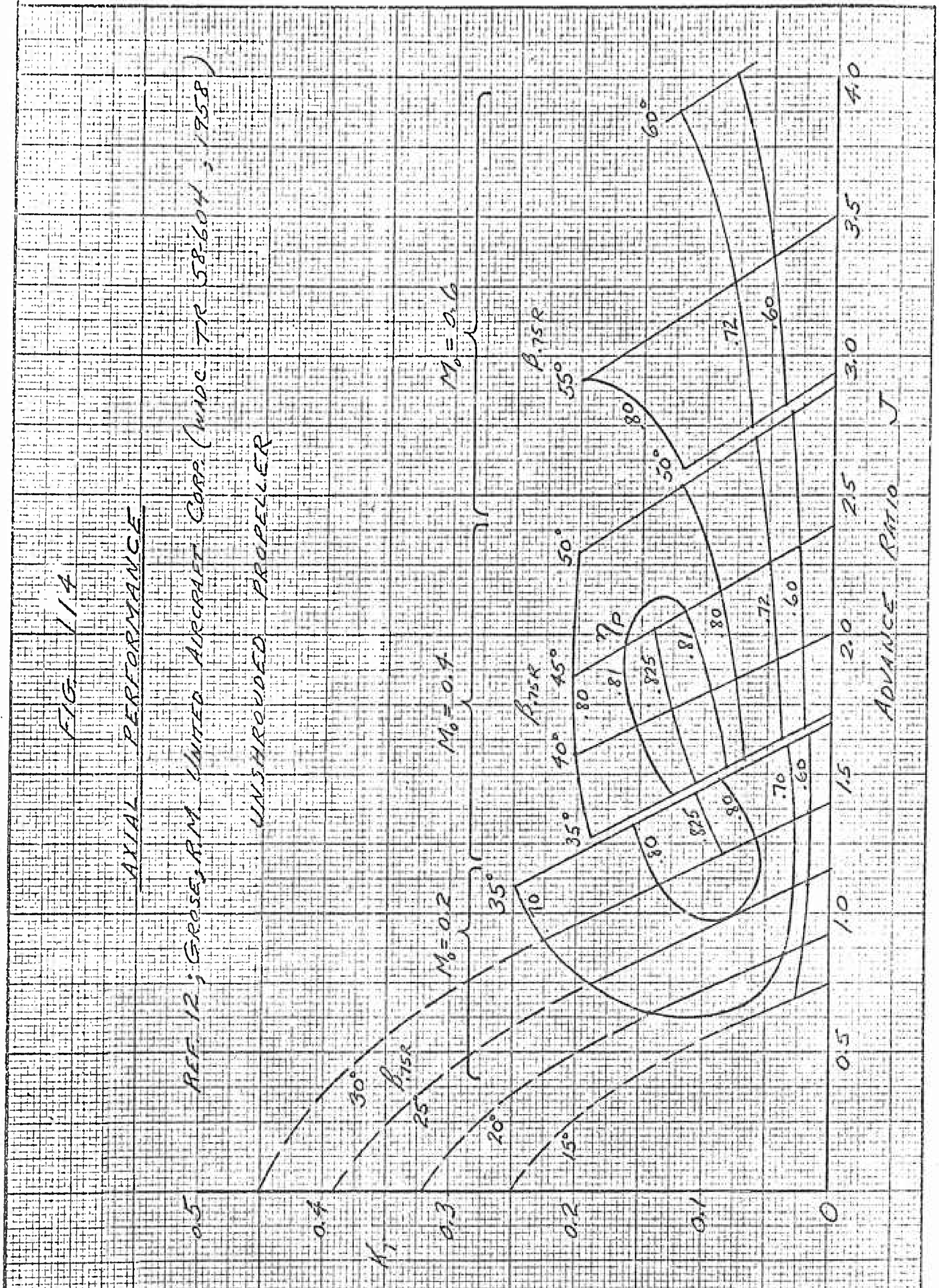

FIG. 114
AXIAL PERFORMANCE
REF. 12; GROSE, R.M. UNITED AIRCRAFT CORP. (WADC TR 58-604, 1958)
UNSHROUDED PROPELLER

Reference	60
Author	Platt, R. J.
Source	NACA
Figs.	115-121

FIG. 115

SHROUD CONFIGURATIONS

REF. 60; PLATT, R.J., NACA RM L7H25, 1948

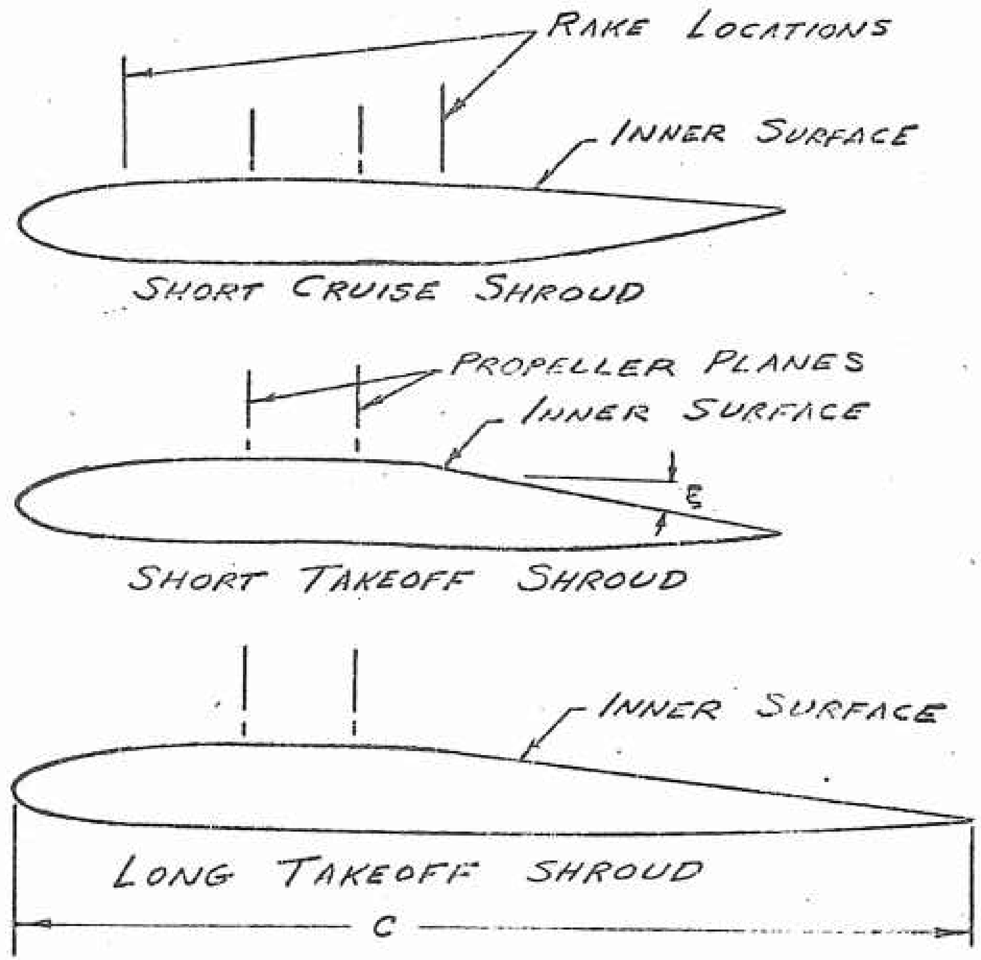

C_S INCHES	C_S/d	A_E/A	ξ DEGREES
32.2	0.671	1.1	3.5
32.2	0.671	1.3	11.2
40.1	0.836	1.3	7.2

PREPARED JRS 1-17-60

CHECKED

REVISED

REPORT NO.

MODEL

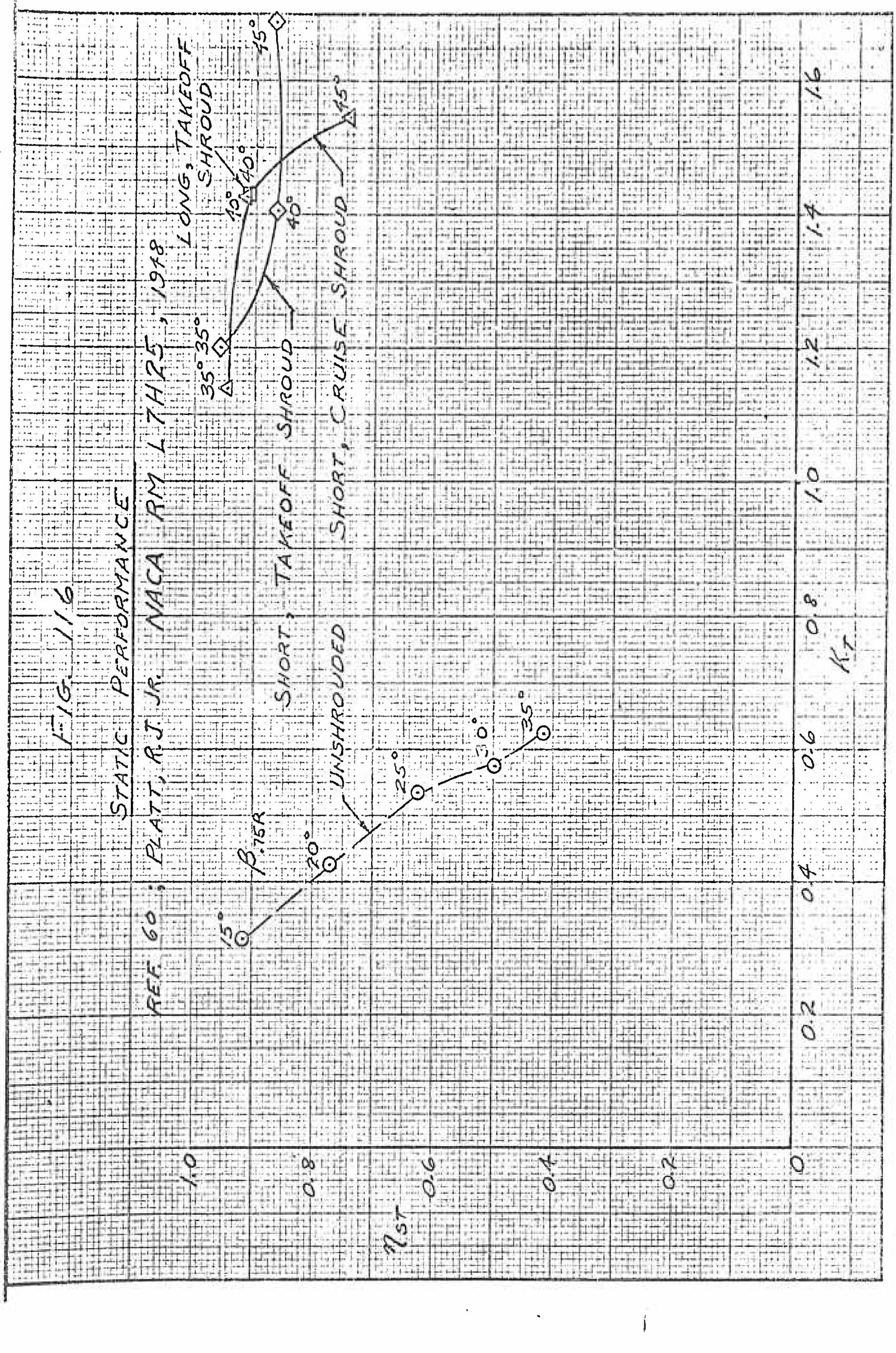

FIG. 117

STATIC PERFORMANCE
SHROUD PRESSURE DISTRIBUTION
REF. 60; PLATT, R.J., NACA RM L7H25, 1948

SHORT TAKEOFF SHROUD

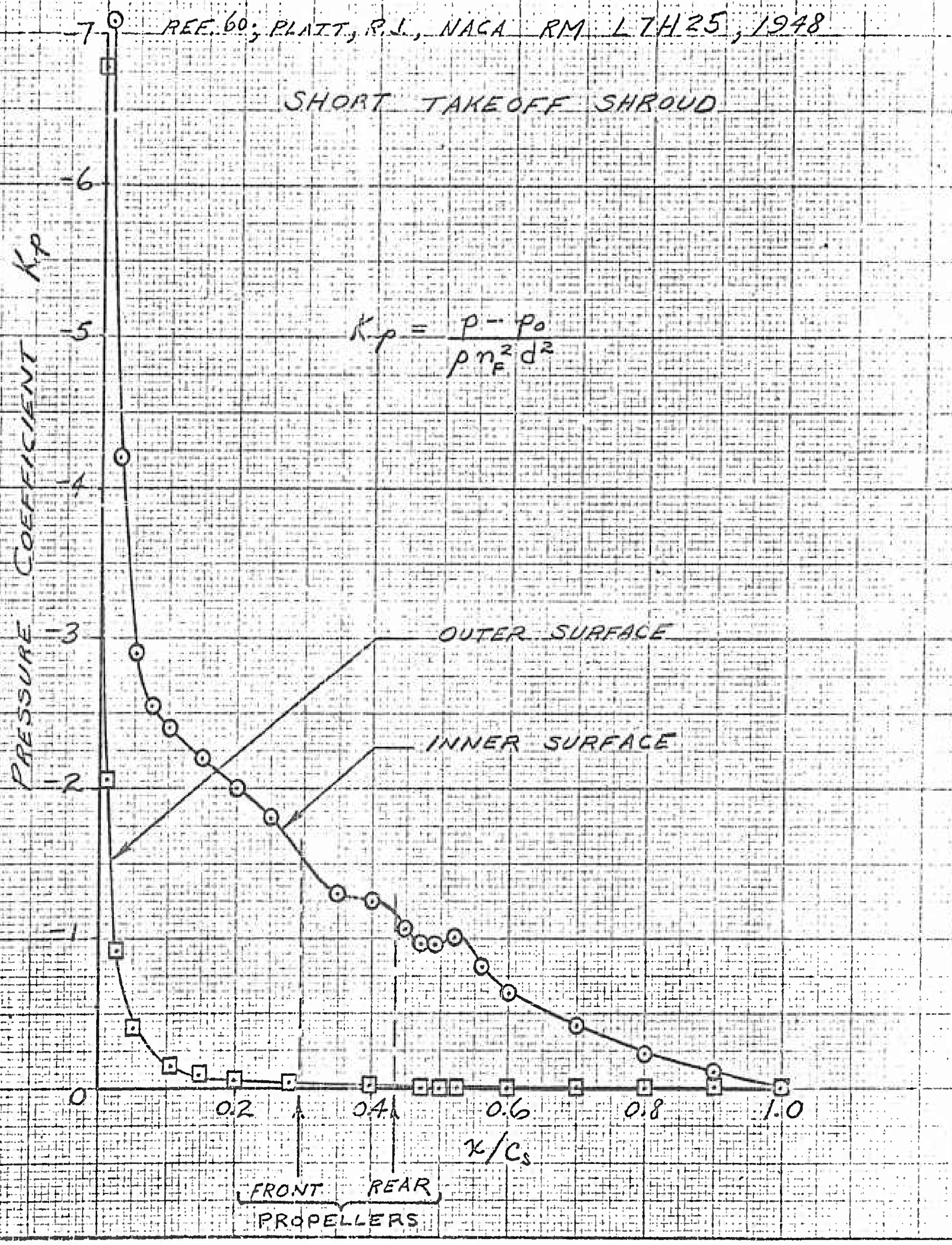

FIG. 118

STATIC PERFORMANCE
AXIAL VELOCITY DISTRIBUTIONS

REF. 60; PLATT, R.J., NACA RM L7H25, 1948

SHORT CRUISE SHROUD
2200 - 2600 RPM

PROPELLERS LOCATED AT 0.3 C_s AND .44 C_s

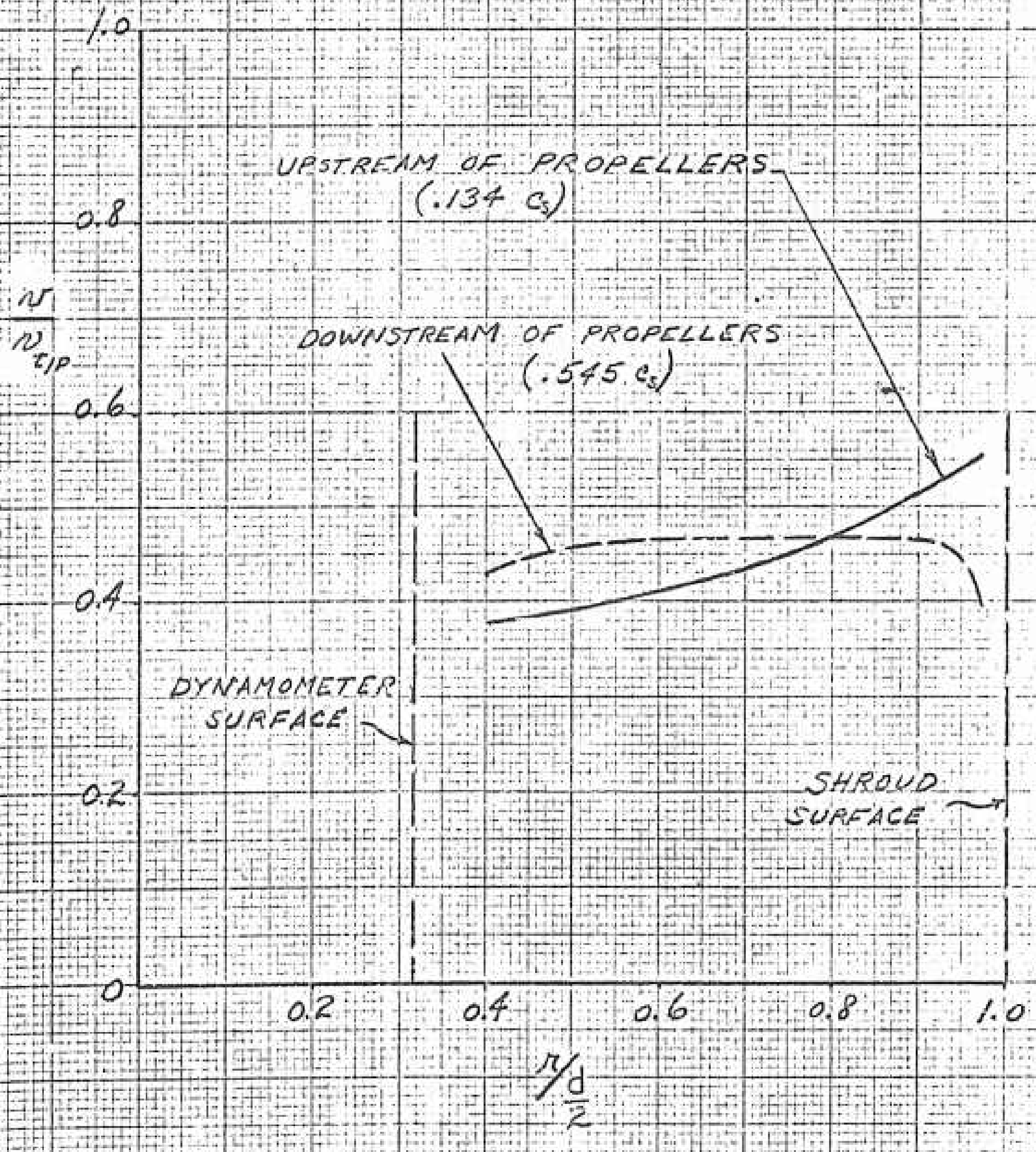

PREPARED JGL 2-24-60 PAGE 260

CHECKED REPORT NO

REVISED MODEL

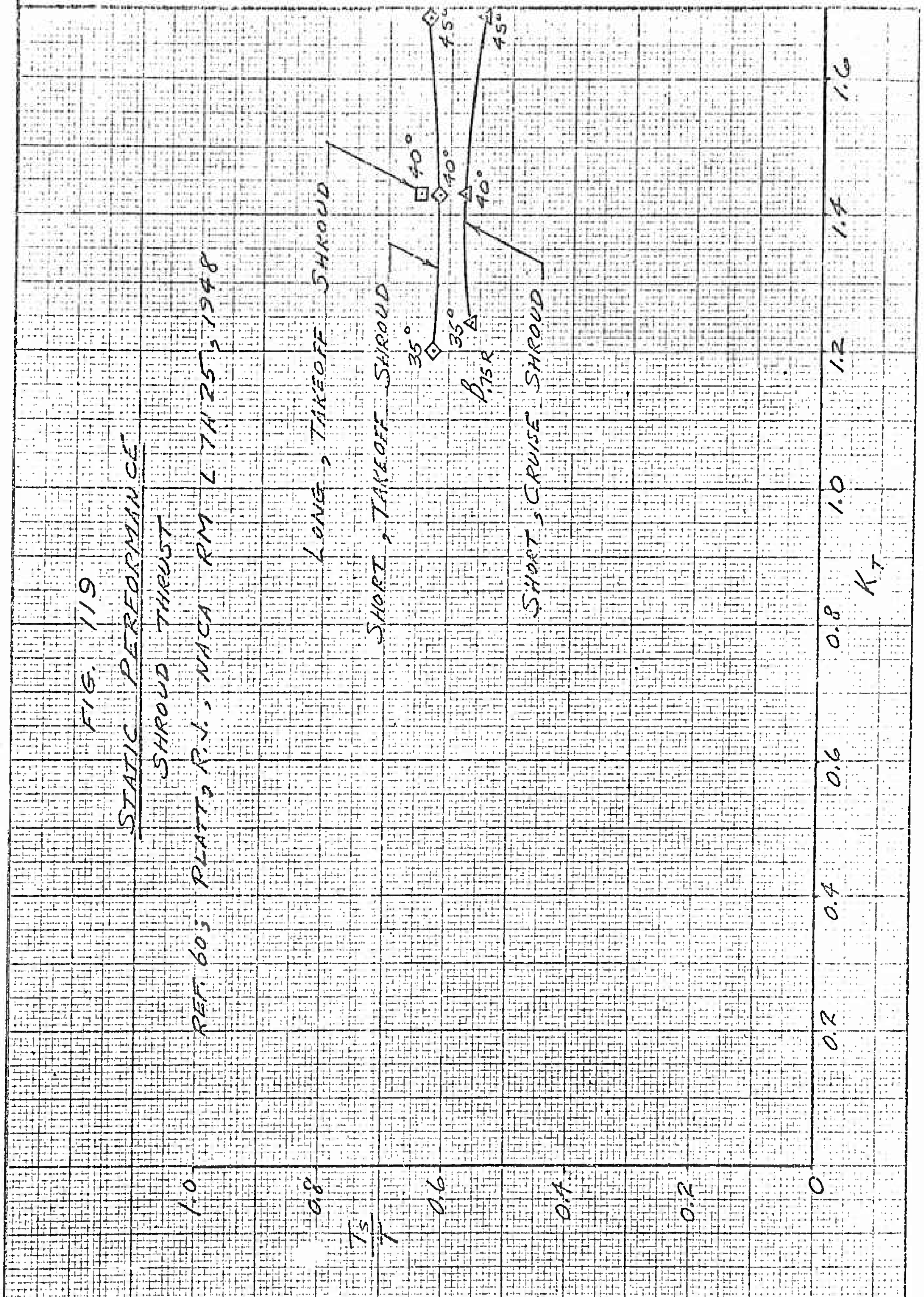

E-10A REV 2/49

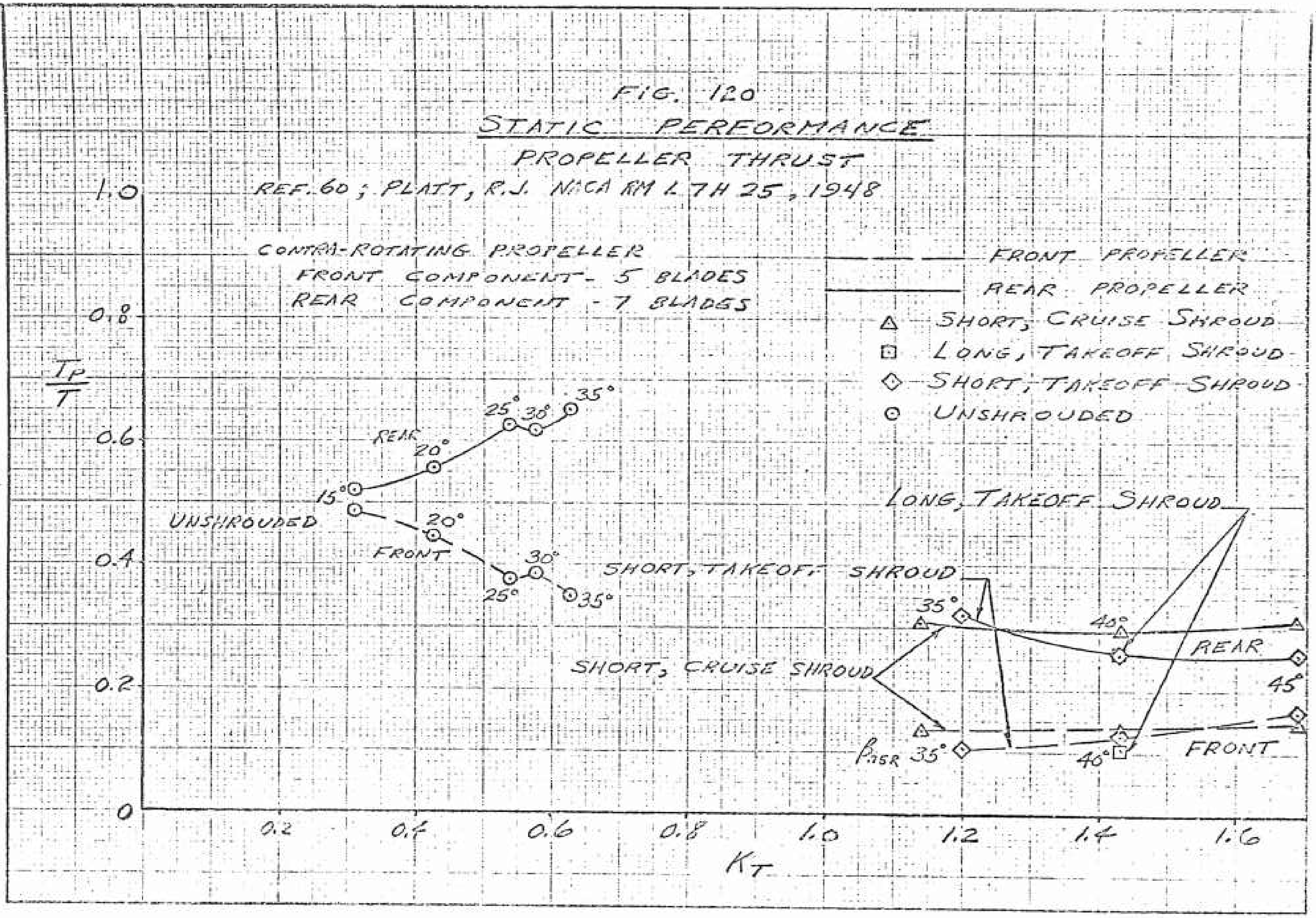

FIG. 120
STATIC PERFORMANCE
PROPELLER THRUST
REF. 60; PLATT, R.J. NACA RM L7H25, 1948

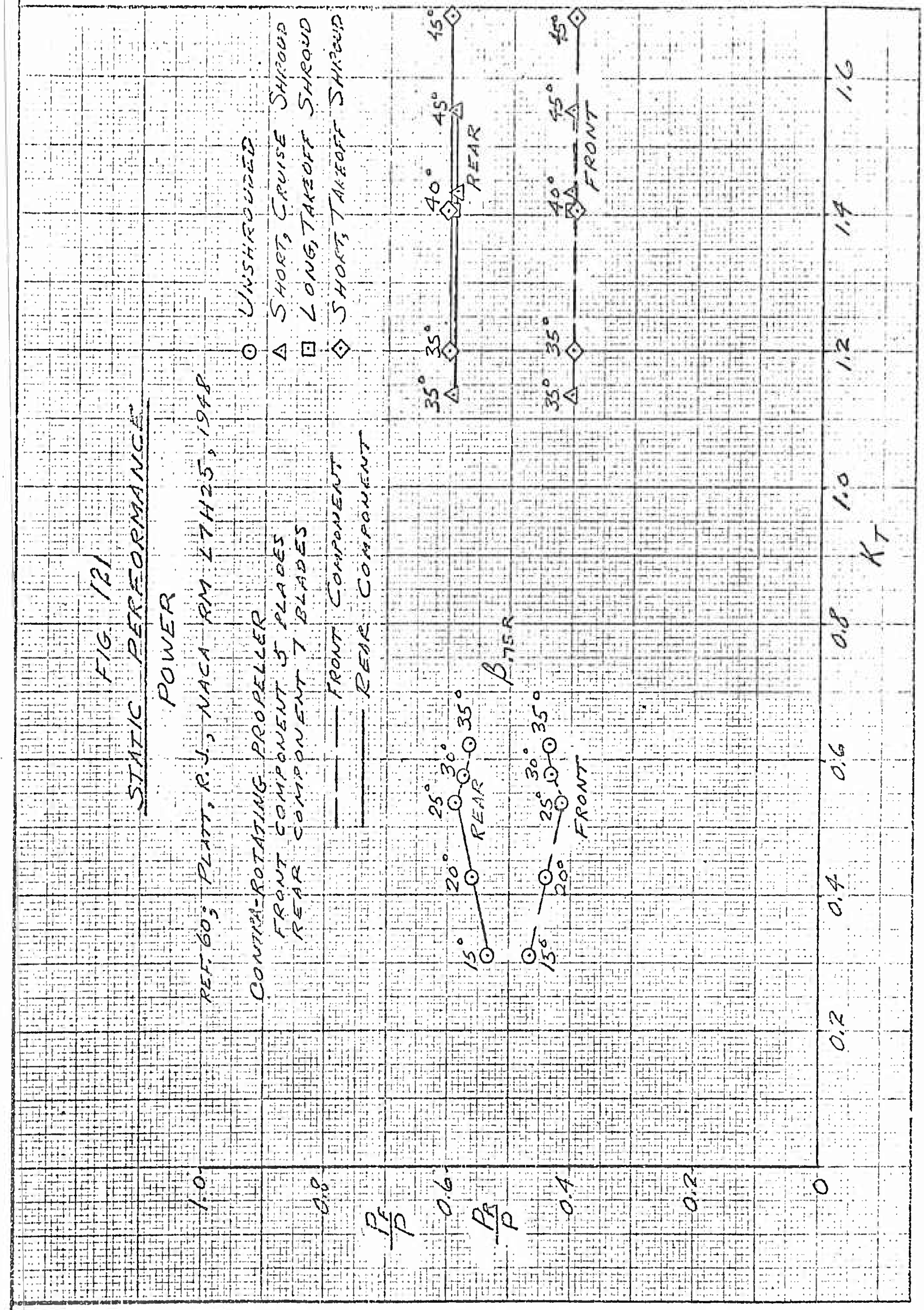
FIG. 121
STATIC PERFORMANCE
POWER
REF. 60; PLATT, R.J., NACA RM L7H25, 1948
CONTRA-ROTATING PROPELLER
FRONT COMPONENT 5 BLADES
REAR COMPONENT 7 BLADES
FRONT COMPONENT
REAR COMPONENT
UNSHROUDED
SHORT, CRUISE SHROUD
LONG, TAKEOFF SHROUD
SHORT, TAKEOFF SHROUD
$\beta_{.75R}$
REAR
FRONT
15°
20°
25°
30°
35°
40°
45°
K_T
0
0.2
0.4
0.6
0.8
1.0
1.2
1.4
1.6
$\frac{P_F}{P}$
$\frac{P_R}{P}$

Reference	31
Author	Krüger, W.
Source	AVA Goettingen, Germany
Figs.	122-130

FIG. 122

CONFIGURATION

REF. 31 ; KRUGER, W. ZWB FORSCHUNGSBERICHT NR 1949
(NACA TM 1202 , 1949)

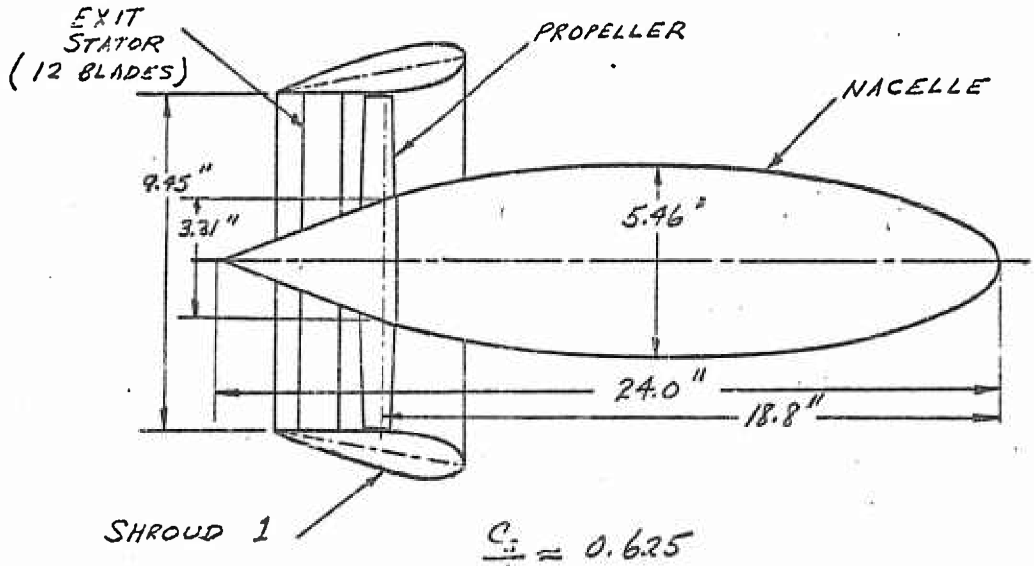

$\frac{c_s}{d} \approx 0.625$

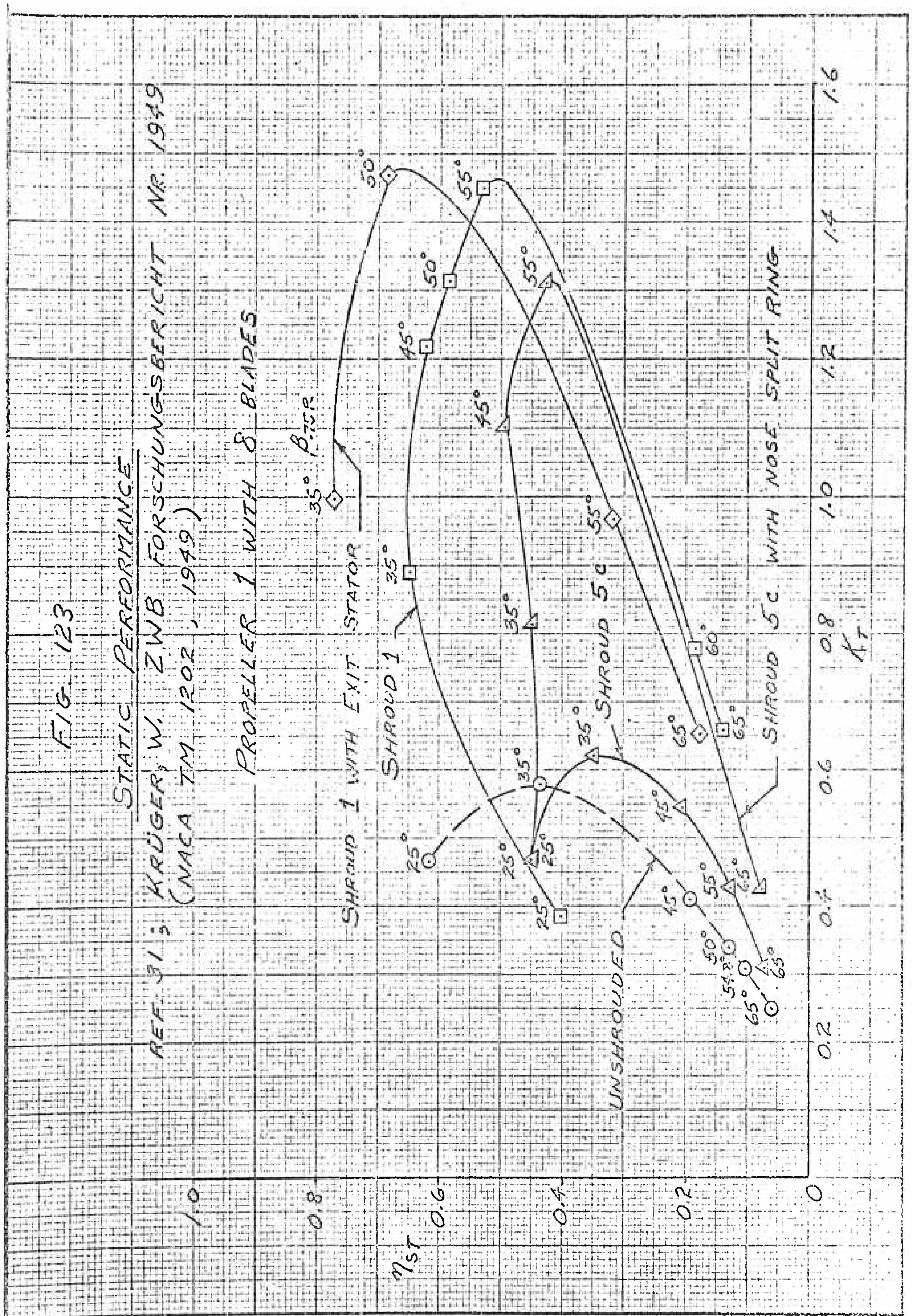
FIG. 123
STATIC PERFORMANCE
REF. 31; KRÜGER, W. ZWB FORSCHUNGSBERICHT NR. 1949
(NACA TM 1202, 1949)
PROPELLER 1 WITH 8 BLADES
SHROUD 1 WITH EXIT STATOR
SHROUD 1
SHROUD 5C
SHROUD 5C WITH NOSE SPLIT RING
UNSHROUDED
$\beta_{.75R}$
η_{ST}
K_T
0
0.2
0.4
0.6
0.8
1.0
1.2
1.4
1.6

PREPARED JBS 1-18-60

CHECKED

REVISED

REPUBLIC AVIATION

REPORT NO

MODEL

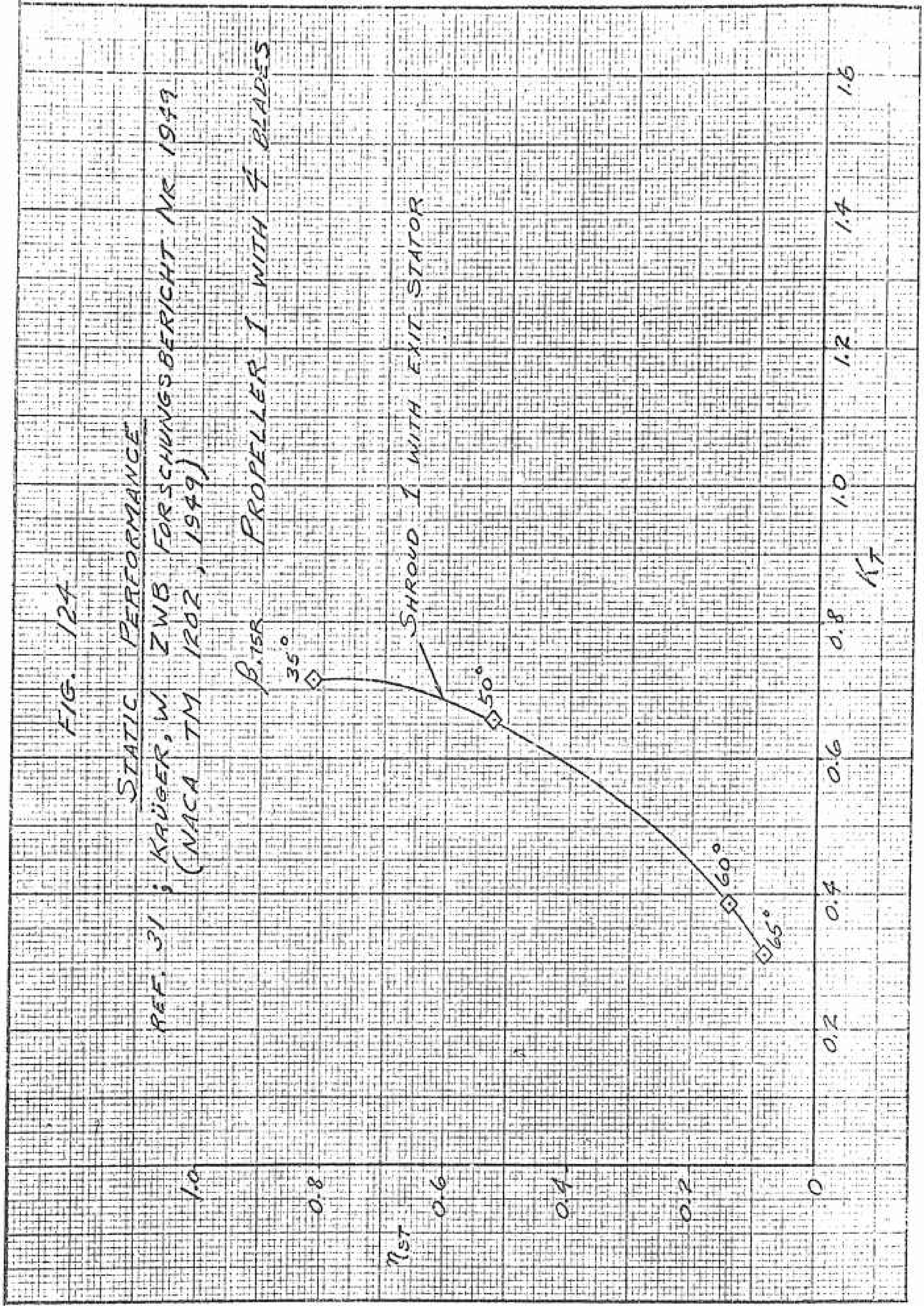

FIG. 124

STATIC PERFORMANCE

REF. 31; KRÜGER, W. ZWB FORSCHUNGSBERICHT NR 1949
(NACA TM 1202, 1949)

PROPELLER I WITH 4 BLADES

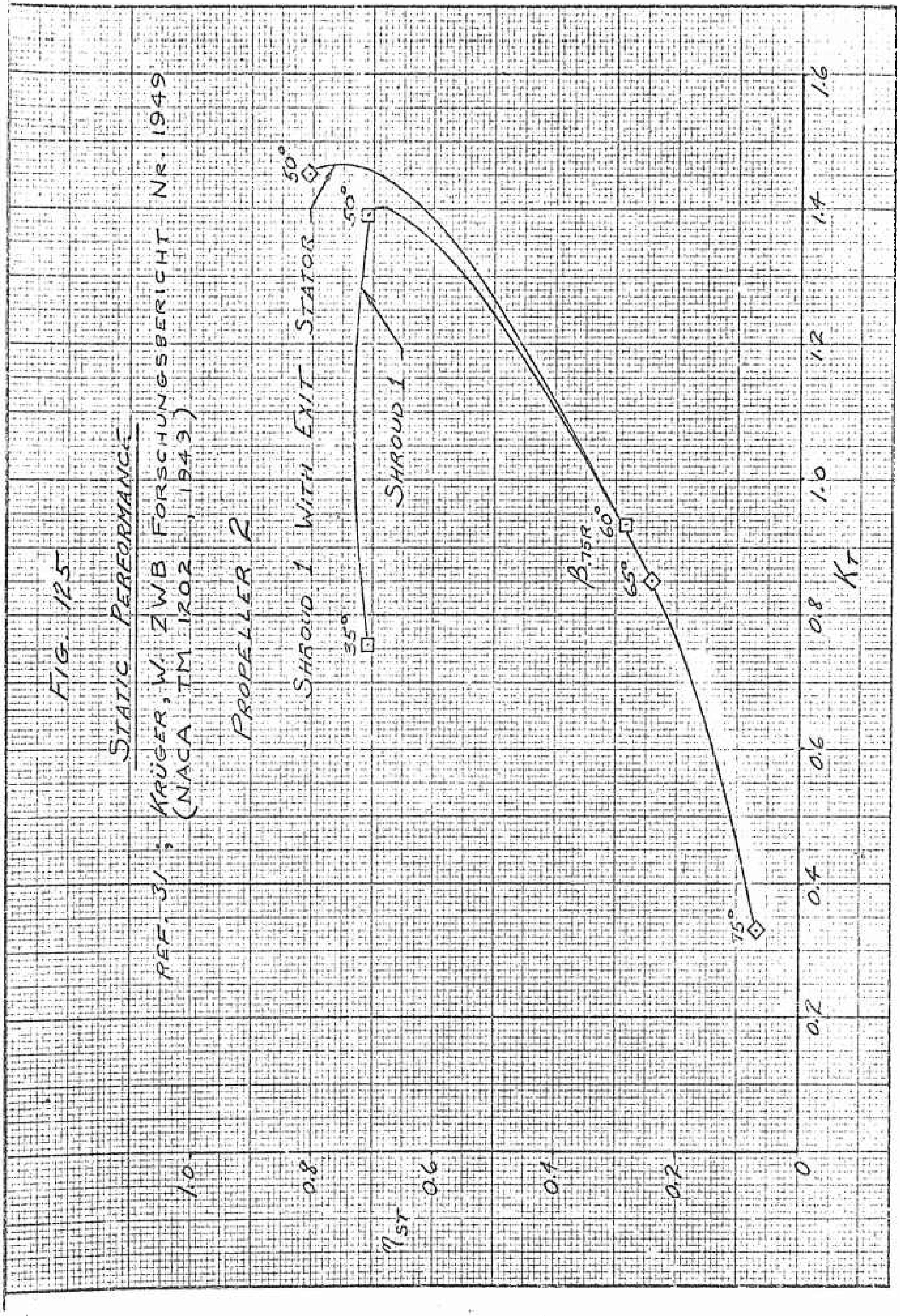
FIG. 125
STATIC PERFORMANCE
REF. 31; KRÜGER, W. ZWB FORSCHUNGSBERICHT Nr. 1949
(NACA TM 1202, 1949)
PROPELLER 2
SHROUD 1 WITH EXIT STATOR
SHROUD 1
$\beta_{.75R}$
50°
50°
35°
60°
65°
75°
η_{ST}
K_T
0
0.2
0.4
0.6
0.8
1.0
1.2
1.4
1.6

FIG. 126

AXIAL PERFORMANCE

REF 31 ; KRÜGER, W. ZWB FORSCHUNGSBERICHT NR 1949
(NACA TM 1202 , 1949)

PROPELLER 1 : (8 BLADES)
UNSHROUDED

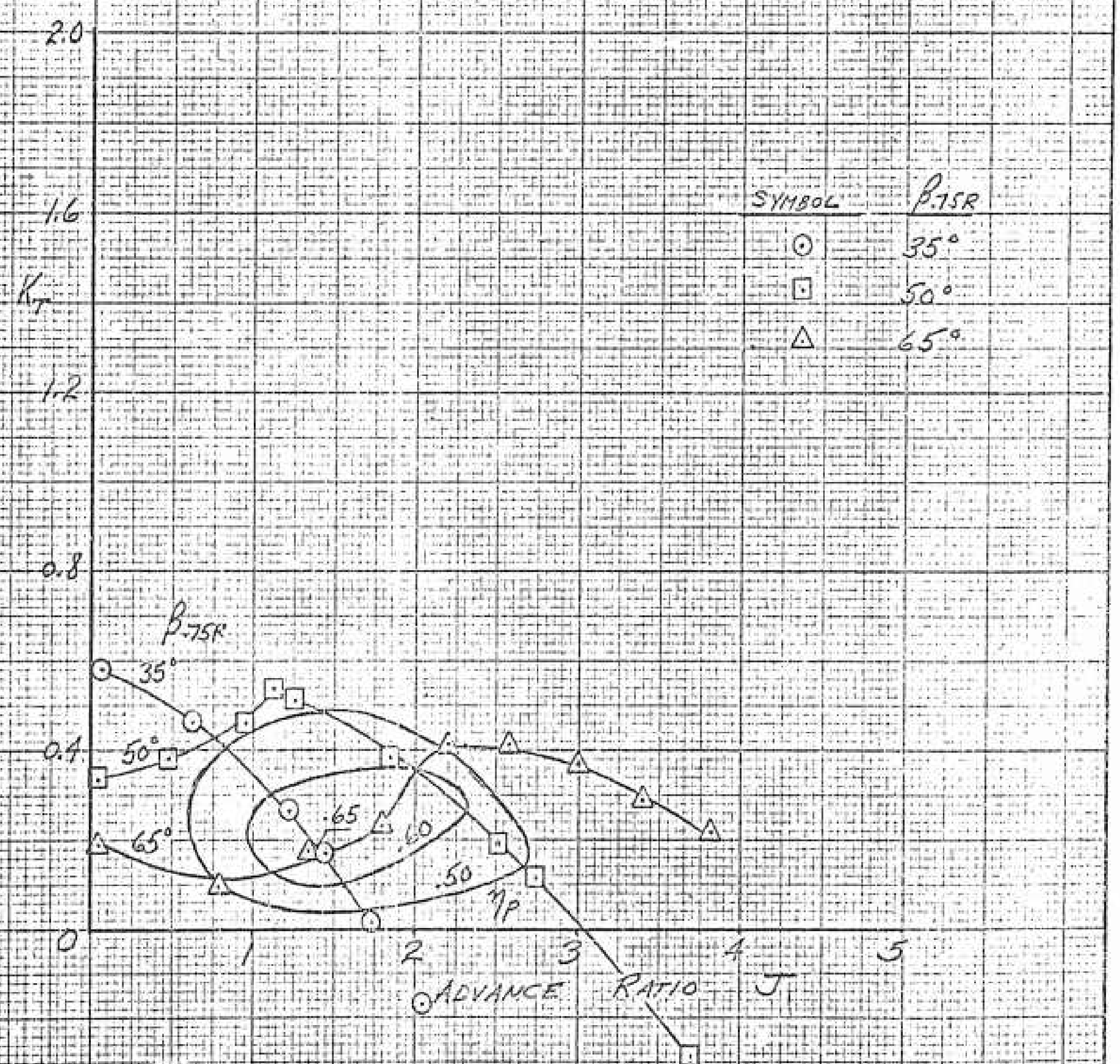

FIG. 127

AXIAL PERFORMANCE

REF. 31: KRÜGER, W., ZWB FORSCHUNGSBERICHT NR 1949 (NACA TM 1202, 1949)

PROPELLER 1 (8 BLADES) WITH SHROUD 1 AND EXIT STATOR

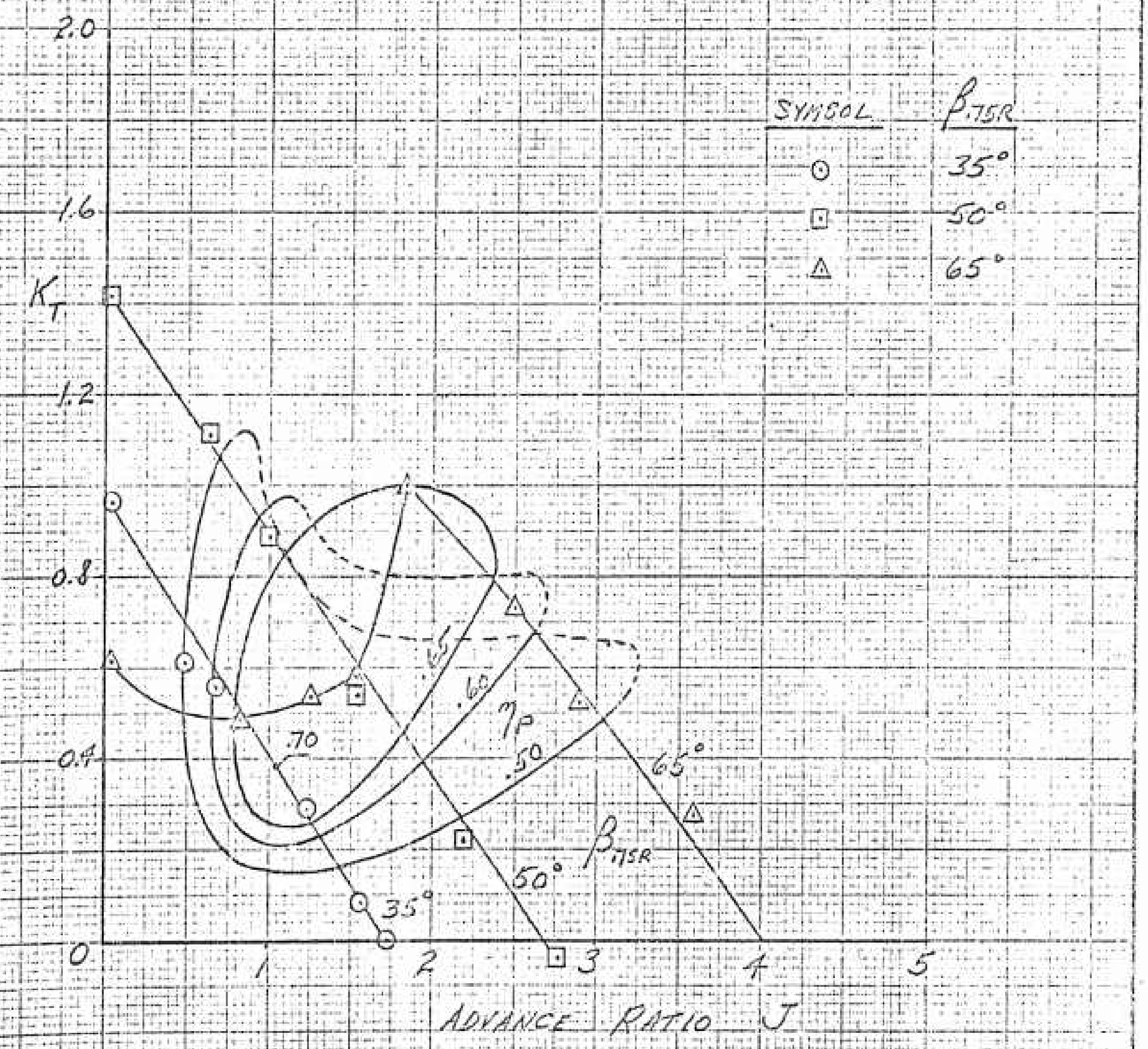

FIG 123

AXIAL PERFORMANCE
THRUST DIVISION

REF. 31 ; KRÜGER, W., ZWB FORSCHUNGSBERICHT NR 1949
(NACA TM 1202, 1949)

PROPELLER 1 (8 BLADES) WITH SHROUD 1
AND EXIT STATOR

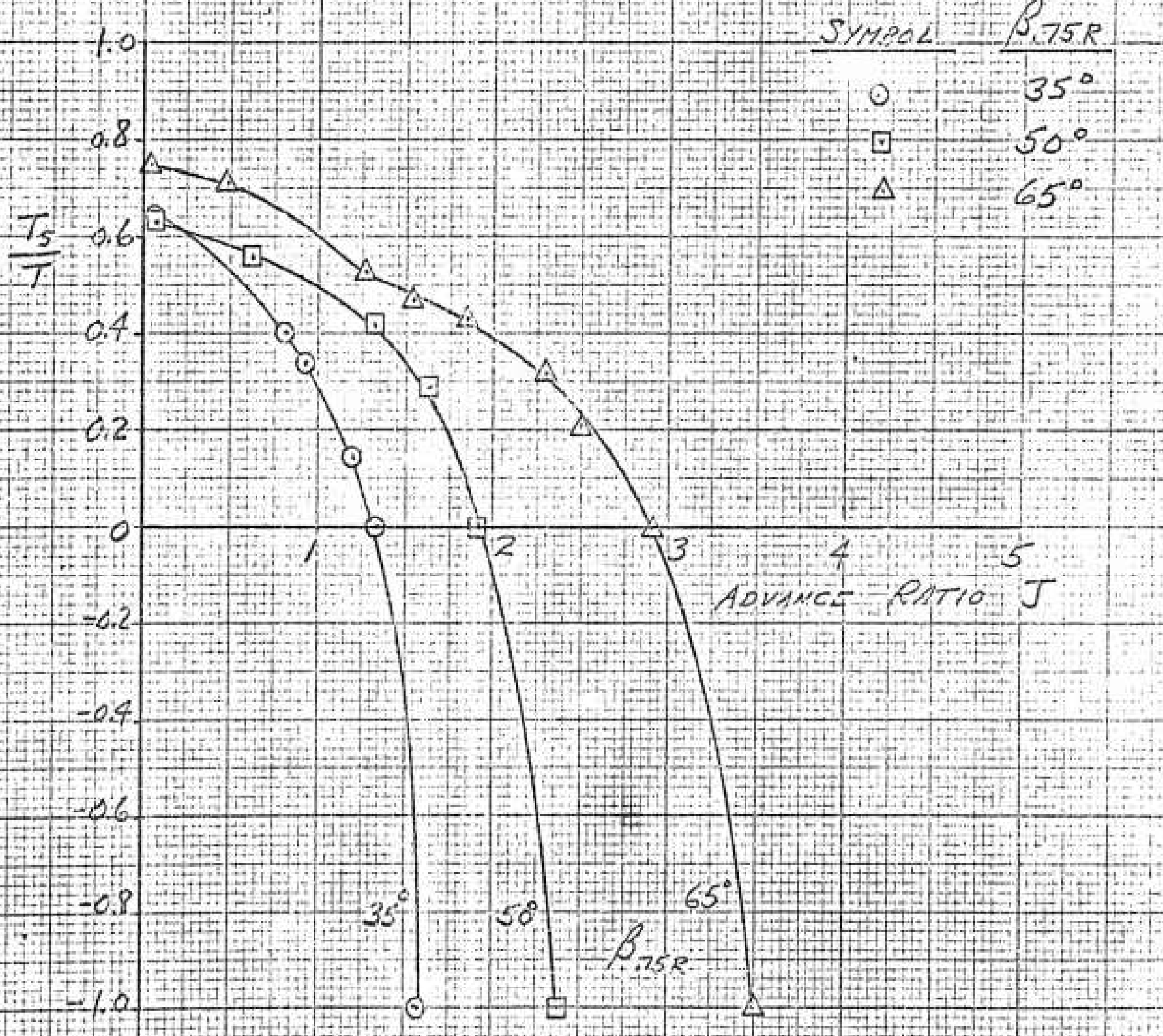

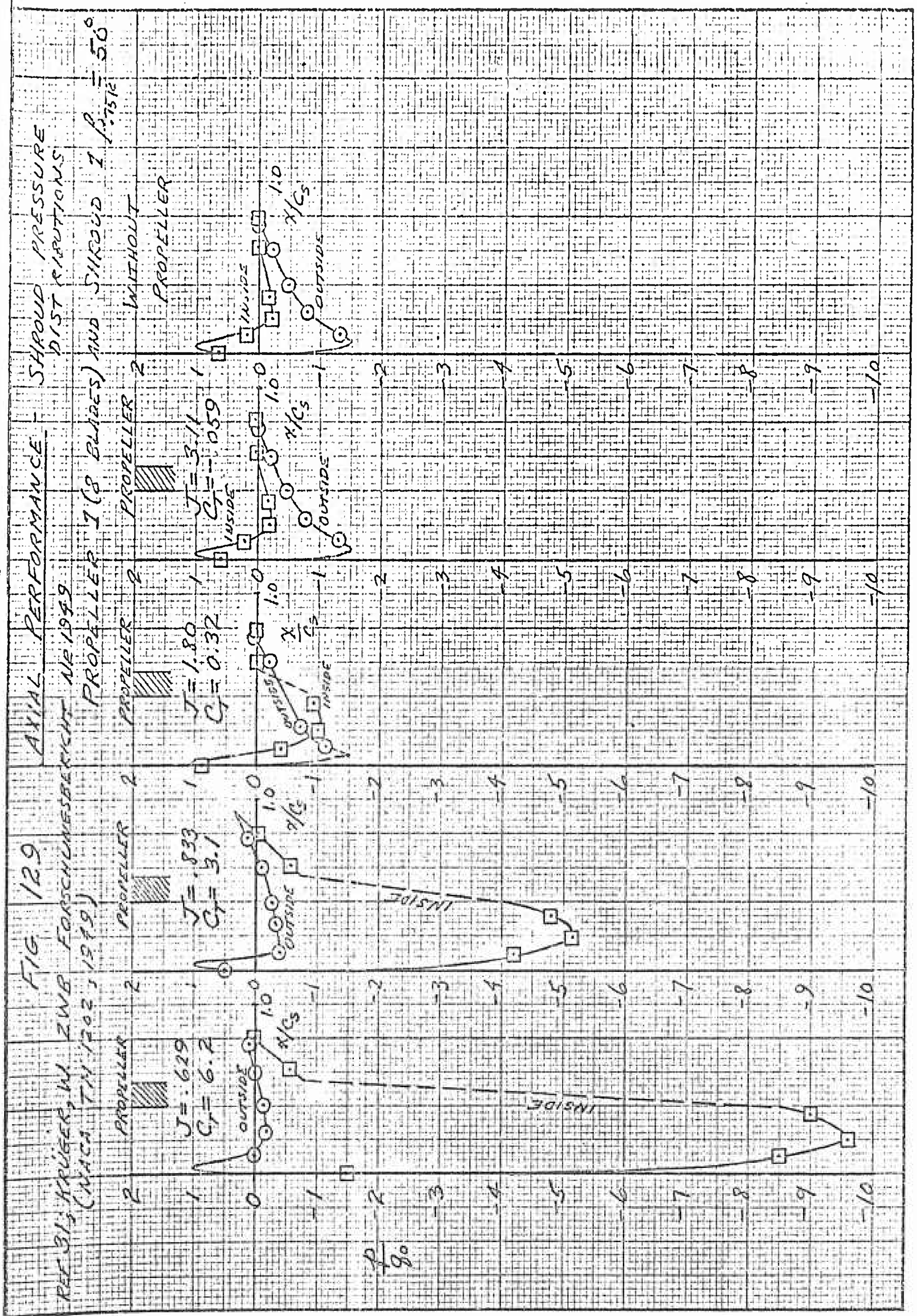
FIG. 129
AXIAL PERFORMANCE - SHROUD PRESSURE DISTRIBUTIONS
PROPELLER I (8 BLADES) AND SHROUD I $\beta_{.75R} = 50°$
REF. 31; KRÜGER, W. ZWB FORSCHUNGSBERICHT NR 1949 (NACA TM 1202, 1949)
PROPELLER
J = .629
C_T = 6.2
J = .833
C_T = 3.1
J = 1.80
C_T = 0.32
J = 3.11
C_T = -.059
WITHOUT PROPELLER
INSIDE
OUTSIDE
x/Cs
P/q_0

FIG. 130

AXIAL PERFORMANCE

REF. 31; KRÜGER, W. (NACA TM 1202, 1949)

VELOCITY DISTRIBUTION IMMEDIATELY AHEAD OF THE PROPELLER PLANE

SHROUD 1 AND/OR PROPELLER 1 (8 BLADES)

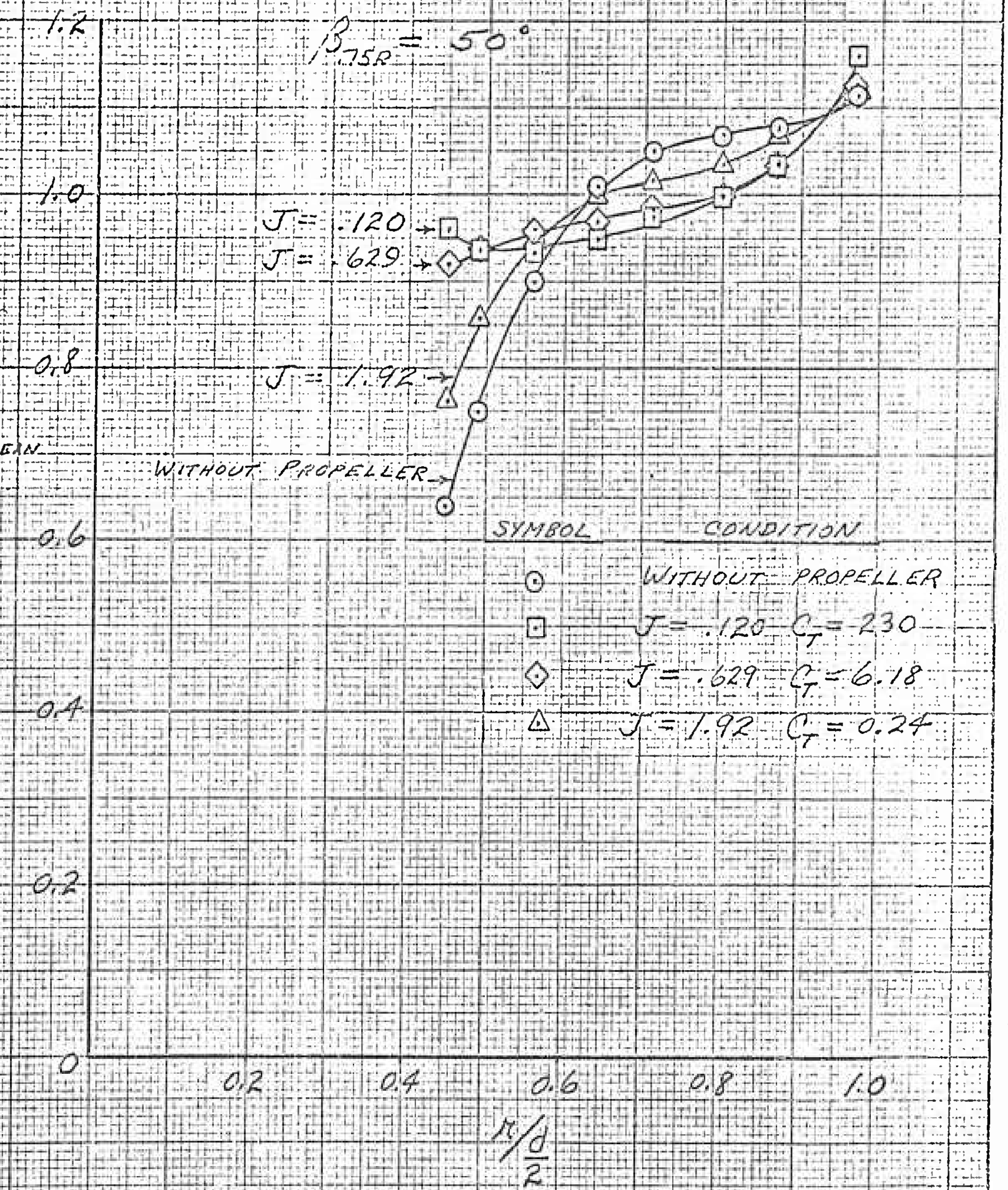

Reference	80, 81
Author	Van Manen, J. D.
Source	Wageningen, Holland
Figs.	131-138

FIG. 131

SHROUD CONFIGURATIONS

REF. 80,81; VAN MANEN, J.D., PUBL. No 115a NSMB, WAGENINGEN, 1954

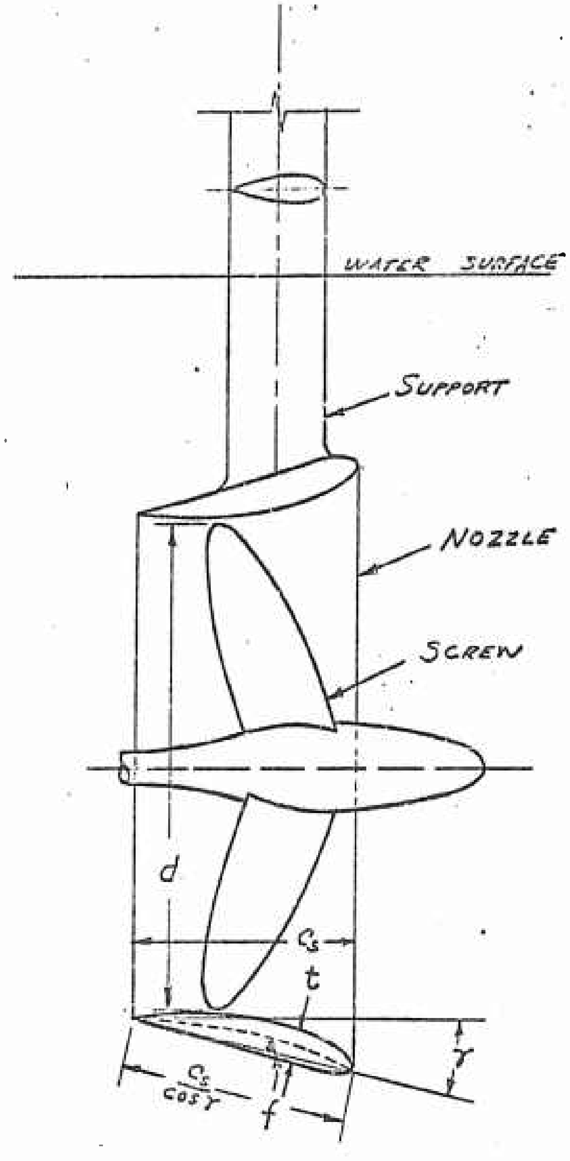

$d = .785'$

NOZZLE	$\frac{c_s}{d\cos\gamma}$	$\frac{t\cos\gamma}{c_s}$	$\frac{f\cos\gamma}{c_s}$	γ	PROFILE
1	1.00	AXIAL	CIRCULAR	CYLINDER	
2	0.67	0.15	0.04	12.7°	NACA 4415
3	0.50	0.15	0.04	12.7°	NACA 4415
4	0.83	0.15	0.04	12.7°	NACA 4415
5	0.50	0.15	0.04	15.2°	NACA 4415
6	0.50	0.15	0.04	10.2°	NACA 4415
7	0.50	0.15	0.05	12.7°	BUILT UP "NACA 5415"
8	0.50	0.15	0.03	12.7°	BUILT UP "NACA 5415"

PREPARED JBL 3-2-60

CHECKED

REVISED

REPORT NO

MODEL

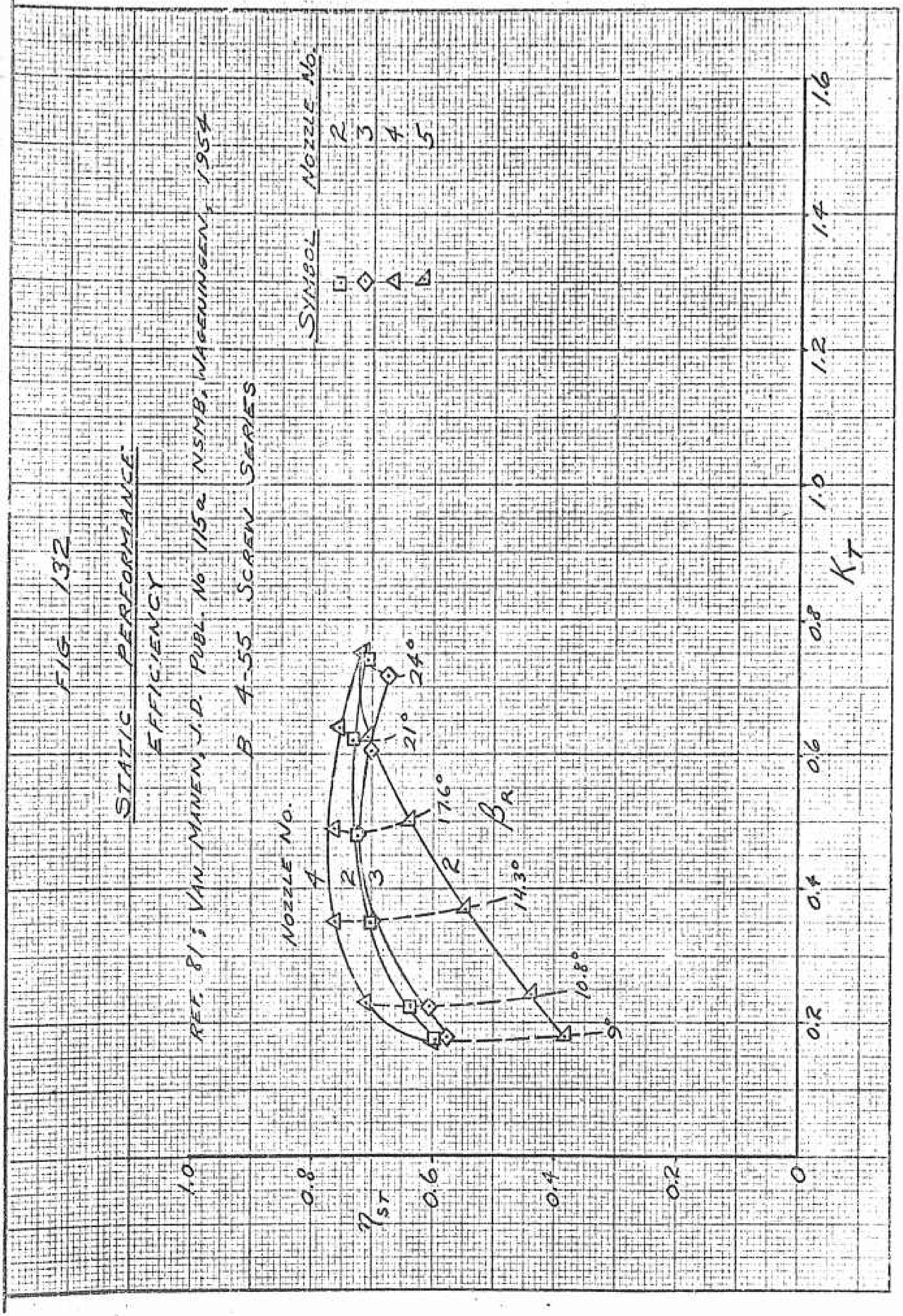

PREPARED ABS 3-2-60

CHECKED

REVISED

REPUBLIC AVIATION

REPORT NO.

MODEL

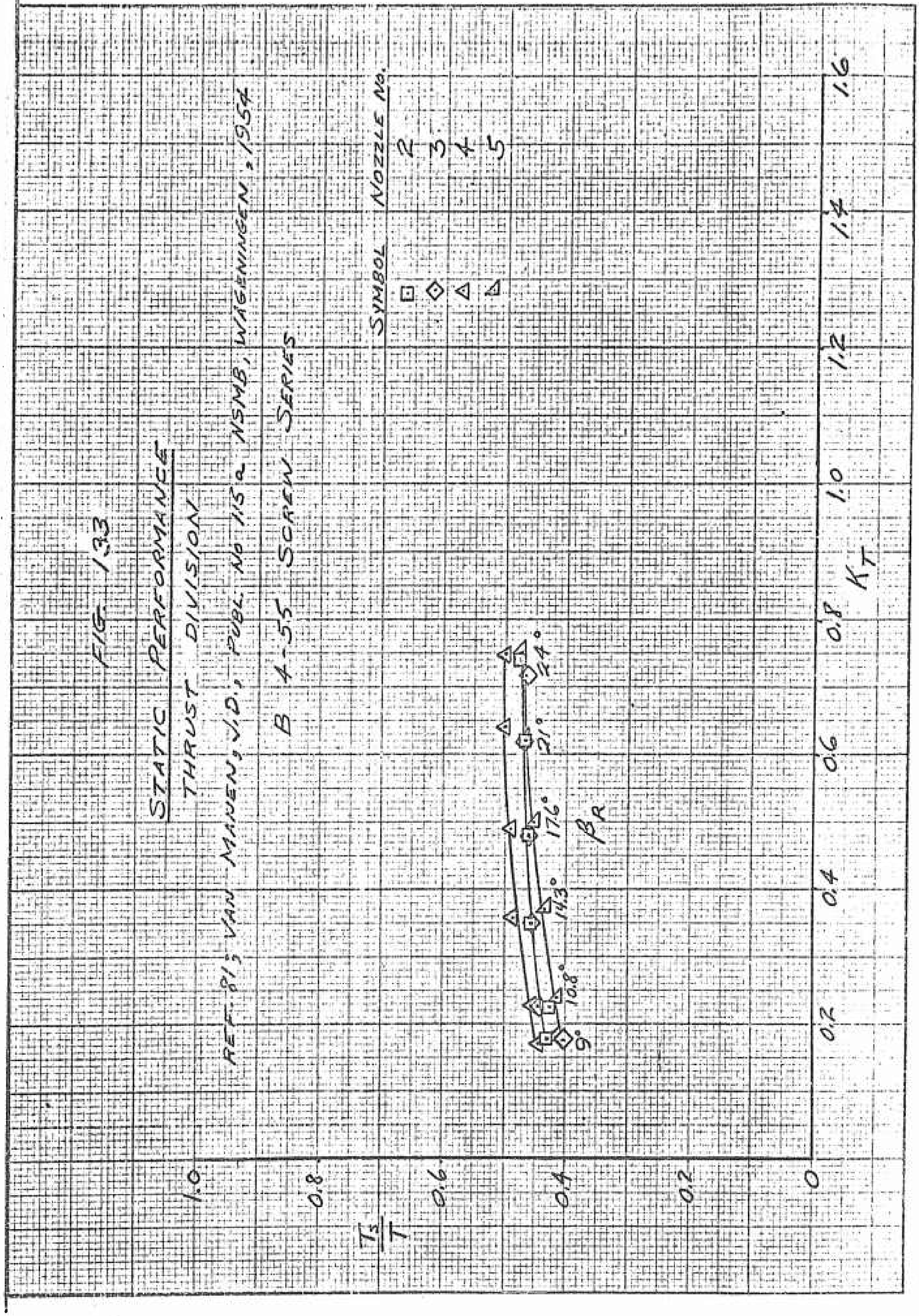

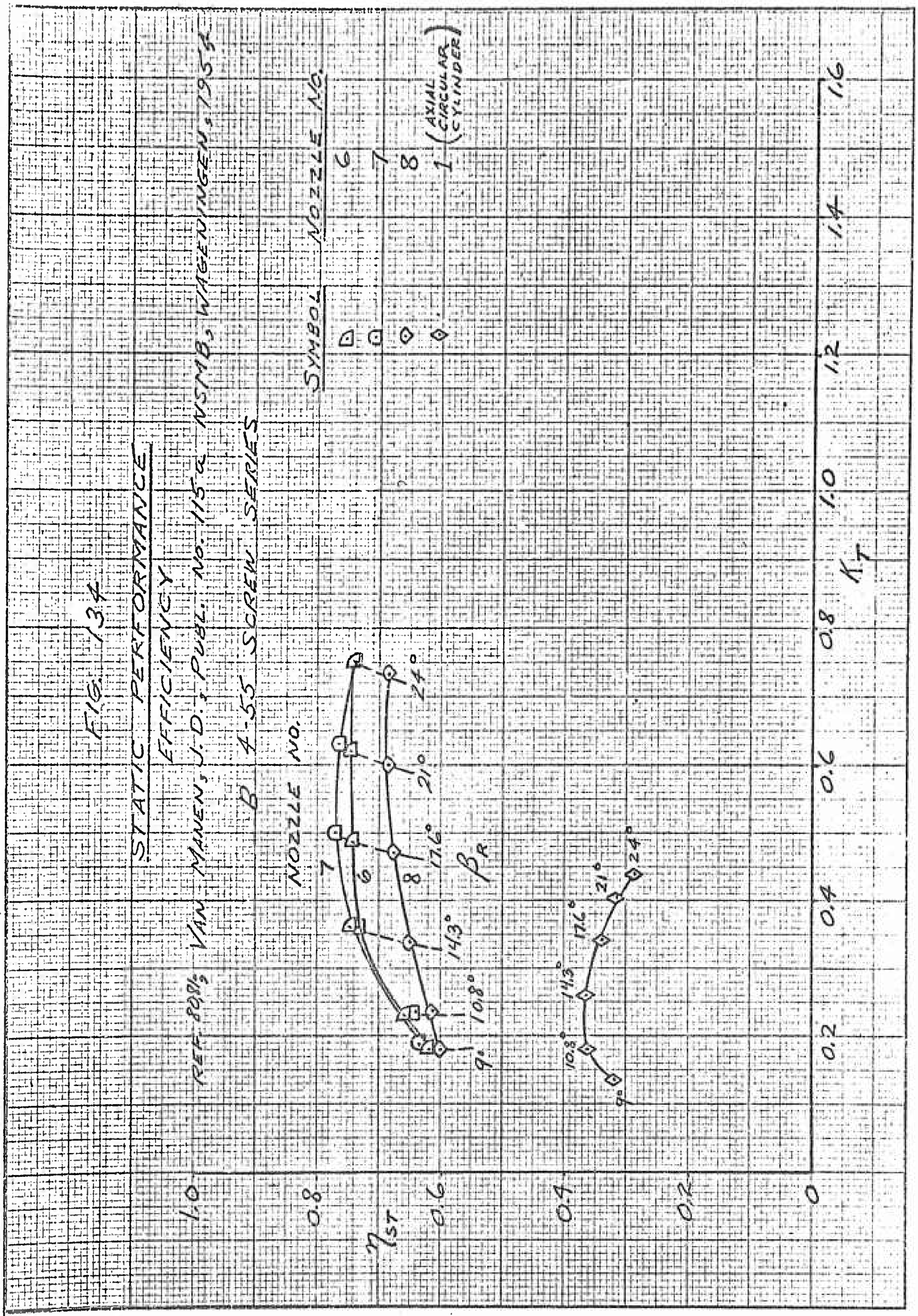
FIG. 134
STATIC PERFORMANCE
EFFICIENCY
REF. 80%, VAN MANEN, J.D., PUBL. NO. 115a NSMB, WAGENINGEN, 1953
B 4-55 SCREW SERIES
SYMBOL
NOZZLE NO.
6
7
8
1 (AXIAL CIRCULAR CYLINDER)
NOZZLE NO.
7
6
8
9°
10.8°
14.3°
17.6°
21°
24°
β_R
η_{ST}
K_T
1.0
0.8
0.6
0.4
0.2
0
0.2
0.4
0.6
0.8
1.0
1.2
1.4
1.6

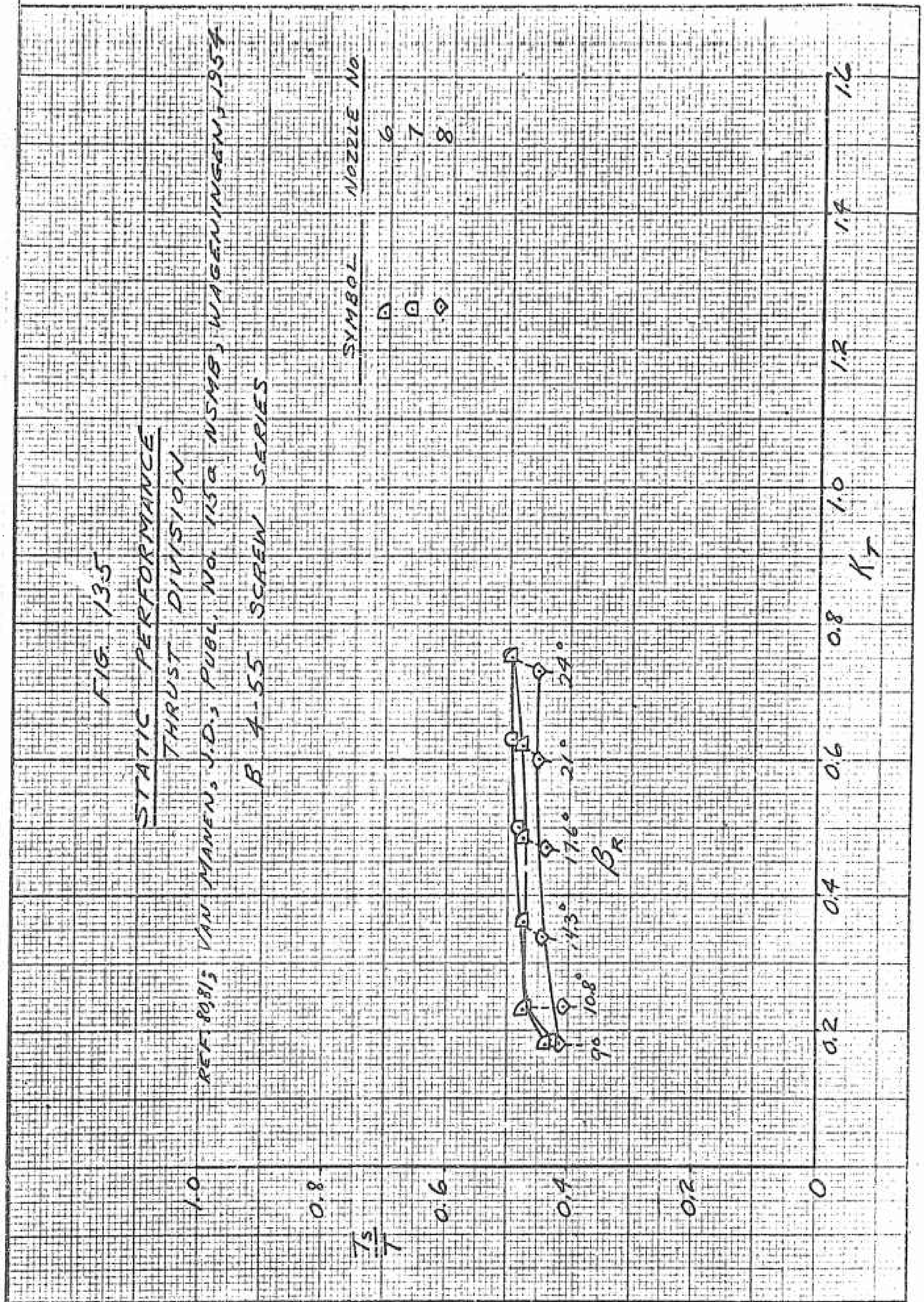
FIG. 135
STATIC PERFORMANCE
THRUST DIVISION
REF 8081; VAN MANEN, J.D.; PUBL. No. 115a NSMB, WAGENINGEN, 1954
B 4-55 SCREW SERIES
SYMBOL
NOZZLE No.
6
7
8
T_s/T
1.0
0.8
0.6
0.4
0.2
0
0.2
0.4
0.6
0.8
1.0
1.2
1.4
1.6
K_T
β_R
9°
10.8°
14.3°
17.6°
21°
24°

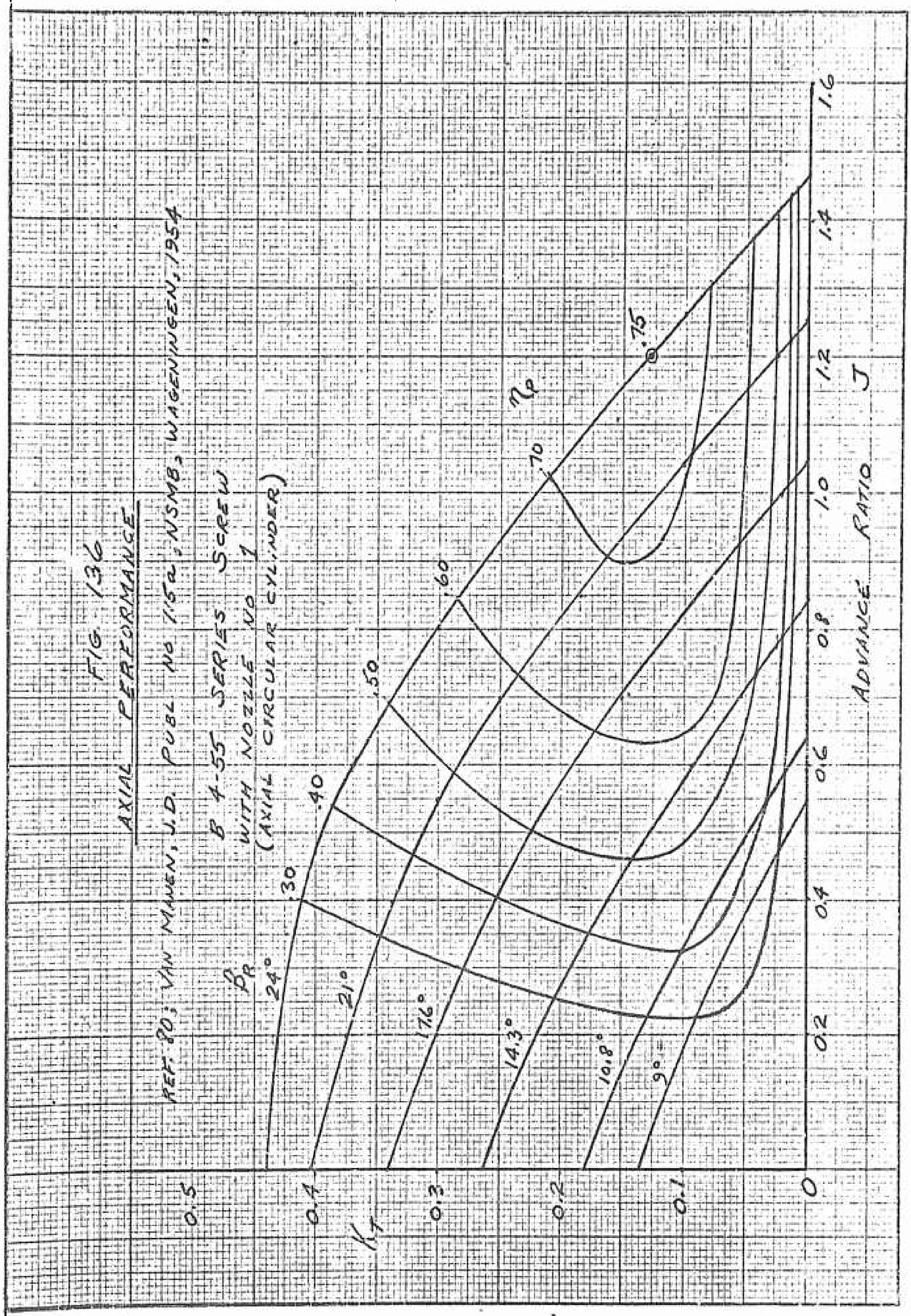
FIG. 136
AXIAL PERFORMANCE
REF. 80; VAN MANEN, J.D. PUBL NO 115a, NSMB, WAGENINGEN, 1954
B 4-55 SERIES SCREW
WITH NOZZLE NO 1
(AXIAL CIRCULAR CYLINDER)
β_R
24°
21°
17.6°
14.3°
10.8°
9°
η_p
.30
.40
.50
.60
.70
.75
K_T
0.5
0.4
0.3
0.2
0.1
0
0.2
0.4
0.6
0.8
1.0
1.2
1.4
1.6
ADVANCE RATIO J

PREPARED JBP 3-3-60
CHECKED
REVISED

REPORT NO
MODEL

FIG. 137

AXIAL PERFORMANCE
EFFICIENCY

REF. 81; VAN MANEN, J.D. PUBL. NO. 115a
NSMB, WAGENINGEN, 1954

B 4-55 SERIES SCREW
WITH NOZZLE NO. 2

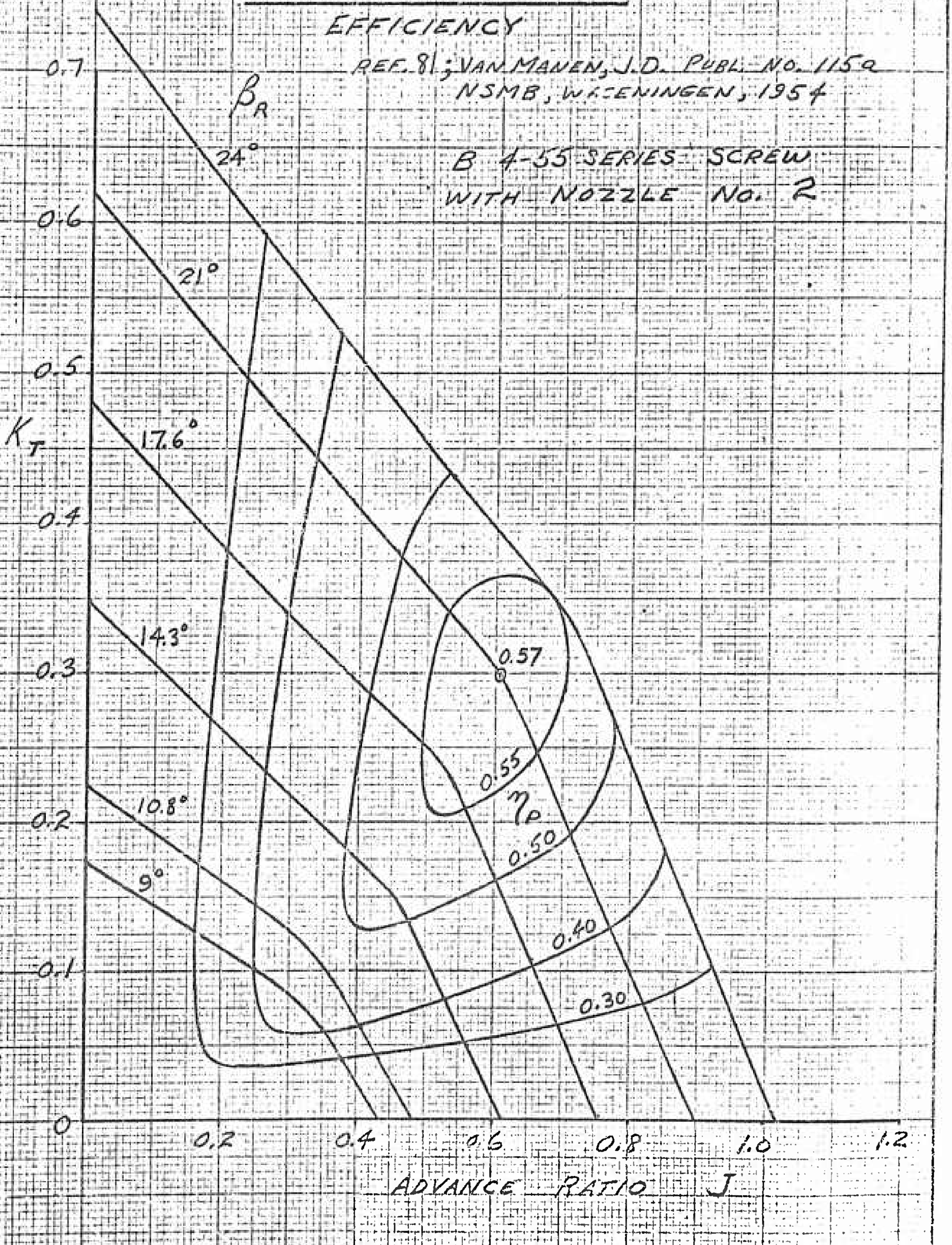

FIG 138

AXIAL PERFORMANCE
EFFICIENCY

REF. 81; VAN MANEN, J.D. PUBL. NO. 115 a
NSMB, WAGENINGEN, 1954

B 4-55 SCREW SERIES
WITH NOZZLE NO 3

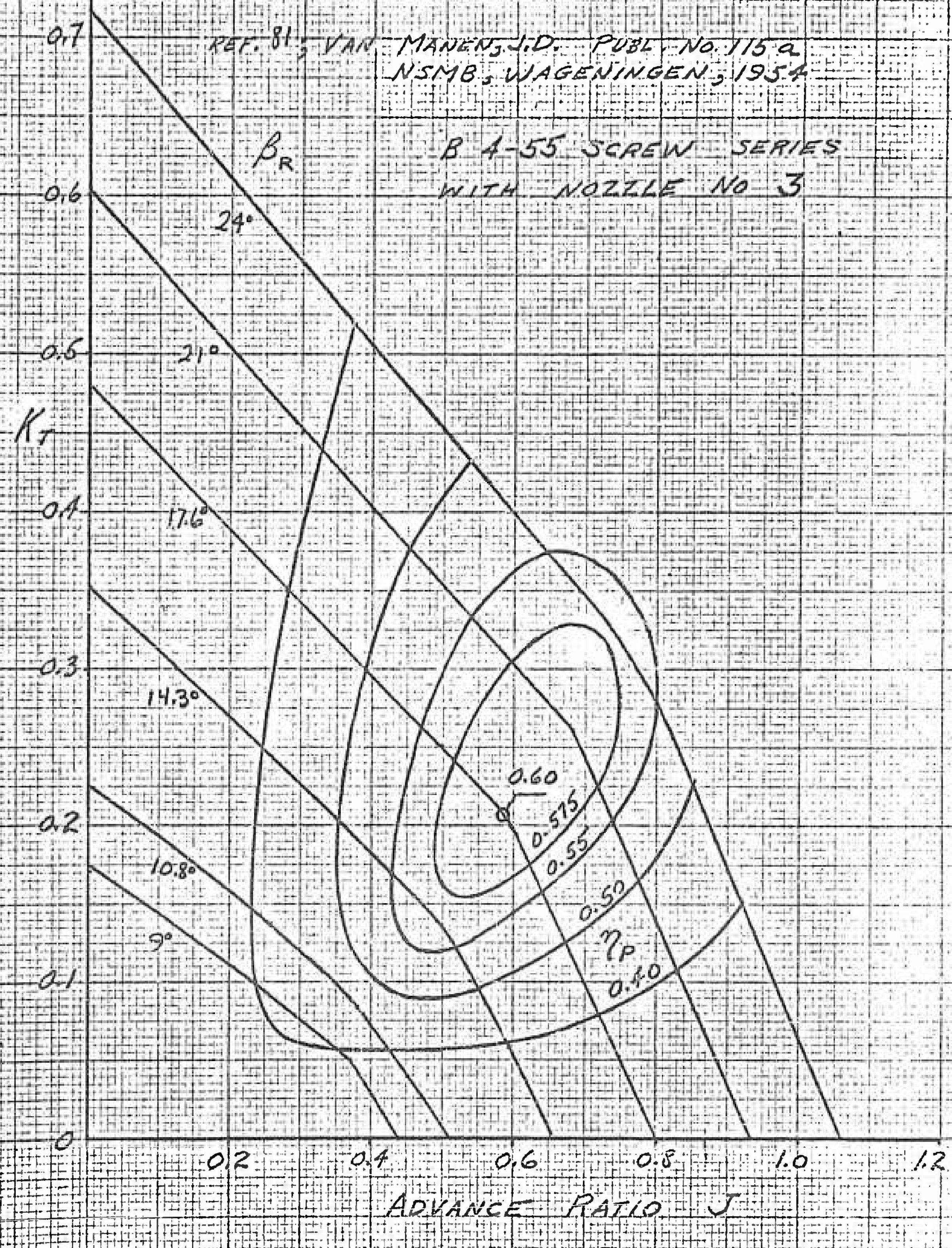

Reference	1
Authors	Allen, H. J. and Rogallo, F. M.
Source	Stanford University
Figs.	139-141

FIG. 139

SHROUD CONFIGURATION

REF: 1 ; ALLEN, H.J., ROGALLO, F.M.
RING COWLED PROPELLERS, THESIS, STANFORD U., 1935

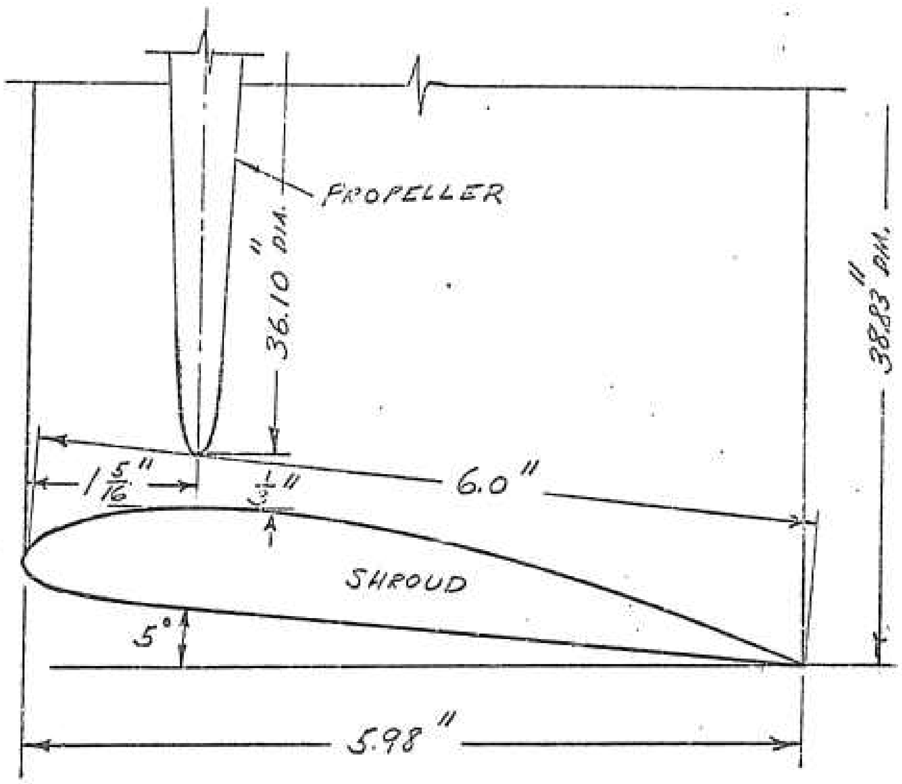

FIG. 140

AXIAL PERFORMANCE

REF. 1; ALLEN, H.J., ROGALLO, F.M.
RING COWLED PROPELLERS, THESIS, STANFORD U., 1935

PROPELLER A WITH SHROUD

$\beta_{.7R} = 25.4°$

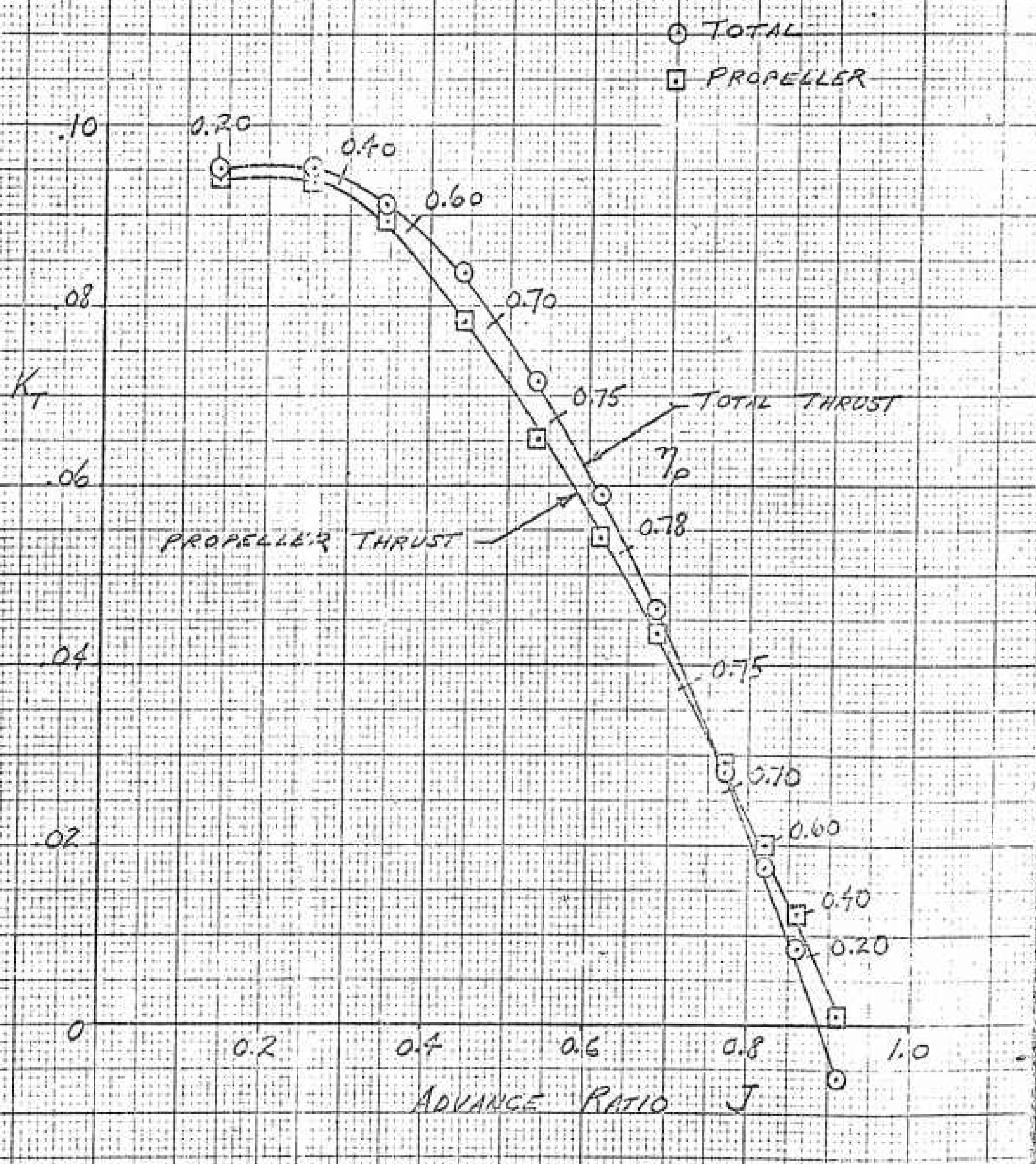

PREPARED ______ 4-20-60 PAGE 285

CHECKED ______

REVISED ______ REPORT NO. ______

MODEL ______

FIG 141

AXIAL PERFORMANCE

REF 1; ALLEN, H.J., ROGALLO, F.M.
RING COWLED PROPELLERS, THESIS, STANFORD U., 1935

PROPELLER A UNSHROUDED

$\beta_{.72} = 25.4°$

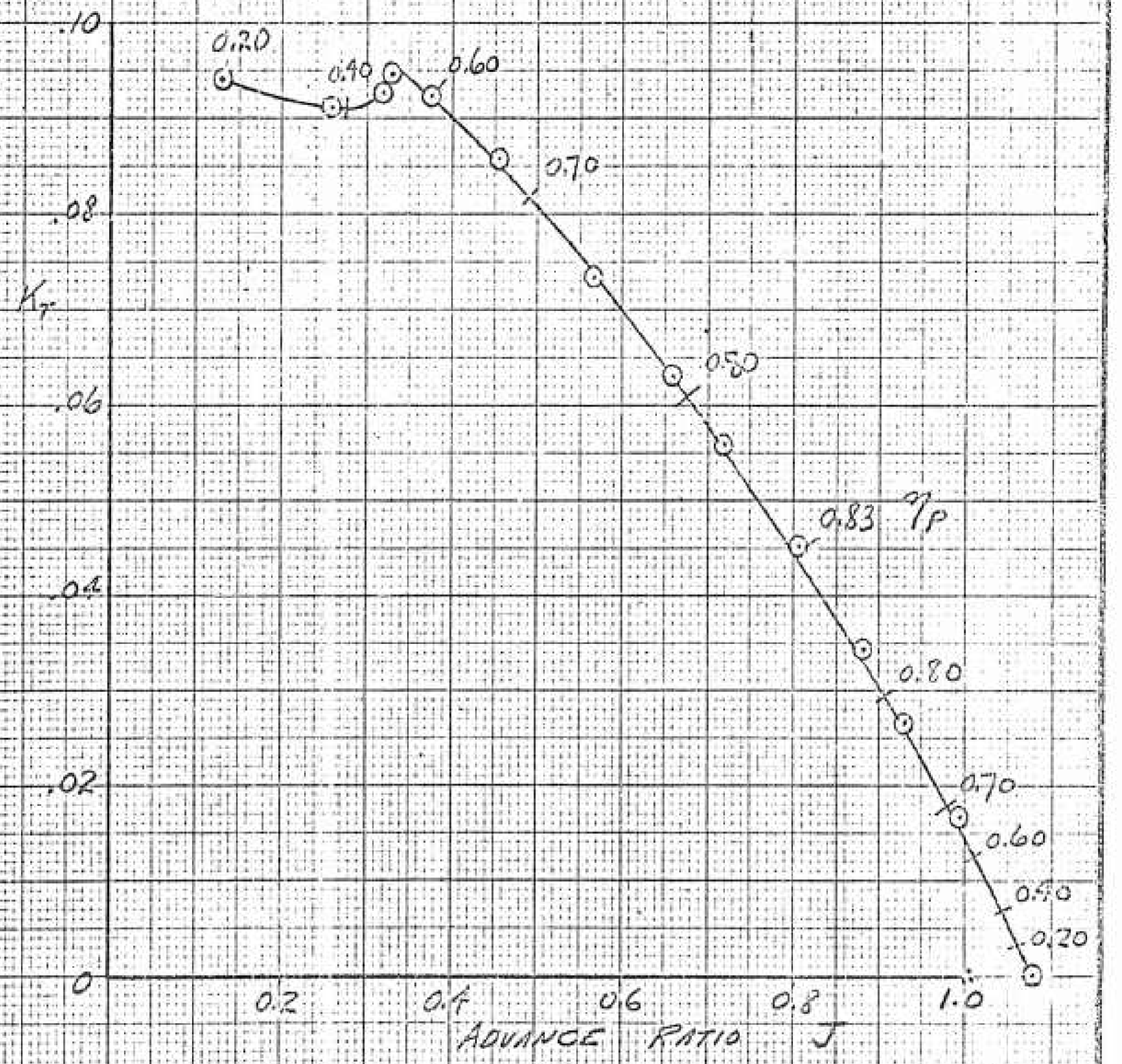

E-1-10A
Rev. 2/49

Reference	52
Auth rs	Moser, H. H., Livingston, C. L.
Source	MIT
Figs.	142-151

FIG. 142

CONFIGURATION

REF. 52; MOSER, H.H., LIVINGSTON, C.L. MIT TR 79-1, 1959

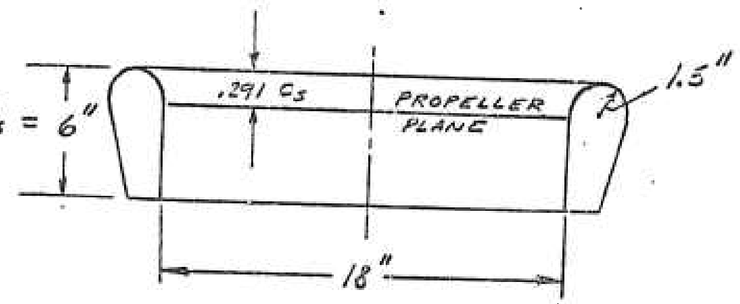

TILTING MODEL

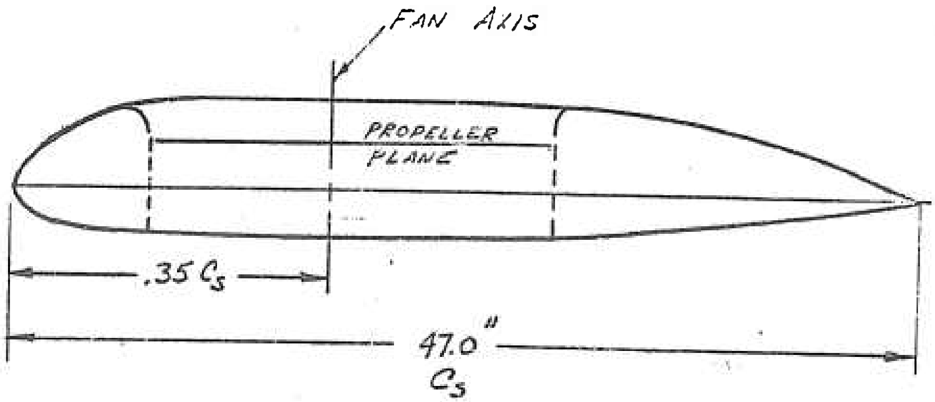

WING MODEL ASPECT RATIO = .766

FIG. 143

STATIC PERFORMANCE

REF. 52; MOSER, H.H., LIVINGSTON, C.L. AEROELASTIC AND STRUCTURES RESEARCH LABORATORY TR 79-1 MIT, 1959

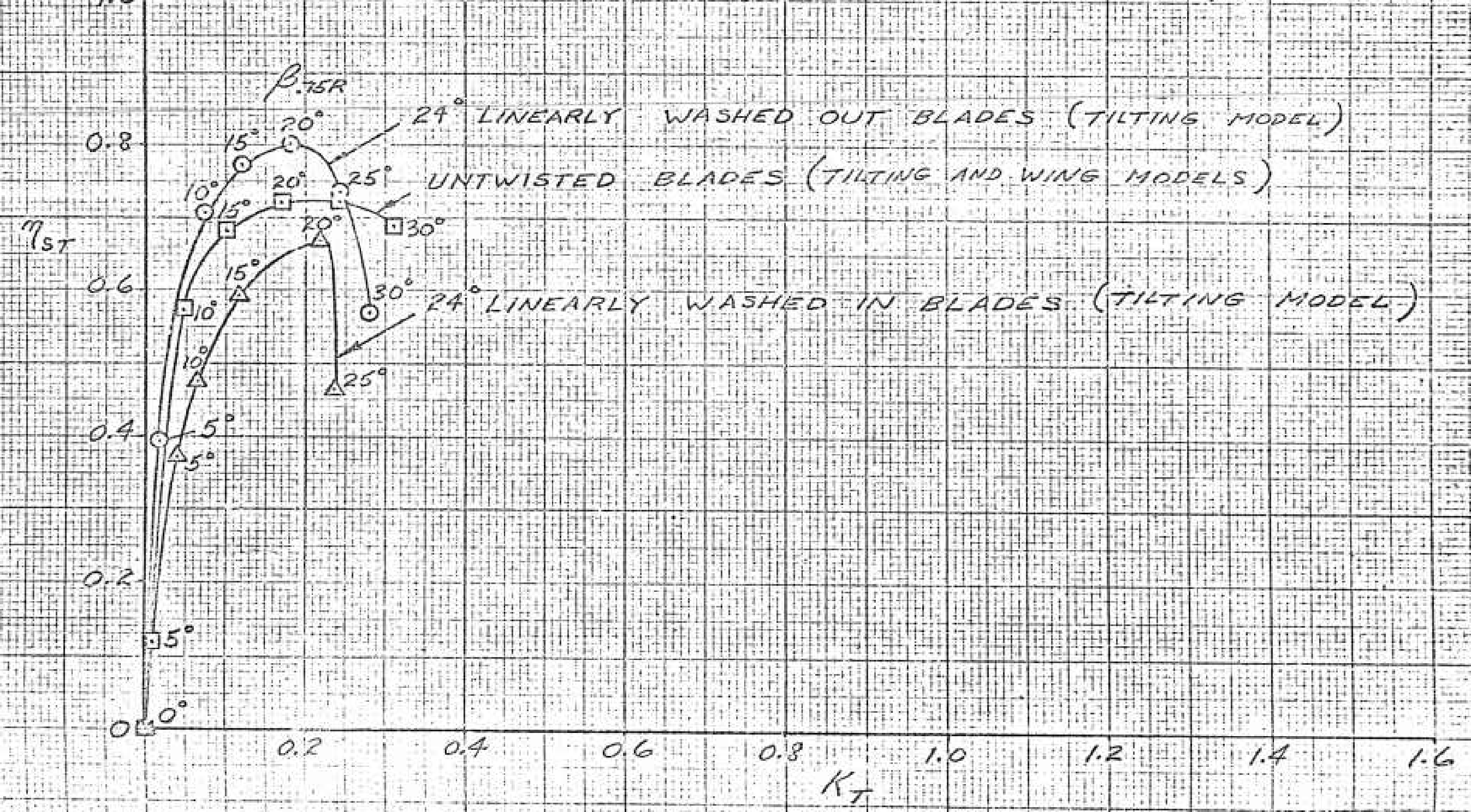

FIG 144

STATIC PERFORMANCE

REF 52; MOSER, H.H., LIVINGSTON, C.L. AEROELASTIC AND STRUCTURES RESEARCH LABORATORY TR 79-1 MIT, 1959

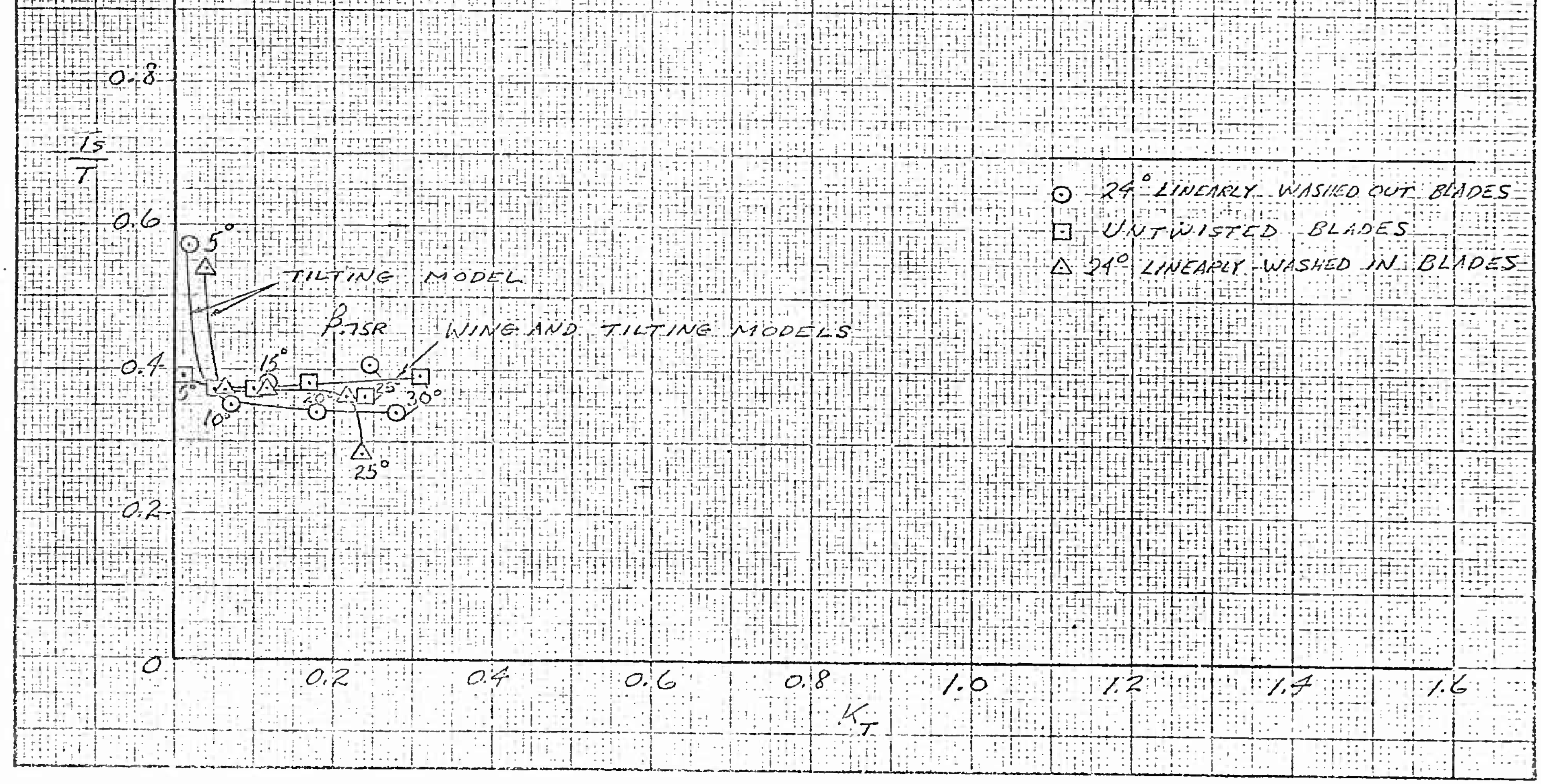

PREPARED JL 4-27-60 PAGE 290

CHECKED REPORT NO

REVISED MODEL

REPUBLIC AVIATION

FIG 145

FAN-IN-WING PERFORMANCE
LIFT

REF. 52; MOSER, H.H., LIVINGSTON, C.L. MIT TR 79-1, 1959

UNTWISTED BLADES
$\beta_R = 20°$

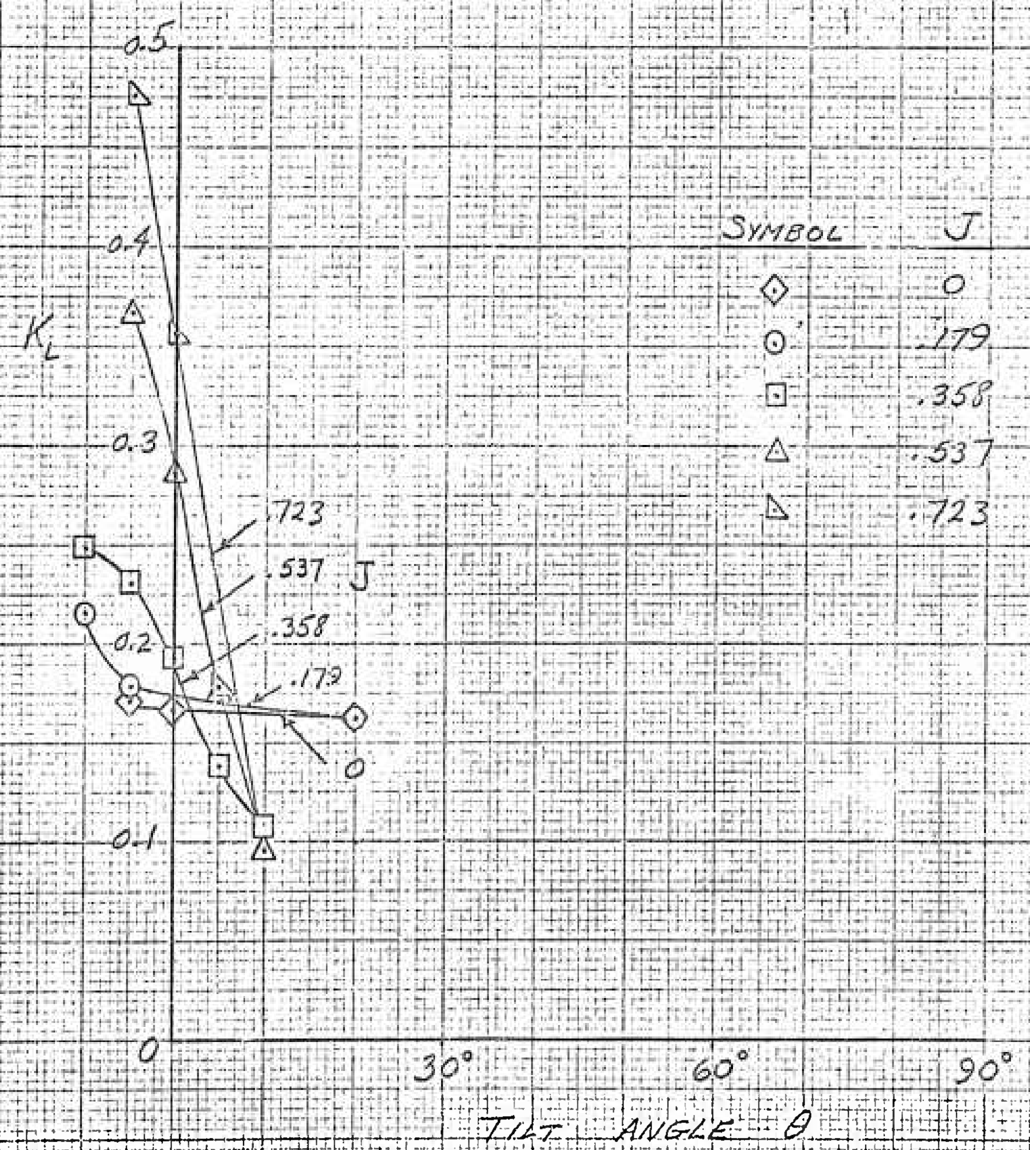

FIG. 146

FAN-IN-WING PERFORMANCE

DRAG

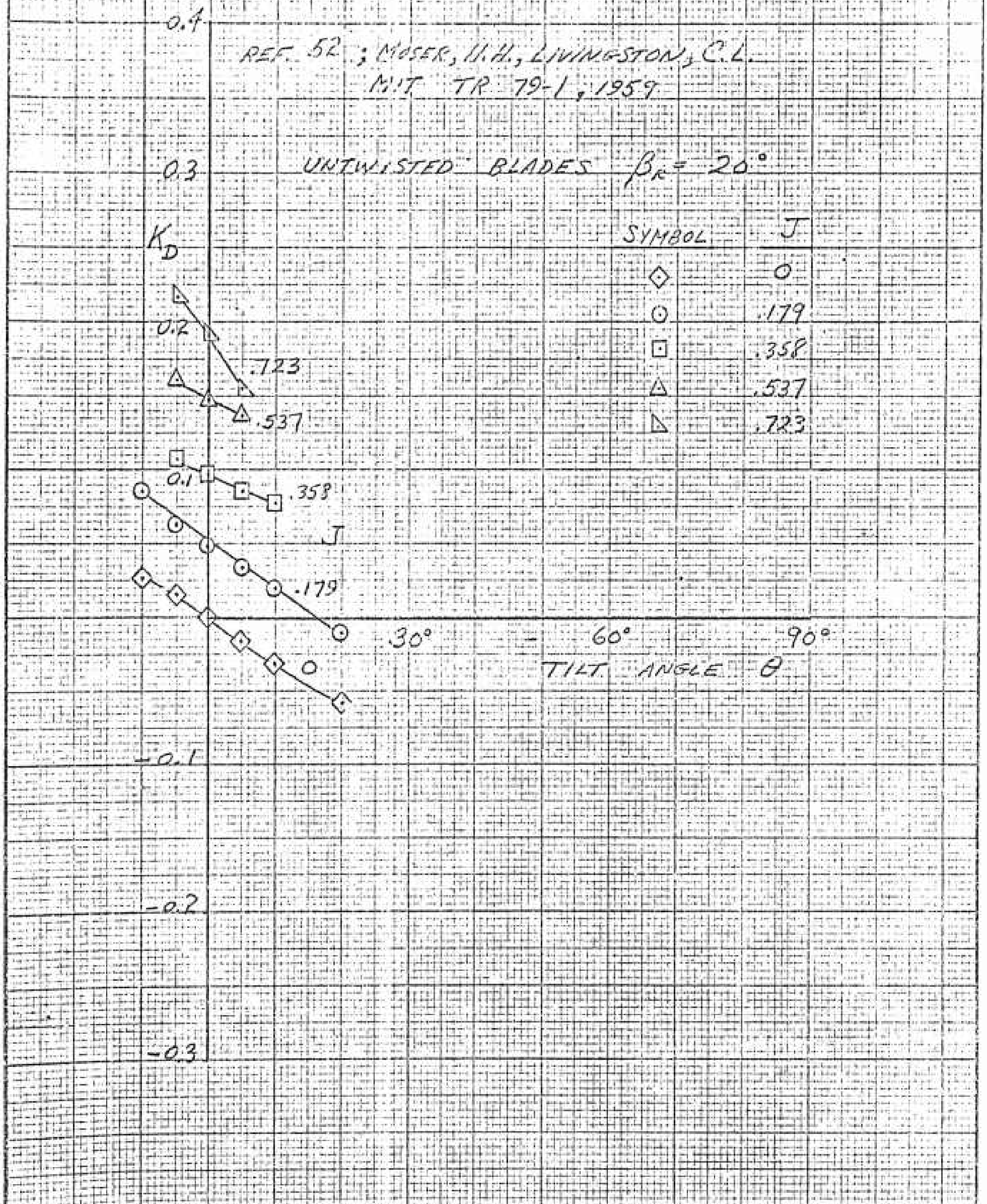

FIG. 147

FAN-IN-WING PERFORMANCE

POWER

REF. 52; MOSER, H.H., LIVINGSTON, C.L. MIT TR 79-1, 1959

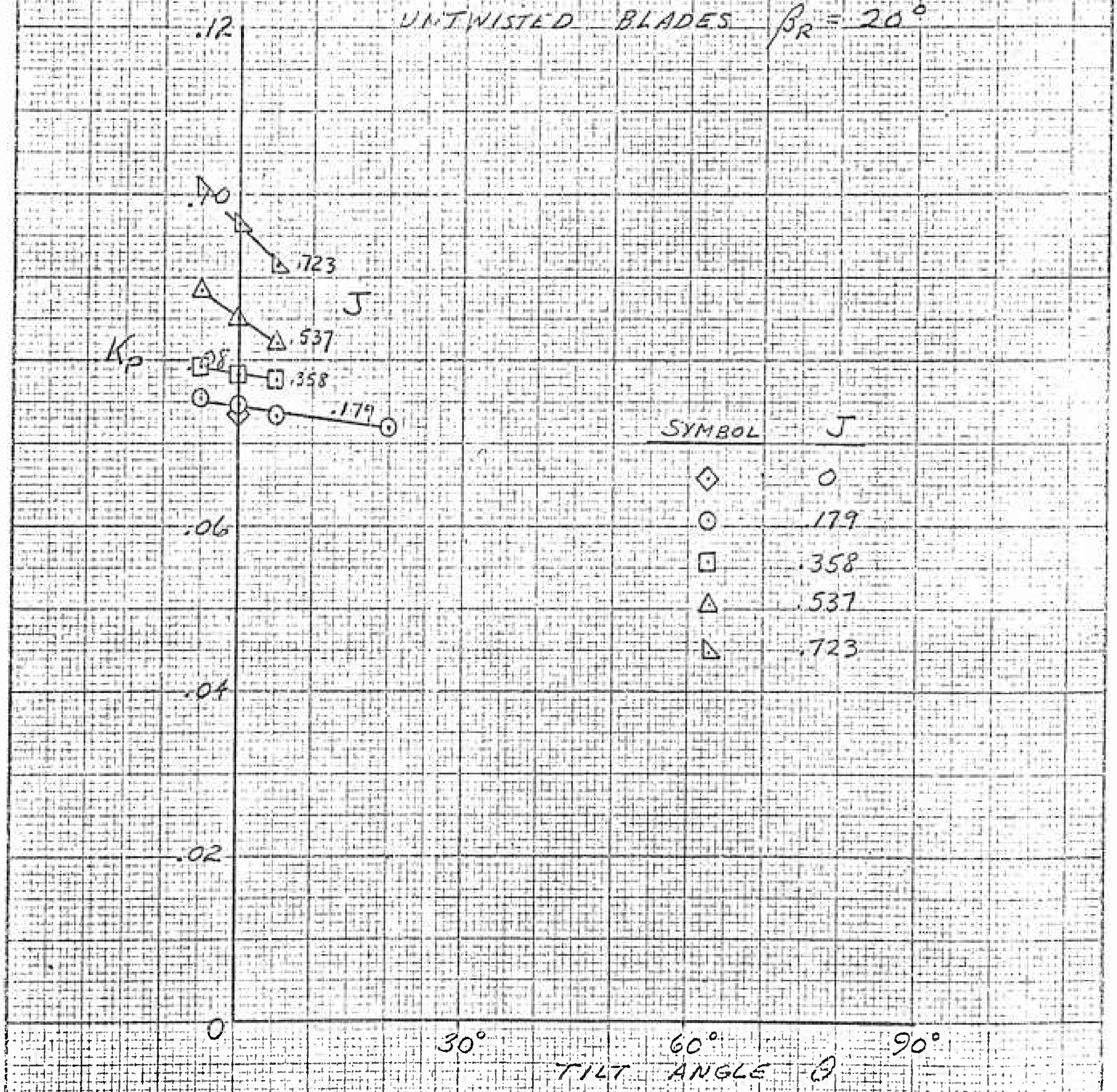

PREPARED BL 1-1-2961

CHECKED

REVISED

REPUBLIC AVIATION

REPORT NO

MODEL

FIG. 148

FAN-IN-WING PERFORMANCE

PITCHING MOMENT

REF. 52; MOSER, H.H., LIVINGSTON, C.L. MIT TR 79-1, 1959

UNTWISTED BLADES $\beta_e = 20°$

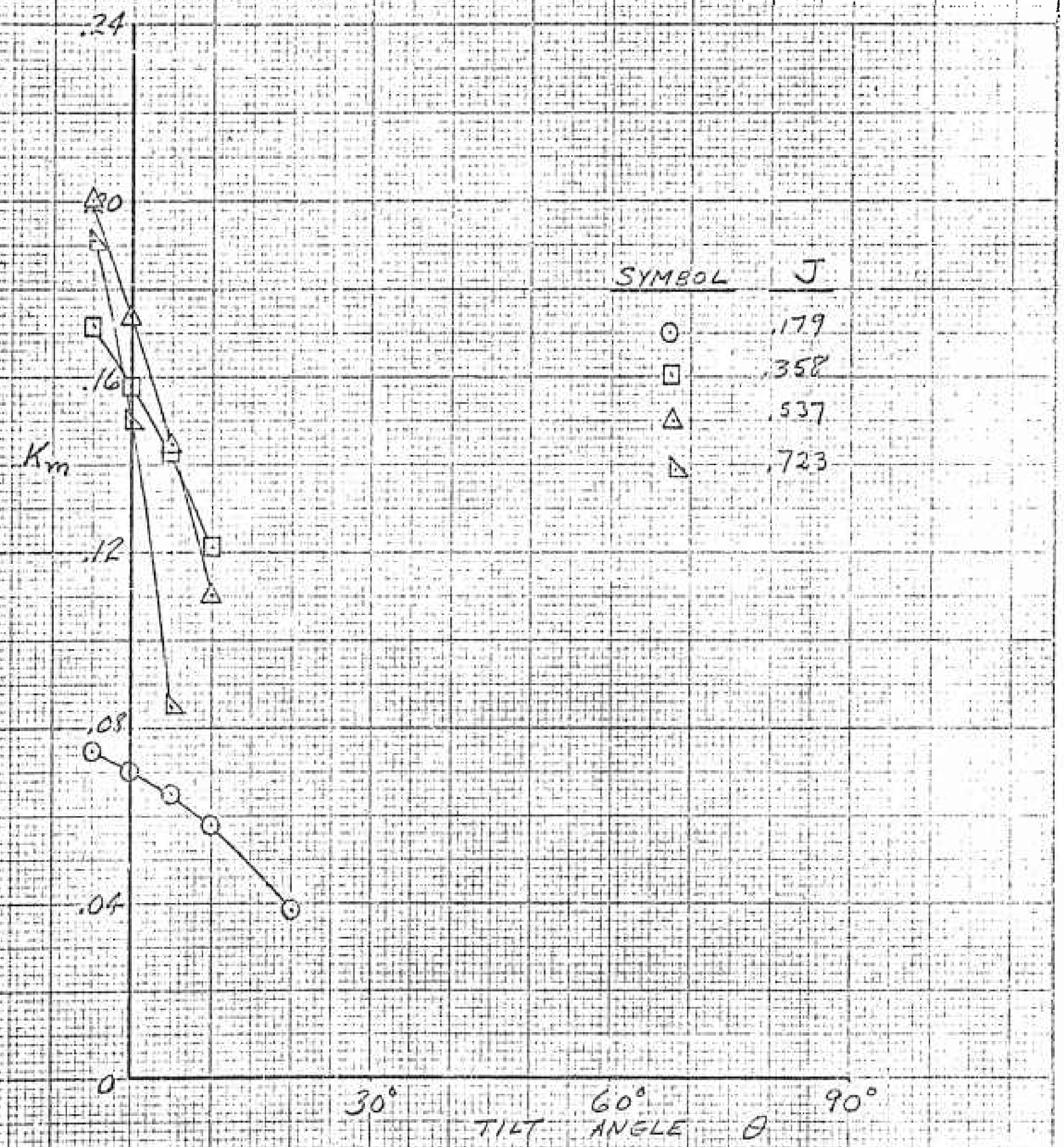

E-1-104 REV. 2/49

FIG. 149

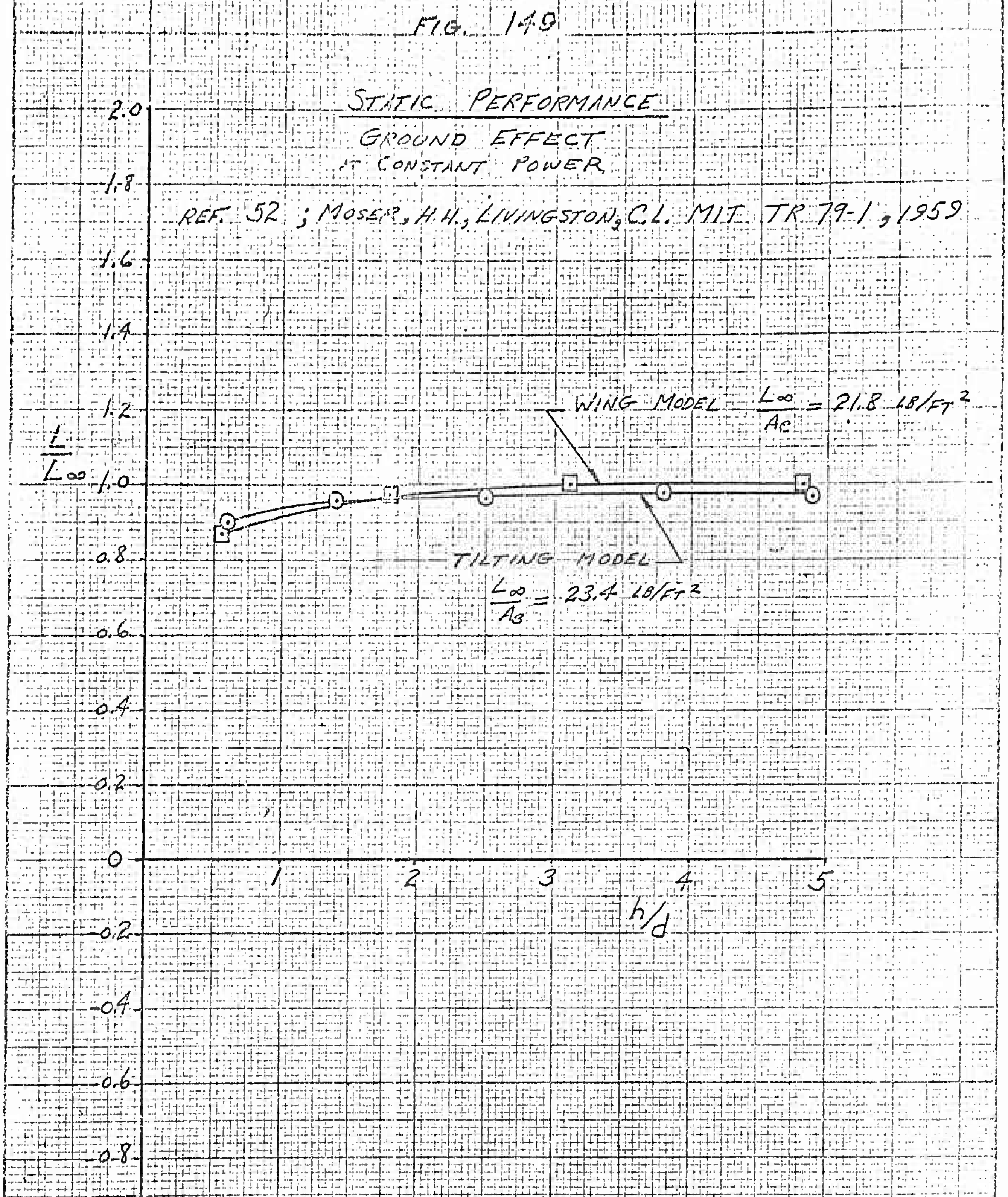
STATIC PERFORMANCE
GROUND EFFECT
AT CONSTANT POWER
REF. 52 ; MOSER, H.H., LIVINGSTON, C.L. MIT TR 79-1, 1959
WING MODEL $\frac{L_\infty}{A_c} = 21.8$ LB/FT^2
TILTING MODEL
$\frac{L_\infty}{A_B} = 23.4$ LB/FT^2
$\frac{L}{L_\infty}$
2.0
1.8
1.6
1.4
1.2
1.0
0.8
0.6
0.4
0.2
0
-0.2
-0.4
-0.6
-0.8
-1.0
1
2
3
4
5
h/d

FIG 150

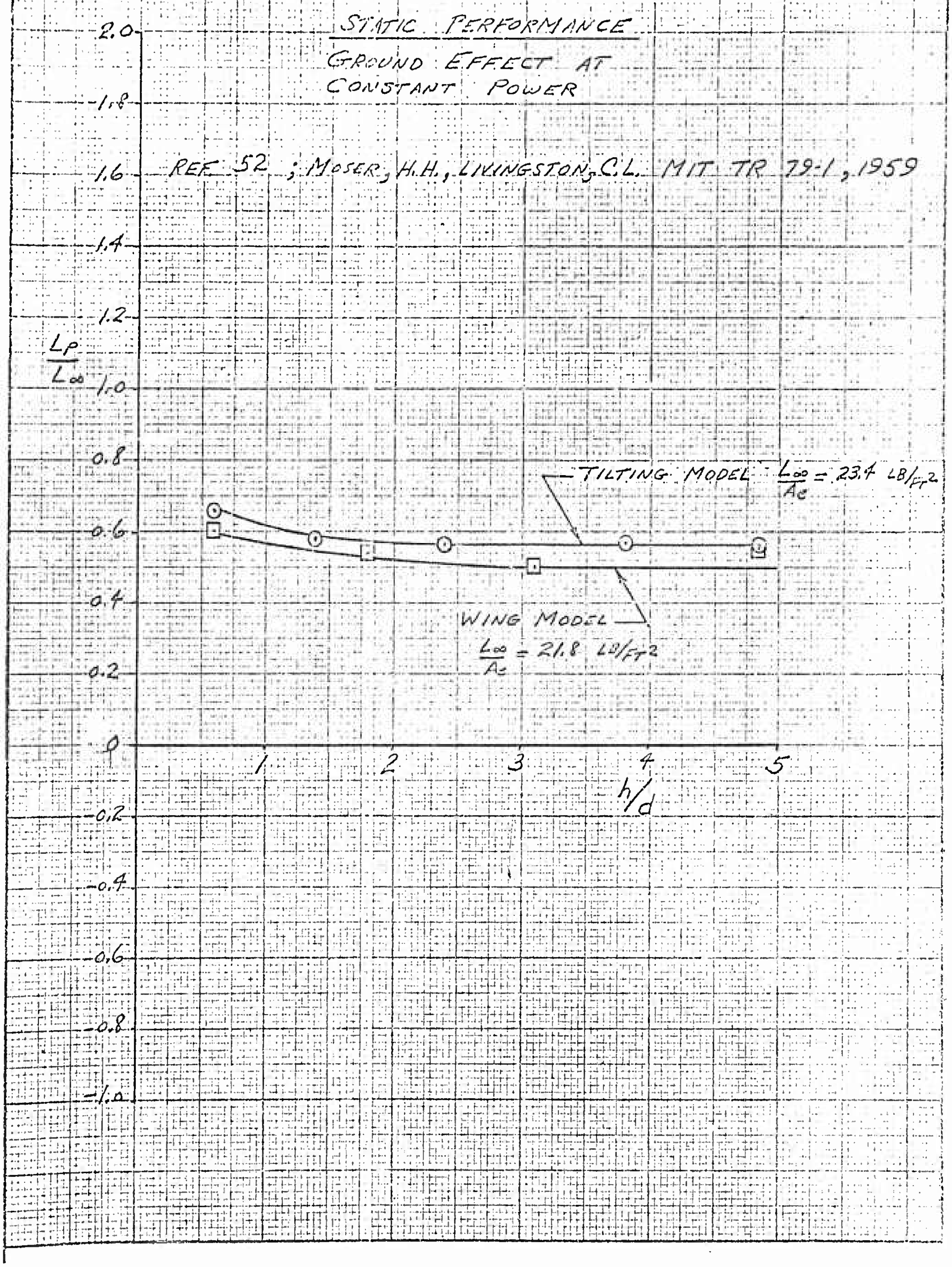
STATIC PERFORMANCE
GROUND EFFECT AT
CONSTANT POWER
REF. 52 ; MOSER, H.H., LIVINGSTON, C.L. MIT TR 79-1, 1959
TILTING MODEL $\frac{L_\infty}{A_e} = 23.4$ LB/FT²
WING MODEL
$\frac{L_\infty}{A_e} = 21.8$ LB/FT²
$\frac{L_P}{L_\infty}$
2.0
1.8
1.6
1.4
1.2
1.0
0.8
0.6
0.4
0.2
0
-0.2
-0.4
-0.6
-0.8
-1.0
1
2
3
4
5
h/d

FIG 151 (a)

STATIC PERFORMANCE REF. 52

EFFECT OF THE GROUND ON INFLOW VELOCITY AND DUCT PRESSURE DISTRIBUTION

UNTWISTED BLADES $\beta_{.75R} = 25°$

TILTING MODEL

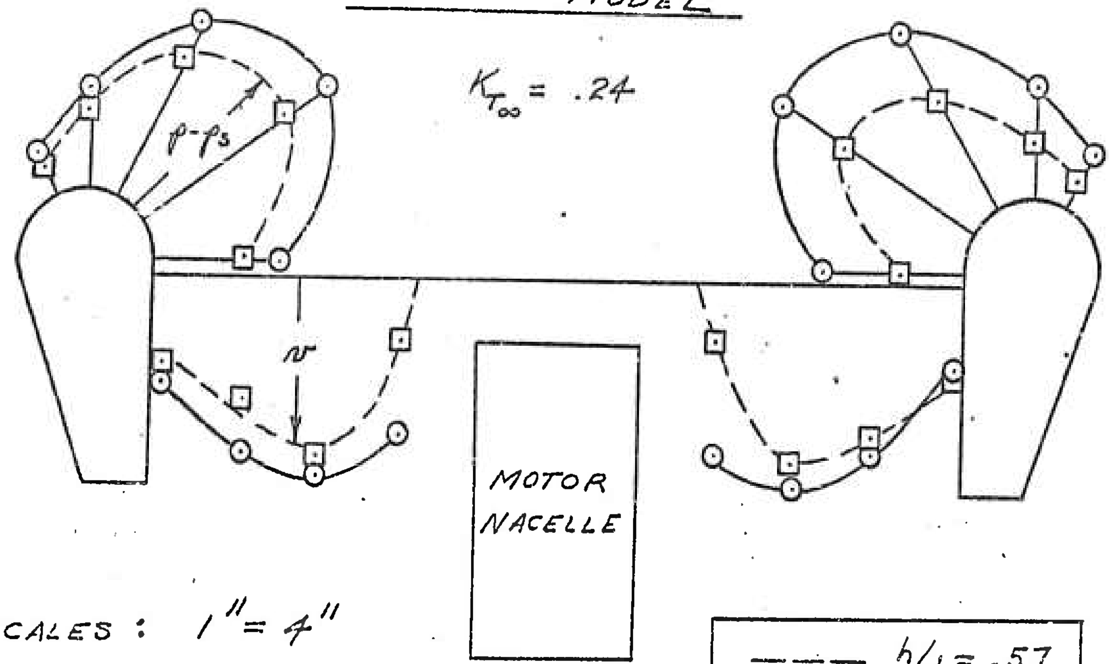

SCALES : $1'' = 4''$

$p - p_s$ $1'' = 37.0$ LB/FT²

$v_{\text{WING MODEL}}$ $1'' = 85.0$ FT/SEC

$v_{\text{TILTING MODEL}}$ $1'' = 107$ FT/SEC

----	$h/d = .57$
——	$h/d = \infty$

WING MODEL FIG. 151 (b)

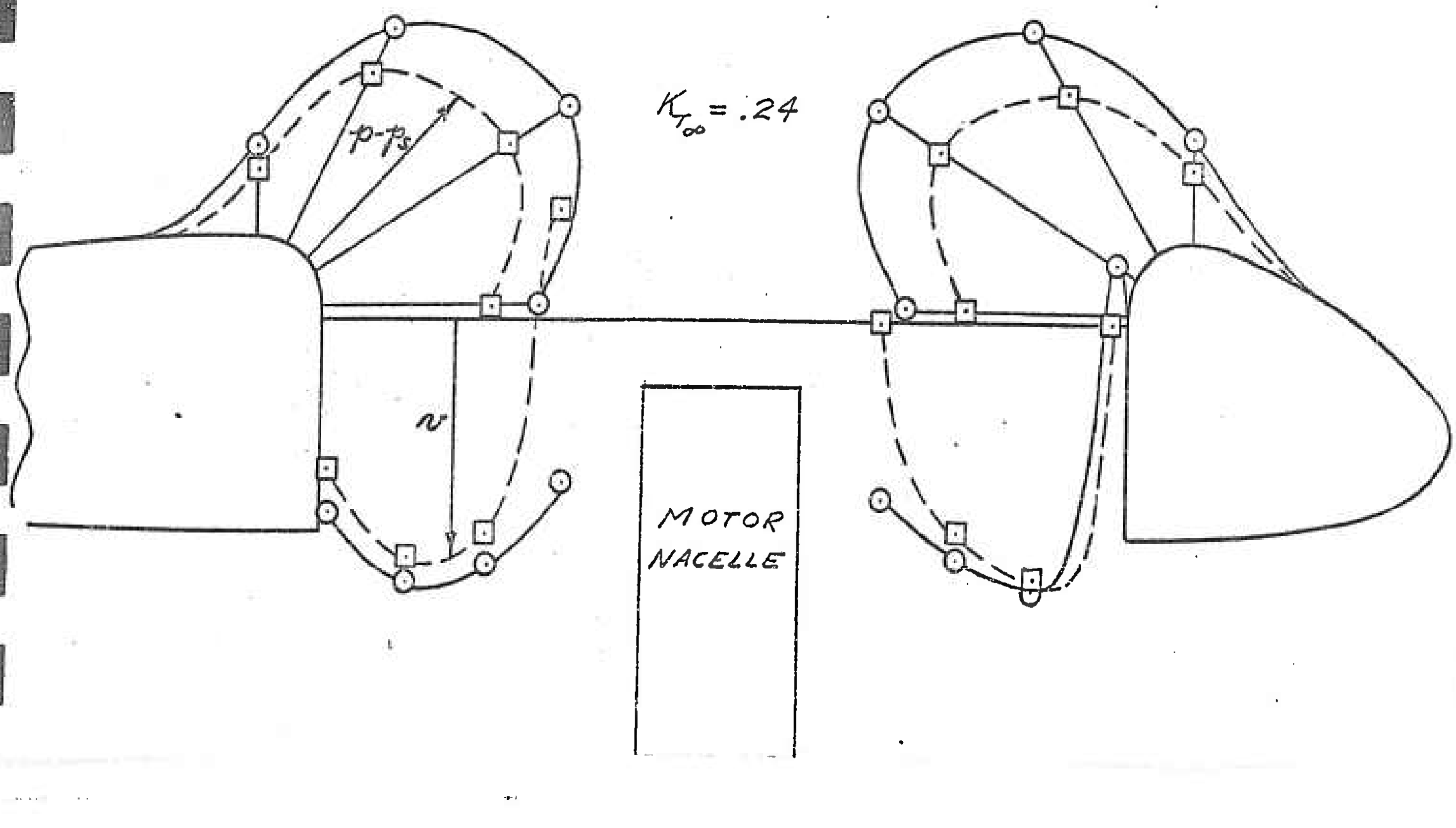

Reference	74
Author	Taylor, R. T.
Source	NACA
Figs.	152-154

FIG. 152

CONFIGURATION

REF. 74; TAYLOR, R.T., NACA TN 4126, 1958

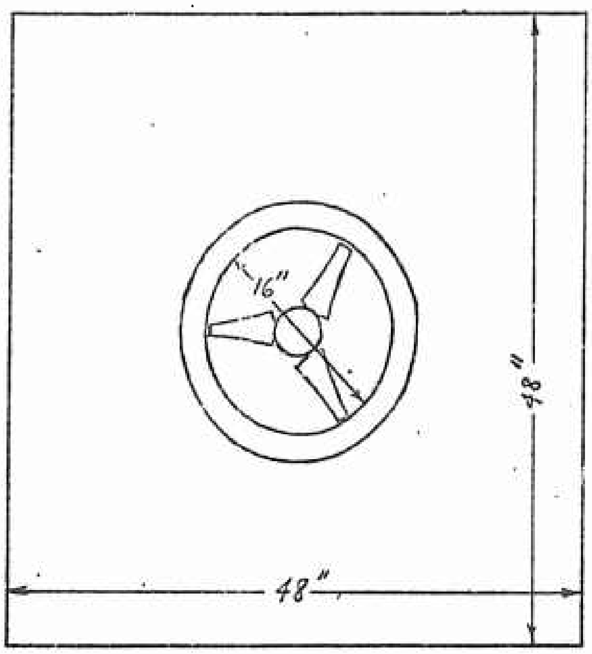

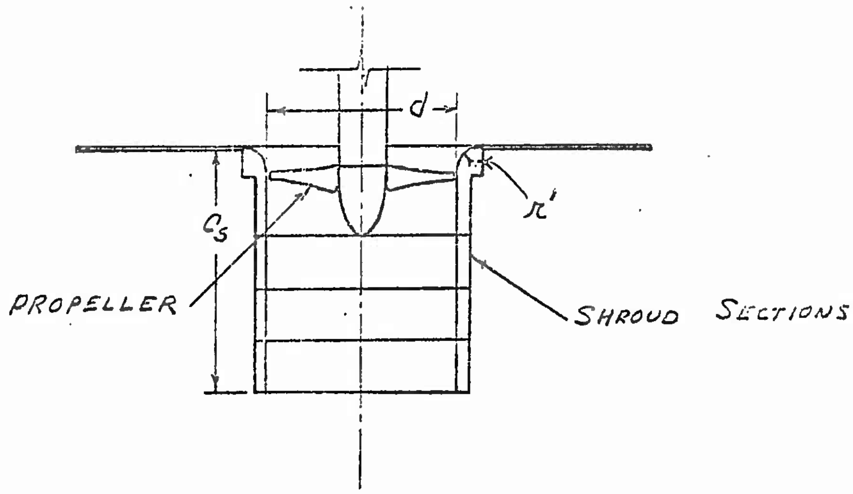

PREPARED 4-28-60 PAGE 299
CHECKED REPORT NO.
REVISED MODEL

FIG 153

STATIC PERFORMANCE

EFFECT OF SHROUD INLET RADIUS OF THRUST DIVISION

REF. 74 ; TAYLOR, R.T. NACA TN 4126, 1958

$\frac{A}{A_3} = 1.0$

$\frac{C_S}{d} \approx 1.0$

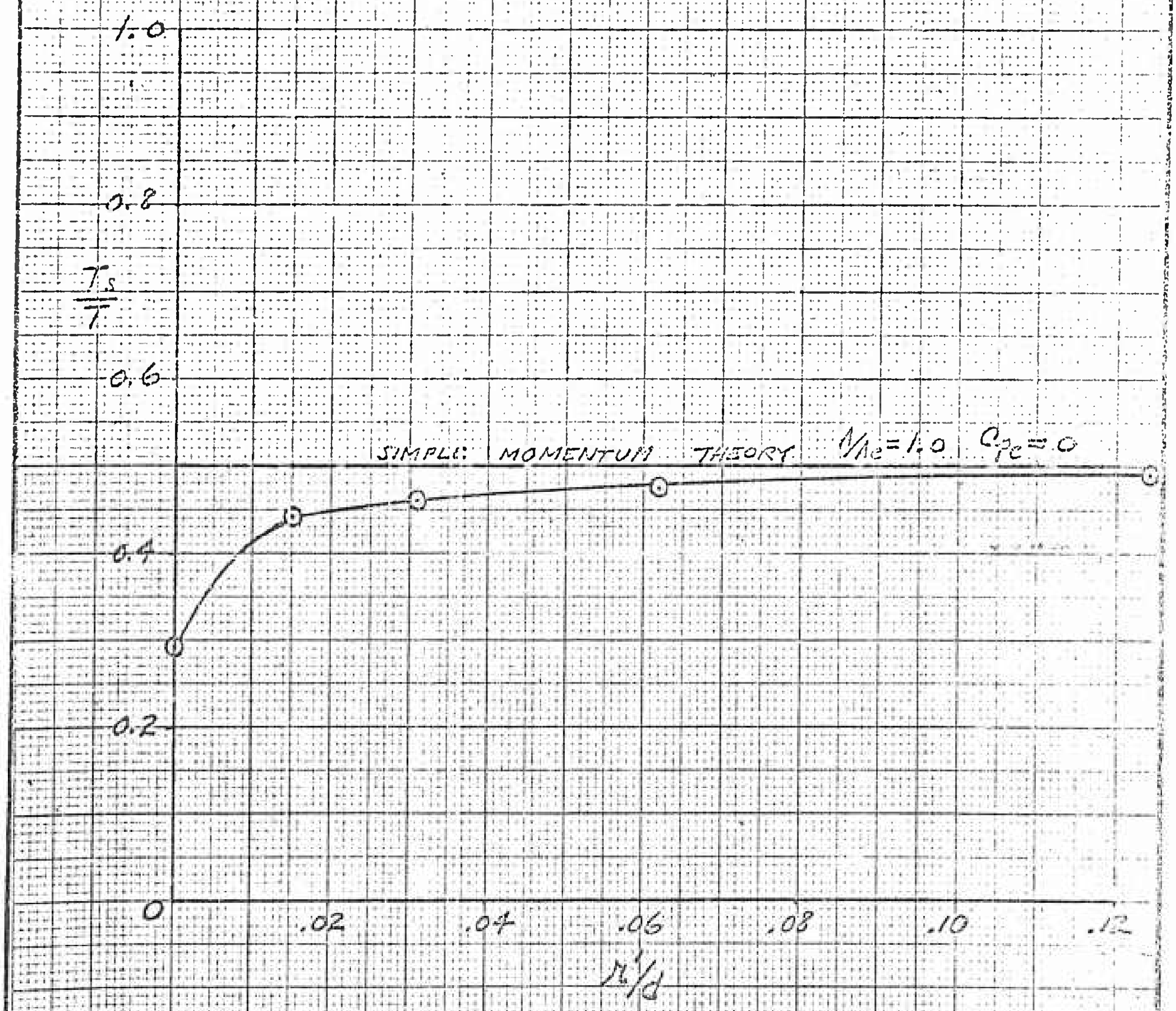

PREPARED 4-28-60 PAGE 300

CHECKED REPORT NO

REVISED MODEL

FIG 154

STATIC PERFORMANCE

EFFECT OF SHROUD DIFFUSION ON THRUST DIVISION

REF. 74; TAYLOR, R.T. NACA TN 4126, 1958

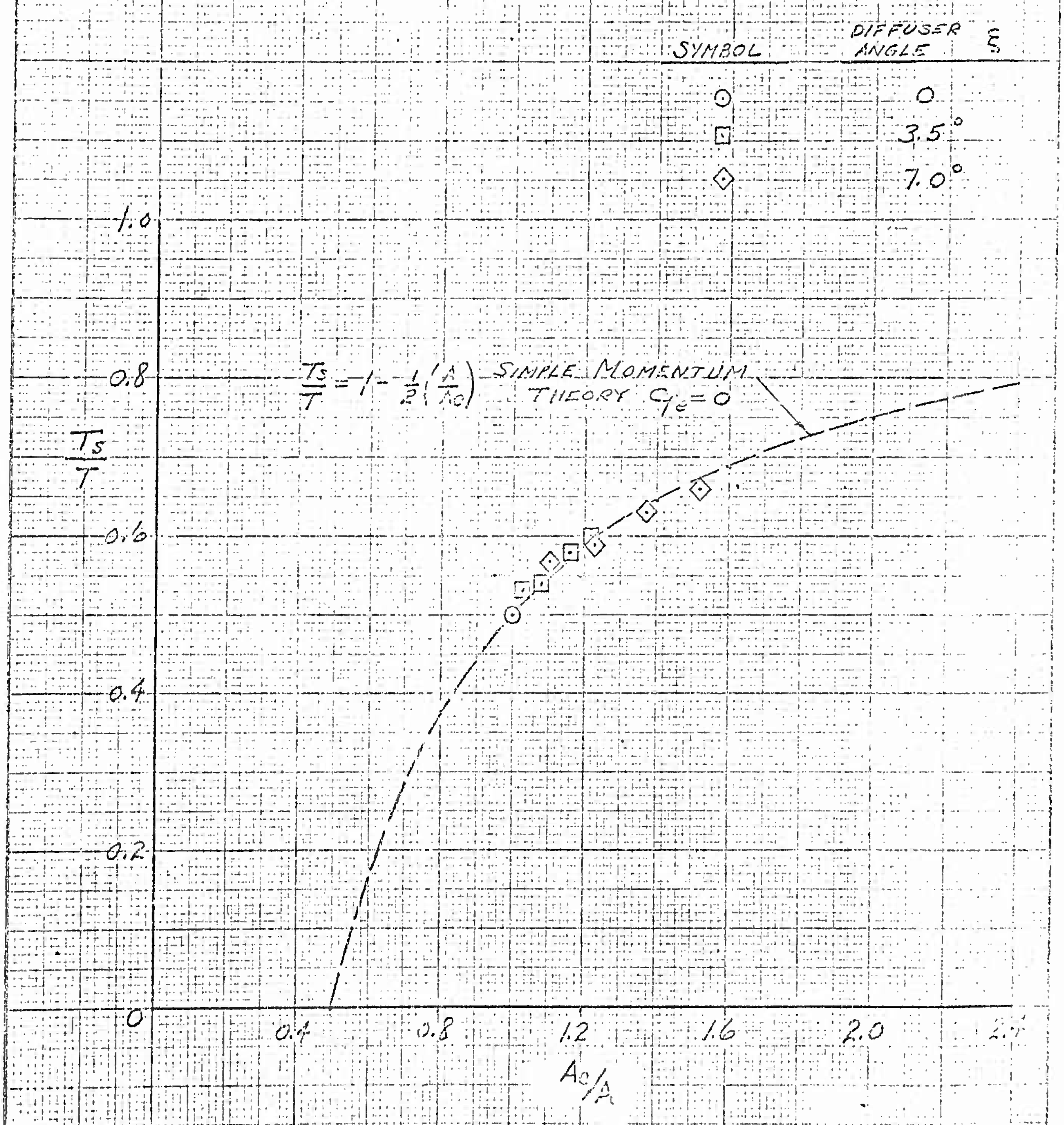

1-10A
2/49

Reference	47
Authors	McLemore, H. C., and Cannon, M. D.
Source	NACA
Figs.	155-167

FIG. 155

STATIC PERFORMANCE
EFFICIENCY
REF. 47; McLEMORE, H.C., CANNON, M.D.
NACA TN 3228, 1954

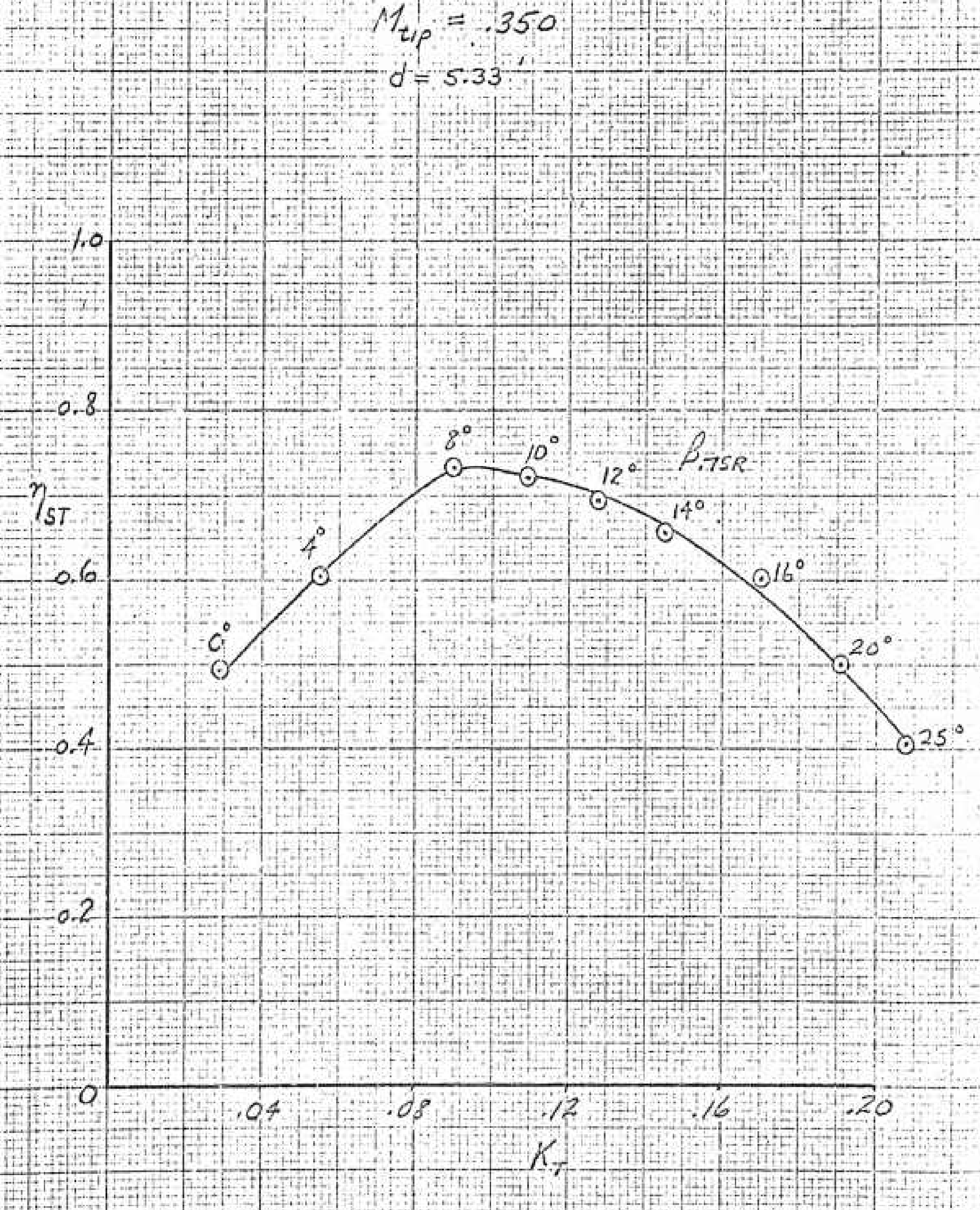

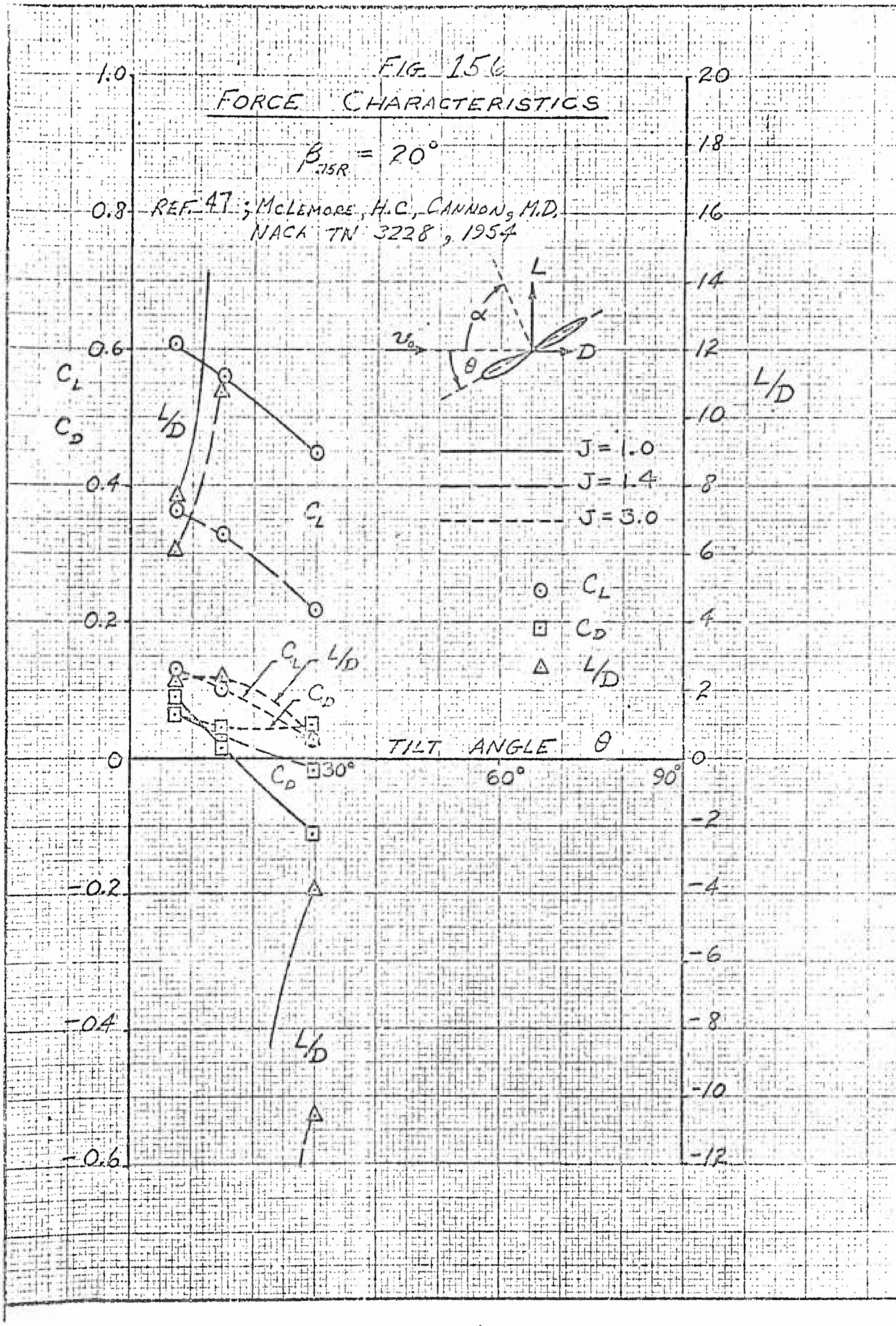
FIG. 156
FORCE CHARACTERISTICS
$\beta_{.75R} = 20°$
REF. 47; McLEMORE, H.C., CANNON, M.D.
NACA TN 3228, 1954
C_L
C_D
L/D
L
D
v_o
α
θ
J = 1.0
J = 1.4
J = 3.0
⊙ C_L
⊡ C_D
△ L/D
TILT ANGLE θ
30°
60°
90°
1.0
0.8
0.6
0.4
0.2
0
-0.2
-0.4
-0.6
20
18
16
14
12
10
8
6
4
2
0
-2
-4
-6
-8
-10
-12

PREPARED J3L 5-18-60

CHECKED

REVISED

REPORT NO

MODEL

FIG 157

NON-AXIAL PERFORMANCE

RESULTANT FORCE

REF. 97; McLEMORE, H.C., CANNON, M.D., NACA TN 3228, 1954

UNSHROUDED PROPELLER

$\beta_{.75R} = 30°$

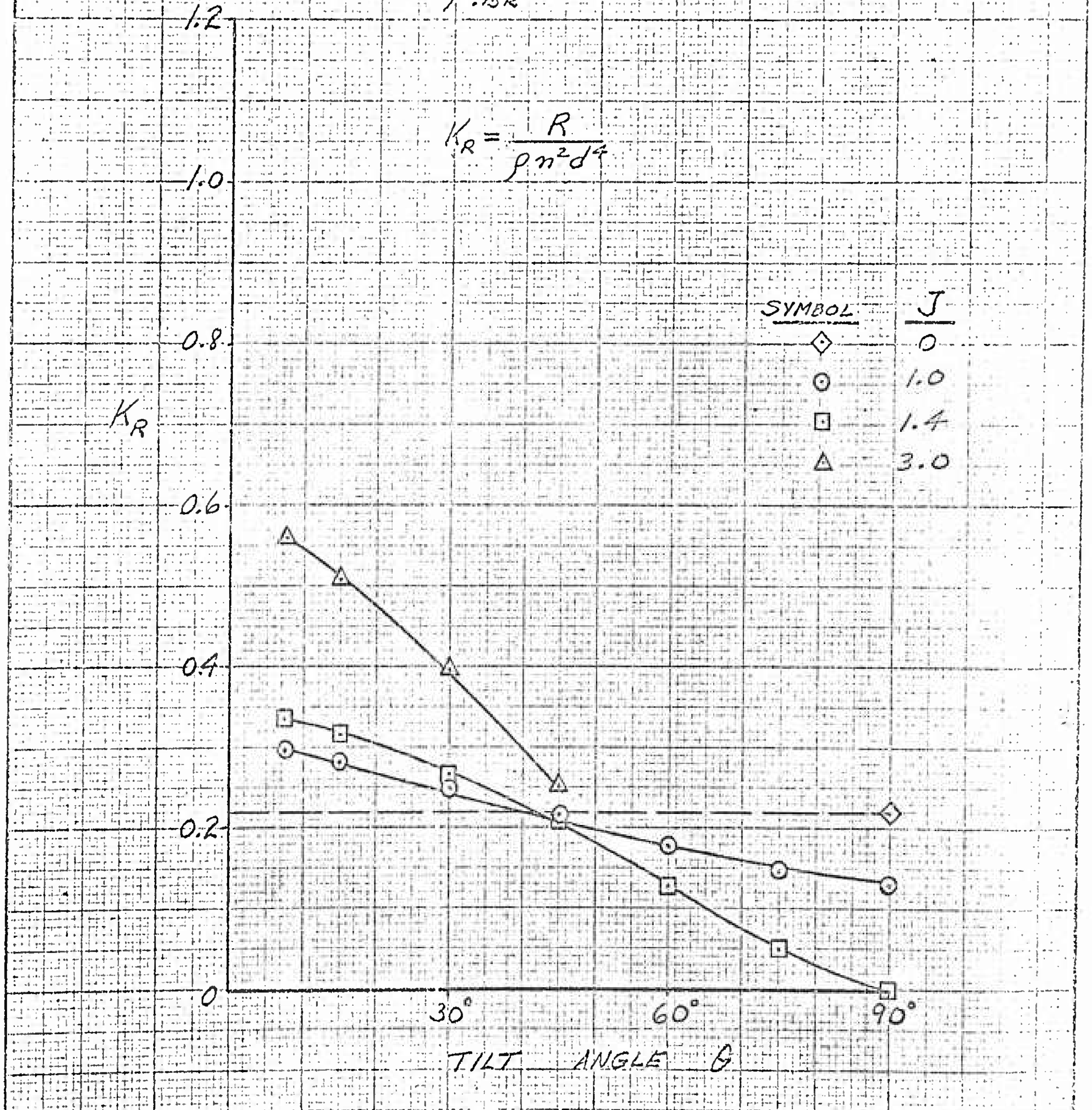

PREPARED JBL 2-18-60

CHECKED

REVISED

PAGE 305

REPORT NO

MODEL

FIG. 158

NON-AXIAL PERFORMANCE

RESULTANT FORCE

REF. 47; McLEMORE, H.C.; CANNON, M.D., NACA TN 3228, 1954

UNSHROUDED PROPELLER

$\beta_{.75R} = 30°$

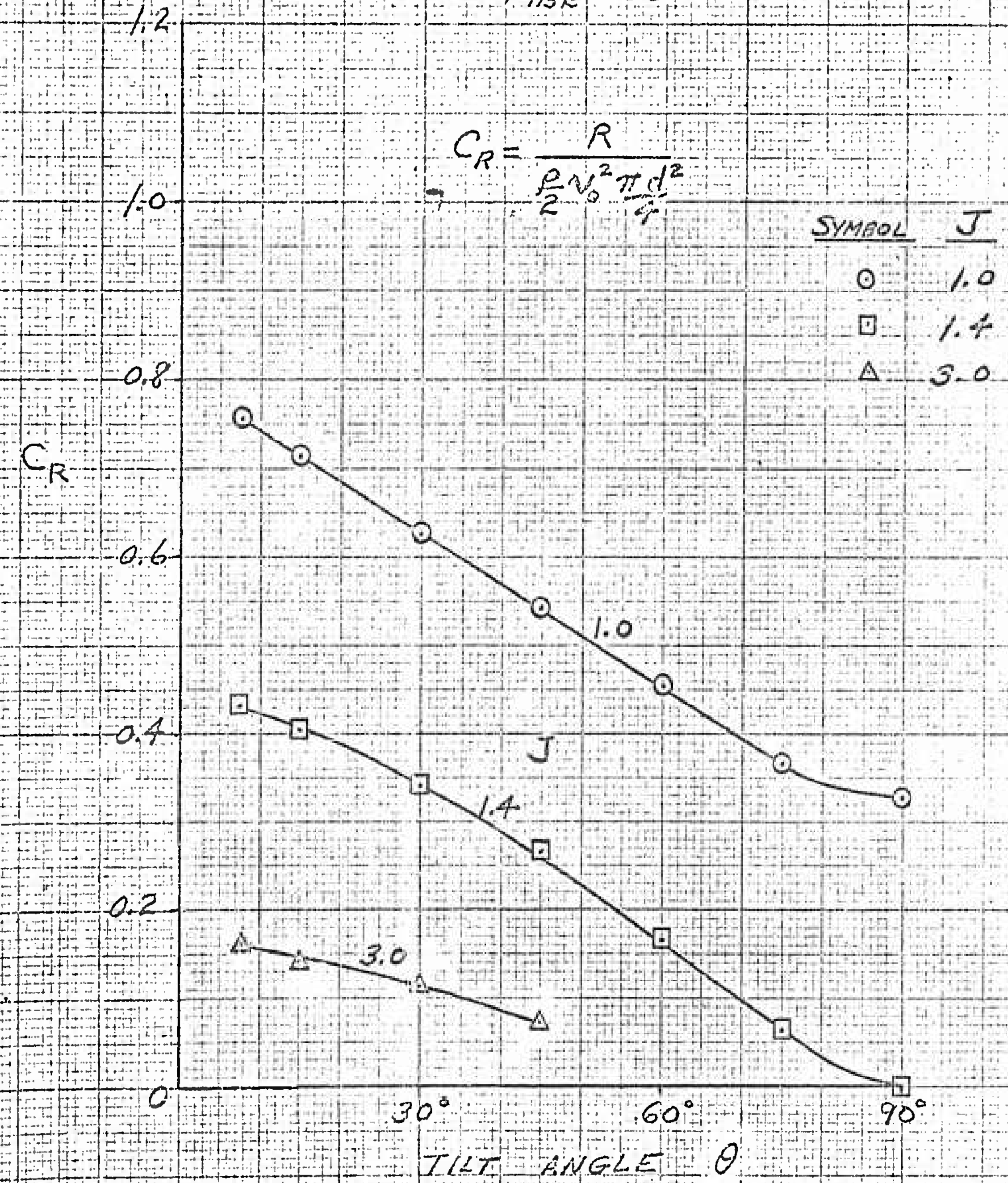

10A
2/49

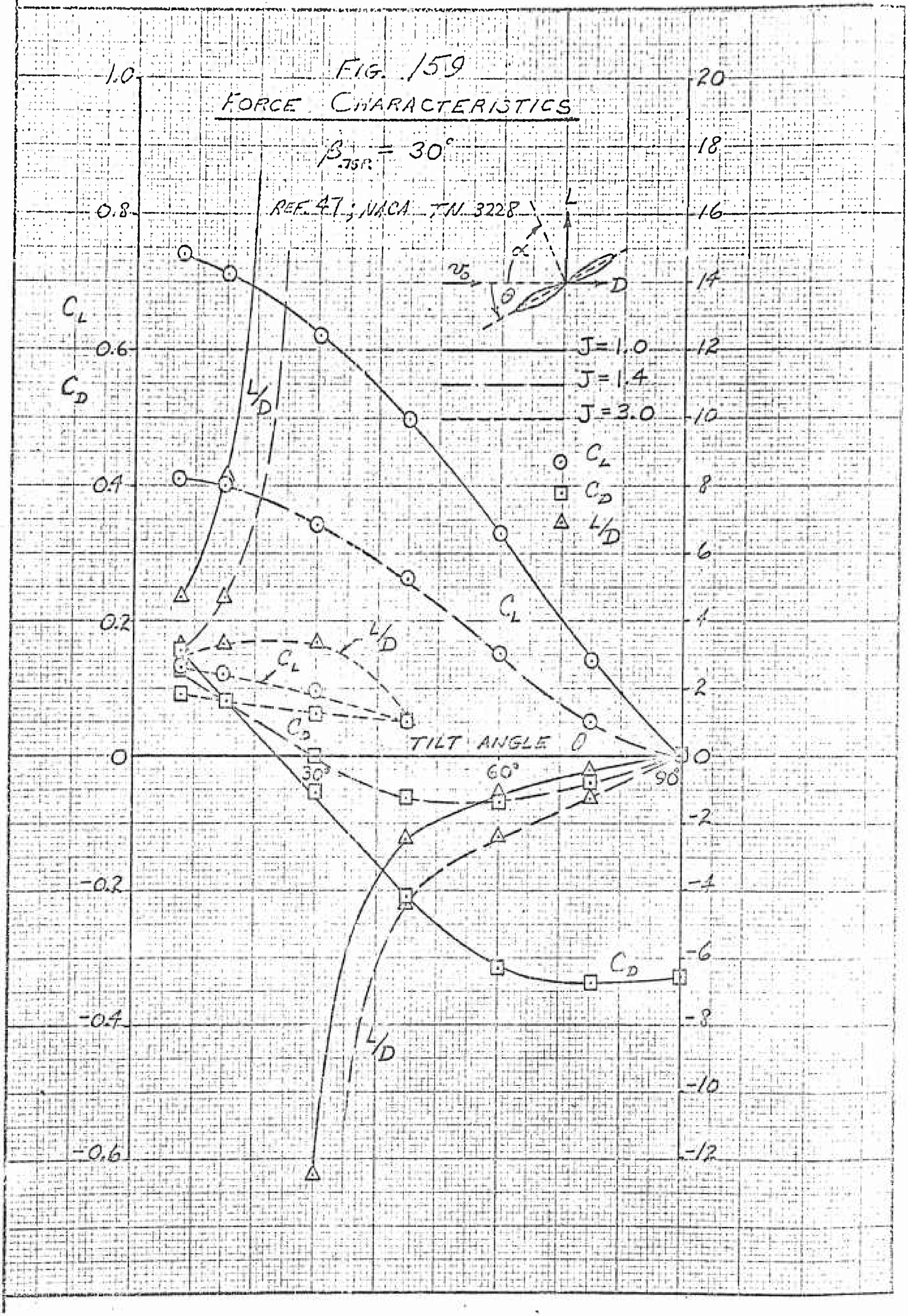
FIG. 159
FORCE CHARACTERISTICS
$\beta_{.75R} = 30°$
REF. 47; NACA TN 3228
L
D
α
θ
V_0
C_L
C_D
J = 1.0
J = 1.4
J = 3.0
○ C_L
□ C_D
△ L/D
L/D
C_L
C_D
TILT ANGLE θ
30°
60°
90°
1.0
0.8
0.6
0.4
0.2
0
-0.2
-0.4
-0.6
20
18
16
14
12
10
8
6
4
2
0
-2
-4
-6
-8
-10
-12

FIG 160

EFFECT OF TILT ANGLE ON THRUST AND POWER

$\beta_{.75R} = 30°$

REF. 47; NACA TN 3228

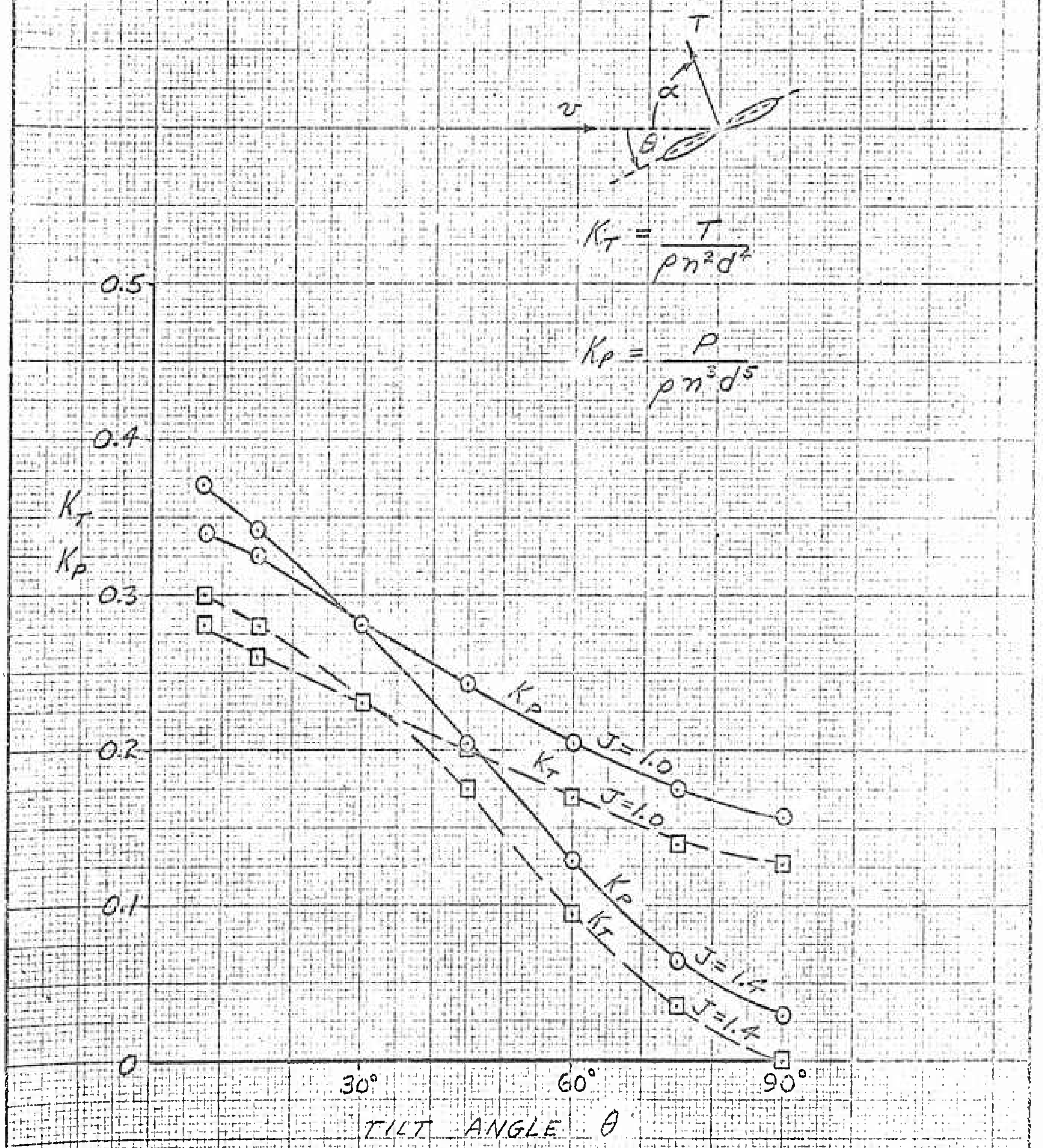

FIG. 161

NON-AXIAL PERFORMANCE
MOMENTS

REF. 47; McLEMORE, H.C., CANNON, M.D., NACA TN 3228, 1954

UNSHROUDED PROPELLER

$\beta_{.75R} = 30°$

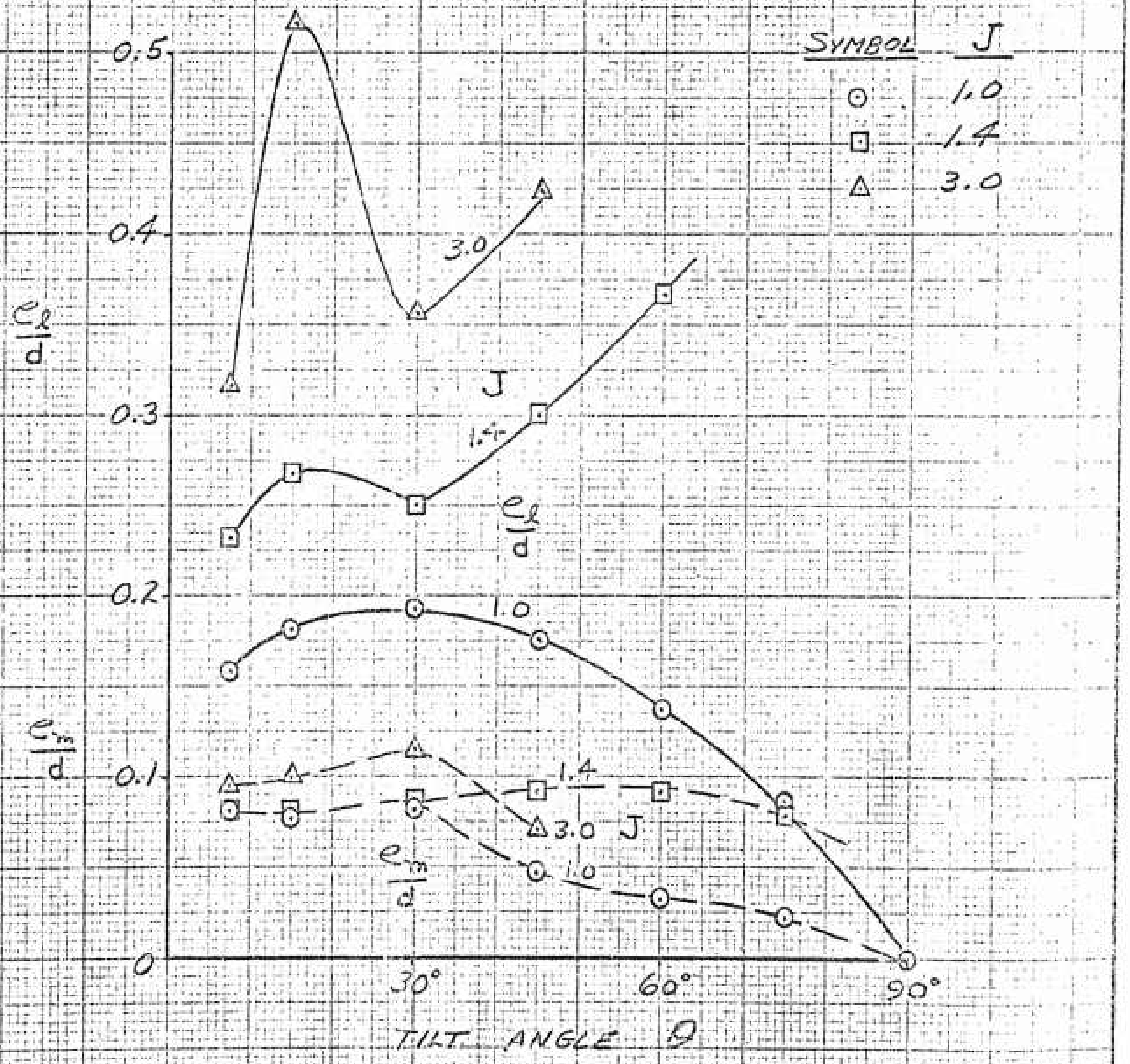

FIG 162

NON-AXIAL PERFORMANCE

RESULTANT FORCE

REF. 47; McLEMORE, H.C., CANNON, M.D., NACA TN 3228, 1954

UNSHROUDED PROPELLER

$\beta_{.75R} = 40°$

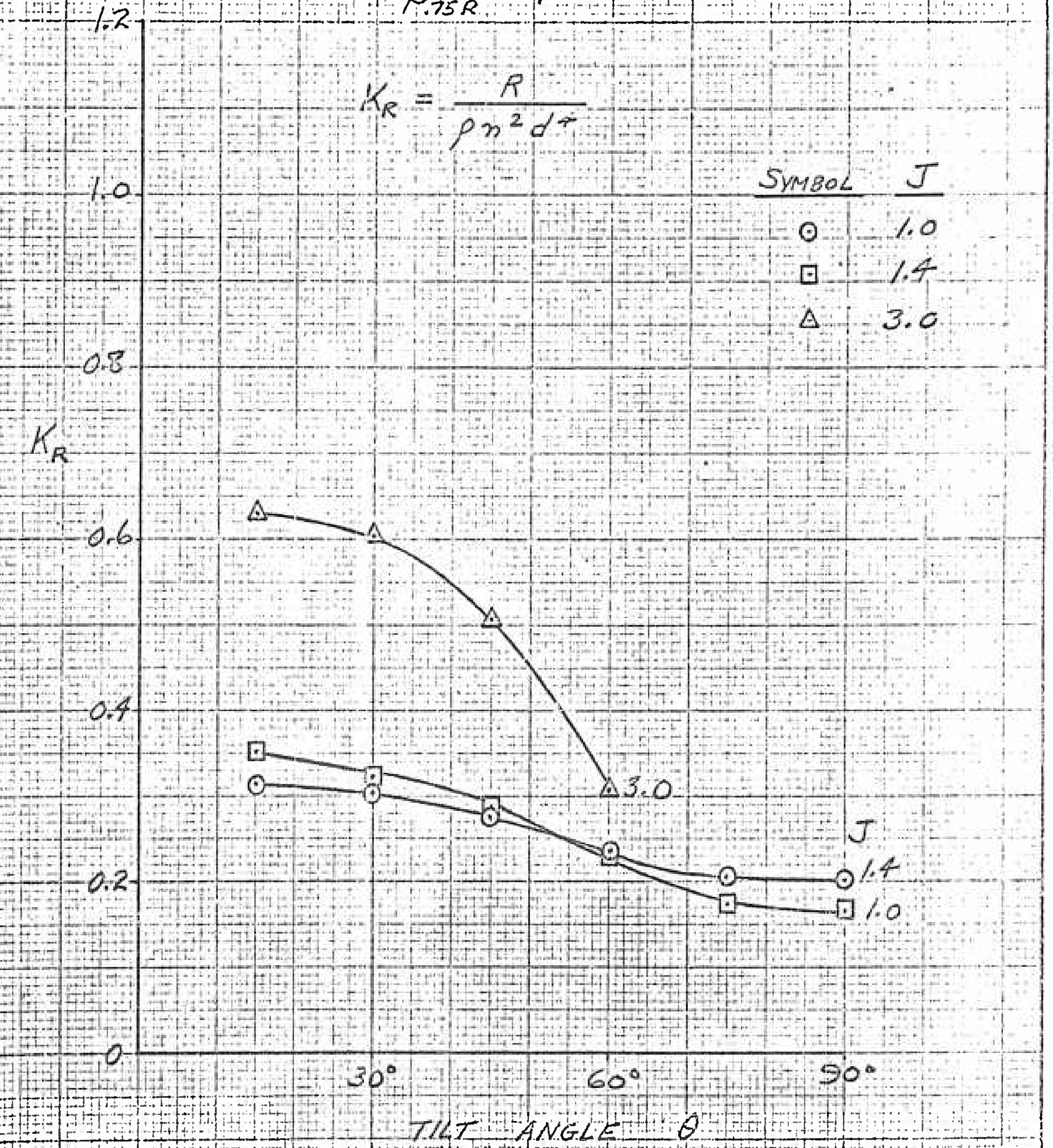

FIG. 163

NON-AXIAL PERFORMANCE
RESULTANT FORCE

REF. 47; McLEMORE, H.C., CANNON, M.D., NACA TN 3228, 1954

UNSHROUDED PROPELLER

$\beta_{.75R} = 40°$

$$C_R = \frac{R}{\frac{\rho}{2} V_0^2 \frac{\pi d^2}{4}}$$

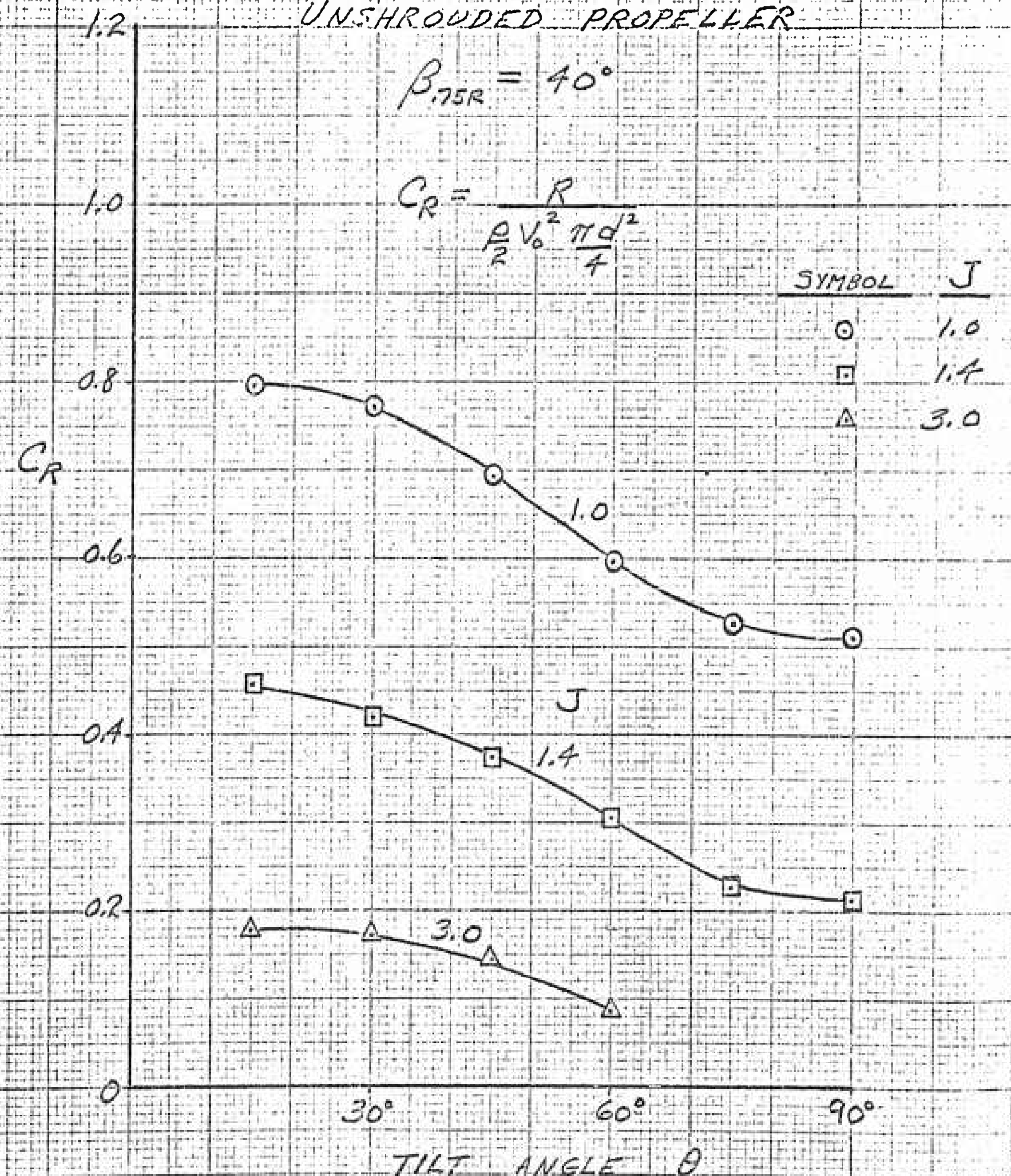

FIG. 164

FORCE CHARACTERISTICS

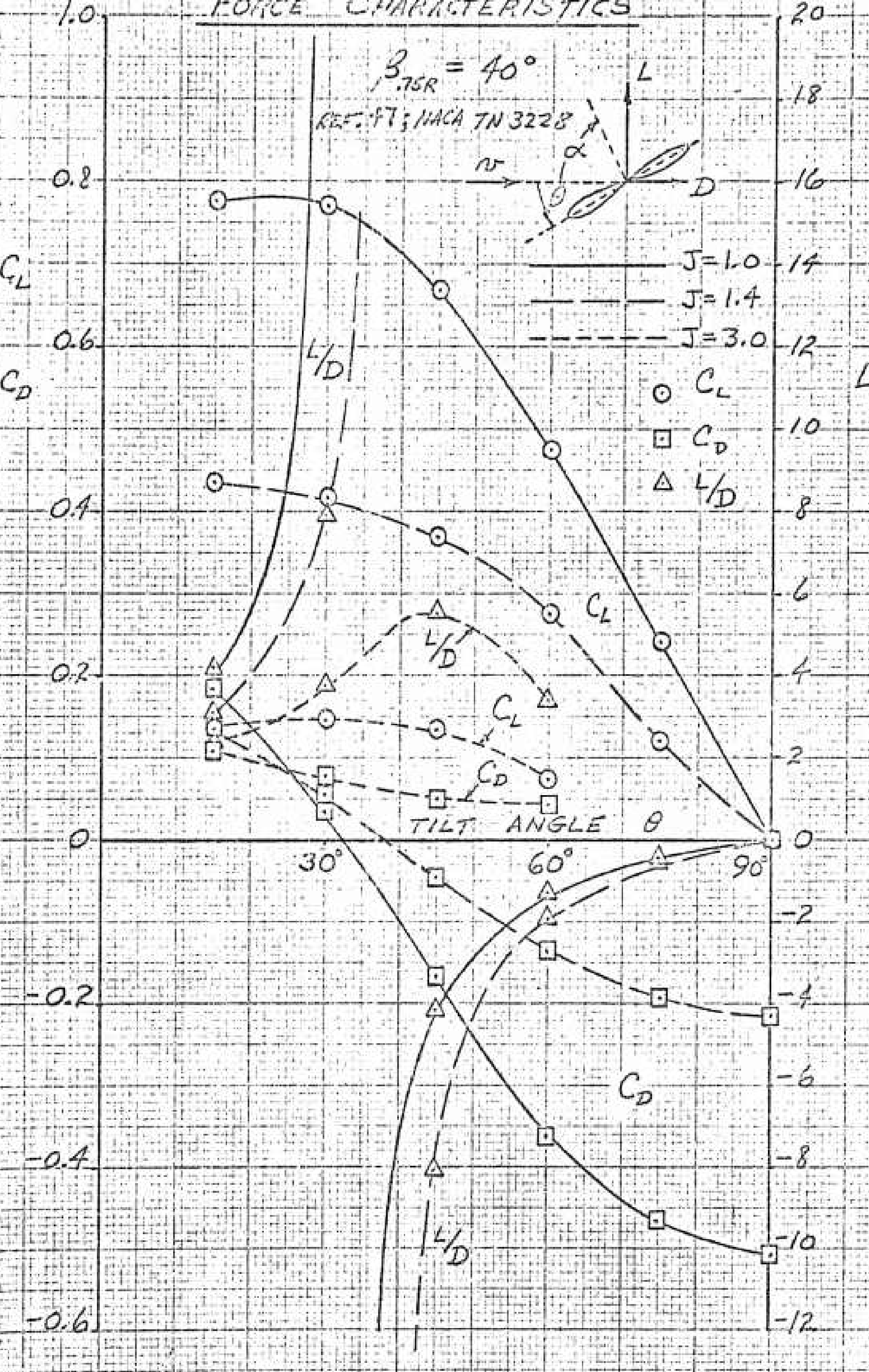

FIG. 165

NON-AXIAL PERFORMANCE
MOMENTS

REF. 47; McLEMORE, H.C.; CANNON, M.D., NACA TN 3228, 1954

UNSHROUDED PROPELLER

$\beta_{.75R} = 40°$

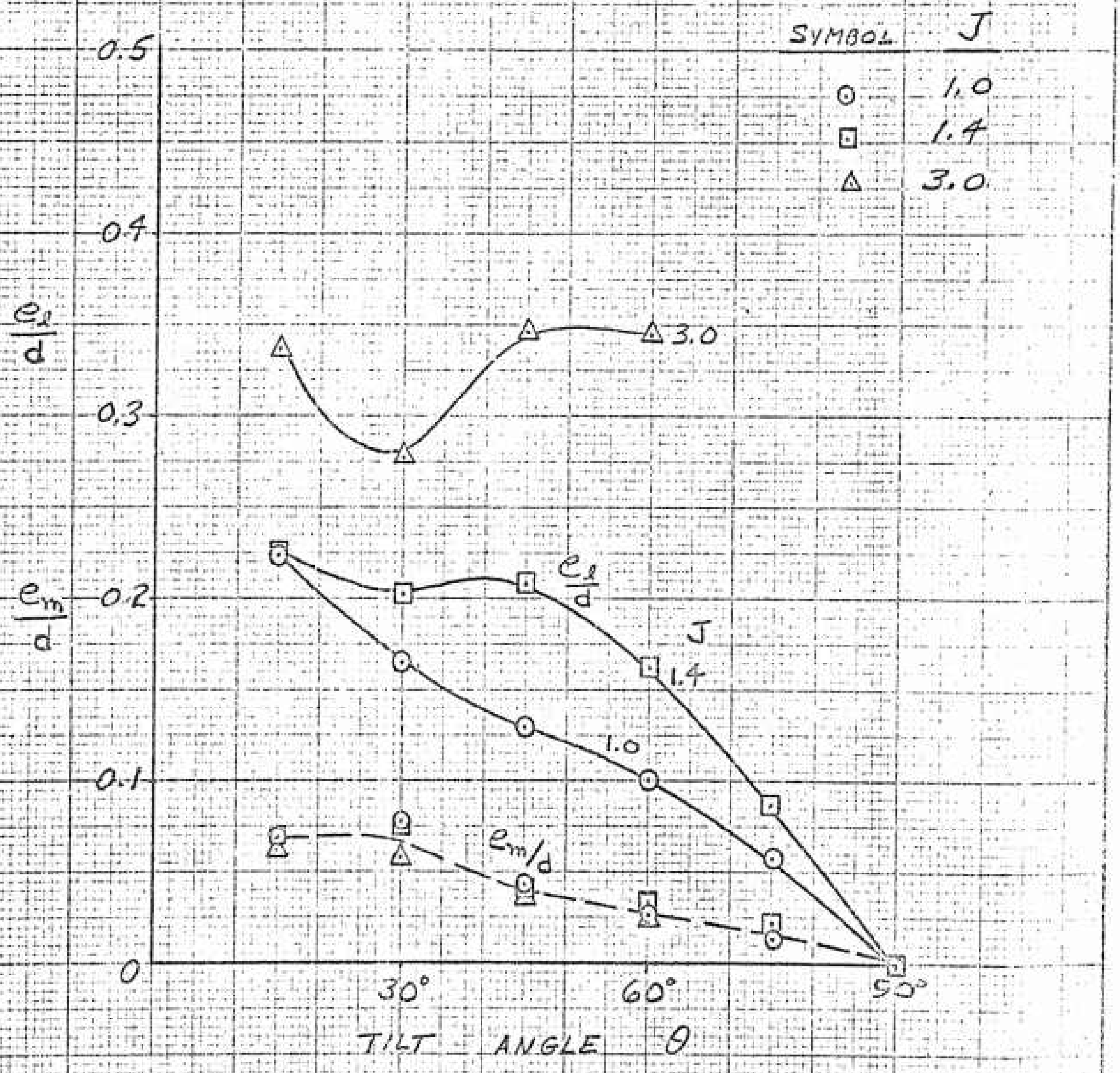

FIG. 166

EQUILIBRIUM CHARACTERISTICS AT CONSTANT LIFT

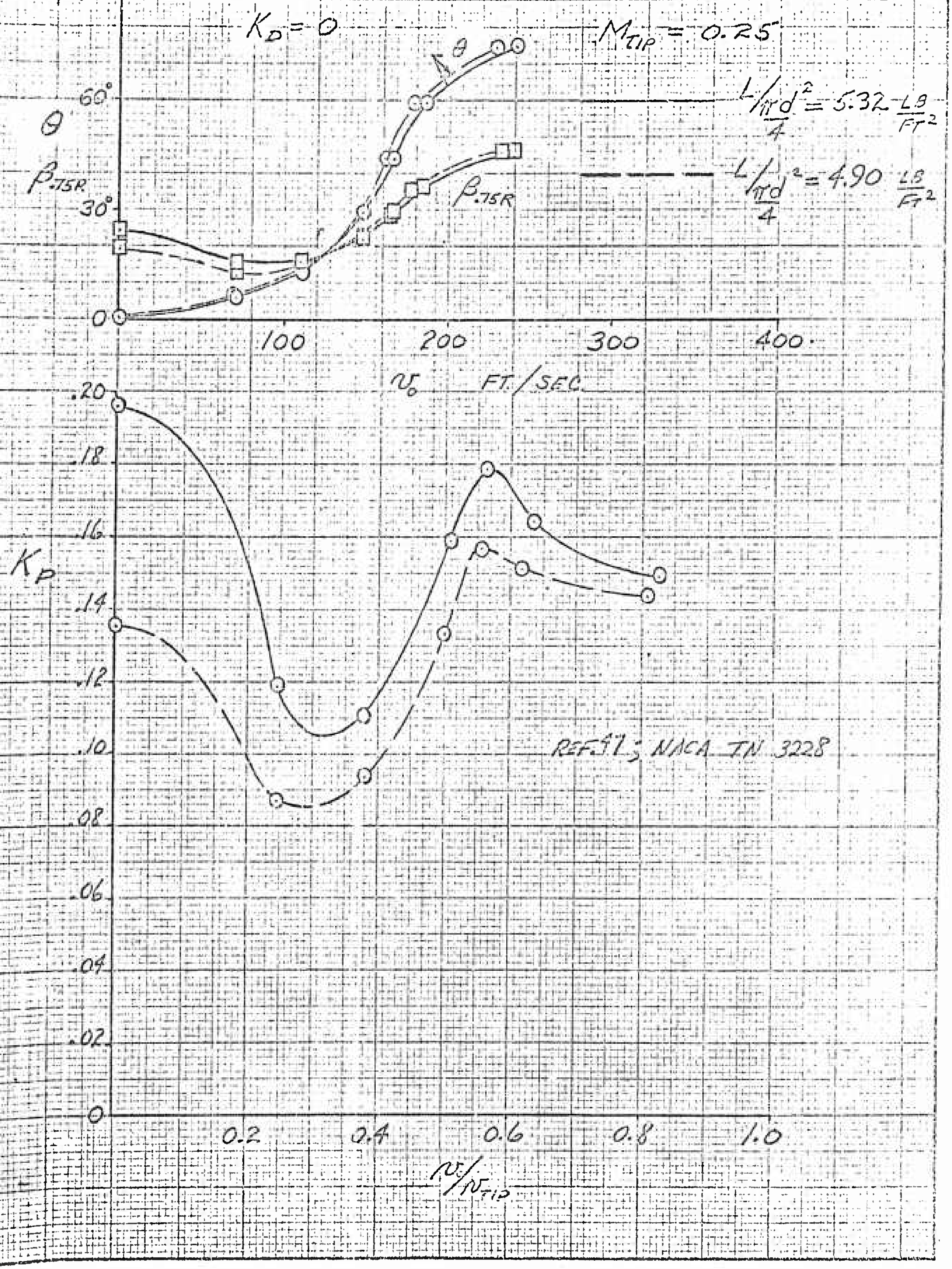

FIG. 167

EQUILIBRIUM CHARACTERISTICS AT CONSTANT LIFT

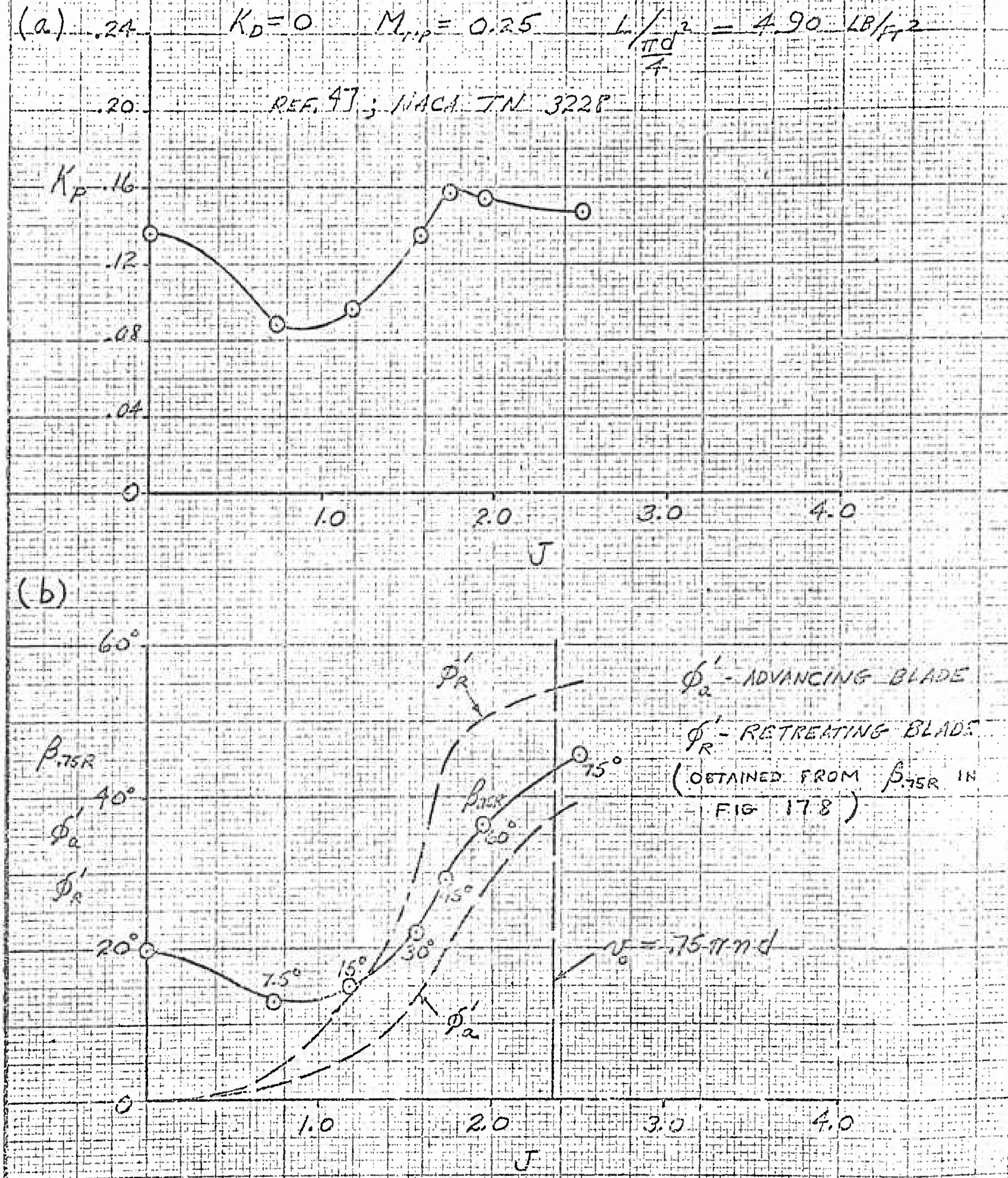

FIG. 168

ZERO BLADE SECTION ANGLE AT 75% RADIUS

$$\tan \beta_{.75R} = \frac{\sin \theta}{\frac{.75\pi}{J} \pm \cos \theta} \qquad \begin{matrix} + \text{ : ADVANCING} \\ - \text{ : RETREATING} \end{matrix}$$

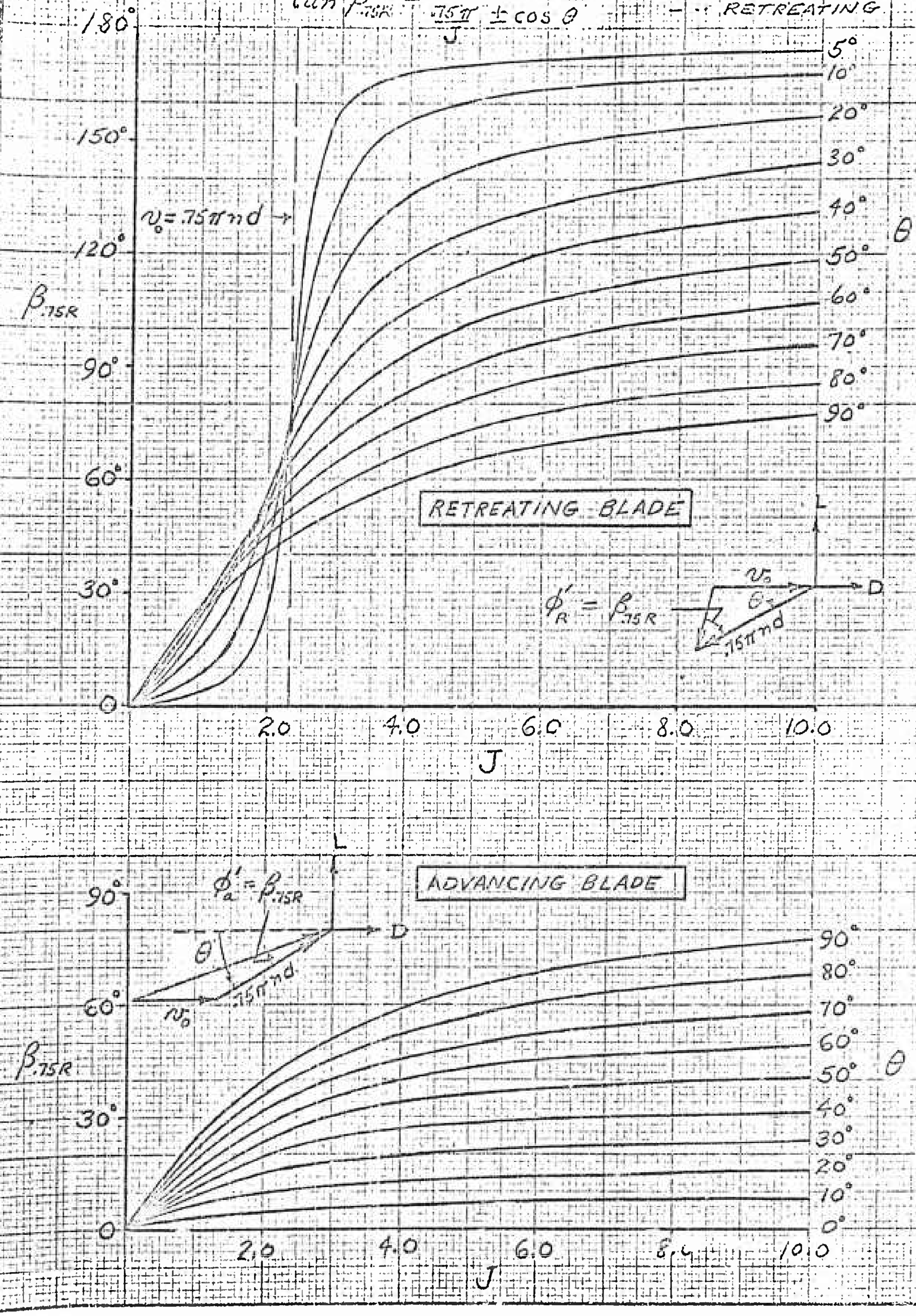

FIG 169

LIFT CHARACTERISTICS OF PROPELLERS AND HIGH SPEED SHROUDS AT SMALL ANGLES OF ATTACK

$$\bar{C}_L = \frac{L}{q_0 c_s d}$$

SYMBOL	REFERENCE	
⊡	7	HILLER ARD-224 D, β_3 S $\beta_{TR} = 9°$ $\lambda = 0.15$
⊙	12	UNITED AIRCRAFT CORP. TR 58-604 HIGH SPEED SHROUD $\beta_{.75R} = 22°$ $M_0 = 0.2$
△	47	NACA TN 3228 $\beta_{.75R} = 30°$ $J = 1.0, 1.4$

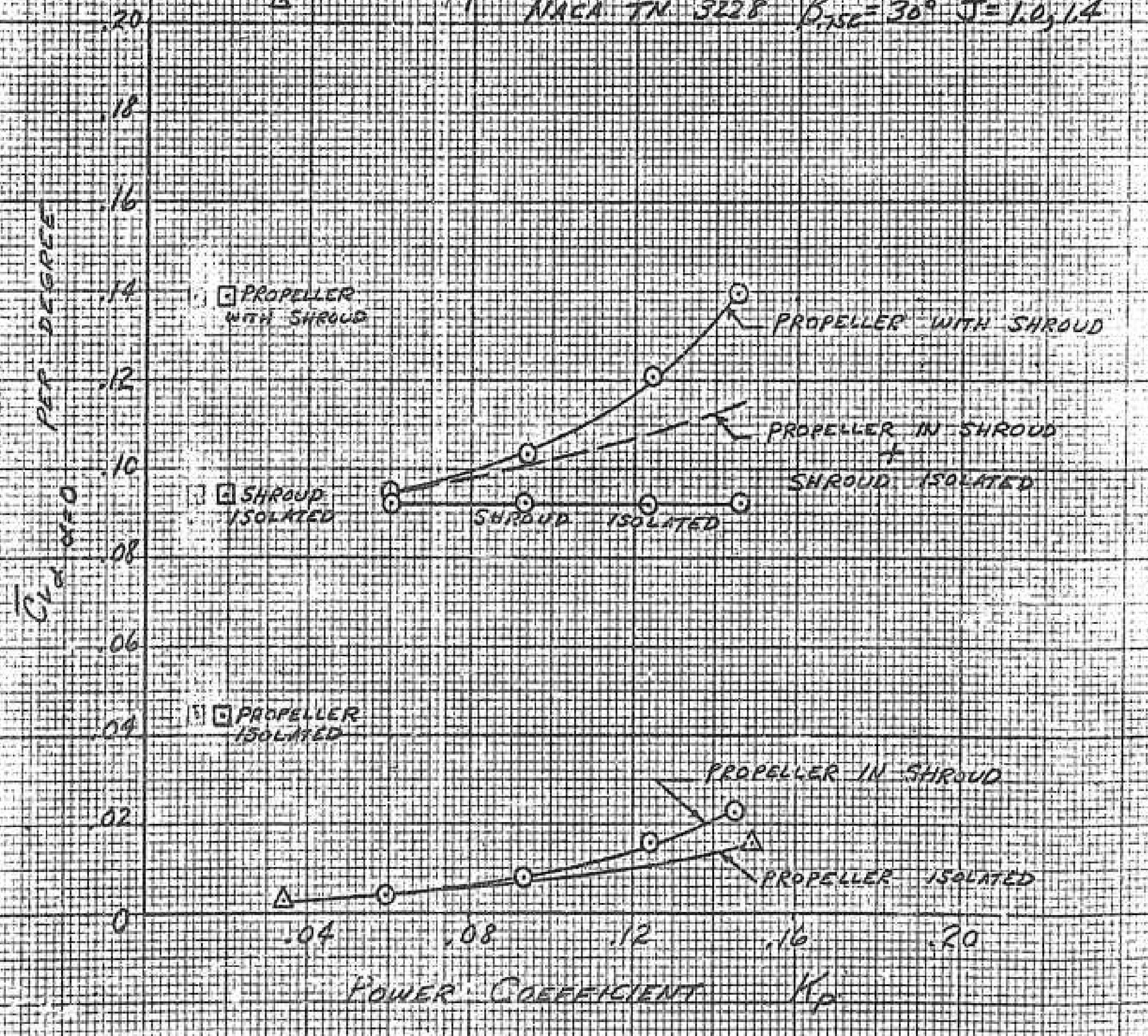

PREPARED [illegible] 1-21-60
CHECKED
REVISED

REPUBLIC AVIATION

REPORT NO
MODEL

FIG 170

STATIC PERFORMANCE

EFFECT OF TIP CLEARANCE ON SHROUD THRUST AND PROPELLER POWER

REF. 26; HUBBARD, H.H. NACA TN 2024, 1950

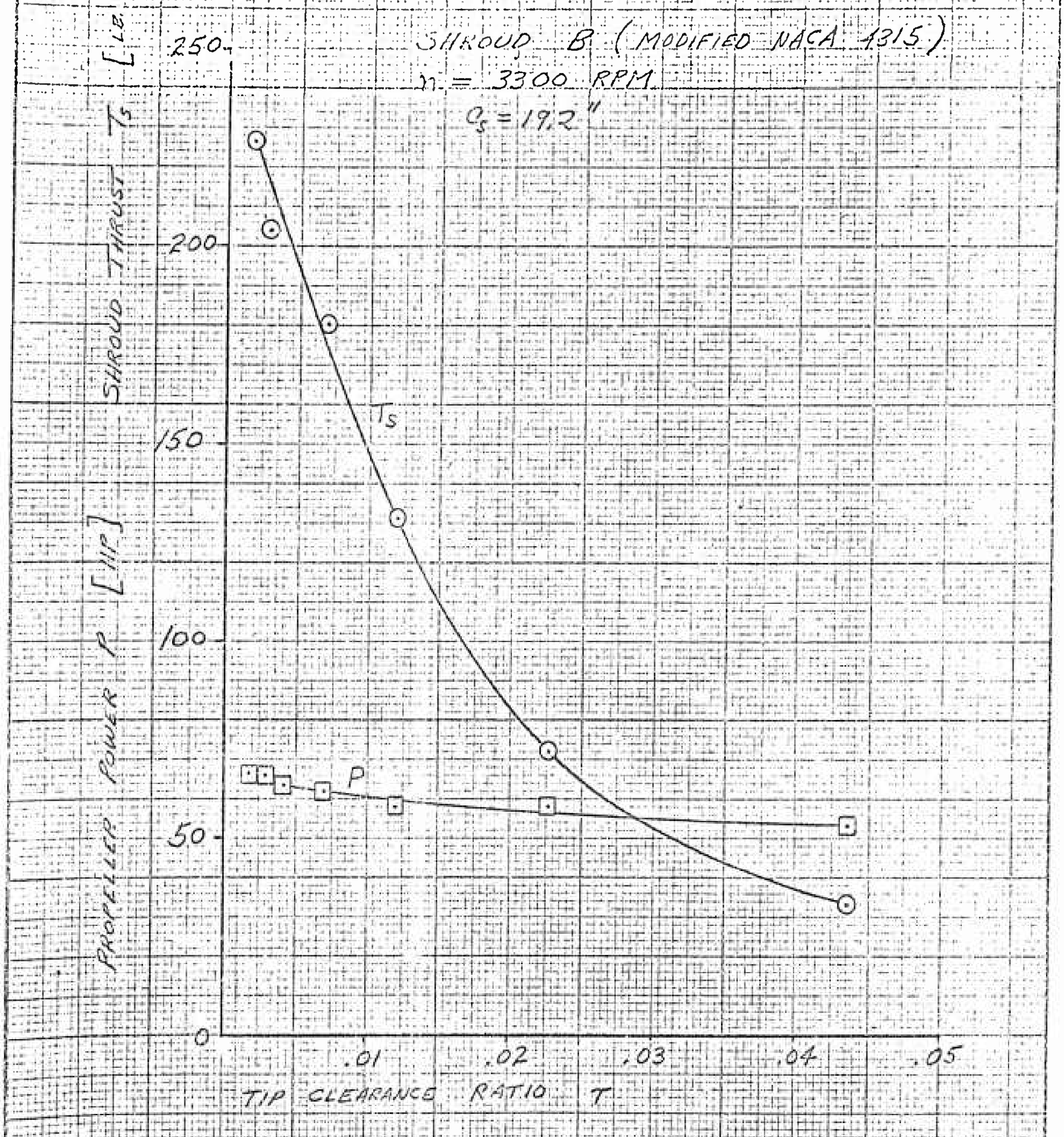

-10A
2/49

FIG 171

STATIC PERFORMANCE OF SIMPLE CASCADES

REF. 76 ; McKINNEY, M. O. ; TOSTI, L. P. ; DAVENPORT, E. E. NACA TN 3198 (1954)

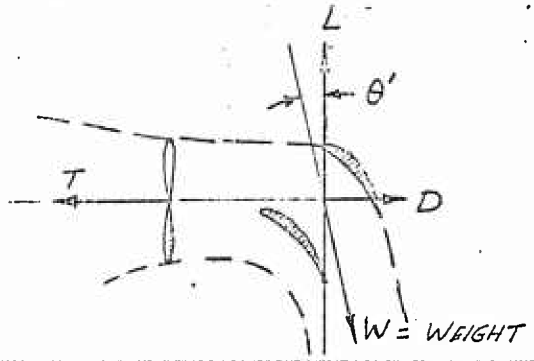

CONFIGURATION		θ' deg.	L/T	D/T	W/T
	1	7.5	0.92	0.88	0.92
	2	12.5	.83	.82	.85
	3	5.0	.85	.93	.85
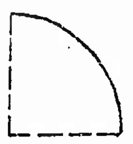	4	38.9	.54	.56	.69
	4PL*	28.2	.68	.64	.77
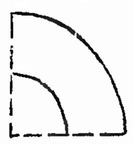	5	27.7	.66	.65	.75
	5PL	21.2	.75	.71	.81
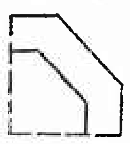	6	21.3	.66	.74	.71
	6PL	11.9	.81	.83	.82
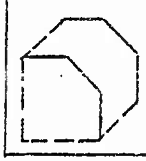	7	20.2	.65	.76	.69
	7PL	13.6	.78	.81	.80

*PL DESIGNATES END PLATES WHICH ARE SHOWN DOTTED IN THE SKETCHES

FIG. 172

STATIC PERFORMANCE

GROUND EFFECT AT CONSTANT POWER

TYPICAL DATA FROM 6 SOURCES